MAX-PLANCK-INSTITUT FÜR PLASMAPHYSIK
GARCHING BEI MÜNCHEN

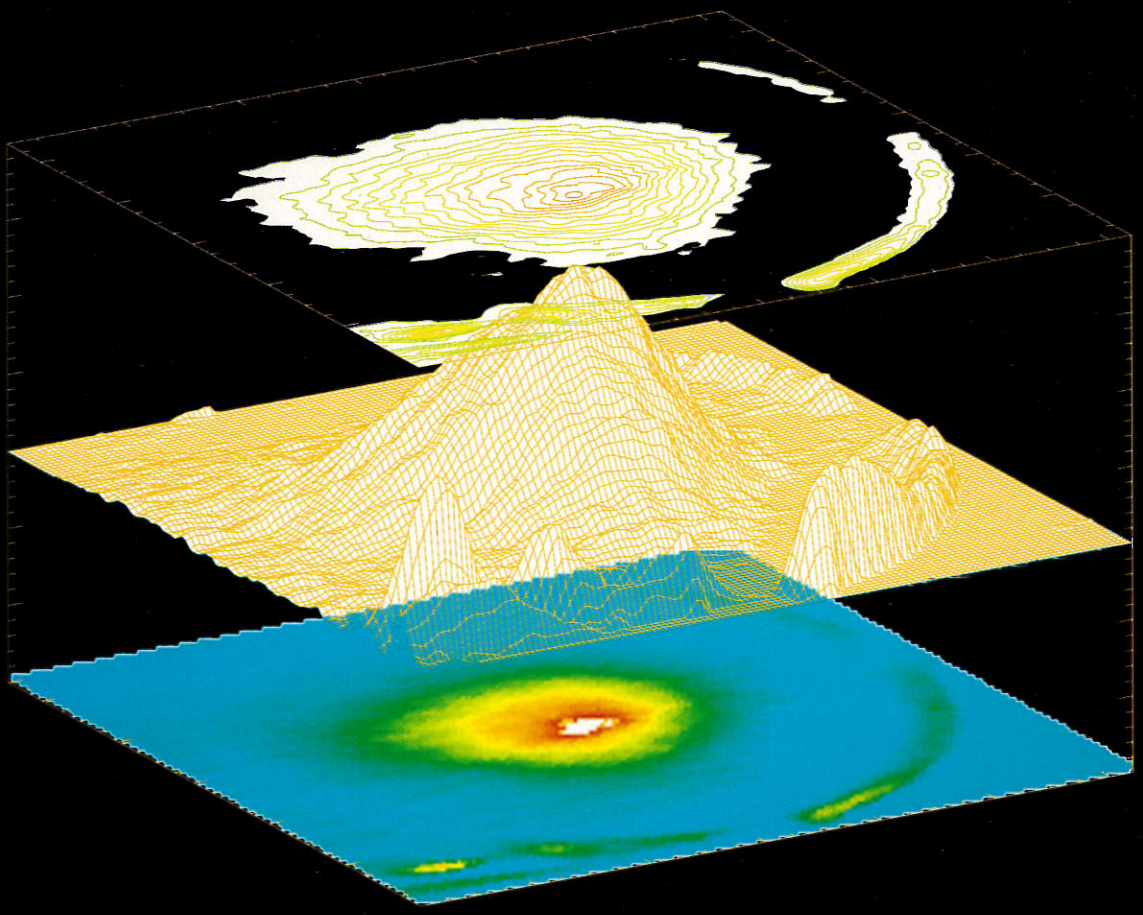

IPP

ANNUAL REPORT 1993

MAX-PLANCK-INSTITUT FÜR PLASMAPHYSIK
GARCHING BEI MÜNCHEN

Annual Report 1993

CONTENTS

PREFACE

Two types of fusion experiments are being investigated at Max-Planck-Institut für Plasmaphysik (IPP): the tokamak and the stellarator. The aim of the ASDEX Upgrade divertor tokamak is to realize a reactor-compatible, open divertor and study reactor-relevant plasma edge physics. Experiments started in 1991. All important plasma configurations with circular and elongated cross-sections, both limiter and divertor bound, can now be realized with great accuracy and controlled in a stable manner. In 1993 the first particle injector was put into operation with up to 6 MW of heating power. The plasma current was raised to 1.2 MA. The main diagnostics were put into operation as also was a newly developed pellet centrifuge. The H-regime of improved energy confinement could easily be achieved independently of the heating method.

At the WENDELSTEIN 7-AS stellarator experiment the cooperation with Russian and German research institutes on electron cyclotron resonance heating was especially successful. The prototype version of a Russian 140 GHz gyrotron was operated at its high power limit of 0.9 MW. This level is considered as target power for ECRH in next-step devices and would even conform to ITER requirements. Besides being used for heating purposes, the microwave generators also served to demonstrate the basic feasibility of a novel scattering method for determining the ion temperature. The plasma experiments concentrated on investigations of the H-regime, density and impurity control and the natural divertor in stellarators.
In addition to plasma start-up by ECRH, which limits the magnetic field strength to two singular values, a new method for WENDELSTEIN 7-AS was developed: Start-up with non-resonant radio-frequency waves works in a large magnetic field range and produces a suitable target plasma for neutral beam heating.

The follow-up experiment for demonstrating the reactor relevance of the Advanced Stellarator principle, WENDELSTEIN 7-X, will be a 5-period Helias configuration with a helical divertor and a superconducting coil assembly. The preparations in 1993 concentrated on design activities for the prototypes and the basic machine. The call for tenders for a full-size demonstration coil was issued and technical specification of a cryostat segment continued. A large part of the physics activity was devoted to the divertor in WENDELSTEIN 7-X.

Work in the new Berlin Division of IPP is largely oriented to the fusion experiments at IPP, concentrating on investigation of the plasma edge by experimental as well as theoretical methods. In Berlin the Division runs a linear plasma generator to study the plasma behaviour near material surfaces, plasma-wall interaction and to develop diagnostics.

On the national level, IPP coordinates its research effort with Kernforschungsanlage Karlsruhe within the "Entwicklungsgemeinschaft Kernfusion" and also with those National Research Centres involved in fusion research. IPP also closely cooperates with a number of German universities, the collaboration with the University of Stuttgart being paticularly successful.
The research conducted at IPP is part of the European fusion programme: IPP are involved in JET, the joint European experiment. The ASDEX Upgrade tokamak and the alternative stellarator concept as embodied in the WENDELSTEIN experiments provide essential information for preparing the next steps in the overall European programme. Furthermore, IPP acts as host to NET, the European reactor study group, who have been working at Garching since 1983.

Coordination of research activities also extends to the worldwide level. IPP is party to two Implementing Agreements: the one with the USA covering cooperation on the ASDEX Upgrade divertor tokamak; the other - with the USA and Japan - regulating cooperation in the joint stellarator programme, to which the WENDELSTEIN experiments make a major contribution. From April 1988 IPP provided the technical site for the American-European-Japanese-Soviet group responsible for the conceptual design activities of ITER, the International Thermonuclear Experimental Reactor. After completion of the conceptual design, IPP was also chosen in 1992 - together with the fusion laboratories in Naka and San Diego - as site for the ITER Engineering Design Phase.

Klaus Pinkau

Projects

TOKAMAKS

A large part of the capacity at IPP is devoted to investigating confinement in the tokamak configuration. With ASDEX, in operation till August 1990, and ASDEX Upgrade, which started scientific investigation in 1991, IPP have concentrated their tokamak research on the divertor principle.

Experimental results from ASDEX and theoretical studies of boundary problems in a tokamak reactor showed the divertor to be the candidate for the experimental fusion reactor ITER for solving problems of plasma-wall contact, such as energy transfer to the wall, erosion, pumping of hydrogen and helium and limitation of impurity production. Therefore, IPP continued and extended its divertor investigations by designing and constructing ASDEX Upgrade. In particular, the necessity of going to sufficient size in a fusion reactor to reach ignition leads to a rising energy flow density in the boundary. This increases the problems of energy transfer to the wall and of impurity control. The aim of ASDEX Upgrade is to realize a reactor-compatible, "open" divertor with distant poloidal field coils, in contrast to the ASDEX closed divertor.

The divertor promises solutions for the plasma boundary because:

- the temperature at the plasma edge (typically 100 eV) can be decoupled from the temperature at the target plates (below 10 eV desired);
- a dense and cold plasma forming in front of the target plates limits erosion and impurity flow into the bulk plasma;
- this dense plasma facilitates pumping of hydrogen and helium;
- this plasma also offers the chance to reduce the energy flow to the target plates by converting it to radiation or redistributing it through charge exchange.

Parallel to simulation of the appropriate divertor configuration, ASDEX Upgrade affords the possibility of investigating a reactor-compatible poloidal field configuration. Plasma control in the unstable position, strategies to prevent disruptions and details of the disruptions themselves can be most realistically tested in ASDEX Upgrade.

The main results in operating ASDEX Upgrade and physical results in 1993 can be summarized as follows:

- In 1993 the in-vessel components were reinforced so that they could withstand the force load of disrupting plasmas up to plasma currents of $I_p = 1.2$ MA, allowing all relevant configurations to be investigated.
- In addition to the ICRH heating system with a capacity of 6 MW the first neutral beam injector was installed and delivered up to 6 MW to the plasma.
- Beta values of $\beta_p \approx 1$ and $\beta_N \approx 2$ were reached, while the density limit was extended to $\bar{n}_e = 1.4 \cdot 10^{20}$ m^{-3} (ELMy H-mode).
- In provoked vertical displacement events halo current and energy deposition were investigated. The thermal energy is deposited on the target plates during the thermal quench phase; in addition about 30% of the plasma magnetic energy is deposited during the decay of the halo current.
- The H-mode was obtained for all heating methods with a low threshold of only $P_{th}\ [MW] \approx 1.7\ \bar{n}_e\ [10^{20} m^{-3}]\ B_t\ [T]$. Whith rising heating power ELM-free and type-I ELM phases were easily reached.
- The pellet centrifuge allowed injection of long sequences of hydrogen pellets. The resulting high density discharge with strong profile peaking showed a doubling of energy confinement.
- The impurity level was low (Z_{eff} typical 1.5) remaining stationary in long-lasting type-I ELM discharges. The Z_{eff}-profile is hollow.
- Chemical erosion at the carbon surfaces of the main chamber seems to be the main source of carbon in the plasma.
- Characteristic properties of the "hot" and the "cold" divertor were investigated with Langmuir probes, spectroscopic measurements, target plate thermography, neutral gas pressure gauges, H_α and bremsstrahlung observations, and bolometer cameras.

- Observations on high-Z materials, originating from inserts in the target plates (W, Mo, Ni, Cr) or laser blow-off (Mo, W) showed only limited erosion even in the "hot" divertor situation, a remarkable retention of target-plate produced material in the divertor chamber and no peaking of radiation in the bulk plasma.
- Pumping with external pumps overcoming variations in wall recycling and balancing neutral injection fuelling could be demonstrated.

The heating will be continuously extended in the coming years. After the installation of the 140 GHz ECRH-system with 2 MW (15 MW total) power, a second injector box will extend the heating capacity to 24 MW. The extended heating power and the need to simulate the ITER divertor will require a redesign of the divertor. The concept of the new divertor II will be fixed in mid 1994 with planned coming into operation in 1997.

Simulation of the plasma boundary (SOL) was a major effort. The experimental data of ASDEX Upgrade were used for validation of the code calculations. Application to ITER resulted in a considerable contribution to the ITER divertor concept evolution.

Cooperation is playing a growing role in the field of fusion research in order to fully exploit the capacity of experimental devices. An IEA Implementing Agreement between EURATOM and the US Department of Energy focuses on investigation of the poloidal divertor. In particular, the problem of plasma shape and position control, plasma disruptions, and vertical displacement effects (VDE) in ITER will be dealt with in ASDEX Upgrade. The plasma dynamics and forces or structures involved in VDEs and current disruptions have been extensively simulated with Princeton's Tokamak Simulation Code.

Besides conducting their own tokamak experiments, IPP have been involved in JET, the joint European large-scale project at Culham (U.K.), since the planning phase. IPP have constructed and operated several diagnostic systems and continue to participate in the exploitation of the JET experiment. In March 1992 JET was shut down for installation of the Pumped Divertor, which will allow effective power exhaust and impurity control in operational conditions close to those envisaged for ITER. The alterations are nearly completed and operational start-up is expected in February 1994.

The results of JET, the IPP divertor programme and the other associations form the groundwork for planning an experimental reactor as a next step, for which IPP are hosting the NET ("Next European Torus") Team. Meanwhile, the European Union, Japan, the USA and the (former) USSR have agreed to prepare a possible next step as a joint venture. An engineering design study (EDA) of the ITER experimental reactor is being carried out by a joint team of the four partners, one of the three groups being stationed at Garching. IPP are contributing to this work through three major channels: (i) direct participation of IPP scientists in the numerous expert meetings called together by ITER to deal with special subjects, (ii) handling of special tasks in support of NET/ITER, and (iii) participating in various NET/ITER committees. Among others, important contributions were the analysis of the confinement data base and the contribution to the development of a divertor model.

ASDEX UPGRADE PROJECT

(Head of Project: Dr. Walter Köppendörfer)

1. OVERVIEW

1.1 Introduction

In 1993 ASDEX Upgrade experiments proceeded essentially as planned. The main goals, Single Null (SN) divertor discharges at high densities, i.e. high plasma current, and high power fluxes in the plasma boundary, i.e. plasma heating powers, could be further approached. The first neutral particle injector was put into operation with up to 6.0 MW of heating power. The plasma current was also stepped up to 1.2 MA. The operational properties and limits, e.g. density limit, L-mode and H-mode confinement behaviour, were investigated and determined for each step. Unstable vertically displaced plasmas with halo current connection to the vessel walls were investigated and compared with model calculations. The vessel walls were repeatedly boronized. Additionally installed diagnostics improved the investigations of the plasma, mainly in the divertor area.

The ITER CDA and EDA considerations emphasized the plasma boundary and divertor problems with regard to large power fluxes. The geometrical size and increased plasma current of ITER lead to unacceptably large power flux densities in the divertor. Radiation from the bulk plasma and boundary is needed to reduce the power flux before it enters the divertor. In addition the role of neutral particles and geometric properties of the divertor is becoming increasingly important. Whether single–particle energies hitting the divertor structure can be sufficiently reduced, so that light material elements (graphite, beryllium) can be used, or whether heavy material elements provide the better solution is still a completely open question. The short–term programme of ASDEX Upgrade and the longer-term programme are therefore currently being revised under these aspects. The next programme steps comprise power flux and temperature control along the scrape–off layer (SOL) for further increased heating powers. ELMs and properly controlled impurity concentrations should serve as a means of tacklig these problems together with magnetic properties which may allow proper power density distribution over inner and outer divertor plates. Samples of tungsten have been integrated into target plates as coatings as well as intarsias in order to learn to diagnose tungsten spectroscopically and to be able to evaluate sputtering yields. First results have already been obtained.

The longer–term programme aims at improving the margin of divertor neutral particle density control by installing a cryopump in the divertor chamber in order to increase the pumping speed beyond the present 20,000 L/s. A major improvement of the divertor (Divertor II) is being designed by geometrically rearranging the divertor target plate structure with the aim of reducing the power load density locally and providing effective neutral particle recycling for charge exchange collision losses. Plasma boundary and neutral particle calculations with the EIRENE code are being used to find proper solutions for suitable divertor geometries.

The following overview summarizes the main results of ASDEX Upgrade machine operation and plasma experiments in 1993. The progress of the ASDEX Upgrade tokamak and the heating techniques are described in Sec. 2. Sec. 3 deals with the plasma bulk investigations, configuration and stability, plasma parameter and confinement properties and the operational limits. The plasma boundary as diagnosed so far is described in Sec. 4. The development and application of new diagnostics are described in Sec. 5.

1.2 Overview and Summary of Progress

The set-up, stable control and controlled ramp–down of ASDEX Upgrade Single Null divertor configurations have been reliably proved. The shape and position of the plasma can be determined with high precision. Nevertheless, disruptions and unstable vertical shifts (VDE) of the plasma are a hazard to the machine. Induced voltages, currents and forces along with disruptions can lead to arcs and mechanical stresses not acceptable for large plasma current discharges. For this reason the plasma current was and is being raised stepwise after sufficient experimental tests in each step. The steps so far were 350 kA, 600 kA, 800 kA, 1 MA and 1.2 MA. Plasma disruptions occurred only at the density limit or in the course of a VDE. The increase of heating power was also properly adjusted to the plasma current values.

The operational boundaries were determined during each step by checking the density limit and the threshold values for

the different confinement regimes: L-mode, H-mode, ELM-free, ELMy type III and I and dithering ELMs. The power threshold for entering the H-mode is rather low in comparision with other tokamaks and is independent of the heating method (OH, NI and ICRH). The different regimes, as characterized by the ELM behaviour, can be classified by the amount of heating power above threshold divided by the threshold power. Heating powers of up to 6.5 MW were applied with predominantly neutral injection of hydrogen of up to 50 kV. ICRH was used up to 1.2 MW at 30 and 60 MHz. But still it could not be reliably applied, partly for technical and partly for plasma physical reasons. The operational regimes were 600 kA $\leq I_p \leq$ 1.2 MA plasma current, $1.0 \leq |B_t| \leq 2.7$ T toroidal field, covering q-values between $2.3 \leq q \leq 6$, and heating powers of 100 kW $\leq P_H \leq$ 6.5 MW. Usually a negative toroidal field was chosen, which results in a B•grad B drift of the ions directed towards the divertor plates. A distinct difference could be observed when the sign of B was positive with regard to a reduced density limit and a more balanced power distribution on the outer and inner divertor plates. The threshold power for attaining the H-regime is also lower for negative toroidal field values. Otherwise the threshold follows in general a $n_e \cdot B_t$ dependence as found in other experiments too. The local power deposition on the inner and outer divertor plates could be measured by thermographic observation with millisecond time resolution. The deposition profiles of up to 20 MW/m^2 vary considerably with the confinement regime, the type of ELMs and ion drift direction. A moveable Langmuir probe yielded radial density and temperature scans of the SOL at the entrance to the divertor chamber. The maxima fit well to the separatrix position as determined by flux surface analysis from magnetic measurements. The decay of the profiles into the vacuum gave hints on thermal and particle diffusion coefficients. This information was used for improved EIRENE calculations.

All plasmas in divertor configuration turned out to be essentially clean, as indicated by $Z_{eff} \leq 2$ and the low radiated power losses. Light impurities such as carbon and oxygen prevail due to the fact that the vessel walls and divertor target plates are graphite clad. Fresh boronization reduced the oxygen content by a factor of up to three. The carbon impurity concentration stayed at the same level independently of the plasma density. The observation of hydrocarbons in the vessel exhaust indicates chemical sputtering on graphite surfaces. Sputtering yields from the target plates could be determined by the measurement of hydrogen particle fluxes and carbon C II and C III lines above the divertor plates. For sufficiently cold divertor conditions the carbon line intensities above the plates are strongly reduced. Chemical sputtering on wall surfaces then seems to be the source of the essentially unaltered carbon impurity content. The question whether graphite walls and graphite divertor target plates provide clean enough plasmas also for reactor–relevant power fluxes is still not answered. A programme to test tungsten for target plate material as a typical material with a sputtering threshold at high energy and with high temperature capability has therefore been started. In a first step small samples were integrated into a target plate and one plate was coated with tungsten. The samples allow one to check up to what distance redeposition occurs. The coating allows spectroscopic measurements as to what lines are dominant and as to how far sputtered tungsten penetrates into the plasma. The diffusion of tungsten into and out of the plasma core was checked by means of laser blow–off.

Cold and dense plasmas with high recycling in the divertor, detached plasmas and MARFEs have been produced under certain conditions. High q-values, moderate heating and high plasma density are favourable. The power radiated from these zones favour the energy flux distribution over larger areas of material structure as compared with the narrow heat conduction channels of the SOL. The questions, however, whether these cold layers are compatible with improved confinement and ELMs and whether they can transport sufficient power also under reactor-relevant power load conditions are still open.

The investigations described will be continued and extended by fully exploiting the machine capability and heating powers, up to 15 MW in the next stage and to 24 MW later. The diagnostics for refined SOL and divertor investigations is already available. The main goal is to find solutions which allow the losses from the plasma to be distributed and controlled over the different loss channels. Controlled impurity radiation, thermal conduction and convection should share in dividing up the extreme power flux densities, so that the material properties of the in–vessel structure can sustain the heat and particle loads. Local control of neutral the particle pressure will play an essential role here. The plasma fan of the SOL into the divertor, the geometric arrangement of target plates and baffles and pumping possibilities govern the distribution of neutrals. After the present Divertor I configuration improvements are to be effected with Divertor II in 1996.

2. TECHNICAL SYSTEMS

The range of discharges could be extended up to 1.2 MA of plasma current (I_p) and 6 MW H^o of neutral injection (NI). Technical problems have limited the Ion Cyclotron Resonance Heating (ICRH) to 1.5 MW. Additional heating by Electron Cyclotron Resonance (ECRH) is under construction. During hard disruptions and $I_p \geq 1$ MA high–current arcs are produced (100 kA) across the insulated gap of the Passive–Stabilizing Loop's (PSL) bridge. To increase the reproducibility of the discharges, helium glowing between shots became a routine operation. Discharges with $I_p > 1$ MA and combined NI (Neutral Injection) and ICRH now require all three available flywheel generators.

2.1 Machine

During 70 days of experimenting 1637 shots were counted. Two unintended shutdowns reduced the operating time. One was caused by a failure of the feedback power supply. Its thyristor fuses were destroyed due to a frequency drop of the grid out of tolerance. The second shutdown required opening of the vacuum vessel; Teflon, evaporated by PSL arcing, had contaminated the vacuum vessel.

During Whitsuntide the assembly of the machine core was finally finished by mounting the last set of NI iron jokes. From August to October the 10 kV net was serviced. This time was used for in-vessel work, dedicated mainly to diagnostic modifications and problems resulting from arcing. Scheduled replacement of the internal thyristor control of the feedback power supply was also effected and an additional protection system installed for it, which switches off in case the grid frequency gets out of the specified range (110 Hz and 85 Hz).

The concept of the ohmic heating (OH) breaker's closing switch had to be changed. The closing switch worked initially in three consecutive parallel stages. First, ignitrons took the arc, then an air-blast switch followed until a vacuum breaker with three parallel tubes finally took over. At switching currents above 15 kA the electrodes of the air-blast switch already wore out after a few operations. Hence this switch could not be used for the envisaged switching currents of 35 kA. There was also a strong intention to dispensing with the ignitrons, being in this particular case a safety risk (mercury). Fortunately, measurements identified a small jitter of the vacuum breaker (1 ms) and estimates predicted a level of arcing coulombs which could easily be taken by one tube of the vacuum switch. However, there was a certain risk of welding the hot closing electrodes. But meanwhile the vacuum tubes alone have switched a current of 30 kA over 700 times without any noticeable deterioration. Recent measurements of the individual tube currents show a switching delay of about 100 μs between consecutive tubes, due to which the first gets two–thirds of the total current at the end of the commutation time of 2 ms. All three currents are well readjusted after 40 ms. A computational circuit model reproducing the measured currents very well shows that an available 1 mH reactance, in series with the vacuum switch, will considerably reduce the arcing coulombs and the deviation of the branch currents. The increased commutation time of 40 ms can be accepted.

The summer inspection of the vacuum vessel showed significant erosion traces mainly on the lower inner and upper outer divertor plates, due to arcing. But also behind the outer carbon protections, in the space between the PSL and vessel wall there were traces of cathode spots found on all metal surfaces normal to the toroidal direction. On the upper branch of the PSL bridge, at the surface pointing towards the vessel wall, a high–current arc (measured ignition at 190 V, burning at 80 V) had ejected a jet of copper, which also hit divertor plates on plasma-facing surfaces. Therefore protection spark gaps with carbon electrodes were mounted on the endangered upper and lower bridge branches. To prevent the arc from escaping to the nearby copper surfaces of the gap, a Teflon strip was inserted in between. The spark gap worked, but one carbon electrode broke rather early. Also small quantities of Teflon were evaporated and spread over the target plates. The Teflon in turn released fluorine during further discharges. The resulting reduction of the density limit then required a shutdown of the machine in late December.

The carbon electrodes and their electrical contacts will now be reinforced and the Teflon replaced by boron nitride. The upper lid of the bridge, which fortunately could be removed, will be coated with ceramic insulation to increase the electrical creep length. Additionally a start was made to investigate the involved arcing phenomena on separate test stands with vacuum, magnetic field and plasma (PLASI) step by step.

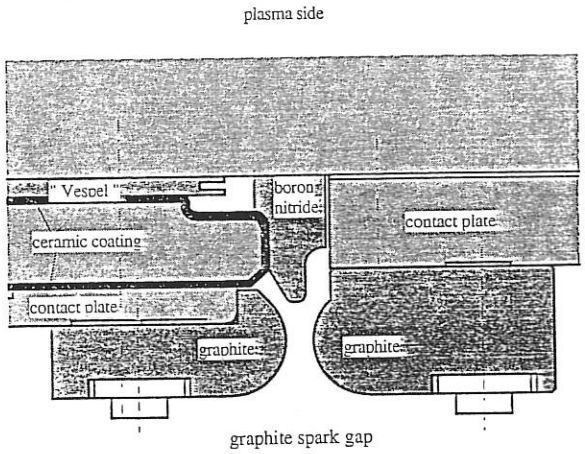

FIG. 2.1: Protection spare gap at the PSL bridge.

2.2 Control Systems and Data Processing

During the past operation period the efforts of the **control system** group were devoted to supporting the experiment's progress, consolidating the control systems (XPM, R1, R2, R4) and further completing those functionalities that will be required for smooth operation in the near future.

For the XPM experiment management system an information management tool was developed to extract the most essential events from the bulk of the protocolled shot data. This gives a quick overview as a basis for discharge control performance evaluation and optimizations between shots. An additional logical trigger facility was created to reduce the amount of diagnostic data and improve their relevance. This is done by the real-time discharge control computer R1, which detects irregular vertical shifts of the plasma centre or drops in plasma current. A disruption trigger is generated and broadcast via the timing system to start fast data acquisition in a narrow time window around the event. Further applications of this universal system are planned.

A substantial amount of effort was spent on the R4 plasma controller project. The structure of the controller's real-time software was defined. The communication software for integration into the XPM environment was completed and a real-time i/o-simulator was provided. The real-time control tasks and the internal and peripheral i/o communication tasks were programmed and tested. By the end of the year the first density feedback control process was being integrated into this framework. Preparations to start up the system and add the feedforward control of pellet injector and heating systems are under way. The hardware required for feedforward control of neutral beam heating and pellet injector systems was completed. The input modules for acquisition of sensor signals required for feedback control of heating and refuelling are in progress.

Being the most essential component of the real-time system, the plasma position controller R2 demands improved reliability and maintainability as well as functional extensions for future operation. Handling and maintenance of the system were simplified by software modules for overall testing of the R2 periphery, full protocolling of input signals and refined reporting of real-time errors and warnings. The extension of the plasma position control to include shape control is being prepared. The existing algorithms are consolidated by streamlining and modularizing the program code. The necessary increase in performance to accommodate these extensions was achieved by installing faster T805 transputers and larger memories. In order to support the design of the shape controller, theoretical investigations are being carried out with the MATLAB and ACSL simulation packages.

Two major changes to the **data processing infrastructure** at ASDEX Upgrade were made in 1993. First an FDDI backbone was built in parallel to the existing network. This was due since the still growing number of diagnostics and the amount of data began to overwhelm the network connection to the computer centre and data archives. (For more details see Computer Science Division.)

Second, the Andrew File System (AFS) was introduced as an installation-wide file system for system and application software and user files. This was a collaboration with the computer centre where AFS was evaluated and selected as a step to a campus–wide distributed computing environment and as replacement for the existing AMOS and HADES mainframe–based file systems. ASDEX Upgrade, as the first group at IPP, introduced AFS because the maintenance of the workstation file systems was due to be concentrated in a central administrable system. While presently only a few users have their files in AFS, in the future all files will be moved to it to allow institute–wide identical access from any workstation. The implementation of Kerberos will in this case ensure authenticated access. Automated backup for data integrity of all files in the AFS is provided and maintained by the computer centre.

Minor changes were the replacement of boot and compute servers by SPARC 10 machines, the introduction of SunOS compatible VMEbus workstations for data acquisition, and the buildup of first diagnostics without VMEbus and CAMAC subsystems using GPIB data acquisition interfaces instead. However, CAMAC developments were also carried out in 1993. So in collaboration with an independent contractor a new programmable and flexible triggerable CAMAC pulse generator with event protocolling was designed. First prototypes of this module will be available for operation in the 2nd quarter of 1994. Also an SBus card as CAMAC controller interface for Sun SPARCstations is under construction by the Computer Science Division.

Standard public domain software packages such as Emacs, Ghostscript, Gnu-C, Gnu-C++, gdb, xfig, xpaint, xv, bash, tcsh, perl, xarchie, xgopher, xplz etc. are available through AFS on all workstations. They are maintained mostly in the actual revision. Also the collection of commercial software has be completed: ORACLE in connection with the ORACLE server of the computer centre provides relational database services; AutoCAD is used for the creation of complex figures for papers from design drawings of other CAD systems.

2.3 Neutral Injection

In 1993 the first injector was successfully put into operation, reaching the nominal neutral power of 6 MW H^o. Significant progress was also made with the second injector: the development of the RF source was considerably advanced and major parts were ordered.

Assembly of the **first neutral beam injector** on ASDEX Upgrade was completed by installing the deflection magnet which had to be modified in order to withstand the higher power loading due to the space charge problem observed on the test stand. Before the beginning of the summer shut-down 5.2 MW were injected for a pulse length of up to 1 s. This heating power, obtained at an extraction voltage of 47.5 kV, corresponds to more than 85% of the nominal power of 6 MW for hydrogen operation. After resumption of beam operation in mid–November the injected power could be further raised to 6.1 MW (50 kV) with a pulse length of individual PINIs of up to 1.7 s. Internal shots onto the calorimeter at 52.5 kV confirmed that the injector is capable of injecting at least 7 MW of H^o beams when operated at the nominal value of 55 kV.

The SIMATIC-based injector control system worked reliably from the very beginning and almost all of the more than 250 signals per pulse (thermocouples, pressures, flow rates, current and voltage measurements) were recorded by the data acquisition system starting from the first shot. A density interlock which inhibits further beam injection within 30 ms if the plasma density or the plasma current falls below preset values was set up and carefully checked before starting the injection experiments.

Beam operation and power loading on ASDEX Upgrade proved to be as expected from the test stand (see Fig. 2.2). The magnetic shielding proved to be sufficient for source operation and ion deflection. A small horizontal shift of the ion beam was detected, which, however, only slightly affects beam transmission through the duct or power loading on duct scrapers for the range of tokamak fields operated so far ($I_p \leq 1.2$ MA). Photodiode signals of visible light from the duct region showed that no significant pressure rise and therefore no excessive reionization losses occur with increasing pulse length, and thermocouple signals from inner wall protection tiles indicate beam shine-through as calculated.

During the first half of the year, final experiments with the bucket sources for the 1st injector were carried out at the **test stand**. During the second half of the year, the work was devoted to the RF source (see Technology Division). A duct simulation with the Box Exit Scraper and the A-port protection scraper was installed. A target tank with an actively cooled calorimeter (TTK) allowed the transmission through this duct to be measured. At optimum, appr. 5% of the neutral beam power intercepts the scrapers. The highest neutral beam power obtained on the TTK was 2 MW from a 55 kV, 94 A beam. A beam modulation as fast as 20 ms "on", 20 ms "off" at nominal

beam parameters for 3 s was demonstrated without any loss of power.

The problem with the ion removal system (IRS), mentioned in the Annual Report 1992, was further investigated. A more accurate measurement of the pressure revealed that the necessary background pressure for space charge compensation is a factor of 4 smaller than previously reported. The power distribution in the IRS with space charge included in the ion trajectory calculations showed that less than 1 % of uncompensated space charge is sufficient to explain the discrepancies to the calculations without space charge.

Concerning the **second injector** the specifications for the PINIs, the grids and the main insulators were finalized and after call for tenders the contracts for all three items were recently placed. These contracts include options for further components suitable for 100 kV, to be released in early 1995. The specifications of the cooling system were completed in autumn and after call for tenders the order is now being placed. Also the prototype RF generator (power-regulation, notch/pulse modulation) was ordered at the end of the year.

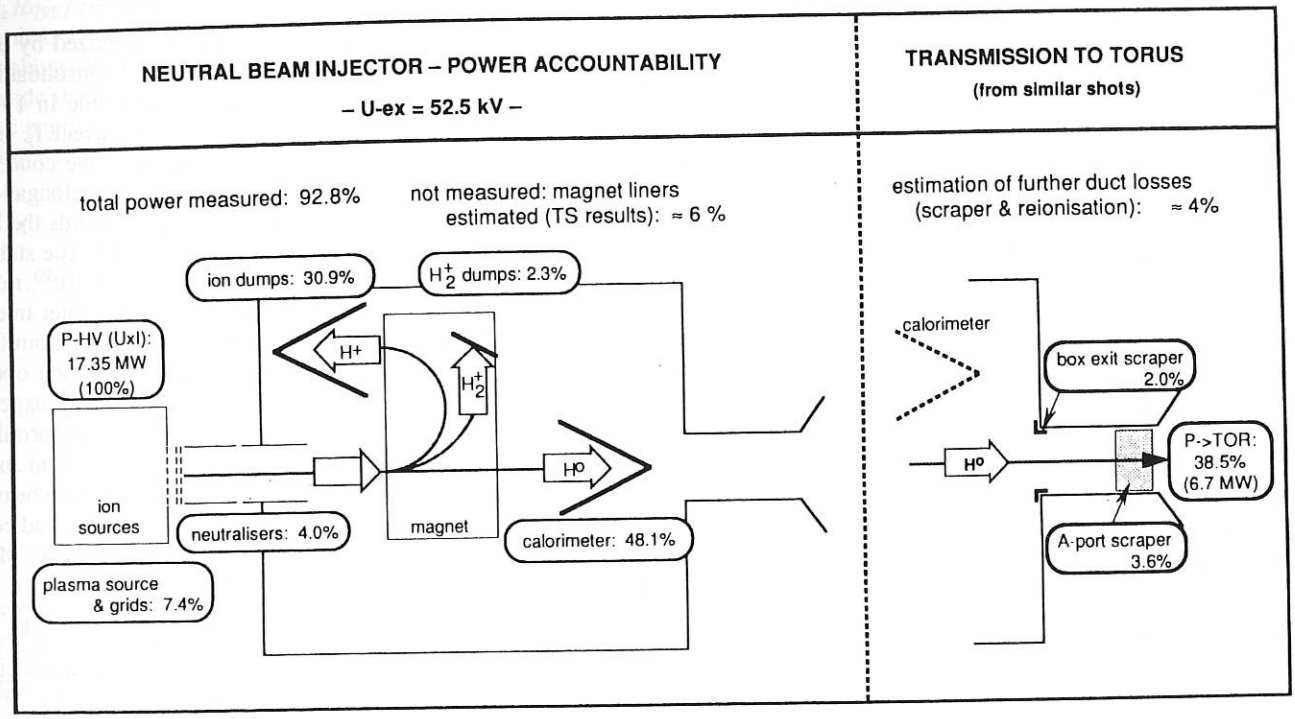

FIG. 2.2: Power accountability of the total beam inside the neutral injector and the neutral beam inside ASDEX Upgrade.

2.4 Ion Cyclotron Resonance Heating (ICRH)

The ICRH system and its first operational results with a heating power of up to 2.2 MW were already described in the Annual Report 1992. Increasing the power in the first half of 1993 was hindered by problems with the generator stability, with damage to the antennas and with the flexibility of the matching system. So, the second half of 1993 was mainly devoted to improving the operational properties of the system.

Generator stability: Self–oscillation and its reasons are investigated by studying the interaction of the resonant circuits of the generator, matching device and antennas (see Technology Division). It can be triggered by load transients in case of too high a reflected power, if unfavourable values of the complex load impedance are transformed to the generator. Stability can be achieved by varying the impedance transformation, e.g. shifting the electric length of the feeding lines. These results shall be applied to improve the reliability of the ICRH operation.

Antennas: In 3 of the 4 antennas arcing occurred at alumina–coated elements used to close the antennas at their lower side against RF leakage and gas influx. The breakdown was obviously initiated at "hot spots" with too high tanδ. Dark spots at other positions of the coating were interpreted as an early stage of a defect. The coating, which should insulate these parts against the adjacent Faraday screen, was replaced by insulating gaps. Similar, but much smaller elements at the upper antenna side, showing no defect, were not changed.

Matching: To achieve satisfactory matching within few shots, an improved method was developed using the complex load impedance measured in the feeder line between tuners and generator. This method, successfully tested at W 7-AS, should bring some progress compared with the scalar measurement used so far. Fast on–line data processing should allow automatic setting of the tuners, but due to their speed only small variations will be possible during a shot.

In cooperation with the electronics group of ZTE, circuitry has been developed to match antenna coupling variations during a shot by controlling the generator frequency according to the reflected power. Limited by the bandwidth of the generator, only small changes of the reactive part of the antenna impedance can be compensated. For the envisaged feedback control of the antenna coupling via the plasma position a hardware device

was prepared, delivering a voltage proportional to the antenna coupling resistance.

Diagnostics in or in front of the antenna, mentioned in the Annual Report (1992), were installed for operation in 1994 (vacuum measurements, gas inlet, plasma surface probes, optical monitoring, reflectometry).

2.5 Electron Cycl. Res. Heating (ECRH)

The parameters of the ECRH system under construction are: frequency = 140 GHz, launched power of 4 gyrotrons = 2 MW, pulse length ≈2 s. The envisaged physics programme has been discussed in a EURATOM ad hoc group, and preferential support phase 1 and phase 2 have been granted.

As a first step we will install in 1994 one gyrotron with 0.5 sec pulse length. Since calculations showed that operation of gyrotrons in the stray magnetic field of a tokamak may be problematic, the gyrotrons will now be placed on the ground floor of the gyrotron hall, where the stray field has mainly a vertical component, while the high–voltage installation (crowbar and modulator) was shifted to the upper floor. The new site for the gyrotrons, however, also required screening against magnetic fields originating from high–current leads installed in the basement. At present the cooling system is under construction. One crowbar and high–voltage modulator unit is installed and being tested. They will finally feed two gyrotrons. The modulator will allow frequencies up to 10 kHz. Construction of the programmable control system is in progress.

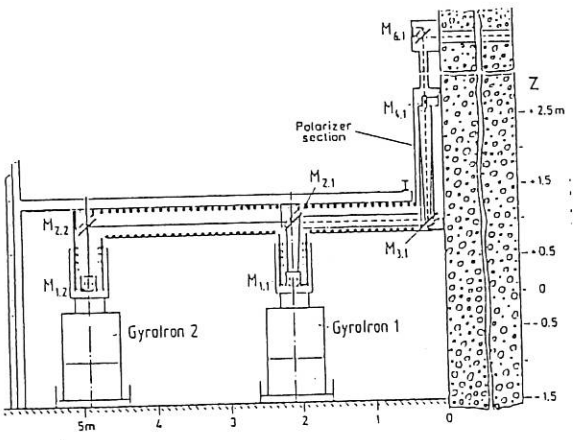

FIG. 2.3: Quasioptical part of the ECRH transmission lines for ASDEX Upgrade

The RF power will be transfered to the torus via four combined quasioptical and corrugated waveguide transmission lines. The quasioptical section in the gyrotron hall for the first two gyrotrons is shown in Fig. 2.3. A pair of grooved mirrors in each line will allow the necessary polarization to be adjusted for oblique launching. In the immediate vicinity of the torus we changed to an HE11 transmission line. The power will be monitored by two directional couplers, one incorporated in a mirror at the gyroton output, the other in a mitre bend at the torus input. Beyond the vacuum window at the torus port transmission is again quasioptical. Moveable mirrors allow the four beams to be directed in different poloidal and toroidal directions.

3. OPERATIONAL REGIMES AND BULK PLASMA PHYSICS

3.1 Expansion of Operational Regime

Since machine development in 1992 was characterized by enlargement of the vessel force load capability and consolidation of plasma position control procedures, we were able in 1993 to improve the density operating space, plasma current I_p and auxiliary heating power level P_{aux} considerably. We concentrated on the lower single-null plasma configuration (elongation b/a $\sim$ 1.6) with standard ion∇ B drift direction towards the X-point, which led to a low H-mode power threshold. The stable density operation space was extended to $\bar{n}_e \approx 1.4 \cdot 10^{20}$ m^{-3} during ELM'y H-Mode as well as with repetitive pellet injection. In parallel, the plasma current I_p was increased from 0.8 MA to 1.2 MA. The hydrogen pellet centrifuge started operation in February and allowed deep particle refuelling experiments demonstrating strongly peaked electron density profiles and correlated improved energy confinement times. From June the first neutral beam heating system injected 4 hydrogen beams of up to 6 MW into the torus. Poloidal β values up to 1 and corresponding normalized β values $\beta_N = \beta_t/(I_p/aB_T)$[%, MA, m, T] $\leq$ 2.1 were achieved.

Relatively high breakdown loop voltages of up to $U^{bd} \approx$ 20 V have been applied in the past since the plasma–facing components were not fully conditioned (see Ann. Rep. 1992, e.g. Sec. 3.4). This induced voltage consists mainly of three contributions : the change of the OH transformer current I_{OH} by the available generator voltage ($\Delta U^{bd}_{gen} \approx$ 4 V) and by an additional resistor R_{aux} connected only shortly into the OH circuit ($\Delta U^{bd}_{aux} \approx$14 V) and the voltage induced by the initial current ramp of the internal control coils ($\Delta U^{bd}_{CoI} \approx$ 2 V).

Accumulative boronizations and advanced conditioning during operation in 1993 allowed the breakdown voltage to be significantly decreased to about 12 V by reducing R_{aux}. This voltage was routinely used to ensure reliable current ramp-up. In conjunction with a slightly modified I_p start-up scenario a further reduction of U^{bd}, which is an important issue for ITER, to about 9 V was possible, corresponding to an electric field of <1 V/m.

During a short period in May a temporary failure of the inner coils allowed only operation with limiter plasmas of circular cross-section. It was demonstrated that a successfull I_p start-up scenario is possible with the available poloidal field coil power supplies (V1 coils disconnected) without the support of the fast inner control coil (see Annual Report 1992). First comparisons of the disruption phase of circular and non-circular plasmas (see Sec. 3.6) have started.

3.2 Density Operating Space

Considering that high–density operation is one of the main goals of AUG, the increase of the density limit is an important aim. In 1992, the boundary predicted by the Greenwald scaling $\bar{n}_e = k \cdot \langle j \rangle$, which is experimentally confirmed in many machines, could not be reached (k is the plasma elongation and $\langle j \rangle$ the area averaged plasma current density). But improved wall conditions in 1993 (see Sec. 3.1) led to stable operation with line-averaged densities approaching the Greenwald limit (see Fig. 3.1). The corresponding experimental Hugill limit is $\bar{n}_e R q_{95} / B_T = 2.8 \cdot 10^{20}$ m^{-2} T^{-1}. With pellet injection the limit is significantly exceeded. This reflects the considerable peaking of the electron density profile which also develops inside the ablation zone of the pellet particles. Concomitantly, the energy confinement time is nearly doubled from 75 ms to 145 ms.

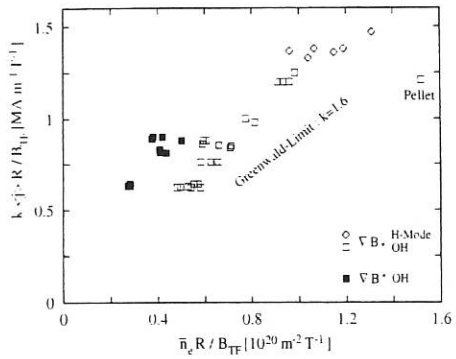

FIG. 3.1: AUG density operating space for OH– and H-mode discharges. The OH data correspond to disrupting density limit discharges. The H-mode discharges do not disrupt at the high $\bar{n}_e$ shown.

Figure 3.1 shows purely ohmically and NBI heated H-mode discharges for both ion ∇B drift directions. The OH data result from discharges which disrupt after reaching the density limit, whereas the H-mode discharges survive the high–density phase, implying that higher densities may be attainable. The highest density achieved up to now is $\bar{n}_e = 1.4 \cdot 10^{20}$ m^{-3}. Reversal of the ion ∇B drift direction clearly has a detrimental effect on the density limit, as demonstrated by the full squares. Modified impurity behaviour seems to be responsible for this degradation.

Investigation of the H-mode density operation space is a favoured topic of the ongoing experiments.

3.3 H-Mode Regime

The improved confinement regime of the H-mode is reached when the heating power exceeds a threshold power, P_{thres}, which depends on the plasma parameters and the device. It is therefore important to determine the operational window of this regime. The H-mode takes different forms (dithering, ELMing with type-III or I ELMs (Edge Localized Mode), ELM-free), depending on the heating power, as described below and in Sec. 4. The dithering H-mode is an oscillatory behaviour between L- and H-mode and ELM is the acronym for Edge Localized Modes. In ASDEX Upgrade, the H-mode has been achieved with hydrogen minority ICRF heating in helium and deuterium, with pure Ohmic and NBI heating. The NBI, put into operation this year, greatly extended the experimental studies of the H-mode. In this section, the operational window of the H-mode in ASDEX Upgrade is presented and the different forms of the H-mode are described and discussed.

3.3.1 H-mode power threshold and operational window

Figure 3.2 shows the H-mode operational window in a heating power ($P_{tot} = P_{OH} + P_{heat}$) versus $\bar{n}_e B_T$ diagram for the three heating methods used in ASDEX Upgrade so far. P_{OH} is the residual Ohmic power, P_{heat} the absorbed heating power, $\bar{n}_e$ the line-averaged density, B_T the toroidal magnetic field. For ICRF 80% RF absorption is assumed, based on experimental analyses. For NBI, the absorption (0.75 – 0.85) is calculated with the FREYA code. The experimental conditions were favourable for easy transition into the H-mode: boronized vessel, deuterium plasma, single-null elongated ($\kappa \approx 1.6$) configuration with ion gradB drift towards the X-point and separatrix distance to protection limiter of the ICRH antennas larger than 3 cm. For the Ohmic studies the plasma current I_p was varied between 0.6 MA and 1.2 MA, B_T from 1 T to 2.4 T and $\bar{n}_e$ between 0.15 and $0.5 \cdot 10^{20}$ m^{-3}. For the NBI cases, B_T was varied from 1.35 T to 2 T at a constant target density of $0.5 \cdot 10^{20}$ m^{-3}. For ICRH experiments B_T was fixed at 2 T for on-axis heating and in this case the range along the X-axis is only due to density variations. The ICRF power was increased with a slow linear ramp with time (2 MW/s) in each discharge such that P_{thres} could be exactly determined.

In most tokamaks, P_{thres} depends linearly on the product $\bar{n}_e B_T$. The results of ASDEX Upgrade are in agreement with these within the experimental uncertainties, at least for $\bar{n}_e B_T > 0.25 \cdot 10^{20}$ m^{-3} T, independently of the heating method (Fig. 3.2). Subtracting radiation losses inside the separatrix, P_{rad} (core), from P_{tot} does not qualitatively change these results, because the fractional radiation power P_{rad}(core)/P_{tot} is almost constant, below 30%, at this stage of the discharges.

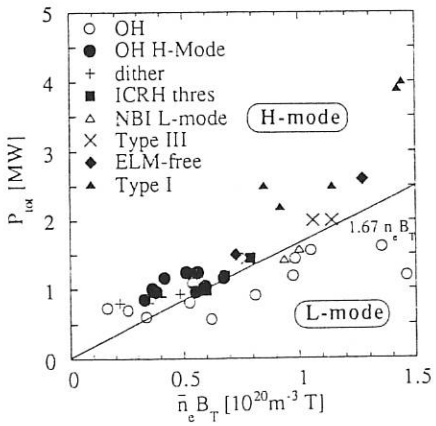

FIG. 3.2: H-mode threshold and operational window: heating power versus $\bar{n}_e B_T$.

For $\bar{n}_e B_T < 0.25 \cdot 10^{20}$ m^{-3} T, obtained at 1.1 T or 1.35 T with Ohmic heating and by reducing the density, the threshold clearly deviates from the linear dependence (Fig.3.2). This feature is not peculiar to the Ohmic H-mode in ASDEX Upgrade, as already observed in ASDEX with NBI. One might speculate that this is due to the decoupling of the electron and ion channels at low density or to confinement degradation at low $\bar{n}_e$.

In comparison with other tokamaks, we normalize the power to the plasma surface area, S, as in the ITER H-mode threshold database work. This gives for ASDEX Upgrade $P_{thres}/S = (0.038 \pm 0.002) \cdot \bar{n}_e B_T$ [MW, m^{-2}, 10^{20} m^{-3}, T], valid at least for $0.25 \cdot 10^{20} \leq \bar{n}_e B_T \leq 1.2 \cdot 10^{20}$ m^{-3} T. This is in agreement with new results from other tokamaks, but is by a factor of 2 lower than the thresholds reported till 1992.

Figure 3.2 further shows that, at a constant value of $\bar{n}_e B_T$, the following H-mode regimes are obtained by increasing the heating power above the threshold power: dithering just above the threshold, ELMing with type–III ELMs up to $\approx 1.2 P_{thres}$ and with type–I ELMs above $\approx 1.7 P_{thres}$, ELM-free in between. We adopt here the DIII-D ELM notation determined by the behaviour with heating power: the frequency of type–I ELMs increases with heating power, whereas the frequency of type–III ELMs decreases with heating power. The physics features of the dithering and ELMs are described in Sec. 4.

3.3.2 *Ohmic H-mode*

The Ohmic H-mode in ASDEX Upgrade was found with $I_p = 800$ kA, $1.0 < B_T < 1.35$, corresponding to $q_{95} < 3$, under easy transition conditions (see Annual Report 1992). ELM-free phases of ≈ 80 ms duration and long (>2 s) stationary dithering or ELMing phases were achieved. The ELM-free phases were obtained for $B_T \leq 1.1$ T. Low q_{95} values are favourable for the ELM-free Ohmic H-mode because P_{OH} increases with decreasing q_{95} due to less peaked temperature profile and because P_{thres} decreases with decreasing B_T.

All Ohmic H-modes exhibit the well-known features of the H-mode: increase of confinement time, density and radiation, and decrease of the D_α light in the divertor and of the loop voltage after the transition. These changes are strong during ELM-free phases and moderate for the dithering and ELMing discharges, for which the plasma features stay, on the average, stationary after the initial evolution following the transition, modulated by the ELMs. Both the electron density and temperature profiles become broader. The evolution of the density profile is in agreement with the assumption of a transport barrier developing at the plasma edge just inside the separatrix during the H-mode and with an increase of the inward drift, at least for dithering or ELMing discharges. During the ELM-free phase, the fall-off lengths in the scrape-off layer (SOL) decreased as measured by IR thermography of the power deposition onto the divertor target plates (Sec. 4). The width of the energy deposition onto the plates decreased by a factor 4 – 5 with respect to the preceding ELMy phase to about 5 mm, whereas the averaged width during ELMy phases is 1.5 times thinner than during Ohmic L-mode phases.

The global confinement time of the H-mode discharges, calculated with the energy from the MHD equilibrium, is shown in Fig. 3.3 versus $\bar{n}_e$ and compared with non H-mode Ohmic points. The confinement improvement is about 1.5 and 2 for the ELMing and ELM-free phases, respectively. The decrease of the confinement time for $\bar{n}_e > 4.2 \cdot 10^{19}$ m^{-3} is probably linked to $P_{OH} - P_{thres}$ approaching zero, where ELMs become more frequent or even dithering occurs.

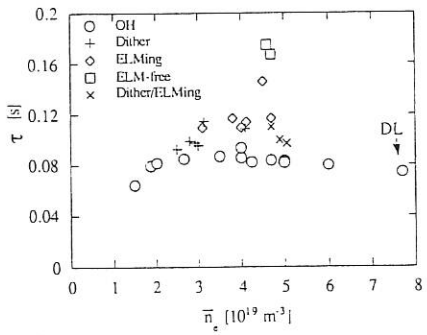

FIG. 3.3: Energy confinement time versus $\bar{n}_e$ for ohmically heated plasmas with I_p = 800 kA, 1.05 T $\leq B_T \leq$ 1.35 T. (DL = density limit).

3.3.3 *Auxiliary-heated H-mode*

The tuneable ICRH power allowed studies of the L-H transition dynamics (see Sec. 4) and clearly showed how type–III ELMs increase in period and amplitude with heating power. Quasi-stationary ICRH-heated discharges with such ELMs could be performed. ELM-free and ELMing type–I discharges have routinely been achieved with NBI, an essential extension of the H-mode operational window this year.

Repetitive ELM-free phases are created in single discharges showing up to 4 ELM-free phases each separated by a short (3 ms) L-mode phase and a 100 ms long dithering phase. During the transient L-phases, the radiation rapidly decreases because it is essentially located at the plasma edge. This increases the power flux at the plasma edge, $P_{tot} - P_{rad}$(core) and allows the plasma to transit again into the H-mode through the dithering phase. No disruptions occur at the end of ELM-free phases, which is attributed to the low impurity concentration in the plasma centre, even at the end of ELM-free phases.

In contrast to type-III ELMs, the frequency of type–I ELMs increases with increasing power, and steady–state discharges are achieved independently of the heating power, as in Fig.3.4. Steady state is reached after 3–4 confinement times (t $\approx$ 2.3 s) and lasts 4–5 confinement times, this being limited only by the NBI pulse duration. Remarkable are the regularity of the ELMs and the low fractional power losses during this phase. As for the Ohmic cases, here also the energy deposition profiles on the divertor target plates become thinner during H-phase (see Sec. 4).

Spectroscopy studies (Sec. 3.4) show that impurity accumulation does not occur during these discharges and Z_{eff} stays low, around 1.5. The oxygen contribution to Z_{eff} obtained

from charge exchange resonance (CXR) spectroscopy exhibits a hollow profile shape (Fig. 3.5), a behaviour which is usually also seen for other light impurity species (B, C). For these experimental conditions with an aged boronization, the C and O Z_{eff} contributions are comparable and about a factor of 2 higher than the contribution of boron.

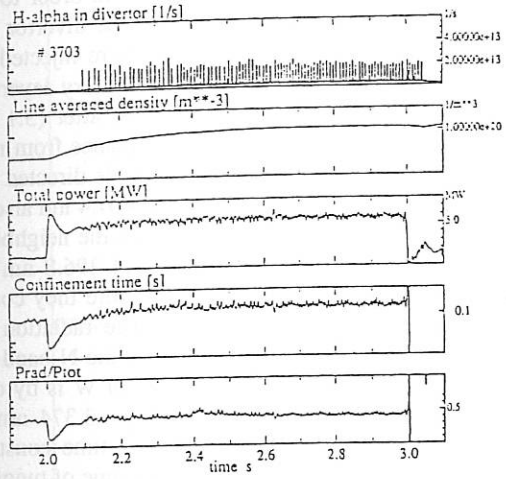

FIG. 3.4: Stationary discharge with type–I ELMs; 1.2 MA, 2 T

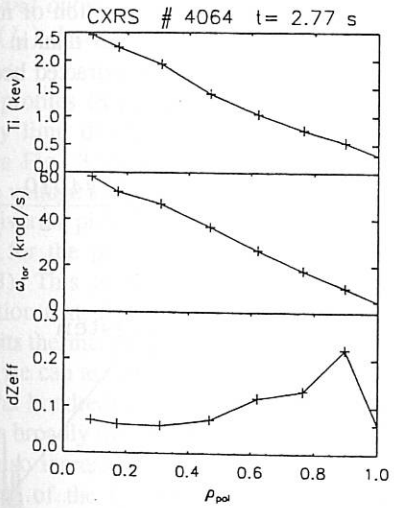

FIG. 3.5: Results from CXR spectroscopy on fully stripped oxygen during a NBI heated H-mode discharge. The crosses mark the flux surface labels of the locations of measurement. dZ_{eff} denotes the contribution of oxygen to Z_{eff} (B_t = 2 T, I_p = 0.8 MA, P_{NI} = 4 MW, $\bar{n}_e = 6 \cdot 10^{19}\ m^{-3}$).

The global confinement time results with additional heating of Fig. 3.6, represented by τ_E/I_p versus power, show a power dependence close to $P^{-0.5}$. Due to the low H-mode threshold, the L-mode power range is limited. The type–I ELMs discharges are comparable to the ELM-free ones within the error bars. This observation, at first glance surprising, is not yet explained. Radiation losses are higher only at the end of the ELM-free phases and therefore do not reduce the confinement time in the early ELM-free phase. The confinement time values are in close agreement with usual H-mode scaling expressions, e.g. the DIII-D/JET scaling.

The radial profiles of the ion temperatures and toroidal rotation measured by CXR spectroscopy show a similar shape (Fig. 3.5). The central ion temperatures agree within 10% with the results from passive CX neutral particle diagnostics. Global momentum confinement times calculated from the velocity profiles are typically a factor of 2 lower than the energy confinement time.

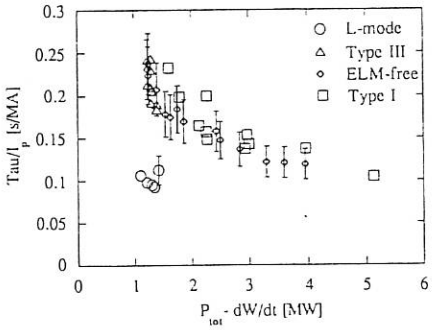

FIG. 3.6: Confinement quality factor versus power for the H-mode with auxiliary heating.

Some discharges clearly show that the power reaching the plasma edge, $P_{tot} - P_{rad}$(core), influences the type–I ELM frequency. The increasing radiation losses due to an external carbon influx event create an ELM-free phase terminated by type–III ELMs. Then the radiation losses decrease again and when they are low enough, type-I ELMs reappear. The discharge recovers because no disruption occurs during the ELM-free phases. This coupling between the ELM activity and $P_{tot} - P_{rad}$(core), which eventually leads to a destroyment of the steady state H-mode, shows the importance of developing active ELM control systems.

3.4 Impurity Accumulation Studies

Since high-Z materials are acquiring increased interest as target plate material for a future reactor, and the injection of medium-Z impurities is planned to obtain radiative cooling, more attention has to be directed to the problem of impurity accumulation. For typical H-mode conditions with flat density profiles and only low-Z impurities present, usually no accumulation of impurities in the plasma centre is observed in ASDEX Upgrade. However, the tendency to accumulation is expected to increase with increasing Z of the impurities involved: the neoclassical forces which try to adapt the peaked profiles increase with the ion charge and may exceed the anomalous transport and sawtooth activities, which tend to flatten the impurity density profiles. Peaking of the electron density profile (or the reduction of the edge density as a result of radiative cooling) will

also increase the neoclassical inward drift.

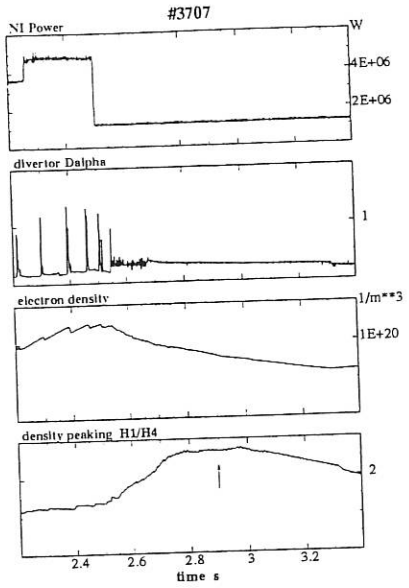

FIG. 3.7: NI power, divertor D_α emission, line-averaged electron density and electron density profile peaking for a discharge exhibiting transient impurity accumulation around t = 2.9 s. (B_t = 2 T,I_p = 1.2 MA).

3.4.1 Argon puffing in NI-heated plasmas

Impurity accumulation phenomena can be studied on ASDEX Upgrade using specifically prepared discharges. Fig. 3.7 shows various traces of a discharge where transient impurity accumulation was observed. Argon was puffed into the plasma before the NI was turned on, to increase the radiative losses. After reducing the NI power from 4.8 to 1.2 MW at t = 2.5 s, the discharge falls back into the L-mode. The loss of part of the edge plasma leads to peaking of the density profile. Radial profiles of the O^{8+} density obtained with CXRS, shown in Fig. 3.8, reveal transient accumulation in the plasma centre. In the following, the accumulation diminishes, probably owing to the continuous reduction of the argon content. First attempts to simulate the observed behaviour with impurity transport calculations using anomalous diffusion superimposed on the neoclassical transport coefficients seem to confirm the importance of the last ones.

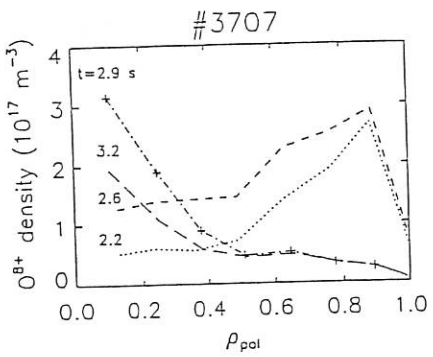

FIG. 3.8: Fully stripped oxygen profiles for the discharge shown in Fig. 3.7. The hollow profiles obtained during the H-mode change to a strongly peaked shape.

3.4.2 Laser blow off of metallic impurities in OH discharges

The intention of the Laser Blow Off experiments (LBO) is to elucidate transport processes, supply spectroscopic information or simply facilitate the identification of spectral lines.

In the last period of the year under review, first LBO experiments were performed at ASDEX Upgrade. In order to assist the spectroscopic investigations of the high-Z divertor plates (see Sec. 4...), molybdenum and tungsten were injected. Figure 3.9 shows spectra measured by the boundary layer spectrometer before (3.0 s, shaded area) and just after (3.1 s) the injection of W. The line near 400.8 nm originates from neutral W (WI) and is also seen if the spectrometer is directed to the W-sector on the divertor plates. The line at 407.4 nm also originates from WI, but is normally blended with the neighbouring oxygen lines. The strong ones at 393.4 and 396.8 nm could not be detected without injection, and therefore they could be attributed to ionized states of tungsten. The radiation of W was also detected by the C-monitor because the N-band X-ray quasicontinuum of several ionization states of W is by chance also at the wavelength of the CVI line (λ = 3.374 nm) normally measured. The signal decays with a time constant of $\tau \approx 100$ ms, which reflects the confinement time of tungsten in the core plasma. This is supported by the bolometer measurements, which show a similar decrease after a strong transient rise of the radiation in the central region.

Spectral lines from different highly ionized states could be identified by the SPRED spectrometer after injection of molybdenum. The line intensities of Mo decay faster than in the case of W, whereas no time constant could be extracted because of the poor time resolution of the spectrometer.

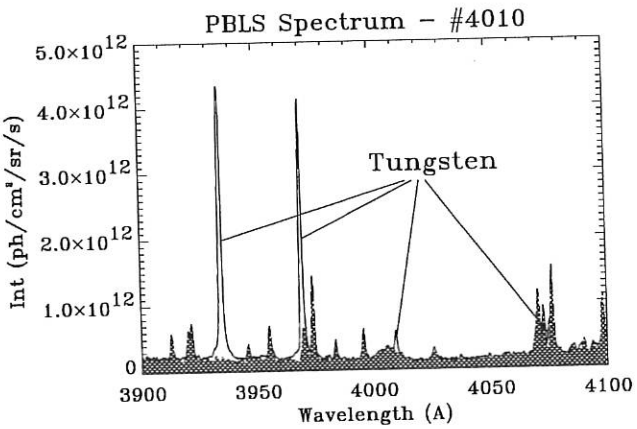

FIG. 3.9: Spectra measured by the boundary layer spectrometer before (3.0 s, shaded area) and after (3.1 s, solid line) injection of tungsten. The four lines indicated originate from tungsten.

3.5 Energy Deposition During Disruptions

The spatial and temporal characterization of energy dissipation and power deposition during disruptions is object of investigation in AUG. The diagnostic apparatus allows reconstruction of the plasma configuration, measurement of the toroidal and poloidal currents in structure and of the radiated energy, and

monitoring of the heat load onto the divertor target plates by means of the high-time-resolution thermography system (see Annual Report 1992).

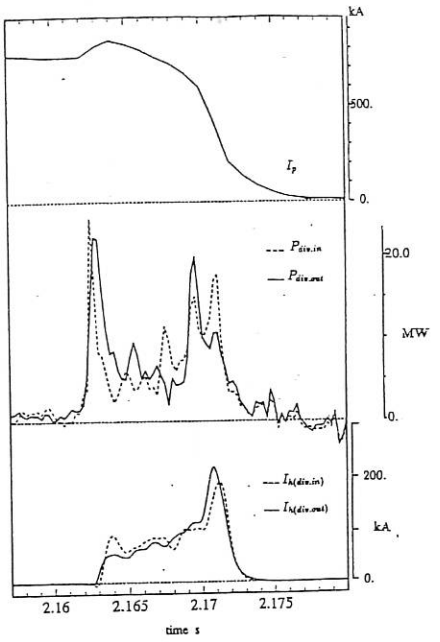

FIG. 3.10: Power flow (P_{div}) and halo currents (I_h) onto inner (div.in) and outer (div.out) divertor plates during the plasma current (I_p) decay phase.

Typical profiles of power onto the target plates (P_{div}) during a density limit disruption followed by vertical instability are shown in Fig. 3.10. The first major peak coincides with the negative voltage spike and the I_p current rise. The power losses to the divertor plates integrated during the first peak duration account for the pre-disruption thermal energy of the plasma (~45 kJ). This is in agreement with the widely confirmed observation that, during the thermal quench, the plasma loses most of its thermal energy. In addition, with a time resolution of 260 μs, we can assess that this process happens on a time scale of several hundreds of μs. The poloidal profile shows that the power is broadly distributed on the plate surfaces. The radiated power also increases during this phase. With the present time resolution of the bolometer (10 ms), we cannot resolve the radiated energy during thermal quench.

The series of peaks which follows the thermal quench coincides with the current decay and halo current (I_h) phase (see Annual Report 1992). In the halo phase a part of the toroidal plasma current flows along open field lines which intersect the vessel structure. The energy deposited onto the divertor during these 10 ms is higher than during the thermal quench and amounts to 30% of the pre-disruption plasma magnetic energy($W_{mag} = LI_p^2/2 \sim 850$ kJ). This indicates that a significant fraction of the magnetic energy is ohmically dissipated during the halo phase and is conducted and convected along field lines to the plates.

Poloidal currents flowing in the SOL and between the plasma and divertor plates are also measured during the ELMy phase of a discharge. Between ELMs, the current (I_θ) is of thermoelectric origin, since the temperature of the outer divertor plate is larger than that of the inner plate. Typically, with 5 MW of auxiliary power, $I_\theta \sim 1.5$ kA. Following the occurrence of an ELM and the rapid inward and downward plasma movement, this poloidal current increases by a factor of two and acts to stabilize the plasma motion. Correlated with these halo currents is the power deposition on the target plates during ELMs (see Sec. 4)

3.6 Results of Ion Cyclotron Resonance Frequency Heating

The combination of ion fundamental and second harmonic ICRH is not a common scenario: few ICRH systems have the necessary wide frequency range to investigate it and at first sight the optimal conditions for the two heating methods do not seem to overlap. Indeed, heating at the fundamental frequency needs a small concentration of the resonant species to optimize the absorption, while heating using the second harmonic is usually performed at high concentration, since its absorption is proportional to the $\beta(\propto nT)$ of the resonant particles, thus favouring a high density of those particles.

But the absorption at the second harmonic is a finite Larmor radius effect, such that good absorption, even at low concentration, can be obtained at sufficiently high temperature for particles with large perpendicular energy. Heating of small concentrations of particles resonant at the second harmonic is thus in principle possible if a tail can be produced (by the second harmonic heating itself or by other means) and has been reported for JT-60 in ohmic plasmas and in plasmas additionally heated by NI for H concentrations in the 10% range. Heating at the fundamental frequency can, in the low minority concentration regime, efficiently initiate or support the production of fast particles, thus providing optimal conditions for the second harmonic heating. On ASDEX Upgrade, second harmonic has been combined with fundamental heating and works successfully at concentrations as low as 3%. The addition of fundamental minority heating improves the conditions for second

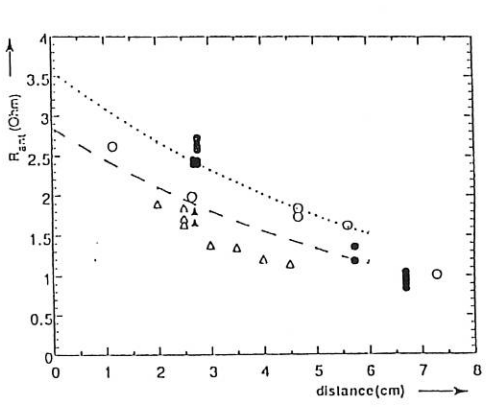

FIG. 3.11: Values of the antenna resistance as a function of the distance antenna limiter to plasma separatrix for L(o,●), and H-mode discharges (Δ▲). Theoretical calculations with the FELICE code used an average central conductor to return conductor distance of 15 cm (...) and 10 cm (– – –), respectively.

harmonic heating at those low concentrations, making it as efficient as monitory heating. Charge exchange measurements confirm that the improvement is due to the doupling at the second harmonic to the tail produced by the minority heating.

To obtain guidance on the plasma surface – antenna distance necessary for sufficient coupling, the antenna resistance in L– and H– mode as a function of the plasma distance was determined and compared with theoretical estimates. The result is shown in Fig. 3.11.

4. EDGE AND DIVERTOR PHYSICS

4.1 Divertor Plasma Profiles and Recycling

4.1.1 In-Vessel Langmuir probe Systems

ASDEX Upgrade is now equipped with two In-Vessel Probe (IVP) systems, which were developed by the Canadian Fusion Fuels Technology Project, Toronto, Canada. The probes scan above the lower divertor plates, providing radial profiles of plasma density and temperature in a period of $\sim$ 100 ms.

Figure 4.1 shows for Ohmic heating the plasma density and temperature radial profiles obtained with IVP1 for a low density discharge (2.3 $\cdot 10^{19}$ m^{-3}) and a high density discharge (6.0 $\cdot 10^{19}$ m^{-3}) with a plasma current of 800 kA and a toroidal field of –2 T. The density in the divertor shows a dependence on central density which is stronger than linear, rising roughly as $\bar{n}_e^{1.5}$. The divertor electron temperature, on the other hand,

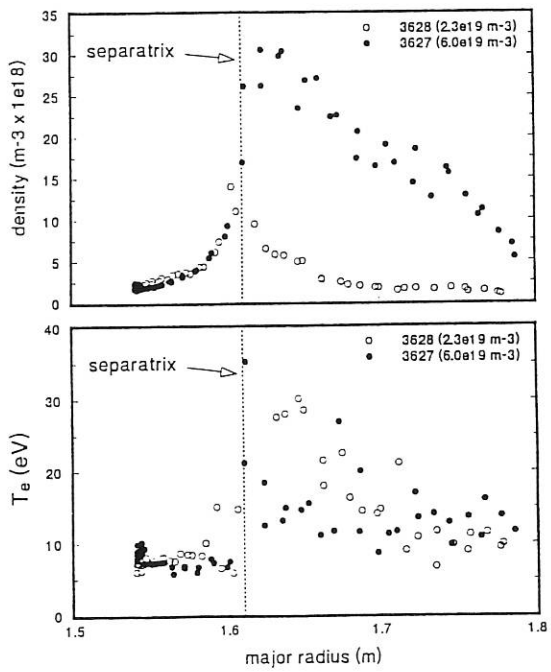

FIG. 4.1: Divertor plasma profiles for two different densities.

is less sensitive to the central discharge density. The radial profiles, for both the density and the temperature, while being quite narrow at low density, become very broad at high density. Such broadening is an encouraging feature of high density operation since it will tend to spread exhausted plasma power over a large area of the divertor structure.

4.1.2 Langmuir Probes in Target Plates

The Langmuir probe system in the divertor plates was expanded to enable routine measurements at up to 20 locations in single, triple, and passive-current modes. The electron temperature and density and the ion flux observed with these probes have been essential diagnostics for the study of ELM's and marfes and the interpretation of spectroscopic data. The evaluation of single and triple probe data is complicated by the fact that the measured electron saturation current is much smaller than that predicted by the standard theory. This suppression is caused by the way current flows across the magnetic field. In conjunction with ongoing theoretical studies, a technique was developed to investigate this current flow, whereby a strong alternating voltage was applied to one electrode, and the return currents on toroidally and poloidally neighbouring electrodes, as well as those at the opposite end of the flux bundle, were measured. Such measurements can also be used to study the magnetic geometry in the scrape-off layer.

4.1.3 Recycling and Pumping

Recycling of the gas-puff–fuelled discharges in ASDEX Upgrade was investigated by means of different diagnostics.

In the divertor the relative poloidal and radial distributions of the D_α radiation were measured with CCD cameras, and absolute intensities were obtained with photodiodes and spectrometers viewing the deuterium radiation along different lines of sight. The recycling at the chamber walls was measured with photodiodes and with the charge exchange spectrometer. In addition, the neutral gas pressure was measured at various positions in the divertor and main chamber. From these results, the particle balance including the wall inventory was qualitatively derived. A more quantitative analysis requires numerical modelling as described in Sec. 4.5.

The effect of external pumps connected to the high neutral pressure divertor region (turbomolecular pumps; 20 m^3/s for hydrogen) was investigated in a series of discharges with and without pumping. The external pump rate turns out to be comparable to the wall pumping and can become dominant when the divertor walls saturate. The absolute exhaust flux is comparable to the particle influx from neutral injection.

4.2 Power Deposition in the Divertor

4.2.1 Power Deposition onto the Divertor Plates

The power deposition is routinely measured with the cooling water calorimetry, wall thermometry and thermography system.

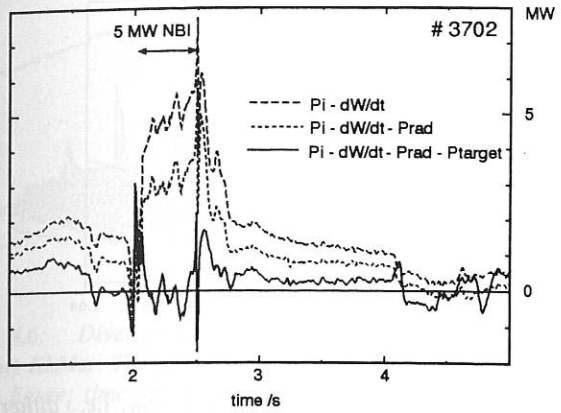

FIG. 4.2: Power balance of a NIB-heated discharge.

The main results of the time-integrated calorimetry measurements are as follows: There are no toroidal asymmetries in the shot-integrated energy deposition on the target plates at ohmic and ICRH discharges in helium or deuterium for a safety factor q_a of about 5 and a toroidal magnetic field directed opposite to the plasma current ($B_t < 0$, ion grad-B drift away from the X-point). The measurements give first hints of toroidal asymmetries in deuterium discharges with ICRH, $q_a \approx 5$ and a toroidal magnetic field in the same direction as the plasma current ($B_t > 0$, ion grad-B drift towards the X-point). There are also significant asymmetries in the toroidal energy deposition profile of the first discharges with Neutral Beam Injection.

There is also an asymmetry in the energy deposition on the outer and inner divertor target plates. The factor for the energy load on the outer target plate compared with the inner targets for discharges with $B_t = -2$ T ranges between 2.2 and 3.5 and, for discharges with $B_t = +2$ T, between 1.2 and 1.7. Thermografically measured power deposition shows the same behaviour of outboard to inboard energy load.

All energy measurements with the cooling water calorimetry diagnostic till now have been consistent with the measurements of the wall thermometry diagnostic within the accuracy of these experimental systems.

A high-time-resolution infrared camera system was put into operation on ASDEX Upgrade to measure the surface temperature of the lower divertor plates. The detector line is oriented along the major radius, viewing both the inner and outer lower target plates. From the time-dependent surface temperature profile the corresponding distribution of power deposited on the divertor plates is routinely calculated by numerically solving the 2D nonlinear heat conduction equation. The total time-dependent power load of the inner and outer divertor plates and the corresponding energies accumulated are also obtained by a routine procedure.

Radial power decay lengths along the target plates of ASDEX Upgrade for different confinement regimes are taken from thermographic measurements. These are less than 1 cm in the ELM-free H-mode and a few 10 cm in the L–mode. Note that in mapping the profiles along the field lines to the torus midplane all decay lengths are reduced by a factor of 10.

The power losses due to radiation from the bulk plasma, measured with the bolometric diagnostics, and deposition on the target plates account well for the difference in power input and the temporal change of the plasma energy (dW/dt) during phases with additional heating. Approximately 60% of the input power is deposited onto the target plates and 40% is radiated from the bulk plasma (Fig. 4.2). About 10% of the input power is not found in the ohmic phase of a discharge. The accumulated energies measured by thermography and calorimetry are in good agreement.

4.2.2 Hot Spots on Divertor Plates

In all phases of Single Null (SN) discharges (OH, L-mode, H-mode, NI, ICRH) hot spots are observed on the target plates in the region of the scrape–off layer (SOL) using a CCD camera with CI filter (Fig. 4.3). The number of visible spots depends on the plasma density and the energy flux into the divertor. With increasing density the incident energy flux will be reduced, the radiating spots getting weaker and their number decreasing. At a critical density characterized by the line–integrated density of the bulk plasma the spots completely disappear. This ciritical density depends on the plasma current and the power of the auxiliary heating system. In the ohmic case it is well below the density limit, and so an operational range with reduced local load of the tiles seems to be possible.

During high–power Neutral Injection (NI) at the edges of the tiles near the strike points the temperatures increase dramatically, following light emission for several hundred milliseconds after termination of NI.

During disruption an enormous number of hot spots are observed on the tiles of the target plates and on the diaphragm ring of the divertor and also a smaller number on the graphite tiles of the lower PSL (Passive Stabilizing Loop). It has not yet been determined whether the hot spots are created by strong local heating due to energy flux along the SOL or whether they are locally ignited arcs.

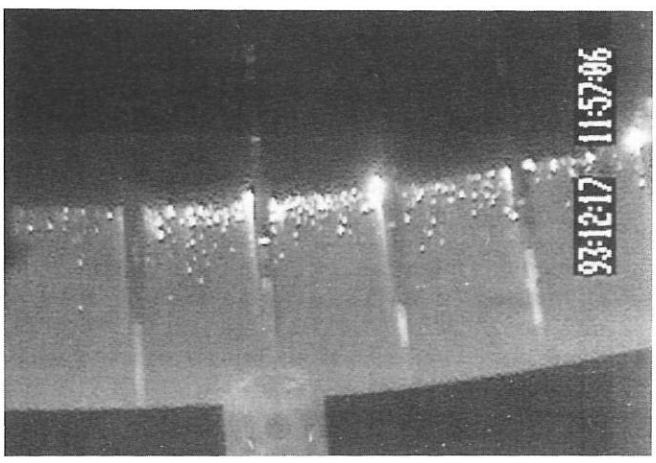

FIG. 4.3: Hot spots on tiles of the lower outer target plate during an 0.8 MA discharge (#4073, t = 3.23 s) with NI (3 MW) observed through a CI filter (945 mmm) with a CCD camera for an exposure time of 20 ms. The strong load at the edge of the tiles is evident.

4.3 H-Mode and Edge

4.3.1 L-H Transition Physics

The L-H transition is not always a single event but may exhibit a series of L-H-L transitions. This phenomenon has been dubbed 'dithering H-mode'. It was shown on ASDEX that in the dithering H-mode the fluctuation levels ($\dot{n}_e, \dot{B}$) switch between typical L- and H-mode values, but never reach the high level of an ELM. In particular, the high-frequency (>100 kHz) fluctuations typical for the ELM are not observed. We therefore distinguish the dithering cycle from an ELM by the fluctuation level, although the shape of the D_α signal may, in some cases, resemble that of an ELM. On ASDEX Upgrade, we find that the number of dithering cycles that appear at the L-H transition varies with the normalized rise of the heating power in excess of the threshold $\tau_{exc} = 1/P_{thr} d/dt(P - P_{thr})$. In the limit of $\tau_{exc} \to \infty$, which eventually occurs in ohmic H-mode discharges, dithering cycles of very regular frequency ($\approx 1 - 2$ kHz) appear for the whole dithering phase of 2–3 s (i.e. $\approx$ 6000 cycles!), limited only by the I_p ramp-down. In usual cases with additional heating, the number of dithering cycles is limited (Fig. 4.4).

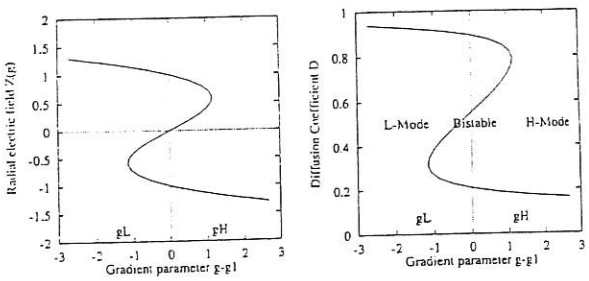

FIG. 4.4: Typical model curve Z(g) and resulting D(g).

The experiments show that there is an intrinsic timescale in the L-H transition. We model the dithering cycles by using an extension of Itoh's model for the L-H transition based on a multivalued curve of the radial electric field Z with respect to the gradient parameters g:

$$g = const. \frac{1}{\rho_{p,i} \nu_i^*} \left(\frac{n'}{n} + \gamma \frac{T'}{T} \right) = g_0 \frac{T}{n} \left(\frac{n'}{n} + \gamma \frac{T'}{T} \right)$$

Transport is assumed to have a high (L-mode) value for positive Z and a low (H-mode) value for negative Z. Fig. 4.4 shows an example of the diffusion coefficient $D(g)$.

We solve a coupled system of diffusion equations for n, T and Z on a spatial domain extending over $\approx$2-3 poloidal ion gyroradii. The boundary conditions are $\Gamma_{in} = const.$ and $q_{in} = const.$ at the left boundary (representing the fluxes from the plasma core into the domain) and $1/\lambda_n = n'/n = const.$ and $1/\lambda_T = T'/T = const.$ at the separatrix.

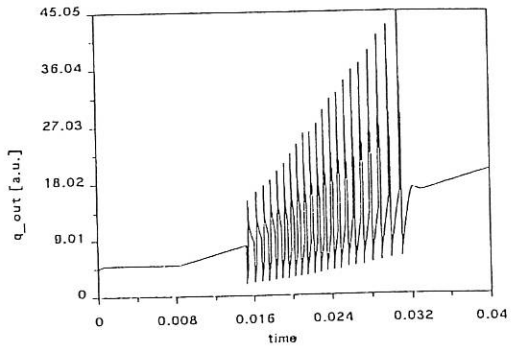

FIG. 4.5: Nonlinear response of q_{out} to q_{in}, i.e. dithering cycles.

As we neglect any energy and particle sources in the domain, we have $\Gamma_{in} = \Gamma_{out}$ and $q_{in} = q_{out}$ in steady state. Due to the nonlinear term, however, the system will respond to a linear rise in q_{in} (simulating a rise in heating power) with nonlinear behaviour of q_{out}. This is shown in Fig. 4.5, where dithers occur at a ramp rate of $\tau_{exc} \approx 20$ ms. This behaviour is known as limit cycle oscillation: In the L-mode, $g_1 > g$, so that $Z > 0$ and $D \approx D_{max}$ (i.e. L-mode conditions). If, as done in the experiment by heating, we increase q_{in}, the temperature gradient rises and for $g > g_H$ the system transits into H-mode ($Z < 0, D \approx D_{min}$). The reduction of transport coefficients leads to an increase in both density and temperature gradients. From eq. (1) it can be seen that the response of g to a change in n and T is different: With our boundary conditions, $n_{sep} = \lambda_n n'$ and $T_{sep} = \lambda_T T'$, so $g_{sep} \propto T/n$ holds. A rise in T drives the system further into the H-mode, whereas the rise in n drives it back towards the L-mode. Therefore, the important ingredient in our model is the T/n dependence of the bifurcation parameter.

A variation of the rise rate of q_{in} reproduces the experimental dependence of the number of cycles on τ_{exc}. Also, in our model, the timescale of the dithering cycle is given by diffusion across the transport barrier, i.e. $\approx$ 2 cm (experimental value) and $D \approx 1$ m^2/s leading to 2.5 kHz in good agreement with the experimentally observed 2 kHz. We conclude that this simple model describes the basic experimental facts of the dynamics of the L-H transition.

4.3.2 Effect of ELMs on SOL and Divertor

(In collaboration with IST Lisboa)

A new difference between type III and type I ELMs is deduced from thermography of the divertor target plates, allowing a measurement of the heat flux to the plates during ELMs. Fig. 4.6 shows the deduced power load during type III and type I ELMs. The shots were run with the ∇B drift towards the X-point. In ELM-free phases, the ratio of the power density between the outer and inner plates is roughly 2:1. During type III ELMs this ratio is unchanged, while in type I ELMs it changes to $\approx$ 1:1. We can therefore distinguish type I and type III ELMs not only by their power dependence, but also by their typical heat load pattern.

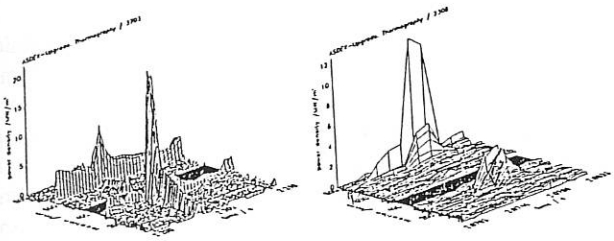

FIG. 4.6: Divertor heat load during type I (left) and type III (right) ELMs. The outer target plate is located on the left of each figure; time propagates from left to right.

With respect to the exhaust problem in a tokamak, ELMs modulate the flux of particles and energy into the divertor. This might be a severe problem for the realization of a cold and dense divertor. It is therefore necessary to characterize the temporal and spatial asymmetries in the power and particle balance due to ELMs.

In a typical type III ELMy H-mode, evaluation of the power balance shows that about 40 % of the total heating power is radiated from the plasma, the remaining 60 % is largely deposited on the divertor plates. In steady state, the total power deposited during ELMs is of same magnitude as that deposited in between ELMs. As the duration of an ELM is short compared with the inverse ELM frequency, the power load during an ELM can be high: Quantitative analysis of thermography data shows that type I ELMs lead to a more symmetric power deposition (consistent with DIII-D), but temporarily increase the load of the plates by a factor of 10-20. With type III ELMs, the increase is only 3-5. Future investigations will focus on the differences in power deposition profiles during the different ELM types.

From the change in density profiles (seen by DCN interferometry and microwave reflectometry) introduced by an ELM, we can estimate the total number of expelled particles. For type III ELMs with a repetition rate of 70 Hz, we find a typical loss of 0.5-2 $\cdot 10^{19}$ particles per ELM (i.e. 2-5 % of the total particle content). The typical energy pulse arriving at the plates during an ELM under these conditions is ≈5-10 kJ (i.e. ≈2.5-5 % of the total energy content). Assuming only convective transport, an average temperature of $< T > \approx 1$ keV is deduced. As the ELM mainly affects the edge region, where the average temperature is much lower, we conclude that the energy loss cannot be explained by the energy carried by the particles alone but has a large conductive component. Within our temporal resolution of 11 μs, there is no time delay between the occurrence of the ELM in the midplane outside and at the plates. Ions flowing at sound speeed need ≈ 0.1-0.5 ms for this distance; therefore, the first energy pulse must be transported via the electron channel; the particles are then lost on the slower ion timescale of 0.1-1 ms. In contrast to DIII-D even giant ELMs show a delayed response of the neutral pressure in the divertor; this may be explained by sorption on the walls.

This suggests that an ELM can be understood as a short opening of the transport barrier. This picture is confirmed by SOL modelling using an improved version of the B2 code with a simple neutral gas model: In a first attempt, an ELM is introduced by enhancing D and χ in both the SOL and the plasma edge region by a factor of 10-50 for 120 μs.

4.4 Impurities in Edge and Divertor

4.4.1 Influence of the carbon and the oxygen concentration on the density limit

It is known from all tokamaks that the maximum achievable density strongly depends on the impurity concentrations. Investigations on ASDEX have already shown a distinct correlation between the value of Z_{eff} and the density limit.

In ASDEX Upgrade carbon and oxygen are the main impurities under normal discharge conditions. The C-O monitor (see Diagnostics) offers a unique tool for examining the dependence of the density limit on impurity species. A statistical evaluation including all standard density limit discharges (B_T = -2 T, I_p = 600 kA) was therefore performed. The concentrations of carbon (C_{car}) and oxygen(C_{oxy}) were deduced from the absolute intensities of their line radiation by transport calculations. For simplicity, the following ansatz for the maximum density n_{fit} was used:

$$n_{fit} \sim C_{car}^{\alpha} \cdot C_{oxy}^{\beta}.$$

The regression was performed for values of the density limit ranging from 4.2 $\cdot 10^{19}$/m^3 to 8.3 $\cdot 10^{19}$/m^3. Good agreement between the experimentally measured density limits and the regression could be achieved with $\alpha \approx 0.0$ and $\beta \approx 0.2$.

In Fig. 4.7 the influence of the respective impurity concentration is shown. n_{norm} is the normalized density, where the influence of the other impurity has already been considered. There is almost no dependence of the density limit on the carbon concentration. In contrast, the influence of the oxygen concentration is very strong. For very small oxygen concentrations (C_{oxy} = 0.05%) shortly after boronization extremely high densities can be achieved ($n_{DL} = 8.3 \cdot 10^{19}/\mathrm{m}^3$), whereas for $C_{oxy} \approx 0.5\%$ only a very smooth dependence of the density limit is found.

At the end of the last discharge period strong radiation of fluorine was found by the SPRED and the CXR spectrometers, as a result of the burning of teflon insulation elements. The further reduction of the DL by this event is illustrated in Fig. 4.7. The stars show n_{norm} for discharges with the additional fluorine impurity. The CXR measurements indicate a F concentration comparable to the O concentration in NBI discharges. On the assumption that this is also valid for ohmic discharges, it seems that fluorine has the same influence on the density limit as oxygen.

Since the density limit is sensitive to the radiation profile near the plasma edge, the above observations are consistent with the fact that flourine should have almost the same radiation characteristics as oxygen, whereas carbon radiates at lower temperatures and larger radii.

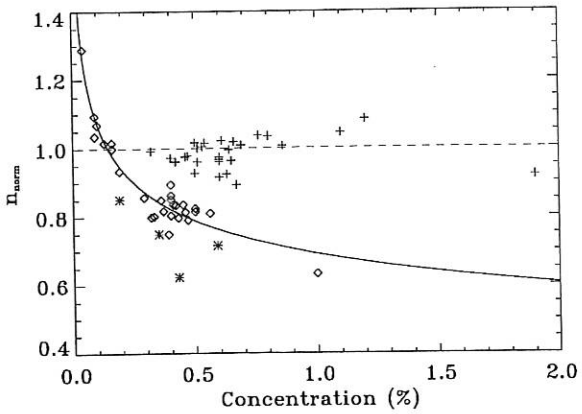

FIG. 4.7: Influence of the carbon (crosses) and the oxygen (squares) concentrations on the density limit. n_{norm} is the normalized density, where the influence of the other impurity has already been considered. The dashed and solid lines illustrate the result of the regression for carbon, respectively oxygen. The stars show the reduction of the density limit due to fluorine.

4.4.2 Marfe Observation and Density Limit

In ASDEX Upgrade density limit discharges, an impurity radiation driven x-point marfe is observed for all values of the safety factor q. The marfe already appears at densities well below the global density limit at another critical density value which depends about linearly on the power flowing into the scrape-off layer. This marfe formation phase was studied experimentally in some detail.

When the density is ramped up, the marfe grows and moves onto closed flux surfaces until a density limit disruption occurs. At the time of current disruption, the distance of the marfe to the q = 2 surface, as determined from bremsstrahlung and bolometer measurements, is still large, e.g. 0.1 m even at a q-value as low as 2.8. It is concluded that edge cooling by the marfe and subsequent peaking of the current profile finally causes the MHD disruption, as already observed in ASDEX. This is supported by the fact that stable operation in the presence of a marfe was possible if the density ramp was stopped at a value between the critical density for marfe formation and the global density limit.

Since the marfe is driven mainly by radiation from low-Z impurities such as oxygen and carbon, the empirical density limit scaling described in the preceding paragraph can be qualitatively understood.

4.4.3 High-Z target plate materials

Preliminary studies have commenced of the suitability of high-Z materials such as tungsten or molybdenum for the divertor plates. Although until now graphite has almost exclusively been used for divertor plates and limiters it has become clear that at reactor relevant heat fluxes unacceptable amounts of material would be eroded and that the 'carbon bloom' effect can result in serious dilution of the plasma. High-Z materials are favorable in this respect because of their very low sputtering rates but are excluded from current designs because they can easily cause tremendous cooling of the core plasma.

As a pilot study stripes of high-Z materials have been inlaid across the outer target plate. These are observed by spectrometer systems which view both tangentially and perpendicularly to the target. A tungsten inlay under the tangentially viewing spectrometer allows direct measurement of the ionisation length of the sputtered atoms. Intensity profiles of a WI (400.8 nm) line measured with this system are shown in Fig. 4.8. Ionisation lengths estimated from these profiles of $\approx$ 2–3 mm are of the order of the gyroradius of the sputtered ions and decrease as expected with increasing density at the target.

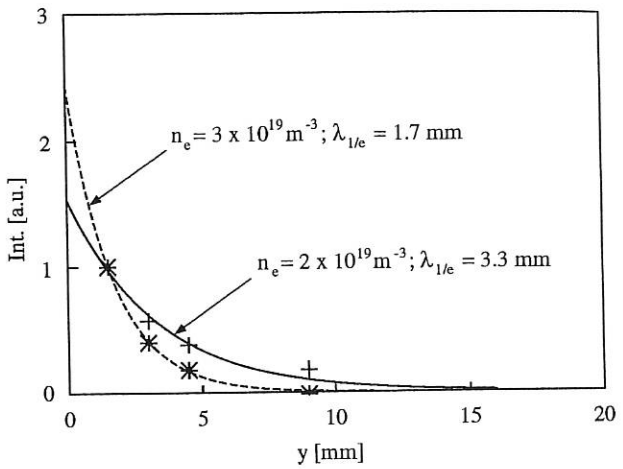

FIG. 4.8: Intensity Profiles of a WI line measured viewing tangentially to the outer target plate (y = chord elevation above target). (I_p = 800 kA, B_t = −2T, D_2 and n_e increasing from 2.0–5.0·10^{19} m^{-3}.)

The perpendicular viewing spectrometer observes either of four inlays of Cr, Ni, Mo or W or the graphite target, thus covering a range of Z = 12–74. This observation geometry is optimal for measurement of fluxes of both sputtered atoms from the various targets and of light impurities recycling at the target. Such observations will be valuable in reaching a consistent interpretation, e.g. with respect to the role of light impurities in the erosion of the high-Z materials.

That the sputtering yield for W is actually strongly temperature dependent is confirmed by Fig. 4.9. The observed WI line intensity, which is approximately proportional to W-influx, decreases markedly as soon as the bulk plasma density is increased (and temperature decreased) even though the D-flux at the target increases. Further measurements, particularly at higher heating power, and their detailed interpretation are in progress.

4.4.4 CXR in the Divertor

Emission profiles were obtained for lines of neutrals and ions of the commonly occurring impurity elements (e.g. C, B) by means of the divertor spectrometer viewing tangentially to the target plate (Fig. 4.10). For neutrals and weakly ionized impurities, these profiles can be explained in terms of stepwise ionization of neutral atoms produced at the target plates and

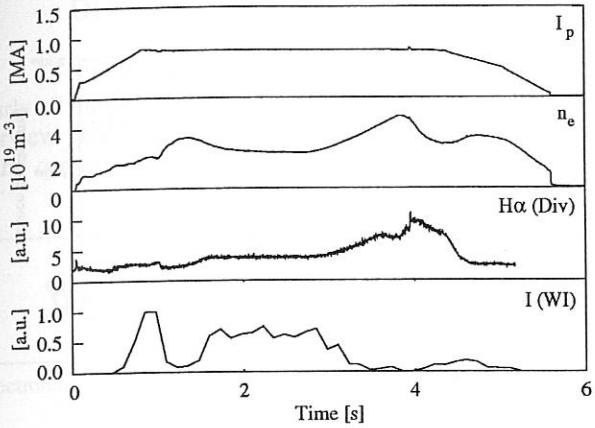

FIG. 4.9: Temporal development of WI (400.8nm) intensity measured viewing tangentially 1.5 mm above the W-inlay. (Shot #3930: I_p = 800 kA, B_t = −2T, D_2 and n_e increasing from 2.0–5.0·10^{19} m^{-3}.)

parallel motion along the field lines. In contrast, electron impact excitation of B^{3+}–levels from ground state is practically impossible for energetic reasons in the low temperature divertor plasma. Pupolation of excited levels of B^{3+} and the shape of the emission profile are a result of charge exchange recombination (CXR) of B^{4+}, produced in the main plasma, with atomic deuterium. Another CXR reaction, C^{4+} with molecular deuterium, could also be confirmed.

CXR of highly ionized ions in the low–temperature divertor plasma leads to electron capture in highly excited levels. This process thus opens a channel of radiative energy loss of ions diffusing from the SOL and reduces the mean charge of ions reaching the target plates.

Low–energy CXR in the divertor could therefore be of importance to decrease the power flux to the target plates and the sputtering rates.

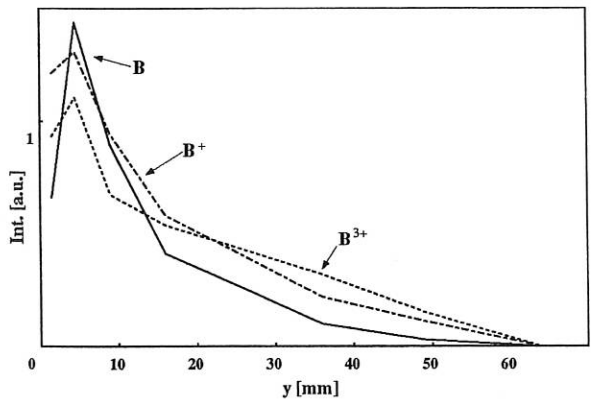

FIG. 4.10: Intensity profiles viewing tangentially to the outer target plate (y = chord elevation above target).

4.4.5 *Divertor Mass Spectrometry*

The investigation of intrinsic gaseous impurities by divertor mass spectrometry was continued. A magnetically heavily shielded total pressure sensor (Baratron) at the location of the quadrupole analyzer has been added to increase the accuracy of the partial pressure data. In addition, differential pumping of the analyzer has been provided to accomodate the quadrupole to the high exhaust pressures ($> 10^{-3}$ mbar) of high density discharges.

Throughout very good agreement between the observed $C_xH_mD_n$ pattern and our model suggested to also employ it for the derivation of in situ carbon erosion yields. Values obtained were typically 5 %. Such values are in fair agreement with data from optical spectroscopy on CD molecules, considering the uncertainties herein, but are about twice as much as laboratory data would suggest. It should be noted here that more than half of the carbon erosion is due to the formation of $C_2H_mD_n$ and $C_3H_mD_n$ as seen by mass spectrometry. There are also several indications that most of the carbon flux is produced by chemical erosion via $C_xH_mD_n$, rather than by sputtering. This might have far reaching consequences for the future use of carbon as first wall material in fusion machines since chemical erosion persists even at impact energies of a few eV.

4.4.6 *Erosion and Redeposition in the ASDEX Upgrade Divertor*

The erosion and redeposition of silicon and tungsten evaporated onto the divertor plates of ASDEX Upgrade were investigated. For comparison with the experimental results the ERO computer program was used. The erosion of Si markers is smaller than expected from plasma ion sputtering, but still exceeds the W erosion by more than an order of magnitude. The observed erosion can only be explained by assuming a protective effect of carbon ions coming from the plasma which are deposited on the marker surfaces, thus reducing the marker erosion.

Redeposition of the sputtered tungsten atoms was found close to the original marker spots mainly because of prompt redeposition during the first gyration.

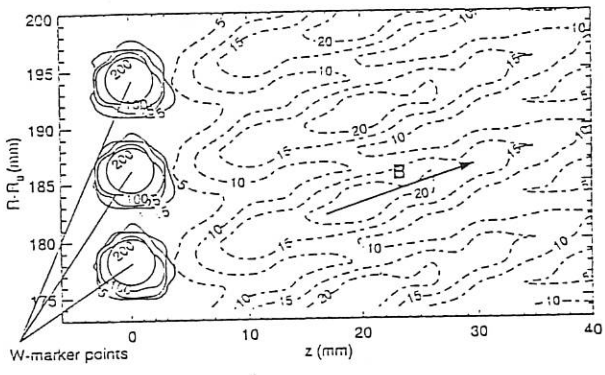

FIG. 4.11: Contour plot of the W distribution after exposure of the original marker spots (solid circles) to about 80 divertor discharges. The levels correspond to thicknesses of the redeposited W in nm. Without taking gyration effects into account (prompt redeposition), the measurement does not agree with the calculated distribution (as indicated by dashed-line contours in the figure)

The pattern of redeposited W after exposure to a more extended discharge period where some W erosion was found is shown in Fig. 4.11. The three marker spots were selected from a position where the erosion along the divertor plate reaches its maximum.

The W distribution indicates deposition close to the original evaporated spots. The version of ERO where the motion of the impurity ions along the magnetic field lines is only determined by friction with plasma ions was used to calculate the deposition at a distance of about 20 mm (Fig. 4.11). This large transport in the toroidal direction is due to the small inclination angle of the magnetic field lines of about 2°. Including, however, the effect of gyromotion and the electric field above the plate results in close agreement with the experimental results.

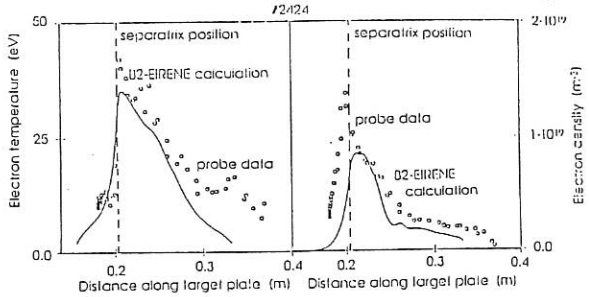

FIG. 4.12: Comparison of measured and calculated divertor plasma profiles.

4.5 Edge and Divertor Modelling and Model Validation

4.5.1 2D Edge and Divertor Modelling and Model Validation

The two-dimensional multi-species fluid code, B2 (Garching version), coupled to the three-dimensional linear Monte Carlo code, EIRENE, is used to describe the ASDEX Upgrade scrape-off layer plasma and the neutral gas dynamics in a fully self-consistent way. After installation of the majority of the ASDEX Upgrade diagnostics system we started model validation using the data for a series of ohmic discharges. The main experimental data used up to now are $n_e(r)$ and $T_e(r)$ just above the outer target plate, measured with the in-vessel probe (C. S. Pitcher, CFFP Toronto and PPPL, Sec. 4.1.1) and the divertor target power load profiles measured by thermography.

To reproduce the density and temperature profiles near the target plate, we had to use a rather low diffusion coefficient $D = 0.1$ m^2/s and moderate heat diffusivity coefficients $\chi_e = 1.5$ m^2/s and $\chi_i = 1.0$ m^2/s. The broad shoulder measured in the n_e-profile is attributed to electrostatic turbulence, and in the 2D modelling it is simulated by a radial outward drift in the outer part of the scrape-off layer. The measured and calculated profiles are shown in Fig. 4.12

. Multifluid simulations including carbon have been started, but still await some improvements in the B2 code. These simulations enable us to compare the spectroscopically measured C fluxes with the simulations by implementing the experimental lines of sight in the code.

Comparison of the measured and calculated power loads on the two target plates shows a discrepancy in the ratio of power onto the outer target to power onto the inner target, $P_{out.target}/P_{in.target}$. Thermography yields a ratio of 2.2 for these ohmic discharges, while modelling gives values of the order of 1.3–1.5 only. The large experimental asymmetry might be attributed to classical drifts. At present, only $\vec{B} \times \nabla T$ is implemented in our code version.

First investigations including this term have shown only a small net effect because the changes in the electron and ion power flows almost cancel each other. This issue is still under discussion.

In addition to these stationary cases, there are experimental situations which clearly require a fully time-dependent treatment. Two cases were treated in substantial detail, but are described elsewhere: radiation–driven MARFEs occurring as precursors to the density limit (see Sec. 4.2.2 and Berlin Division) and ELMs appearing during the H-mode phase (see Sec. 4.3.2.).

5. DIAGNOSTICS

Nearly all diagnostics for the investigation of the ASDEX Upgrade plasma are now installed and more or less in operation. A short overview of these diagnostics with its main characteristics is given in the following table. Special physical results are presented in the corresponding sections of the annual report.

Diagnostic	Quantity to be measured	Chan.	Space resol. [mm]	Time resol. [ms]	Comment
Electromagnetic probes *	electromagnetic signals (current, voltage, magnetic field)	160 64 8		1 0.5 0.1	bulk, high precision because of feedback control
Mirnov probes	MHD activities	32		$\leq$0.002	bulk
Halo currents	halo currents	51		0.2	
Mass spectrometry	gas pressure + gas composition	1			pump tube
Neutral gas pressure gauges	gas pressure of H_2, D_2	17		1.5	in vessel, outside plasma, $10^{-5} - 10^{-1}$ mbar
He u. D/H partial pressure	partial pressure of H_2, D/H	1		10	behind PSL, partial pressure $> 5 \times 10^{-5}$ mbar
Photographic diagnostic (visible region)	observation of different parts of vessel and plasma	6 cameras	1 - 10	20	PSL, X-point, divertor plates, overview of total vessel
H_α normal * H_α with posttrigger *	hydrogen flux	18 4	100 - 500	0.1 0.01	PSL, bound., div. may be used for CI, CII, CIII and bremsstrahlung also
DCN interferometer	$\int n_e \, d\ell$	8		1	bulk, density feedback control
Bremsstrahlung	bremsstrahlung (IR)	3	100	0.01	bulk, for density control (redundant)
2 mm interferometer	$\int n_e d\ell$	1		1	bulk, density feedback control (now dismounted)
Calorimetry	energy deposition	157	1 segment	1 disch.	divertor plates
Wall thermometry	tile temperature	62	1 tile	3000	
Thermography	energy deposition	256	2.7 - 3.3	> 0.130	on inner and outer div. plates
Langmuir probes fixed position *	T_e, n_e	60 (120)	divertor 15	$\geq 0,05$	div., in tripel mode operation 20 (40) chann.
Manipulator boundary **	electron temperature	1	15	0.1-100	moving probe across boundary, 1/disch.
Manipulator divertor **	particle flux	1		200	rotating probe in div. plate
Pitcher probe	electron temp., density	2		0.1-100	above inner and outer div. plate, 1/disch.
Fast moving probe **	electron temp., density	1		0.1-100	choosable traces in div., 1/disch.
Collecting probe	particle deposition and erosion			long term	distributed over vessel
Thomson scattering VTS Thomson scattering HTS *	T_e, n_e, vertical T_e, n_e, horizontal	16 16	40 10 - 40	0,0001 0.0001	bulk, 6 lasers, 20/s each bound.-bulk, 6 lasers, 20/s each
Relativistic Thomson-Scattering	runaway electrons	4	$\approx$ 100	$\approx$ 1000	bulk, density, energy distribution
Bremsstrahlung profile, vertic.	Z_{eff}-profiles	16	40	0.05	bulk, JR, using Thomson detectors
Bremsstrahlung IR-arrays	MARFE observation	2 x 35	30	1.1	bulk, 1 vertical, 1 horizontal array
ECE polychromator	$T_e(r,t)$	8	40 - 70	0.1 - 1.0	bulk

Diagnostic	Quantity to be measured	Chan.	Space resol. [mm]	Time resol. [ms]	Comment
ECE Michelson	ECE spectra, $T_e(r,t)$	1	120	25	bulk, identification of nonthermal electrons
ECE heterodyne radiometer *	$T_e(r,t)$	8 (16)	10 - 20	0.01	bound.
SPRED spectrometer	impurities	1		≥ 7	bulk, VUV, overview
C, O and B monitors **	Lyα of C, O (and B)	1	100	≤ 1	2 (3) Bragg spectrometer
CX recombination spectrometer	T_i, plasma rotation, n_z	8	100	30-500	bulk, visible, He, B, C, O, F
Divertor spectrometer	emission profiles of impurities	16	2	0.01-20	div., 2d-CCD + multipliers erosion, ionization lengths
Provisional boundary layer spectrometer	impurity flux, T_i	2048	3	6	div., ant., 200 - 800 nm, either 1 local, 2048 spectral ch. or vice versa
Boundary layer spectrometer **	impurity sources, transport, plasma rotation	1	5	25	div., bound., VUV, UV, VIS 2 x 2048 channels, spacial scan
Grazing incidence spectrometer *	high z impurities	1	10	≥ 5	bulk, 2 $\times$ 1024 spectral channels, 1 - 200 nm
Johann spectrometer	T_i	1	50	100	bulk, high spectral resolution, 512 channels
Bragg spectrometer *	medium and high z impurities	1	20	1	bulk, 0.1 - 10 nm, spectral resolution 200 - 2000
Laser blow off system *	injection of metallic impurities				1/disch., final design 20/sec
Soft X-ray diagnostics *	plasma dynamic, impurity radiation	92 (124)	50	0.005	bulk, 3 of 5 cameras installed, MHD, ELMs, disruptions
Bolometer cameras *	total radiation	88 (72)	≈ 50	10 (1)	bulk, div.
Hard X-rays	runaway electrons	4	none	1	bulk, fixed detectors outside AUG
Neutron flux detector	total neutron rate	1	none	1	bulk, absolutely calibrated, epithermal neutrons
Neutron spectrum	T_i, ion energy distribution	1		100	bulk, He^3-detector
Pellet centrifuge	bulk refuelling				40/s up to 1200 m/s, $\leq 4.2 \cdot 10^{20}$ particles/pellet
Pellet observation	pellet ablation	3		0.001	bulk, 3Hα-diodes (CI, CII)
CX neutrals *	energy distrib. and T_i of H°, D°	1 (2)	50-100	5-500	10 energy/mass - chann., bulk, up to now no local scan
LENA (Low Energy Neutral Analyzer) *	T_i of H°, D°	1	20	100	bound., 20-1000 eV (TOF), depth $3 \cdot 10^{17} cm^{-2}$
Lithium beam **	$T_e(r)$, $n_e(r)$, $n_z(r)$	20 - 40	3 - 6	0.1	bound.
Microwave reflectometry *	$n_e(r)$, n_e-fluctuations	5 (12)	5	0.1 - 0.01	bound., 2 ch. high, 3 ch. low field side, $0.4\text{-}2 \cdot 10^{19} m^{-3}$
ICRH-diagnostics					see Sec. 2.4

Agenda:
T_i: ion temperature
T_e: electron temperature
n_i: ion density
n_e: electron density
n_z: density of impurities
bulk: plasma centre
div.: divertor region
bound.: boundary region
ant.: antenna
disch.: discharge
( ): final design
TOF: time of flight
*: not yet completed
**: not yet installed

INTERNATIONAL COLLABORATION

1. DOE – ASDEX Upgrade

The main activity in this IEA Implementing Agreement for the joint work on the investigation of toroidal physics and plasma technologies in ASDEX Upgrade was personnel exchanges and a technical workshop in connection with the annual (8th) IEA ASDEX Upgrade Executive Committee meeting on March 2, 1993, at IPP. The personnel exchanges were from laboratories in the US (PPPL: 6 scientists) to IPP Garching, and from IPP Garching (6 scientists) to GA, ORNL, PPPL, and Texas University and involved participation in experiments, computer code analysis of results, theory, and technology development. The workshop, held at IPP on March 1-2, 1993, was on the topic of "Edge and Divertor Physics". The workshop provided an opportunity to exchange information on plasma edge modelling, divertor data analysis, and divertor design.

1.1 Plasma Control

ASDEX Upgrade with its poloidal field coils outside the toroidal field coils and its "open" divertor has a magnetic configuration similar to that planned for ITER, especially that of the first EDA studies. Thus, the problem of plasma shape and position control, plasma disruptions, and vertical displacement events (VDE) in ITER can be dealt with in ASDEX Upgrade, including their time scales of > 0.1 s. The dynamics and forces involved during VDE's and current disruptions has been extensively simulated with PPPL's **T**okamak **S**imulation **C**ode (TSC) code. The design of a disruption data bank for ASDEX Upgrade has been started to obtain – together with results from other experiments – scalings for extrapolations towards ITER.

1.2 Edge Physics

There is an ongoing joint activity in the field of tokamak edge modelling, which is based on the B2 tokamak edge multifluid code of B. Braams (NYU/PPPL), the EIRENE Monte Carlo neutral gas code of D. Reiter (Jülich), and the grid generator SONNET of H.P. Zehrfeld (Garching). Within this effort, the numerical solver was further improved for the case of extreme sources and sinks as obtained with strong impurity radiation or for neutral gas dominated ITER divertor scenarios and was implemented in the B2 tokamak edge code. A very general ansatz for the thermal forces for arbitrary impurity concentrations was developed. In addition, kinetic corrections to the fluid equations were further discussed and a viscosity limit was implemented.

The retention capability of the DIII-D divertor for recycling impurities was investigated by means of short gas puffs to study the containment of such impurities as a function of global parameters such as density, auxiliary heating power, and magnetic geometry. Within the frame of an heuristic global transport model, the divertor retention can then be compared with the results obtained on other devices with different divertor geometries.

A simple Langmuir probe manipulator for divertor profile measurements (IVP 1) was developed by S. Pitcher (Toronto/PPPL) and installed in ASDEX Upgrade. A second probe (IVP 2) for the inner divertor leg was ordered and built into ASDEX Upgrade.

Within the framework of plasma-wall interaction the thermal stability of ion implanted dopants (B, Si, Ti, Mo) in graphite was investigated by methods such as X-ray photoelectron spectroscopy and transmission electron microscopy, which are available in the Solid State Division of Oak Ridge. The development of high thermal conductivity CTC materials with the Material & Ceramics Division of ORNL with the emphasis on neutron irradiation testing was discussed.

1.3 Transport, Heating and Refuelling Issues

Collaboration for the bulk plasma issues concentrated on transport and confinement studies and heating and refueling issues.

Plasma transport analysis and simulation work both for ASDEX Upgrade and for ITER predictions need 1.5-D transport codes, such as PPPL's TRANSP and BALDUR codes. Both are used at IPP. An issue of further common interest was the simulation of electrostatic turbulence and its comparison with experiments.

Collaborative work also treated pellet ablation and vapour shield modelling studies, especially collisional energy transfer from incident plasma particles to the vapour shield.

RF heating and applications: In preparation for ICRH modulation experiments in ASDEX Upgrade Fast Wave and ECRH

modulation experiments in DIII-D were analyzed. Computer codes in the area of transport, kinetic theory and wave propagation were exchanged to complement each other's strengths and for comparison purposes.

2. DEMOKRITOS, Greece

There is ongoing cooperation between IPP and Demokritos in the field of divertor physics and especially divertor plasma diagnostics by movable Langmuir probes.This activity started with extensive divertor profile measurements on ASDEX, which, over the past years, contributed a lot of data to the ASDEX edge and divertor data base..

In parallel, Demokritos conducted feasibility studies for an advanced, reciprocating Langmuir probe for the ASDEX Upgrade divertor, which should allow measurements over a large area in the lower outer divertor chamber. Probe exchange and maintenance should be possible without breaking the vacuum. On the basis of this study, IPP and Demokritos agreed in 1990 to build such a Langmuir Probe System (LPS). After a few design iterations between IPP and Demokritos, the construction of LPS by Demokritos was nearly completed in 1993 and, after some remaining tests, LPS will be shipped to IPP and mounted on ASDEX Upgrade in spring 1994.

3. University of Cork, Ireland

The collaboration with the University of Cork concerning the MHD equilibrium identification using magnetic measurements and function parametrization of an equilibrium data base was continued. This method is the central part of our diagnostic data evaluation procedures and is currently checked against other observations. Function parametrization technique has also been used to model neutral beam power deposition profiles for different plasma parameter profiles.

4. Cooperation with Russian Institutes

Most of the collaborations are organized in the framework of WTZ, the Agreement between the Federal Minister of Research and Technology of the FRG and the State Committee for the Use of Atomic Energy of the USSR on Scientific-Technological Cooperation for the Peaceful Use of Nuclear Energy. Four topics relate to ASDEX Upgrade.

1. Pellet injection — Technical University of St. Petersburg: The theoretical work concentrated on ablation theory. A diagnostic pellet injector for carbon pellets, a microwave system for pellet mass measurements and a CCD camera are contributions from the Technical University of St. Petersburg, which are installed and routinely used at ASDEX Upgrade.
2. ECRH — Institute of Applied Physics, Nizhni Novgorod (IAP): The construction of the ECRH system has been started with strong technical and personnel support from IAP.
3. Control of plasma parameters — Efremov Institute, St. Petersburg: This collaboration takes the form of common workshops.
4. Neutral particle analysis — Kurchatov Institute, Moscow: A code is being developed for fast interpretation of data with the aim of evaluating the ion temperature profile.

Two contracts outside WTZ exist in the field of neutral particle analysis: Ioffe Institute, St. Petersburg, contribute to the measurement and interpretation of neutral particle spectra and Kurchatov Institute perform a detailed sensitivity study to the neutral particle interpretation code.

5. University of Budapest, Hungaria

In the framework of the EU TEMPUS programme, directed at improving professional training in East-European countries, a young scientist of the Dept. of Fluid. Mech., Technical University of Budapest commenced a 10–month stay at IPP Garching, Tokamak Theory Division (Th3), in Nov. 1993. He is participating in a research study pertaining to pellet fuelling in fusion machines.

Two IPP scientists (L Lengyel and J. Schweinzer) were invited to present papers at the Workshop on the Use of Atomic Beams in Plasma Experiments organized jointly by the Hungarian Academy of Sciences, Central Research Institute for Physics, and the German Research Foundation (DFG) in Budapest, March 1993. The titles of the two talks presented: "Pellet Ablation and Wall Erosion: Physics and Modelling" (L. Lengyel) and "Lithium Beam Diagnostics on ASDEX Upgrade and W7–AS" (J. Schweinzer et al.).

6. Centro de Fusão Nuclear, EURATOM IST Association, Lisbon, Portugal

In 1993, major parts of the reflectometry diagnostic in ASDEX Upgrade were completed. Two Ka-band channels (26–40 GHz) were installed opposite the high- and low-field sides of the plasma midplane, and first measurements of density profiles in the scrape-off layer were made. In addition, two V-band channels (50–75 GHz) in X-mode were installed to probe the outer edge of the plasma. One of these systems will be used to measure the density profile in front of an ICRH antenna. The total accessible density range is now from ≈ 0 to $2 \cdot 10^{19}/\mathrm{m}^3$. A prototype of a 200 MHz VME-bus data acquisition board to be used for the V-band was also built. A high-speed optical transmission system is under development to cope with the high sampling frequencies occurring at sweeping times of 10 – 100 μs.

7. AEA Culham, United Kingdom

The collaboration with AEA Culham on MHD and RF heating and current drive was continued and extended in 1993. M. O'Brien of AEA performed BANDIT-3D calculations of ECRH/ECCD power deposition and current drive efficiency for ASDEX Upgrade. Also, members of IPP and Culham discussed possibilities of MHD control by ECRH/ECCD. These results contributed to the proposal of the new ECRH system for ASDEX Upgrade. H. Zohm of IPP visited Culham to discuss COMPASS-D H-mode results, especially MHD characteristics of ELMs. According to the classification established on DIII-D, the ELMs occurring on COMPASS-D so far are of type III.

JET COOPERATION PROJECT

(Head of Project: Prof. Dr. Michael Kaufmann)

Meanwhile an extension of the project until 1996 (four years beyond the originally foreseen closure in 1992) was adopted in order to introduce a new Pumped Divertor Phase before the final two year tritium phase. The objective of this new phase is to establish effective control of plasma impurities under operating conditions close to those of the Next Step Tokamak. A further extension of the project until 1999 is under discussion by the relevant bodies.

Various diagnostic devices essential for investigating the JET plasma have been built by IPP and installed in JET. The presently used diagnostic systems are: a bolometer array for spatially and temporally resolved measurements of the total radiated power, soft X-ray diode arrays to detect MHD instabilities and locate rational q surfaces and two crystal spectrometers for the X-ray regime to investigate the impurity behaviour (especially the evolution of impurity density profiles).

To run the diagnostic devices and to contribute to the exploitation of JET in specific research areas, personnel are assigned to JET under several task agreements concluded with JET. Two of these agreements are still in force. The first one provides for the investigation of bulk impurity physics and for the use of impurity related diagnostics. The second one refers to the study of plasma-wall interaction. During 1993 the number of scientists who were temporarily (up to one year) assigned to working at JET within the framework of JET cooperation totalled 5, including 2 scientists of institutes other than IPP. In addition, 9 scientists have been seconded to JET by IPP for long-term stays, including two from institutes other than IPP. They are members of the JET-team staff.

In February 1992 JET completed successfully the 1991/1992 experimental programme and entered into a major shutdown to incorporate modifications and changes to JET to meet its new objective of demonstrating effective methods or power exhaust and impurity control in operational conditions close to those envisaged for ITER. The shutdown continued throughout 1993 and is expected to be completed in January 1994 after a prolonged period of intensive work. When operations resume in the pumped divertor configuration, the interior of JET will have been essentially replaced.

The shutdown has been undertaken in three major stages:

- Stage 1 involved the removal of components and preparation of the vacuum vessel for installation of the divertor coil (February - September 1992);
- Stage 2 involved assembly of the four divertor coils and casings inside the vacuum vessel (October 1992 - May 1993);
- Stage 3 involved the installation of the Mark I inertially-cooled divertor, cryopump, RF antennae, limiters and saddle coils (May 1993 - January 1994).

The installation of components of the pumped divertor and its associated system modifications, included:

- Mark I divertor structure;
- four internal divertor coils and power supplies;
- divertor cryopump;
- poloidal limiters;
- a set of eight new ICRH antennae, with modified protections;
- a new high power LHCD launcher with modified grill and protections;
- divertor diagnostics;
- saddle coils for use in feedback control of disruptive instabilities, TAE mode excitation and error field compensation.

A large number of new divertor diagnostics were installed for spatially resolved characterisation of the divertor plasma. Amongst these are a divertor interferometer, reflectometer and LIDAR as well as a divertor bolometer array. Conditions at or near the divertor target plates will be diagnosed by more than hundred Langmuir probes, infrared thermography, emission spectroscopy, and neutral particle pressure sensors. For improved magnetic reconstruction of the plasma position, particularly in the divertor area, additional divertor flux loops and coils were installed.

Planning for the experimental start-up in early 1994 and throughout the Divertor Characterisation Phase of 1994 has gone ahead. Experiments will concentrate on establishing and characterising plasma behaviour in the Pumped Divertor configuration. The Programme will focus on:

- establishing reliable operation in the new configuration;
- studying the control of impurities, plasma density and exhaust, and power handling using the full range of ancillary equipment;
- extending performance to high power, long pulse operation; and
- studying specific ITER related physics issues.

At the end of the current shutdown, the RF capabilities of JET will have been enhanced significantly with the installation of the new set of eight RF antennae and of the full power LHCD launcher. The exploitation of these systems in a range of heating and current drive scenarios will be an integral part of the Programme during this phase.

CFC (carbon fibre composite) divertor target plate tiles will be installed for most of the operational period with the Mark I divertor (inertially-cooled plates). Later during the programme, it is intended to make a comparative assessment by replacing the CFC tiles with beryllium tiles during a short intervention.

1. TASK AGREEMENT NO. 1

R. Barnsley[1], N. Gottardi[1], Ch. Fuchs, H.J. Jäckel[1], G. Janeschitz[1], K.F. Mast, R. Reichle
[1] JET Joint Undertaking, Abingdon, UK

The diagnostics systems built by IPP and still installed in JET are the bolometers, the soft X-ray diode arrays and the two double-crystal monochromators for soft X-ray plasma spectroscopy. These diagnostics contribute to the understanding of plasma radiation losses, impurity behaviour, and the fast behaviour of the plasma observed through its X-ray emission.

For the JET pumped divertor experiment a new bolometer diagnostic was developed and installed in JET. It partly replaces the previous KB1 system and will provide information on the local radiation power density in the bulk plasma and in the divertor region by two-dimensional reconstruction based on a new tomography programme developed for the ASDEX Upgrade bolometer diagnostic. Space and time resolution will be much higher than before. The principal component of the new JET bolometer diagnostic is a novel metal resistor bolometer with MICA foil which represents a high-temperature version of the ASDEX Upgrade 4-channel low-noise metal resistor bolometer. Low-resistance gold resistor layers are deposited on the thin MICA substrate and can be baked to temperatures higher than 400°C without any degradation. The new bolometer can be operated at temperatures of up to 400°C and is excited with a 50 kHz AC-current. After amplification, the bridge output signal is demodulated and filtered by an 8-pole Bessel filter. A modified version of the JET MICA bolometer will be installed in the divertor region of ASDEX Upgrade.

In the frame of an Article 14 Contract, IPP gave advice and support for the design and construction of a centrifuge pellet launcher for edge refuelling. The centrifuge is similar to that for ASDEX Upgrade, but it accelerates larger pellets (up to 64 mm^3) to reduced velocities.

2. TASK AGREEMENT NO. 2

R. Behrisch, G. Haas, A.P. Martinelli, D. Naujoks

From the carbon and the beryllium tiles at the JET vessel walls about 20 representative probes were cut along a poloidal cross-section. The surface layers of these probes were investigated with ion beam techniques in respect of erosion as well as hydrogen isotope and impurity trapping. The amount of collected deuterium ranges from $5 \cdot 10^{15}$ to $5 \cdot 10^{17}$ D/cm^2. Metal impurites, such as Ni, Cr and Fe, are in the range of 10^{15} to $3 \cdot 10^{16}$ /cm^2 and Cl is in the range of 10^{16} to 10^{18}/cm^2 - the lower concentrations apply to erosion-dominated areas, while the higher concentrations represent lower limits for the deposition-dominated areas. The total amount of collected D and impurites, other than Cl is a factor of up to 10 lower than in previous discharge periods.

As an extension of Task Agreement No. 2 investigations of the neutral particle flux and recycling in the pump divertor and elsewhere on the wall of JET are envisaged with ASDEX-type pressure gauges. IPP's involvement to date has consisted in designing a new sensor head, testing a prototype and providing advice during development and construction by the PTS Company of Freiburg under IPP licence. The hardware was delivered to JET and installed for the next experimentation phase.

3. THEORETICAL INVESTIGATIONS

W. Feneberg, Yu. Igitkhanov, P. Martin

JET - Fast Boundary Code

This code, called LACWIR (W. Feneberg, K. Lackner, P. Martin, Nov. 1993), was developed for JET and describes a fast method of identifying the plasma boundary using results of magnetic measurements. Having been in routine use at JET for 10 years, it was now necessary to change it to a new version fitting to the configuration of the JET pumped divertor. The change consisted essentially in the use of a grid with high resolution near the x-point and a distribution of currents on the outer control surface C obtained on the basis of test functions with cubic splines. Results calculated for a "fat" equilibrium (see Fig. xxx) show an accuracy in localizing x-points of <2 cm. Its boundary was compared with the boundary of the full "PROTEUS" equilibrium identification code, showing excellent agreement at the inboard and outboard sides of the plasma.

Advanced Sheath-Boundary Conditions

One of the critical issues in edge plasma modelling is that of proper boundary conditions for the fluid equations at the divertor target. A conventional approach employed in 2D fluid codes is based on limitation of the upper value of the fluid velocity at the target (Bohm criterion). The main shortcoming of this approach is the incorrect description of momentum transfer at the sheath region, which overestimates the fluid velocity and underestimates the plasma density and temperature near the divertor plate. More general and advanced sheath boundary conditions for fluid equations were suggested, on the basis of conservation laws of particles, momentum and energy in transition from the fluid to kinetic region at the upstream boundary of the pre-sheath, where they have to be imposed at the last computational mesh at the upstream end of the pre-sheath region. Plasma in this region is assumed to be collisionless and can be taken as Maxwellian (shifted and truncated according to the electric field action) in calculation of boundary flows and the corresponding transmission coefficients. The developed boundary conditions are internally more consistent because they are imposed at the same point where they are assumed to be set and the pre-sheath plasma, which is generally non-fluid, remains outside the computational region. The new boundary conditions allow improvements following from refined kinetic treatment: they are valid for arbitrary kinetic boundary distribution function and for example can be applied for simulation of non-local transport effects.

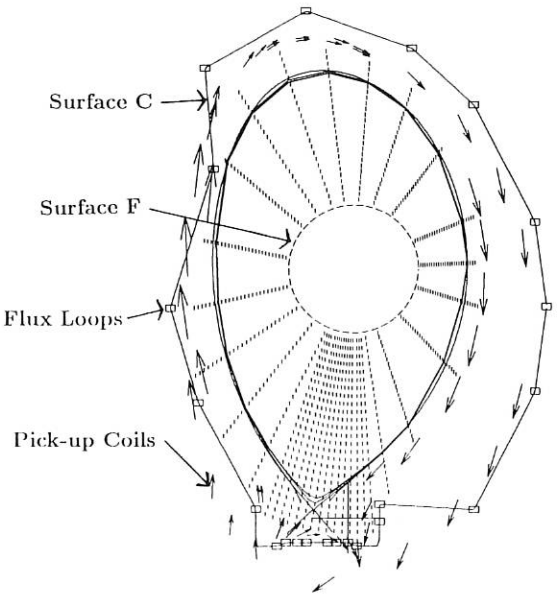

FIG. 1: LACWIR boundary (inner thick solid curve) superimposed o the PROTEUS boundary for a single null x-point configuration.

- *Plasma current:* I_p *(calcul.)* $= 4.94$ *MA*
  I_p *(required)* $= 5.0$ *MA*

- *x-point:*	*R (m)*	*Z (m)*
x (req.):	*2.64*	*-1.57*
x (cal.):	*2.65*	*-1.55*

The corresponding programme package was developed for implementation in the EDGEB2 code. The new boundary conditions are typically more efficient: only a small fraction of computer time required to advance the computation at each time step is spent in evaluating the boundary conditions.

NET/ITER COOPERATION PROJECT

(Head of Project: Dr. Günter Grieger)

Since its foundation IPP have hosted the NET Team, a group of scientists and engineers from the European countries participating in the EURATOM programme. They were called together to prepare the design of NET, the Next European Torus. NET is conceived as the next major step in the European fusion programme, and a considerable fraction of its objectives are in the technology area. IPP contribute to the NET activities both by direct secondment of personnel to the NET Team and by performing NET supporting work.

From May 1988 to the end of 1990, IPP hosted the full ITER Team (International Thermonuclear Experimental Reactor), a project with objectives similar to those of NET but with equal participation of EURATOM, Japan, Russia and USA. IPP strongly supported the ITER activities through its support of NET and are still doing so.

With the signing of Protocol 1 of the ITER-EDA phase it has been decided that from now on the ITER Team will reside at three locations, one of them being IPP Garching again. The Garching part of the ITER Team will concentrate its activities on physics questions and on in-vessel components. IPP will also continue to host the NET Team, which, at the same time, will function as the EC home base to ITER.

IPP has made numerous and essential contributions to the ITER EDA work, the major ones of which are described in the following. Mentioned, however, are only those research activities, which were part of specially organized international collaboration efforts or sponsored by special NET-contracts. Besides this, however, most of the research work of ASDEX-UPGRADE is directly dedicated to the generation of the physics base for ITER. Also the stellarator experiments at IPP make significant contributions to this aim, which are described in a separate section of the chapter on W 7-AS.

1. DEVELOPMENT AND ANALYSIS OF ITER ORIENTED DATABASES

(The H-mode Database Working Group:
From ASDEX: O.J.W.F. Kardaun, F. Ryter, U. Stroth, A. Kus.
From DIII-D: J.C. DeBoo, D.P. Schissel, G. Bramson, T.N. Carlstrom.
From JET: K. Thomsen, D.J. Campbell, J.G. Cordey, J.P. Christiansen.
From JFT-2M: Y. Miura, N. Suzuki, M. Mori, T. Matsuda, H. Tamai, T. Takizuka.
S.-I. Itoh*, K. Itoh**. (* Kyushu University, ** NIFS).
From PBX-M and PDX: S.M. Kaye.)

The H-mode database working group (consisting of representatives from ASDEX, DIII-D, JET, JFT-2M, PBX-M, and PDX) has continued its collaboration in the fields of global thermal energy confinement and H-mode power threshold databases. It has started activities on a plasma profile database. Progress in the refinement and the analysis of the global confinement Database (ITERH.DB2) has been described in an IAEA paper (Würzburg) and an EPS paper (Lisbon). A summary of the work has been presented at the H-mode Workshop in Naka, November 1993, and a documentation of the ITERH.DB2 database is to appear in Nuclear Fusion. An important improvement with respect to ITERH.DB1 is the availability of a good and consistent estimate of the thermal energy content and of the power losses due to charge exchange and unconfined orbits. The standard dataset defined in the EPS paper consists of 858 ELM-free and 769 ELMy time slices from only NBI heated discharges, but with no restriction on wall material or evaporation. The standard dataset in the IAEA paper included ICRH and combined NBI/ICRH discharges. Roughly speaking, the standard dataset excludes shots with low q_{cyl}, high radiation, high fast particle contents, and transient behaviour. The precise selection criteria are made available to the user by including 'selector' variables. The analysis yields simple power law expressions as first order approximations with reasonably small residual error (about 13%), yielding confinement time predictions of about 4.5 ± 0.7 seconds for both ELMy and ELM-free discharges in ITER CDA and about 6.5 ± 1 seconds for a recent ITER EDA concept. A simple power law model has been fitted to the EPS standard ELMy dataset without the JET shots. The corresponding scaling deviates little from the scaling based on the full ELMy dataset, and predicts the confinement time of the ELMy JET shots within about 20%. It should be remarked that, nevertheless, the R and κ scaling, and hence the prediction for ITER are sensitive to the rescaling of PDX from closed to open divertor. Moreover, interesting deviations of simple power laws have been found. They can be described by interactions (i.e.: cross products of the regression variables on logarithmic scale) or by fitting offset linear models, which write W_{th} as the sum of two power laws, one independent, and the other proportional to the power absorbed by the plasma. The quadratic terms of the ELM-free scaling described in the EPS paper are

$$\ln(\tau_{th_E}) = L + 0.3\ln(n_e)\ln(B_T/j) + 0.1\ln(j)\ln(P_L/S) + \\ +0.5\ln(M)\ln(P_L/(n_eV)),$$

where $\tau_{th,E} = W_{th}/P_L$ is the thermal energy confinement time, not corrected for radiation, j is the current density, S is the plasma surface area and V the plasma volume. L denotes the linear term of the scaling. This means, for instance, that the effective density exponent, $\alpha_n^{eff} = \alpha_{n0} + 0.3\ln(B_T/j) - 0.5\ln(M)$, decreases with current density and with effective isotope number M. Not yet fully concluded investigations of offset-linear scalings indicate that the M_{eff} exponent is higher and the density exponent is lower in the offset term than in the linear term, which is in agreement with the interactions described above, as well as with results of some individual experiments. Both the interaction and the offset linear models give a more optimistic prediction (20-50%) for the confinement time of ITER CDA in the ELM-free as well as ELMy case. Offset-linear scalings are not easy to fit numerically. A better determination of the exponents is expected from more varied isotope experiments from each of the machines, and a better quantification of the openness of the divertor.

2. ITER H-MODE POWER THRESHOLD DATABASE

The work started in 1992 on the H-mode power threshold database, which covers five divertor tokamaks (ASDEX, DIII-D, JET, JFT-2M, PBX-M), was continued this year. The present version of the database contains about 3,000 time slices with NBI heating for each device and, in addition, ICRF heating for JET. Besides some corrections made to the previous version of the database, the essential extension was the addition of more than 450 recent discharges from JET covering a large operation al window.

The preliminary results obtained last year were confirmed. Under the conditions known to lead to easy L-H transition, e.g. single-null configuration with ion grad B drift toward the X-point, deuterium target plasma, and separatrix far enough ($\approx$ 3 cm) from protection limiters, the threshold power P_{thres} is found to increase linearly with $\bar{n}_e B_T$. Agreement between the different tokamaks within a factor of 2, which otherwise are more than one order of magnitude apart, is obtained by dividing P_{thres}, by the plasma surface area S. The averaged fit of the heating power from time slices taken just before the L-H transition yields $P_{thres}/S = 0.0089\ \bar{n}_e B_T$ [MW,m^2,T,10^{19}m^{-3}]. The database does not include the latest results obtained with boronization in DIII-D and PBX-M, for which the threshold is at least a factor of 2 lower. Discriminant analysis suggests a somewhat stronger size dependence, $S\ a^{0.3}\ A^{0.64}\ \kappa^{-1.2}$, where A is the aspect ratio R/a and κ the elongation.

Analyses using the plasma energy content and an averaged temperature clearly separate the L and H-mode regions.

These results are not yet understood, and work a long this line is being pursued.

Dimensionless studies yield an $R^{2.5}$ size dependence if the $\bar{n}_e B_T$ dependence is assumed to be real, and an $\bar{n}_e^{0.75} B_T$ dependence if the size dependence S is assumed to be correct. The two possibilities cannot be sorted out within the experimental uncertainties of the present data.

Preliminary analyses of edge data from DIII-D and JET were started this year. The results suggest that the electron temperature or collisionality just inside the separatrix is not the universal parameter determining the L-H transition.

The database is now being improved and will be released in 1994 accompanied by a report describing the database in detail and summarizing the analyses performed by the group.

3. DIVERTOR MODELLING

(R. Schneider, D. Reiter (IPP Jülich), K. Lackner, J. Neuhauser, H.-P. Zehrfeld, A. Kukushkin)

3.1 ITER Divertor Modelling with DDC83 Code

DDC83 code has been extensively used for modelling the divertor performance in ITER-relevant conditions. The code is based on 2D fluid equations for electrons and ions in simple rectangular geometry. It employs Monte-Carlo techniques for modelling the transport of atoms and molecules. Power enters the SOL across the separatrix and spreads along and across magnetic field. In the divertor region, below the x-point, plasma is surrounded by gas with prescribed density and temperature, which provides the only paticle source. There is no natural recycling, i.e. every particle, charged or neutral, coming to the target plate or the side walls gets lost. There is also no plasma recombination in the volume, and particle flux across the separatrix is assumed to be zero. Particle balance is therefore maintained by competition of ionization of the neutral gas and sink of the plasma to the side walls and target. The length of the divertor domain from plate to x-point was artificially increased, corresponding approximately to 4.5 m distance in poloidal direction. The gap between the separatrix and the wall was 15 cm. Cross-field diffusivities were $\chi_e = 1\ m^2/sec$, $\chi_i = 0.5\ m^2/sec$, $D = 0.33\ m^2/sec$.
The flame-like solutions, where the plasma temperature in the divertor drops below 1 eV and the power and momentum flows are reduced by more than 2 orders of magnitude before they reach the target, were found for a range of the input power P_{SOL} from 50 to 200 MW. Profiles of plasma temperature and density in the divertor region for P_{SOL}=200 MW are shown in Figs. 1 and 2. The dominant energy loss channel is the transport of potential energy, which is released when the plasma recombines, to the side walls and the target (60%), while the carge exchange and hydrogen radiation take no more than 15% each. A sufficiently high plasma density upstream in the SOL is found to be essential for the flame detachment from the target, and the trend is quite natural: the higher the input power, the higher the upstream density is needed for the same divertor length.

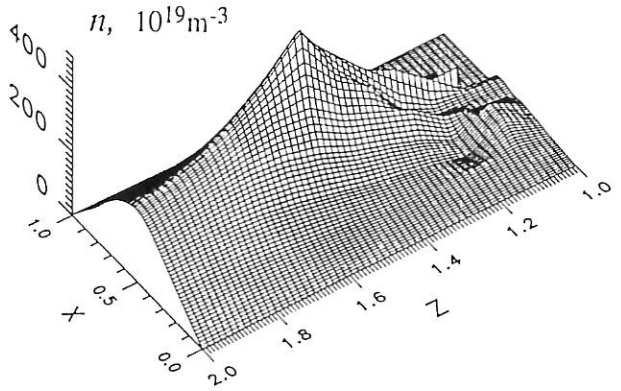

FIG. 1: Profile of plasma density.

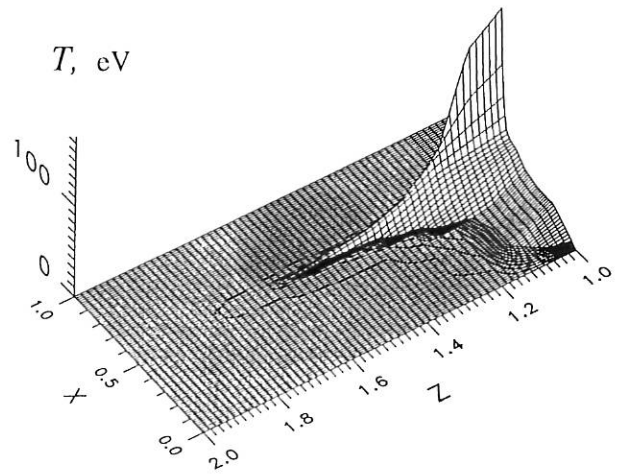

FIG. 2: Profile of plasma temperature ($T_i \cong T_e$ due to the strong Coulomb exchange) in the divertor region. Target is located at Z=2.0; x-point is at Z=1.1, X=0.6. Level lines at the bottom of the hill correspond to the T range from 0.5 to 5 eV. length (l=1 cm)

3.2 ITER Modelling with B2-Eirene (in collaboration with IPP Jülich)

To study neutral dominated divertor regimes, the B2-Eirene-Sonnet code package was used. An ITER single null geometry was set up (see Fig. 3) to analyse as well gas puff scernarios with external gas puffs replacing the recycling sources (same scenario as introduced by Kukushkin's DDC-83 calculations) as a more realistic scenario with V-shaped extremely inclined target plates and baffles up to

the X-point to confine neutrals and replace external puffs by recycling sources (target recycling and wall recycling) (see Fig. 3). We were able to obtain detached gas target solutions in both cases. The gas puff scenario results agree quite well with the DDC-83 results, also demonstrating that the dominant loss channel is the energy loss of electrons due to line radiation of hydrogen atoms and dissociation of molecules. The charge exchange losses are small due to the surface effect nature of this process at high plasma densities (very short mean free path of neutrals). In the realistic scenario target recycling gets small compared to wall recycling in the gas target condition. In Fig. 4 for 100 MW input power and a midplane-density at the separatrix of $1.7 \cdot 10^{20} m^{-3}$ the contour plots of ion temperature and electron density are shown. A detached outer divertor can be seen, whereas the inner divertor is still attached. The geometry (concentration of neutrals in high-energy zone) triggers formation of this detached gas target state. Broad radial profiles at midplane show that the outflux of energy in parallel direction is blocked by strong flow reversal due to strong neutral sources in the outer divertor. Dominant loss channel is the plasma flow to the walls mainly in the main chamber. Bremsstrahlung losses are also high and concentrated in the outer divertor (high density region with ion densities up to $10^{22} m^{-3}$). Neutral losses are dominated by losses due to the interaction of neutrals with neutrals, e.g. with hydrogen atoms (radiation and ionization) and molecules (dissociation). The maximum power load on targets and on side walls is below $0.75 MW/m^2$. The balance between inner and outer divertor is a very delicate problem (introduce additional baffles?) and it is not clear how to obtain detachment for both. The flow pattern with very strong flow reversal demonstrates the blocking of the outer detached divertor, indicating that for these kind of divertor scenarios helium ash removal will be a severe problem.

3.3 Conclusions from ITER Divertor Simulations (DDC-83, B2-Eirene)

It seems to be impossible to deposit the SOL input power for ITER (300 MW) onto divertor side walls by neutrals alone due to the necessary high midplane densities. The formation of a gas target can be triggered by the target geometry. Once the gas target state is formed, its parameters are nearly independent(within a factor of 2) of the geometric details (comparison of DDC-83 results obtained with a simple slot geometry and B2-Eirene results for a full single null geometry). For a reasonable ITER midplane separatrix density of $1 \cdot 10^{20} m^{-3}$ the corresponding power entering the divertor is limited to about 50 to 75 MW, i.e. that is $17\% - 25\%$ of total ITER input power of 300 MW. Even in this case a lot of this power might be going to the walls or baffles.
This means that ITER needs at least 80% radiation losses by impurities.
The most promising ITER divertor concept seems to be an in-series arrangement of different power loss mechanisms: radiation losses from the core and the edge (divertor region and whole scrape-off layer) and neutral losses (mainly in the divertor). The problems connected with the different loss channels (radiation: controllability, stability, compatibility with central confinement; neutrals: baffling of high

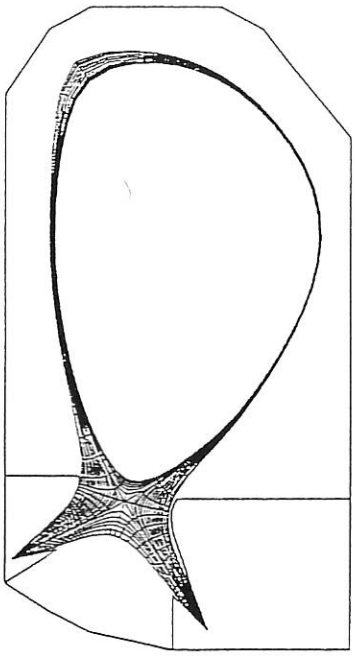

FIG. 3: Geometry used for the B2-Eirene ITER simulations.

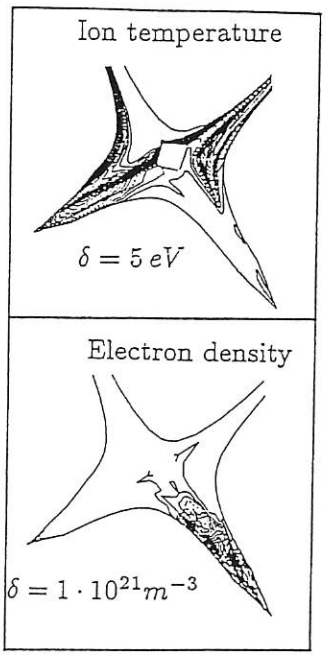

FIG. 4: Contour plots of ion temperature and electron density for the divertor region. The increment between contour lines is 5 eV and $1 \cdot 10^{21} m^{-3}$ for ion temperature and electron density, respectively.

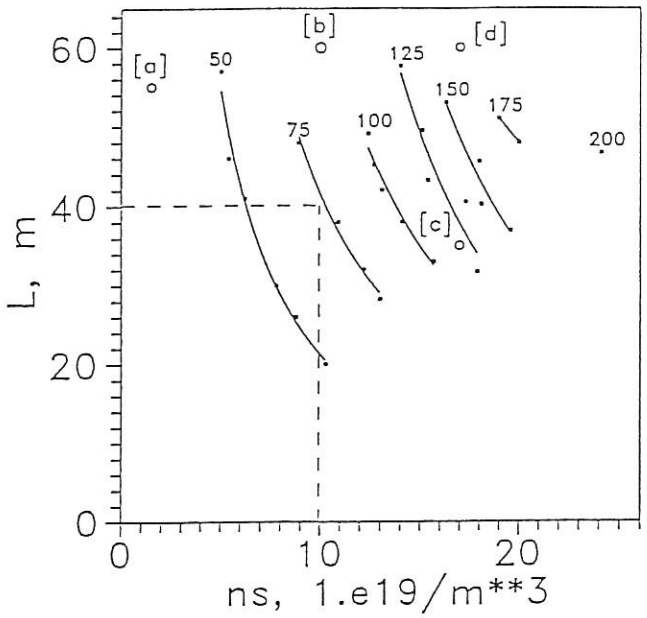

FIG. 5: Flame extinction length, L, against upstream plasma density, n_s, for different values of power entering the SOL, P_{SOL}. Values of P_{SOL} in MW label the $L(n_s)$ curves. L is the distance along field line from the x-point to a point where the parallel heat flux goes below 10 MW/m^2. The points from B2 results are shown with open circles; all the rest are DDC83 data. The B2 point are: 24 MW, gas puffing [a]; 100 MW, gas puffing [b]; 100 MW, natural recycling, outer leg [c]; 100 MW, natural recycling, inner leg [d].

neutral pressure in the divertor to reduce backflow to the main chamber and sputtering by neutrals) have to be solved compatible with H-mode, ELM's and helium ash removal. This divertor concept can only be found by an extensive collaboration of experiments and simulations.

4. NUMERICAL SIMULATION OF WALL EROSION DURING OFF-NORMAL (DISRUPTIVE) TOKAMAK OPERATION

(L. Lengyel, P. Spathis)

The objective of this study was the development of a predictive code, based on a physical model that includes all relevant physical effects, for the purpose of calculating the erosion rates of solid surfaces exposed to fluxes of high-energy plasma particles by taking into account the major shielding effects: collisional, electrostatic, magnetic, and radiative cooling. Two time-dependent high-collisionality (continuum) models, corresponding to different geometrical approximations, were started. Both include the following common features: (a) collisional energy transfer to the solide surface and the vapor layer evolving over it (stopping-length calculations with simultaneous determination of the self-consistent electrostatic shielding field induced); (b) erosion rate of the solid surface based on the energy flux balance at the surface; (c) gasdynamic expansion of the vapor and the resulting hydrodynamic and state parameter distributions; (d) atomic processes: finite rate ionization and recombination, radiation emission; (e) MHD interaction of the high-beta ionized vapor fraction with the magnetic field (slowing-down and stopping of the cross-field motion); (f) distortion of the magnetic field topology; (g) energy transport in the cloud interior by thermal conduction and radiant energy transport; (f) energy losses to the environment by conduction (into the solid) and by radiation. The physical model thus defined can readily be extended to simulate the current decay phase of disruptions as well (time-dependent interface conditions for the developing halo-currents, etc.). Two geometries were considered: (a) 1-D model corresponding to an infinite plate in an initially uniform magnetic field of given angle of incidence. The model is well suited for analyzing the effects of the various physical processes considered. (b) $1\frac{1}{2}$-D model in which the SOL - locus of localized energy input - is represented by a straight strip of given width extending to infinity. Parameter variation across the SOL is neglected in this approximation. With the help of this model, the effects of the lateral expansion of the vaporized material and the lateral radiative losses are analyzed.

5. NET/ITER-RELEVANT RESULTS OF W 7-AS

(J. Baldzuhn, V. Erckmann, U. Gasparino, H.J. Hartfuß, A. Kus, H. Maaßberg, U. Stroth, A. Weller, E. Würsching)

W7-AS contributes with eight tasks to the ITER Physics R&D Programme. The results are summarized as follows:

In 1993 W7-AS was very successful in improving global energy confinement. High-power (0.5 MW or 0.9 MW, 0.4 s) ECRH at 140 GHz was performed, and the plasma density was increased up to the cut-off density $1.2 \cdot 10^{20} m^{-3}$. During high-density operation, the H-mode was observed for the first time in a stellarator. The H-phases display all the characteristics known from tokamak H-modes, including ELMs. The achievement of the H-mode in a shear-free stellarator without net toroidal current has consequences on H-mode transition and ELM theories.

ECRH was also used in combination with NBI to control the density despite the beam particle fuelling and for current drive (long-pulse operation). In the description of the ECCD net current as a function of the launch angle, density and trapped particle fraction, excellent agreement with theory was achieved. For optimized stellarators such as W7-X, global Monte Carlo simulation and local analysis show good agreement and demonstrate favourable neoclassical transport and near elimination of the bootstrap current in this configuration.

Pellet ablation, which is important for long-pulse operation, was found to be governed by self-shielding of the pellet by

already ablated material, leading to an oscillatory process. The nearly shear-free configuration of W7-AS can uniquely contribute to the role of rational surfaces in the striation formation. Apart from the magnetic axis rational values seem to play a minor role.

Theoretical investigations show that transport in the net-current-free stellarator has gyro-Bohm-like properties; this predicts favourable scaling of the confinement properties when projecting to larger devices. Density limit experiments in W7-AS always led to a smooth thermal collapse without any disruptive instability. At high density, close to the thermal collapse the highest β-values are obtained ($\langle\beta\rangle \leq 1.2\%$). These values are still power limited. MHD does not play a limiting role.

Beam driven Alfven eigenmodes, which can play an important role in the fusion reactor, were clearly demonstrated and studied in W7-AS with NBI. Unlike the tokamak, global Alfven waves are induced.

In diagnostics higher stability of a conventional reflectometry system was obtained by measuring the phase of the amplitude modulation of a carrier rather than that of the carrier itself.

6. ICRF RELATED WORK

Extensive calculations on antenna coupling and power deposition profiles were made in preparation for the European contribution to ICRF heating and current drive on ITER. (M. Ballico, M. Brambilla, C. Hoffmann, J.-M. Noterdaeme).

Temporary secondment of personnel provided the necessary emergency support for the task of writing the ITER Report to be presented at the 4th meeting of the Technical Advisory Committee (J.-M. Noterdaeme).

A proposal was worked out for an in-beam irradiation experiment on ceramic samples at Munich research reactor (FRM) and simultaneous testing with RF power as a collaborative project with KFK (H. Wedler, R. Heidinger[1], H. Gerstenberg[2]).

Measurements of tg δ of ceramic samples and samples with plasma-sprayed Al_2O_3 layers were made in collaboration with KfK (H. Wedler, H. Heidinger[1]).

[1] Kernforschungszentrum Karlsruhe

[2] Forschungsreaktor München

7. CHARACTERISATION AND EROSION STUDIES OF POTENTIAL PLASMA FACING MATERIALS FOR NET/ITER

(B.M.U. Scherzer, J. Roth, C. Wu*)

The chemical erosion of CFC materials doped with B and Si exposed to hydrogen plasmas is expected to be strongly reduced compared to pure carbon materials. Further, a reduction of radiaton enhanced sublimation was observed in doped materials. However, at elevated temperatures evaporation of boron or silicon from doped CFCs is expected. This evaporation may be enhanced by simultaneous hydrogen ion bombardment.

The objective of the contract with NET/ITER was, therefore, the characterisation of newly developed doped CFC materials. The measurements performed under this contract were

- Ion beam surface and in-depth analysis of boron and silicon concentration in doped CFC materials, which have been developed by industry following the specifications made by NET/ITER
- measurement of a possible depletion of boron and silicon after annealing as a function of temperature and time up to 1800 K
- measurement of the erosion yield and change in dopant concentrations due to 1 keV D^+ irradiation at 300 K, 800 K and 1500 K.

This experimental program has been started with 4 boron doped and 2 silicon doped probes. The first results showed a considerable inhomogeneity in the dopant concentration of the material. This is especially true for samples where B_4C was introduced into the fibre structure. Local differences were found larger than a factor of 20 on the same material. Because of these large variations, the concentration after annealing must be determined in the same spot where it was measured before annealing. This has been done for two spots of each material, the analysed surface being cut from the bulk of the material. No difference could be found in the boron concentration up to 1800 K within the statistical error limits of the analysis.

For Si-doped CFCs the erosion yield was measured during deuterium irradiation at elevated temperatures. Indeed, around 800 K a strong reduction of the chemical erosion yield was found. At temperatures above 1300 K a strong outgassing of the samples occurred, making weight loss measurements to determine the erosion yield impossible. The experimental program will be continued on more dense and better defined CFC materials.

STELLARATORS

IPP's activities in the stellarator field are concentrated on exploiting the WENDELSTEIN 7-AS experimental facility and on developing the next-step facility in the WENDELSTEIN line, WENDELSTEIN 7-X. Work on the first topic is done by Experimental Division 3, headed by F. Wagner, work on the second topic by Experimental Division 2, headed by G. Grieger.

The results from W 7-AS were characterized by new technical and diagnostic means which provided further insight into the structure and behaviour of the stellarator plasma.

The plasma wall problem, crucial to the reactor, was tackled on a broad front. Notwithstanding the complicated three-dimensional structure of the island strings at the edge, it was possible to get a better grasp of the natural divertor of the stellarator plasma, both in the experiment and in the numerical model. Newly discovered connections between the distributions of the flux line connection lengths and plasma potential near the edge also afforded insights into possible causes of the H-mode development in W 7-AS in a narrow iota range.

Investigations of the H-mode in ECRH plasmas were made possible by the Russian 140 GHz gyrotron, whose output was raised to 900 kW. The H-mode was also obtained at half the main field (1.25 T) and in hydrogen. The microwave generators, otherwise serving only for heating purposes, were used to demonstrate the basic feasibility of collective scattering for determining the ion temperature.

In addition to the previous preionization by ECRH, a non-resonant RF method was developed. Only then could the main field freely be chosen, allowing for the first time definite identification and detailed investigation of NI-driven global Alfven eigenmodes, avoidance of which could be decisive for a future fusion reactor.

Another major area of investigation was plasma fluctuations and their connection with plasma transport. For the first time it was possible to measure temperature fluctuations, in the plasma centre by a new ECE correlation method and at the edge by means of a fast-sweep (1 MHz) probe.

With respect to W 7-X, work was determined by preparing the basis for the Phase II application. In particular, it was concentrated on the evolution of the divertor concept. Both island and ergodic divertor concepts are considered and their magnetic field properties and plasma flow patterns are investigated. Comparisons are made with results coming from W 7-AS. Both of these concepts can be realized in W 7-X by dc-action of "sweep coils". Non-local ballooning modes were investigated for their potential influence in configurations of the W 7-X type. Again the particular criteria satisfied by the W 7-X fields exhibit a very beneficial influence on reducing the danger of such modes. Advanced equilibrium calculations concerning fine-scale finite-β island structures down to the ion-gyroradius scale have begun.

Continuation on force and stress distributions on the W 7-X magnet have led to a further optimization of the coil support structure and a saving of cold mass. Similar studies are performed with respect to the vacuum vessel and its combination with the magnet cryostat.

The W 7-X superconductor is developed for fabrication in industry and is under test at present. A full-size DEMO coil and a half-period long test cryostat are fully designed and ready to be launched for construction in industry.

Assessment of the reactor properties of Advanced Stellarators of the HELIAS type were continued. They clearly benefit from their inherent potential of stationary operation, the lack of need for intense feed-back stabilization, absence of disruptions, etc. A relatively low amount of circulating energy is the consequence resulting in comparatively high overall efficiency. This part of the work is done to guide the evolution of the Advanced Stellarator line to result in an attractive reactor concept.

WENDELSTEIN 7-AS

(Head of Project: Prof. Dr. Friedrich Wagner)

W7-AS Team

R. Balbin[1], J. Baldzuhn, K. Behringer[13], R. Brakel, R. Buechse, R. Burhenn, G. Cattanei, J. Das, A. Dodhy, D. Dorst, A. Elsner, M. Endler, K. Engelhardt, V. Erckmann, T. Estrada[1], Y. Feng, U. Gasparino, J. Geiger, T. Geist, S. Geißler, U. Gerstel, L. Giannone, P. Grigull, H. Hacker, M. Haese, H.J. Hartfuss, O. Heinrich, G. Herre, C. Hidalgo[1], M. Hirsch, J.V. Hofmann, E. Holzhauer[13], K. Ida[7], R. Isler[5], R. Jaenicke, J. Junker[14], M. Kaiser, F. Karger, A. Kechriniotis[8], M.A. Kedves[10], M. Kick, A. Kislyakov[2], J. Kisslinger[14], C. Konrad, H. Kroiss, G. Kuehner, A. Kus, A. Lazaros[9], T. Luce[5], H. Maassberg, C. Mahn, W. Mandl, N. Marushchenko[4], K. McCormick, S. Morita[7], M. Murakami[6], H. Niedermeyer, M. Ochando[1], W. Ohlendorf, M. Peters[11], V. Plyusnin[4], F. Rau[14], H. Ringler, A. Rudyj, N. Ruhs, J. Saffert, J. Sapper[14], F. Sardei S. Sattler, F. Schneider, U. Schneider, G. Siller, E. Sizov[3], U. Stroth, G. Theimer, M. Tutter, E. Unger, F. Wagner, R. Waltz[5], A. Weller, H. Wobig[14], E. Würsching, S. Wurdack, H. Yamada[7], M. Zerbini[12], D. Zimmermann, M. Zippe, S. Zöpfel

ICRH (Ion Cycl. Resonance Heating)

M. Ballico, W. Becker, F. Braun, C. Hoffmann, F. Hofmeister, J.M. Noterdaeme, S. Puri, Ph. Verplancke, H. Wedler, F. Wesner (Technology Division)

NBI (Neutral Beam Injection)

K. Freudenberger, W. Ott, F.-P. Penningsfeld, F. Probst, E. Speth, R. Süß, A. Teubel (Technology Division)

W. Melkus (Central Technical Services)

Computer Centre

J. Gassmann, S. Heinzel, H. Lederer, I. Weidl

ECRH (Electr. Cycl. Resonance Heating)

W. Kasparek, G.A. Müller, P.G. Schüller (IPF Stuttgart)

H.U. Nickel, M. Thumm (KfK Karlsruhe)

A. Borschegovsky, S. Filchenkov, V. Isaev, A.G. Litvak, L. Lubyako, V. Malygyn, E. Suvorov, (IAP, Nizhny Novgorod)

V. Kurbatov, S. Malygyn (Salut, Nizhny Novgorod)

V. Il'in (Kurchatov, Moscow)

Plasma Surface Interaction Group

R. Behrisch, K. Ertl, R. Fischer, W. von der Linden, J. Roth, A. Schiavi, E. Taglauer, H. Verbeek

Division Berlin

A. Herrmann, D. Hildebrandt, B. Jüttner, P. Pech, H.-D. Reiner, H. Wolff

1) Guest from CIEMAT, Madrid (Spain)
2) Guest from IOFFE Institute, St. Petersburg (Russia)
3) Guest from Gen. Phys. Inst., Moscow (Russia)
4) Guest from Kharkov Inst. (Ukraine)
5) Guest from General Atomics, San Diego (USA)
6) Guest from Oak Ridge National Laboratory (USA)
7) Guest from Nat. Inst. for Science, Nagoya (Japan)
8) Guest from University of Patras (Greece)
9) Guest from Demokritos, Attiki (Greece)
10) Guest from KFKI Research Inst., Budapest (Hungary)
11) Guest from FOM-Instituut, Nieuwegein (Holland)
12) Guest from ENEA, Frascati (Italy)
13) Guest from IPF Stuttgart (Germany)
14) Experimental Plasma Physics Division 2

1. OVERVIEW

In 1993 the work on W7-AS was roughly divided into two parts: an experimental period until August and a technical phase continuing till February 1994. The experimental results were characterized by numerous insights into the structure and behaviour of the stellarator plasma, some of them only made possible by technological innovations and by the ongoing successful collaboration with Russian institutes, the IPF Stuttgart and KfK, as well as the Berlin Division.

The plasma wall problem, so crucial to the reactor, was tackled on a broad front. Notwithstanding the complicated three-dimensional structure of the island strings at the edge of W7-AS, it was possible to get a better grasp of the natural divertor of the stellarator plasma, both in the experiment and in the numerical model. It was found that the radial electric field always changes its sign at the transition between long and short con-

nection lengths of the flux lines. These connections between the distributions of the flux lines and plasma potential near the edge afforded insights into why the H-mode exists in a narrow ι-region in W7-AS.

Investigations of the H-mode in ECRH plasmas were made possible by the Russian 140 GHz gyrotron, whose output was raised to 900 kW. This marked a milestone in the application of high-power ECRH. The H-mode was also obtained at half the main field (1.25 T) and in hydrogen. The microwave generators, otherwise serving only for heating purposes, were used to demonstrate the basic feasibility of a novel scattering method for determining the ion temperature.

In addition to the previous preionization by ECRH which allows the operation only at the resonant main field strength, a non-resonant RF method was developed. Only then could the main field be freely chosen, allowing for the first time definite identification and detailed investigation of NI-driven global Alfvén eigenmodes. Because of their possible detrimental effect in connection with α-particle heating their avoidance could be decisive for a future fusion reactor.

Another major area of investigation was plasma fluctuations and their connection with plasma transport. For the first time it was possible to measure even temperature fluctuations, in the plasma centre by a new ECE correlation method ($\Delta T_e > 0.1\%$) and at the edge by means of a fast-sweep (1 MHz) probe.

Further developments in diagnostics prepared during shutdown are: a multichannel ruby laser Thomson scattering system allowing profiles to be measured in one shot (already in operation), a periodic multichannel Thomson scattering system using a pulsed Nd:YAG laser, a high-energy lithium beam diagnostic allowing density measurements to the centre of the discharge for $n_e < 4 \times 10^{13}$ cm^{-3}, spatially resolved H_α detection, toroidal rotation measurements, etc.

Two major assembly projects were carried out during the autumn shutdown period. All nine remaining endangered modular field coils were reinforced by an additional support structure of the type successfully tested in spring on one coil. Normal operation of the machine without severe restrictions will be possible after this difficult assembly. The second major modification was the assembly of five pairs of auxiliary limiters at the inner wall.

2. EXPERIMENTAL RESULTS

2.1 Boundary Layer and Plasma-Wall Interaction Studies

2.1.1 Resonant magnetic field structures and radial plasma parameter profiles at the edge

In W7-AS, large "natural" boundary magnetic islands belonging to the local rationals $\iota = 5/m$ offer the potential of open divertor operation. As a pre-study in this context, the impact of the islands on the edge plasma parameter profiles was investigated by two fast reciprocating Langmuir probes for varying configurations in the edge rotational transform range $\iota_a = 0.45$ - 0.6, including the 5/11, 5/10 and 5/9 resonances. The discharge conditions were chosen to keep the configurations close to the vacuum field: currentless, flat-top ECRH discharges with $P_{heat} = 160$ kW and $\langle n_e \rangle = 1 \times 10^{19}$ m^{-3}. The two main limiters were fixed at their outermost positions. Both probes were placed at a triangular plasma cross-section ($\phi = 72^o$): probe #1 at the outside triangular tip (x-point position for all resonant cases), probe #2 more towards the bottom (as a function of ι_a, also intersecting islands).

The edge plasma parameter profiles show strong, quasi-periodical variations with ι_a, which are clearly correlated to the 5/m separatrix positions. Fig. 1 shows examples of typical profiles measured by probe #2: In a) the probe intersects the 5/9 island. The limiters introduce finite, but very long connection

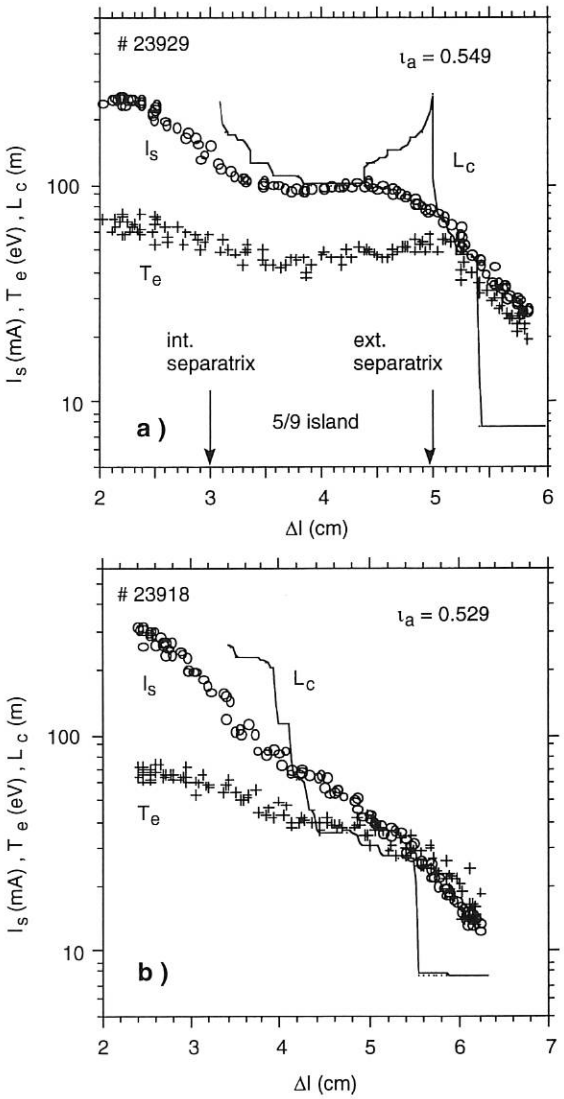

*FIG. 1: Edge profile broadening by 5/m boundary islands. Radial profiles of the ion saturation current I_s and electron temperature T_e from Langmuir probe #2 for low-ß, currentless ECRH discharges with (**a**) the probe line-of-sight intersecting the 5/9 island, and (**b**) the island formation suppressed by short connection lengths L_c.*

lengths L_c. Both the ion saturation current I_s and the electron temperature T_e profiles show pronounced flat regions inside the island. In case b), the island cannot be formed due to short L_c. The profile shoulders vanish almost completely. The space potential (not shown here) has, in the first case, a flat region inside the island, while in the second case there is a sharply pronounced maximum at the calculated separatrix position. By varying ι_a these profile types return quasi-periodically in keeping with to the occurrence and radial shift of the 5/m separatrix in very good agreement with vacuum field calculations. An exemplary overview on probe #1 results is given in Sec. 2.2.7, Fig. 9.

We conclude that the 5/m islands are a reality with respect to particle and energy transport. In cases with sufficiently long L_c they introduce a radial short-circuit by strong parallel components. Most of the profile shoulders we found can be explained in this way. The identified separatrix positions agree very well with vacuum field calculations, spatially as well as with respect to the ι scale (the latter within 10^{-3} of the current ratio I_{tor}/I_{mod}). This serves as basic information prior to further divertor studies.

From type b) radial density profiles, particle transport coefficients (averaged in the parallel direction) were zero-dimensionally estimated for $\iota_a = 0.34$ (limiter-bounded) and 0.53 (separatrix-bounded). They show a unique scaling with the inverse of the LCMS plasma density. For low to moderate densities and for the two poloidal probe positions, no indications of an ι-dependence or poloidal asymmetry were found within the limits of the simple model.

2.1.2 *Resonant flux coordinates for modelling plasma edge transport in separatrix-dominated configurations*

For "high ι" configurations ($\iota \geq 0.5$), the boundary topology of W7-AS exhibits open, divertor-like field structures (Fig. 2a) which are responsible for highly non-homogeneous recycling and wall load distributions. However, even in these cases field line tracing outside the LCMS generally shows ordered patterns reflecting the field structure of the dominant "natural" edge resonance $\iota = 5/m$. This common property of low-shear stellarators has been exploited to parametrize the space outside the LCMS by "open magnetic surfaces", which are spanned by field lines and smoothly match the LCMS and the separatrix of the main resonance.

A sample of the new surfaces, covering both the weakly stochastic region between the LCMS and the separatrix as well as the open regions ("island" and "private flux" regions) outside the separatrix, is shown in Fig. 2b. The surfaces well reproduce the patterns of a Poincaré plot including small cross-field diffusion. They are also consistent with the contours of the ion saturation current from 2D Langmuir probe array measurements. The new surfaces only depend on the magnetic topology, not on material structures.

In order to optimize the numerical treatment of plasma transport, a helically symmetric poloidal flux coordinate is defined by shifting the field lines towards resonance within the given surfaces. (Plasma transport is "as 2D as possible" in flux space.)

In a first application to a typical low-density ECRH discharge at $\iota(a) = 0.52$ with fully retracted limiter, the open magnetic surfaces were mapped onto the wall, yielding highly localized magnetic fluxes on a small impact area along the "helical edge" close to the "triangular" cross-section. Here, recycling fluxes consistent with Langmuir probe data were defined and used to simulate the 3D neutral gas distribution with the EIRENE code.

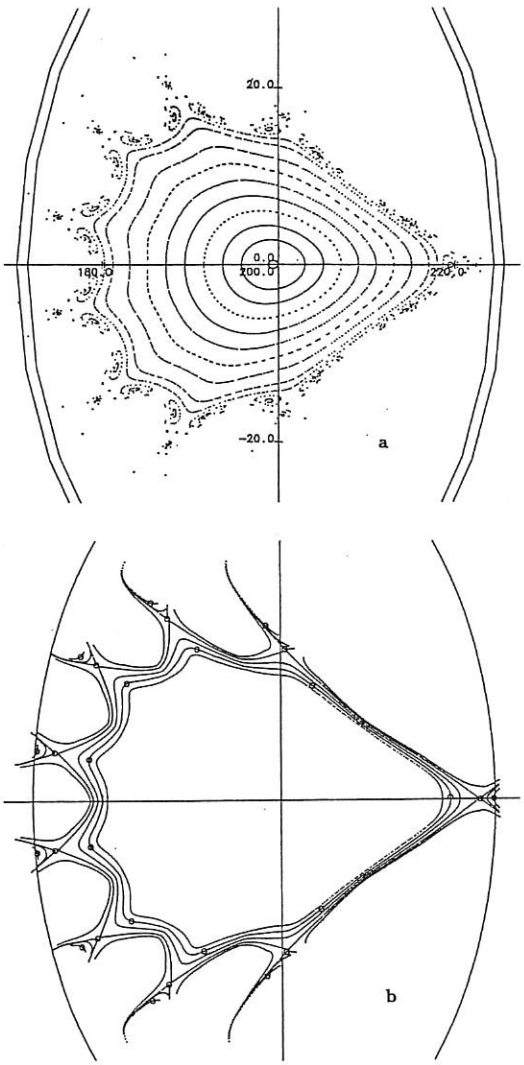

FIG. 2: Poincaré plot and radial coordinate system outside the LCMS. The dots on the new surfaces represent resonant flux coordinate lines.

2.1.3 *Correlation of low-energy CX fluxes from LENA with other plasma parameters*

The low-energy neutral particle analyser (LENA) was installed to deliver information on the T_i profiles near the plasma edge from the energy distributions of the CX neutrals. To achieve

reasonable statistical significance, this requires the addition of several hundred time of flight (ToF) distributions, which restricts the time resolution to ~100 ms. If integral quantities such as the total CX flux Γ or the mean energy <E> (which depends on the shapes of the energy distributions) are considered, the time resolution is only limited by the ToF repetition frequency of 7 kHz. Rapid events such as ELMs in the plasma edge can thus be observed in the LENA signals. By correlation techniques these events can be detected in spite of the rather large fluctuation levels due to counting statistics. Rapid fluctuations due to ELMs have been detected in Γ with a correlation of up to 0.7 with the H_α light observed at the limiter. ELMs hardly show up in the H_α light measured at the LENA port. The observed CX flux fluctuations are therefore mainly due to fluctuations of n_i rather than of n_0 (wall recycling). There are no significant changes of <E> during ELMs and therefore no changes of T_i at the edge are observed. Also in the case of ECRH modulations we observe modulation of Γ. There was some hope of this yielding information on the ion transport. However, the correlation of Γ with the ECRH power is < 0.3 in most cases and even smaller for <E>, and the observed time shifts of 2 to 6 ms are not yet reproducible.

2.1.4 *Sniffer probe analysis*

(in collaboration with U. Furuyama (Kobe University of Mercantile Marine, Japan))

The sniffer probe was moved to port 3/8 and initially used for isotope changeover monitoring. In contrast to earlier measurements (Ann. Rep. 1991) the isotope changeover was completed within about 40 standard shots, whereas in the period beginning with shot # 16126 (with hydrogen glow discharges during baking of W7-AS) it took approximately 400 shots. Boronization with B_2D_6 resulted in extremely clean deuterium discharges with less than 5% hydrogen during the pulse.

2.1.5 *Recycling studies*

Recycling of particles escaping from the bulk plasma by radial transport and refuelling the plasma after surface reflection or by surface release is the key to density control and thus operational flexibility. We investigated hydrogen recycling in W7-AS for various surface conditions. The influence of the limiter (boron-doped graphite) bulk temperature and the long-term behaviour after helium glow discharge cleaning (He-GDC) and boronization of the vessel was studied.

Experimentally, the decay of the plasma density was measured after the external gas feed was turned off at a stationary plateau $<n_e> = 1.5 \times 10^{19}$ m^{-3} (limiter-dominated plasmas at $\iota = 0.34$, B = 1.25 T, and heated by 360 kW of applied ECF power). The time constant $\tau_p^* = -N_p / (dN_p/dt)$ of the initial density decay (Fig. 3) can be related by a simple model to a generalized reflection coefficient r at the surface, a fuelling efficiency f of the scrape-off layer, confinement times τ_p of the plasma and τ_s of the surface, and the ratio N_{ex}/N_p of the numbers of externally supplied particles and plasma particles:

$$1/\tau_p^* = (1 - R)/\tau_p - S/\tau_s(N_{ex}/N_p - 1),$$

where R = rf/(1 – r(1-f)) and S = f/(1 – r(1-f)). The reflection coefficient r includes both elastic and inelastic reflection and approaches the value 1 for a hydrogen-saturated surface.

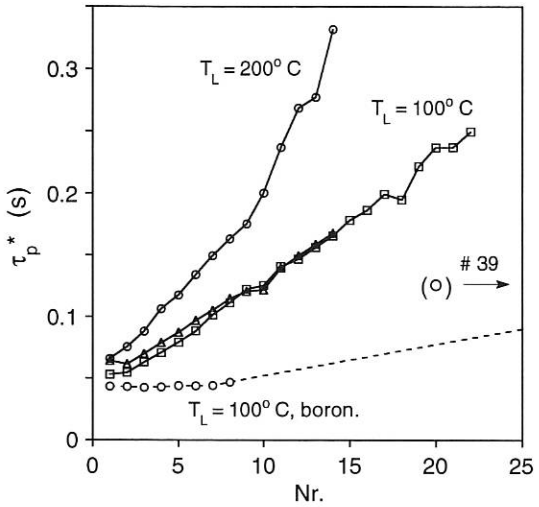

FIG. 3: Shot to shot evolution of the plasma density decay time after He-GDC (at 200 and 100° C) and after boronization (at 100° C). The dashed line interpolates to # 39 after boronization.

He-GDC is found to establish reproducibly low recycling conditions (low r) by hydrogen-depleted surfaces for the first shots after conditioning. In the course of subsequent plasma discharges a steady increase of recycling due to hydrogen enrichment in the surface is observed. The shot-to-shot increase is considerably faster for the higher limiter temperature (200° C). After boronization, recycling is initially comparable to the He-GDC conditioned surface but proves to be long-term stable at low level. Furthermore, the surface particle confinement time τ_s, which can be derived from the residual steady-state plasma density after decay, increases by an order of magnitude from about 0.5 s to about 3 s. The boron-coated surface therefore exhibits greatly improved pumping efficiency.

The analysis does not differentiate between limiter and wall surfaces. The sensitivity to the limiter temperature seems to indicate that recycling concentrates at the limiters (in accordance with the limiter-dominated boundary topology). However, the behaviour after boronization indicates that recycling is dominated by the wall rather than the limiters, because it is known from earlier results that the coating deposited by boronization is quickly eroded from the limiters. A possible explanation for this contradiction is that a significant fraction of wall recycling occurs after primary reflection at the limiters.

2.1.6 *Surface probe analysis*

The analysis of long-term collector samples gives evidence of localized erosion of surface layers from the wall by ion sputter-

ing during the operational period 1992/93. Wall erosion by ion sputtering has been observed for the first time in W7-AS and is most pronounced on wall locations with the closest proximity to the plasma (outboard midplane at triangular plasma shape). Earlier investigations showed dominant impurity deposition (Annual Report 1991) or melting phenomena (Annual Report 1992) at these locations.

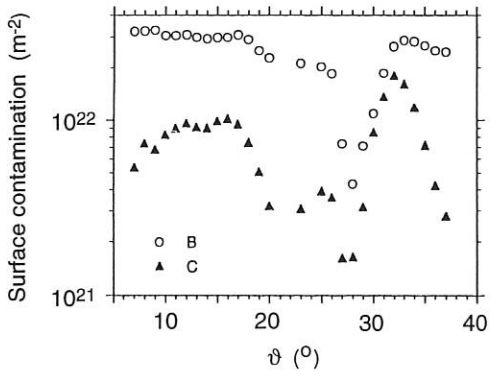

FIG. 4 : Impurity deposition on a long-term sample located at PHI = 221° (module 4). ϑ is the poloidal angle.

Fig. 4 shows the amount of boron and carbon measured on a long-term sample. Due to boronization a uniform boron coverage of about 2×10^{22} atoms/m^2 is expected. The measured boron distribution gives clear evidence of strongly localized erosion during successive plasma discharges at a theta of 28°. From earlier investigations and calculations we expect ion fluxes moving parallel to the magnetic field at a theta of about 28°, and those moving antiparallel to the magnetic field at a theta of about 15° at this toroidal location. This indicates that wall erosion is caused by ion fluxes moving parallel to the magnetic field. In contrast, significant wall erosion was not detected for ion fluxes moving antiparallel to the magnetic field. Similar observations were also made for modules 2 and 5.

With a new retractable wall sample, it was found that this erosion occurs during discharges with high iota values (ι = 0.53, B_t = 1.25 T) and retracted limiters. Obviously, particles with high kinetic energy reach the wall in these separatrix-dominated discharges. During the last operational period a large number of discharges were made with an iota of about 0.53, making the results from the long-term samples plausible.

Apart from sharp minimum at a theta of 28°, the carbon distribution shows two broad deposition maxima whose position is in accordance with earlier results. However, in contrast to earlier observations the larger deposition on the wall is found for particles moving parallel to the magnetic field.

The impurity flux measurements in the boundary plasma using the movable collector probe were continued. The collected boron fluxes with the BC limiter and boronized wall were as high as in the period with the TiC limiter and boronized wall in limiter-dominated discharges (ι = 1/3, open limiter). They were an order of magnitude lower with the BC limiter and a metallic wall (see Fig. 5).

An explanation is that the BC limiter surface was covered by contamination layers of carbon and oxygen, which prevented erosion of the limiter material during this period with the metallic wall. Effective and durable cleaning of the wall and limiter surface was not achieved during this period. Reduction of the carbon and oxygen contamination of all inner surfaces could only be achieved after boronization. This led to increased erosion of the limiter material and higher boron influxes from the limiter, which is also demonstrated by spectroscopic measurements. However, a beneficial effect of solid target boronization could not yet be confirmed. On the basis of a 1D impurity transport model a comparison of Langmuir and collector probe measurements with spectroscopic measurements in the core plasma was made, supporting this explanation.

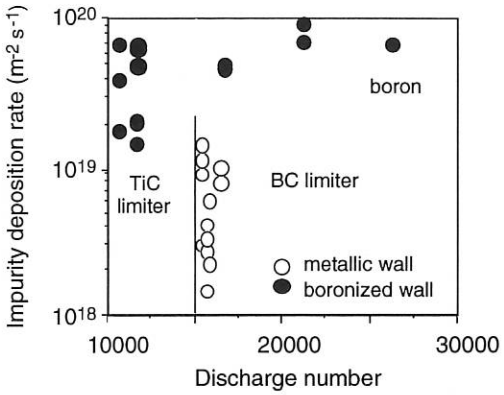

FIG. 5: Boron deposition rate in the boundary plasma in periods with different wall conditions and limiter materials.

2.2 Confinement and Transport

2.2.1 Isotope effect

In view of the favourable scaling of tokamak confinement with the ion mass it is of interest to look for a corresponding isotope effect in stellarators. In contrast to tokamaks, isotopic dependences are missing in the W7-AS H-mode properties. To investigate the ion mass scaling of W7-AS confinement, two series of equivalent discharges (B_t = 2.5 T, ι = 0.53, $n_e = 4.5 \times 10^{19}$ m^{-3}, 360 kW ECRH) in hydrogen and deuterium were analyzed.

A general trend of slightly improved confinement in deuterium was observed for most of the transport-relevant quantities investigated. The global energy confinement was 20% better in deuterium, whereas the electron thermal conductivity χ_e from heat wave analysis was lower by approximately the same amount. Impurity confinement times τ_{Al} deduced from laser blow-off injected aluminium were 30% higher in deuterium than in hydrogen. The central electron temperature (from ECE) slightly improved from 1.5 keV (in hydrogen) to 1.6 keV (in deuterium). No effect could be observed on the edge density and density decay length as measured by Langmuir probes.

These preliminary observations agree with an ion mass scaling of confinement like $\tau_E \propto A_i^{0.2}$, which is weaker but in the same

direction as in tokamaks. It must be stressed, however, that the observed differences are close to the reproducibility of single discharges and partly within the error bars (χ_e , τ_{Al}). In conclusion, the isotope effect in W7-AS is small, if it exists at all. It is necessary to improve the database to rule it out or quantify it with reliable accuracy.

2.2.2 *Iota dependence*

The statistically deduced scaling of the global energy confinement time τ_E of ECRH plasmas in W7-AS is found to be close to plateau scaling (P is the ECRH power):

$$\tau_E \sim a^{1.92}\, B^{0.61}\, n_e^{0.7}\, P^{-0.53}\, \iota^{0.3}.$$

It is different in form to scaling laws typically found for tokamaks which are expressed in terms of the plasma current. If the current scaling is rewritten in terms of B_t and ι, the tokamak scaling expressions become similar to the stellarator ones.

In order to explore the ι-dependence, which might also give a clue to understanding current scaling, discharges at ι-values with optimum confinement properties were studied in detail. For that purpose, discharges at $\iota \approx 1/2$ and $\iota \approx 1/3$ (B = 1.25 T, a = 0.13 m, 360 kW ECRH) were compared at the same density. In addition to the energy confinement, also the electron heat and the particle and impurity transport were analyzed.

The total plasma energy measured by the diamagnetic loop (W_{dia}) is used for studies of the energy confinement time. For local information the electron heat conductivity χ_e was calculated from a stationary power balance and from the investigation of heat wave propagation in the plasma. The particle diffusion coefficient at r = 0.8 a (≈ 0.1 m) was obtained from 3D-DEGAS code simulations and calibrated H_α-emission, measured at both limiters, which at a = 0.13 m were the dominant sources of neutral gas. Finally, the impurity transport coefficient was obtained from a simulation of the time traces of spectroscopic line emission from laser blow-off experiments.

On the assumption of an unperturbed magnetic configuration at the two ι-positions compared, there is evidence of a general improvement of confinement: A factor of 2-3 for the particle, 1.6 for the electron heat and only a small amount for the impurity diffusion coefficient. The unexpected strong scaling of τ_E ($\sim \iota^{0.7\text{-}0.8}$) diminished and disappeared, when operating with larger limiter apertures. This problem is the subject of the ongoing investigations.

2.2.3 *Density scaling*

In previous experiments in W7-AS, a strong favourable dependence of τ_E on density was demonstrated. From database regressions, a stronger scaling was observed ($\sim n^{0.7}$) for low to medium-density ECRH discharges than for NBI heated discharges ($\sim n^{0.5}$), which also could be sustained to very high densities. A strong density scaling of τ_E would be beneficial to a stellarator reactor because high confinement times could easily be achieved by increasing the density. Previously, the scaling behaviour at high densities could be studied in NBI plasmas only. Because of radiation, non-steady-state and power absorption effects, the analyses of high-density NBI discharges was, however, ambiguous.

Successful implementation of a 140 GHz gyrotron has now allowed the density scaling of pure ECRH discharges to be investigated for the first time up to a line-averaged density of 9×10^{19} m^{-3}. For this purpose, density scans were performed at $\iota \approx 1/3$, P ≈ 0.5 MW and B_t = 2.5 T. First results are shown in Fig. 6. τ_E improves up to a line-averaged density of $\approx 6 \times 10^{19}$ m^{-3}, where it turns into saturation similar to that observed in the tokamak SOC regime. The radiation losses never exceed 30% of the input power. The ion energy increases somewhat up to the highest density, whereas the electron energy content seems to saturate already at lower densities.

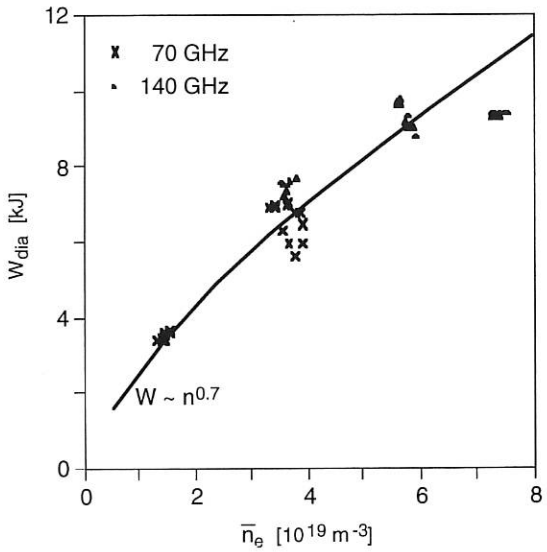

FIG. 6: Diamagnetic energy content as a function of line-averaged density for ECRH discharges (P = 420 kW and 470 kW in the 70 and 140 GHz phases, respectively) at ι = 0.34.

2.2.4 *International stellarator database*

A stellarator database working group has been established, working with data from ATF, CHS, Heliotron-E, W7-A and W7-AS. A working mode has been found and a detailed list of parameters for the data to be stored was defined. It contains global parameters which describe the device, discharge and plasma condition sufficiently accurately. Up to now, 822 observations have been contributed from the different stellarators and stored on the IPP VAX, which serves as host of the database activities. The goals of this work are: (i) availability of comparable databases of global confinement data for different stellarators, (ii) creation of a basis for investigating the influence of the magnetic field configuration on confinement and (iii) determination of a reliable scaling law for stellarator properties to predict the performances of future stellarator devices.

Furthermore, a mode has been found for the exchange of profile data. The relevant parameters, the radial grids for the pro-

files and the format of the data have been defined. First profiles have been exchanged between CHS and W7-AS and the transport and equilibrium (VMEC) codes used at the two institutions have been successfully benchmarked.

2.2.5 *Calculated plasma equilibria*

Calculations with the NEMEC free-boundary 3D MHD-equilibrium code mainly addressed two topics: configurations with different toroidal mirror ratios and configurations with toroidal net currents.

Model calculations for the configurations with different toroidal mirrors at $\iota = 0.34$ (see Sec. 2.2.6) were made to provide the transformations from real space to magnetic coordinates. For the different configurations, Fig. 7 shows the dependence of the axis shift on the central β value. In the triangular plane ($\phi = 0$) the shift is maximal for the configuration *R* with the largest radial excursions of the flux surfaces corresponding to the minimum in field strength.

Changes in the configuration are also expected from toroidal currents driven either internally like the bootstrap current or externally like the ohmic or ECCD current. Since NEMEC can take into account arbitrary toroidal current profiles, their effect on the magnetic configuration can be examined. Preliminary results show two apparent effects. Firstly, there is the change in the iota profile due to the additional poloidal field from the toroidal current density. This is expected and can be roughly described by means of the large-aspect-ratio approximation with circular flux surfaces. Nevertheless, with the effective plasma radius kept constant, the more complex 3D geometry leads to a stronger change of ι (a factor of 1.3 to 1.4) than estimated from the large-aspect-ratio approximation used in the W7-AS database. Secondly, the toroidal current leads to less

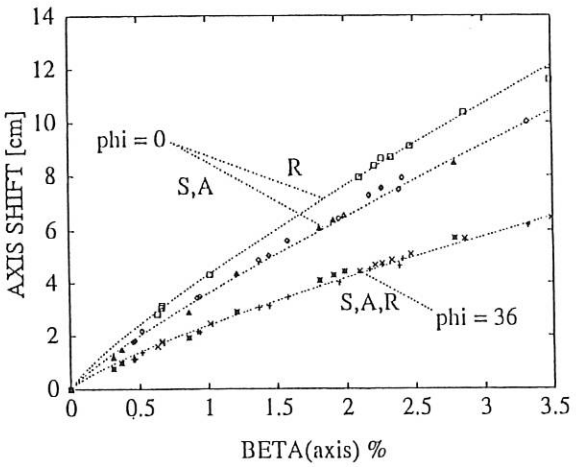

FIG. 7: Axis shift in the two main planes ($\phi = 0$ and $\phi = 36$) as calculated with the NEMEC free-boundary code for the three configurations described in Sec. 2.2.6. The equilibria have no toroidal net current density, and the pressure profile is taken to be $p_0*(1-s)$ <=> $\beta_0/\langle\beta\rangle = 2$

elongated flux surfaces. The results were compared with a calculation done with the KW code for a large plasma current (18 kA at 1.25 T). There is agreement concerning the iota profile but the flux surface geometry differs. This difference is currently being investigated. The bench marking of NEMEC with the DIVA tokamak equilibrium code used at ASDEX Upgrade shows full agreement in both the iota profiles and the flux surface geometry.

2.2.6 *High-β discharges at various mirror ratios*

Pilot experiments on NBI-heated high-β discharges in magnetic configurations with various values of the magnetic mirror were conducted. The configurations were inward-shifted for ECRH start-up with $\iota(a) = 0.34$, a = 0.15 m and $B_t = 1.26$ T at the heating location ($\phi = 36^o$). The standard configuration (*S*) with a mirror ratio MR ≈ 1% was compared with configurations with MR ≈ 10%. In the mirror configurations, the toroidal field assumed either a maximum (*R*) or a minimum (*A*) value at $\phi = 36^o$. Hence, the toroidal average of B_t was different by ≈ 20% in the extreme configurations. Another difference relevant to neoclassical transport and possibly also to stability is the fraction and location of the trapped particles: From *S* to *A* and *R*, the fraction increases from ~ 30% to ~ 45%. Furthermore, the majority of the trapped particles are shifted from a region of favourable to unfavourable curvature for stability when changing from *R* to *A*.

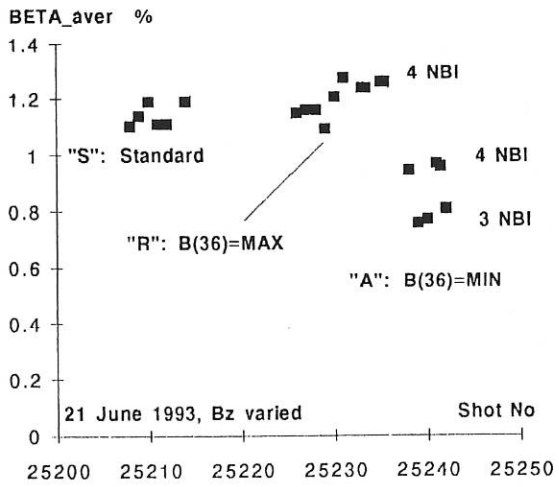

FIG. 8: Preliminary comparison of average β-values obtained in NBI experiments in W7-AS at various mirror ratios.

In the various configurations, the measured stored energies at full NBI power range between 8 and 11 kJ. Diamagnetic β-values of 1 and 1.2% were derived form these data, see Fig. 8. Marginally larger values are obtained in configuration *R*, where the average magnetic field was about 10% smaller than in the *S* configuration. The lowest values are found for configuration *A*, which has the highest average B_t value. For the electrons,

$\beta(0) / \langle\beta\rangle \approx 3$ was deduced from Thomson profiles. The experimental conditions have to be improved for the *R*-configuration, where a higher impurity radiation level was found.

2.2.7 *H-mode*

In W7-AS the H-mode was observed for the first time in a currentless stellarator plasma. H-modes are achieved with 0.4 MW Electron Cyclotron Resonance Heating with 140 GHz at 2.5 T and high density, but also with 70 GHz at 1.25 T and lower density and with neutral beam injection. The H-phases display all characteristics known from tokamak H-modes, including development of an edge transport barrier, increase of the poloidal impurity flow velocity at the edge, reduction of edge turbulence and ELMs (see Ann. Rep. 1992). The power threshold for the H-mode seems to be lower than that in tokamaks but is in agreement with $\bar{n}_e B_t$ scaling . The power threshold is shown in Fig. 9 in comparison with the results from tokamaks.

The documentation of H-mode transition was expanded with more detailed documentation on edge poloidal flow and edge fluctuations. For the first time density fluctuations were measured via true phase fluctuations in the reflectometry signals. True spectral measurements are possible with heterodyne detection only. The RMS level of turbulence fluctuations decreases by a factor of about 10 for $f \leq 10$ kHz and about 3 for the frequency range up to 200 kHz (see also Sec. 2.4.4).

An intriguing aspect of the H-mode of W7-AS is its limitation to a narrow range of ι around $\iota_a \approx 0.53$. In the following we describe the peculiarities in the vacuum configuration in this ι-range. Magnetic shear of the vacuum field configuration is small and positive and grows with ι_a and minor radius r. The variation of iota in the range of interest is shown in Fig. 9a. From edge studies it is known that the major features of the vacuum configuration remain at the edge even with plasma (see Sec. 2.1.1).

The plasma edge is shaped by the inner separatrix of the 5/9 (= 0.556), 10/19 and the 15/28 field perturbations. The 10/19 island chain has a typical island width of about 1 cm. This zone might be partly ergodized. An important aspect could be that the plasma cross-section is large at $\iota_a \approx 0.53$ and the separatrix zone is in a radial range of comparatively large magnetic shear (see Fig. 9a).

At $\iota_a \approx 0.53$, the plasma size is large and the plasma surface is well defined by a short connection length within the SOL. As a consequence, this ι_a-range is characterized by the existence of a well-defined and singular velocity shear layer even in these non-H-mode discharges. Figure 9b shows the radial variation of the space potential. The relevant iota range is qualified by a precise definition of the edge.

It seems that the iota range $\iota_a \approx 0.53$ has the potential to realize the required H-mode transition conditions. There is no other iota range within the W7-AS field configuration with the same match of properties. It is not yet known whether the iota range for H-mode operation can be extended by more heating power.

The W7-AS results first confirm the tokamak findings that a separatrix eases the spontaneous transition into the H-modes. The separatrix-specific aspect could be to shift ionization predominantly into the SOL and thus give rise to a reduction of energy and momentum losses inside the separatrix. Another aspect of this iota range is the precise formation of the velocity shear layer and of short magnetic shear length at the periphery. This will limit the radial correlation length of the turbulence and thus may make shear flow decorrelation work.

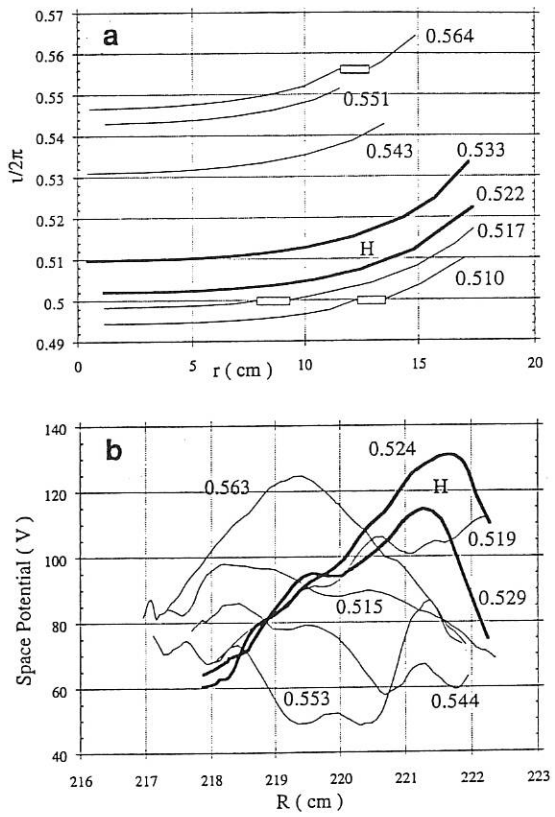

*FIG. 9 (**a**) Iota profiles of the vacuum field in the ι_a-range of interest here. The thick line is the corresponding profile where the best H-mode development occurs. (**b**) Radial profiles of the space potential around the plasma edge (200 cm is the major radius).*

2.2.8 *Neoclassical ion transport*

Ion temperatures of up to 0.8 keV measured by active charge exchange diagnostics have been obtained in W7-AS. The heating was done by combined off-axis ECR (400 kW at 140 GHz, 325 kW at 70 GHz) and NBI heating (510 kW absorbed power) at moderate densities of $n_e(0) = 9 \times 10^{19}$ m^{-3} ($T_e(0) = 1$ keV) and at $B_t = 2.5$ T. A similar experiment with combined on-axis ECRH (400 kW at 140 GHz) and NBI (~170 kW) at a lower density of $n_e(0) = 6 \times 10^{19}$ m^{-3} resulted in $T_i(0) = 0.7$ keV and $T_e(0) = 1.75$ keV. Different heating scenarios always yielded lower ion temperatures: In discharges heated by ECR only ($P \leq$ 0.725 MW) at densities of up to 6×10^{19} m^{-3} the central ion temperature never exceeded 550 eV. In purely NBI heated ($P \leq$

1.5 MW) discharges at densities between 6 and 30×10^{19} m^{-3} ion temperatures of 300-400 eV have been obtained.

The above described discharges with pure ECR, pure NBI and combined ECR and NBI heating were analyzed in a power balance. The neoclassical DKES code was used to assess the level of the ion energy transport. The experimental energy transport of the ions is consistent with neoclassical theory only if the ambipolar electric field is taken into account. This holds for the ion plateau regime (pure NBI) as well as for moderate LMFP conditions (combined ECRH / NBI) (see Fig. 10). The radial electric field calculated from ambipolar diffusion, however, is rather small ($e\Phi \approx kT_i$ only in the gradient region). Higher fields would be desirable in order to reduce the neoclassical ion heat transport, which at medium and high densities is the dominant loss process in W7-AS.

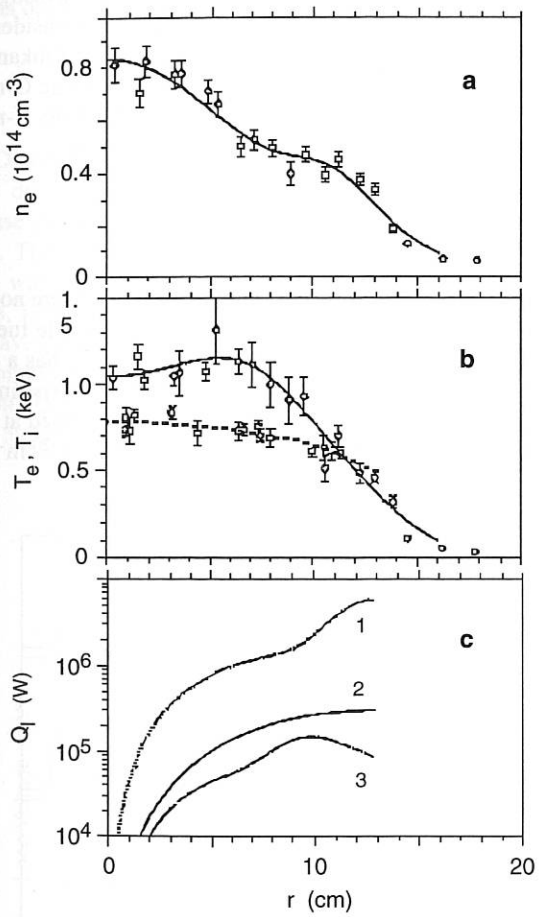

*FIG. 10: (**a**) n_e, (**b**) T_e and T_i profiles and (**c**) ion power balance (2: experimental ion heating power, 1: neocl. ion heat loss without, 3: with ambipolar electric field) for a combined heating discharge.*

In experiments further into the LMFP or with a different helical ripple which can be produced in W7-AS the validity of neoclassical predictions can be checked.

2.2.9 *Impurity transport*

In addition to laser blow-off and profile measurements of impurity lines, a new method of studying the transport behaviour of impurities has been implemented on W7-AS. The method, which was developed on ASDEX, works as follows: a sinusoidally modulated influx of a tracer impurity is detected by time- and space-resolving spectrometry of radiation due to different ionization states within a wide spectral range from soft-X ray to visible. A transformation of the continuity equation for the tracer particles gives expressions for the diffusion coefficient and drift velocity. By measuring the phase and amplitude of the line radiation, experimental transport coefficients can be obtained from these expressions.

Series of steady-state ECRH discharges at $B_t = 1.27$ T, P = 370 kW, $\iota = 0.34$ and $n_e = 1.2 \times 10^{19}$ m^{-3} were analyzed with sulphur as tracer impurity. The modulation frequency was 5 Hz. First analysis of the data could be performed for the core plasma up to an effective radius of a = 0.1 m. The results are depicted in Fig. 11. Up to now data at B = 2.53 T cannot be analyzed self-consistently. An improved experimental technique will be applied in the next period of experiments.

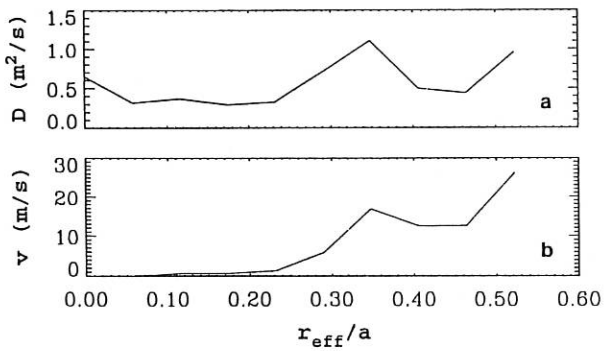

*FIG. 11: Diffusion coefficient (**a**) and inward drift velocity (**b**) from experiments with sinusoidally modulated influx of sulphur.*

2.2.10 *Transient transport studies*

To clarify possible dependences of the energy transport coefficient (χ_e) on heating power and electron temperature, we investigated the transient behaviour of discharges during energy increase and decay after switch-on or -off of a large amount of heating power. The experiments were performed on ECRH plasmas at low densities. τ_E ranged from 6 to 12 ms at B_t = 1.25 T and $\iota \approx 1/3$. Power balance analyses were carried out in the transient phases relying on density profiles from Thomson scattering and electron temperature profiles from ECE with a time resolution of 0.1 ms. The radial and temporal evolutions of χ_e deduced from the power balance analysis are shown in Fig. 12. It can be seen that χ_e reacts to changes in heating power in times as short as 1 ms. The change is much faster than the modification in T_e or the temperature gradient. χ_e therefore cannot depend in a simple form on the electron temperature. A heuristic model for χ_e which simulates changes with heating

power on a much faster than the diffusive time scale has been successfully used in time-dependent simulations of the temporal evolution of the ECE electron temperature. Furthermore, the model was also successfully used in the simulation of the main experimental features found from heat wave studies in W7-AS.

The investigation of transport by power balance and heat wave techniques is especially fruitful if the results from the two methods can be compared. Comparisons of the χ_e deduced from the two methods gives information about its dependence on the temperature gradient. In W7-AS, the fact that the χ_e values from heat wave and power balance analyses agree within a factor ≤ 1.5 indicates that χ_e is not a strong function of the temperature gradient. Finally, a temperature dependence of the transport coefficient would make χ_e, as deduced from heat waves, modulation frequency dependent. The experimentally found weak dependence (see Fig. 13) of the heat wave χ_e on the modulation frequency is another indication that χ_e is not a simple function of T_e.

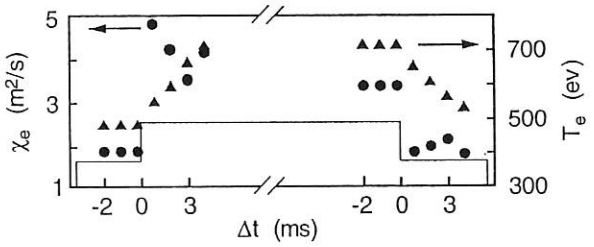

FIG. 12: Radially averaged T_e and χ_e values as a function of time relative to the switch-on and -off of 0.6 MW ECRH power, indicated in the box diagram.

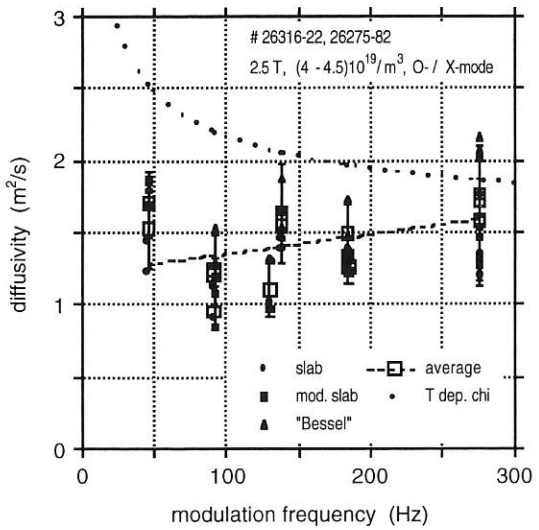

FIG. 13: χ_e deduced from heat wave analysis using different analysis techniques as a function of the modulation frequency. The dotted line shows the expectation if χ_e depended on the electron temperature.

2.3 ECRH / ECCD

2.3.1 *High-power 140 GHz experiments*

First plasma experiments with 140 GHz ECRH were performed with a microwave power of up to 0.9 MW from a single source, and 0.7 MW was launched into the plasma (for details see Sec. 5.3). An advanced prototype gyrotron with a power output of 0.5 MW for 1.1 s or 0.9 MW for 0.4 s from the development line of IAP Nizhny Novgorod, Russia, was successfully operated at W7-AS in collaboration with the Russian institutes, IAP (Nizhny Novgorod) and Kurchatov (Moscow), IPF (Stuttgart) and KfK (Karlsruhe). The application of 140 GHz ECRH overcomes the density restrictions imposed by the cut-off condition of the previous 70 GHz system and opened a new parameter window with respect to density and power for plasma physics investigations. Plasma start-up, pure ECRH and the combination with NBI were investigated. The 140 GHz ECRH system at W7-AS may be considered a reference system for both next-step stellarators and tokamaks, because it satisfies ITER requirements at 1st harmonic O-mode and W7-X stellarator requirements at 2nd harmonic X-mode operation except for the CW operation requirement.

2.3.2 *Combination of ECRH and NBI*

Typical high-power NBI-heated plasmas in W7-AS are nonstationary, because the combined effect of beam particle fuelling (typically 1×10^{20} s^{-1} (for 0.35 MW) and recycling has a comparable contribution which causes a density rise. Experiments with combined ECRH and NBI heating were performed at densities of around $n_{e0} \approx 5\times10^{19}$ m^{-3} and $n_{e0} \approx 1\times10^{20}$ m^{-3}, re-

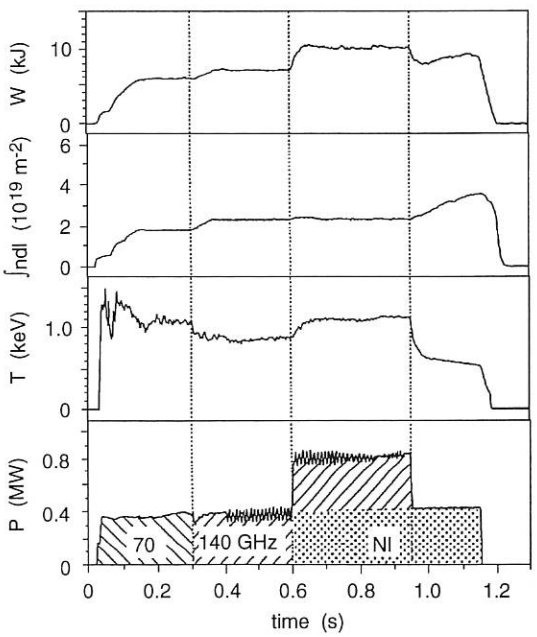

FIG. 14: Time evolution of the stored plasma energy W, the line-integrated density ∫ndl, the central electron temperature (SX) and the input power P for combined heating with on-axis ECRH and NBI.

spectively, with both on- and off-axis power deposition of ECRH. An example with on-axis ECRH at $n_{e0} \approx 5 \times 10^{19}$ m^{-3} is seen in Fig. 14. During the ECR-heated prephase and the combined heating phase density control is maintained by feedback-controlled gas puffing, whereas after switch-off of ECRH the density increases with the external gas feed turned off. The density could also be controlled with a combination of 0.75 MW ECRH and 0.7 MW NBI heating. As a rule, the density control could be maintained only if the ECRH power was approximately equal to or larger than the NBI power. Evidence of degraded particle confinement in presence of strong ECRH emerges from the profile development in the different heating cases.

The impurity confinement was investigated by Al laser blow-off experiments and degrades also during combined heating, i.e ECRH may provide tools for impurity control in steady-state plasma operation.

2.3.3 *Electron cyclotron current drive*

ECCD was investigated at W7-AS, where the comparatively small driven currents can be measured with high accuracy because of the absence of large 'obscuring' current as in tokamaks. The sensitivity of ECCD with respect to trapped particles was investigated in different magnetic field configurations, i.e. with different populations of trapped particles in the wave-particle interaction region. The required loop voltage for compensation of the EC-driven current and the bootstrap current ($I_p = 0$) is plotted as a function of the launch angle in Fig. 15a for two cases.

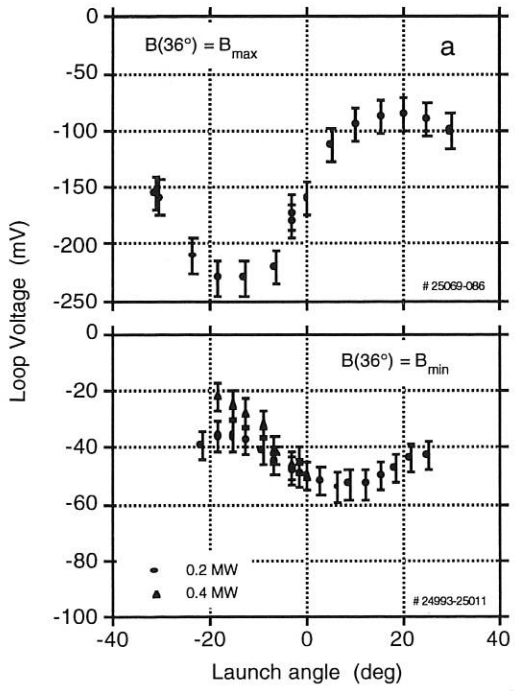

FIG. 15a: Loop voltage response on a launch angle scan with plasma net current $I_p = 0$ for two magnetic field configurations. The discharges are heated with 0.4 MW ECRH, and the launch angle scan is performed with 0.2 MW (dots) and 0.4 MW. (▲)

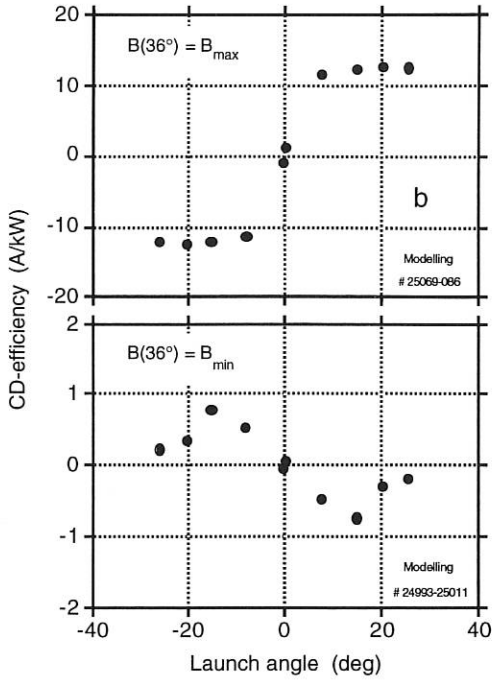

FIG. 15b: Theoretical modelling of the experiment. Note the different scales.

For case 1 the maximum of the magnetic field is located at the poloidal plane, where ECRH is launched, i.e. the trapped particles are mainly located outside the wave-particle interaction region and their impact on the ECCD efficiency is mainly due to friction with the current-carrying passing particles (standard case). In case 2 the minimum of the magnetic field is placed in the plane where ECRH is launched and consequently a considerable fraction of the injected ECRH power interacts directly with trapped particles, which do not contribute to ECCD.

The loop voltage for perpendicular launch (no ECCD) is non-zero and indicates compensation of the bootstrap current alone. Two effects are clearly seen, viz. the loop voltage and thus the driven current are much smaller in case 2 and the ECCD efficiency even changes sign. This is in agreement with theoretical predictions using linearized theory in the long mean free path. The reversal of the sign as compared with the usual current drive mechanism is a consequence of ECRH-induced trapping of otherwise barely passing particles.

2.3.4 *Power modulation and deposition profile*

The power deposition profile was measured by fast modulation of the microwave power with modulation frequencies of up to 8 kHz and a modulation amplitude in the range of 10-30% of the launched power. The well-known 'stimulated heat wave propagation method' is generally used to examine the heat dif fusivity. For sufficiently high modulation frequency, however, the characteristic radial amplitude decay length of the perturbed electron temperature becomes comparable to the power deposition profile and the relation between the deposited power and the amplitude of the temperature perturbation converges to

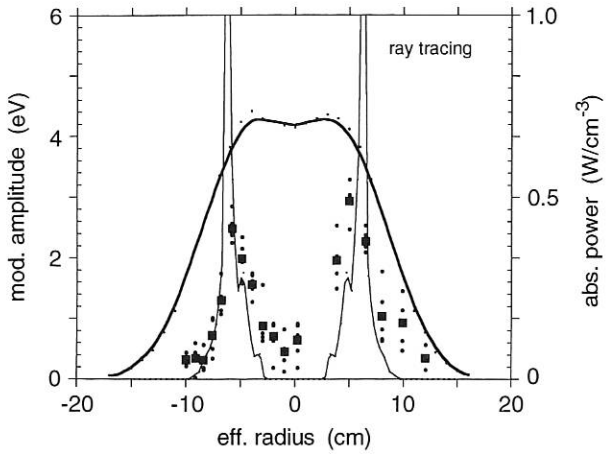

FIG. 16: Electron temperature modulation amplitude (dots, squares: averaged) measured by ECE diagnostics and the electron temperature profile as a function of the effective minor radius for off-axis ECRH at r_{eff} = 6 cm. Ray tracing calculations are included for comparison.

$\delta P_{abs} = 3/2\ \omega_{mod}\, n_e\, \delta T_e$. Thus the power deposition profile can be directly measured by this method. An example is given in Fig. 16 for a discharge with 0.2 MW ECRH and characterized by $n_{e0} = 2.5 \times 10^{19}$ m^{-3} and T_{e0} = 1.1 keV, where the microwave beam was launched 6 cm off-axis in the vertical direction.

The electron temperature profile is flat within the power deposition region and is also plotted in Fig. 16 as a reference. The microwave beam power was square-wave modulated with 2 kHz and a modulation amplitude of about 20%. The FWHM of the power deposition profile from ray tracing calculations is about 3 cm and is slightly smaller than that measured.

2.4 Modes and Fluctuations

2.4.1 Global Alfvén eigenmodes

(in collaboration with D.A. Spong, ORNL)

Some experimental and theoretical aspects concerning neutral beam destabilized global Alfvén eigenmodes (GAE) were investigated in detail. In particular, the issue of the relation between the observed mode frequencies (15-35 kHz) and the Alfvén velocity (v_A) was clarified by a magnetic field scan using a 900 MHz RF generator to create the NBI target plasma non-resonantly. The measured frequencies of the observed (m,n) = (3,1) modes (X-ray measurements) are compared in Fig. 17 with the calculated threshold shear Alfvén frequencies $(k_{\|,m}\, v_A)_{min}$, which correspond approximately to the theoretical GAE eigenfrequencies. In the calculations the value $k_{\|,m} = 3.2 \times 10^{-4}$ cm^{-1} derived from the rotational transform profile was used. This result is considered as clear evidence of GAE's in W7-AS.

MHD calculations including a gyrofluid model for the fast particles show that the energetic particle destabilization of GAE's in W7-AS mainly occurs by ions with parallel velocities clear-

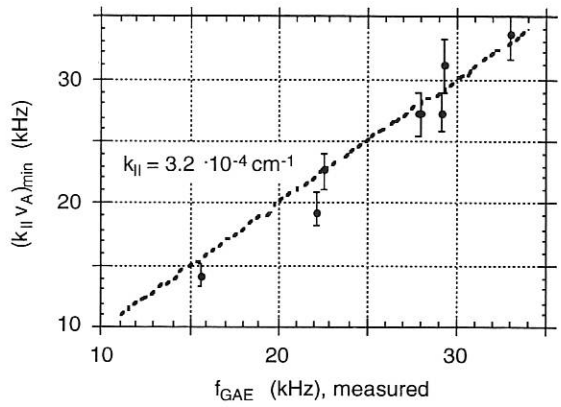

FIG. 17: Predicted GAE frequencies plotted versus the (3,1) mode frequencies observed during a magnetic field scan.

ly below v_A. In most cases, where GAE's are found, the full destabilization therefore takes place via the toroidal m±1 sideband drift resonances at much lower particle velocities $v_{res} = |\omega_{GAE} / k_{\|,m\pm1}| \ll v_A$, because $|k_{\|,m\pm1}| \gg |k_{\|,m}|$ due to weak shear in W7-AS. The contributing particles in the slowing down distribution are mainly those injected with 1/3 of the full NBI energy. It could also be verified experimentally that the resonance conditions of co- and counter-injected particles can be different. These details of the fast particle distribution, however, are not presently included in the gyrofluid model.

In addition to the X-ray and ECE emission, the modes are also observed as density fluctuations in μ-wave reflectometer, μ-wave scattering and H_α signals. A global mode structure extending from the plasma interior to the edge can be inferred from all these measurements. Radial displacements of the equilibrium magnetic surfaces due to the modes of up to ≈ 1 cm, consistent with observed magnetic field perturbations of

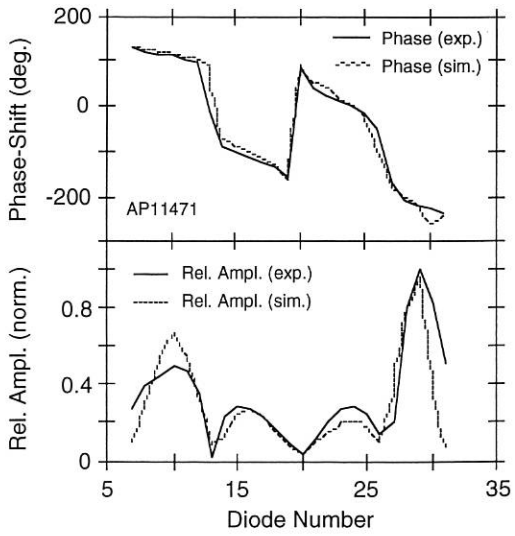

FIG. 18: The poloidal and radial mode structures (m=3) and the direction of propagation are determined from fitting the amplitudes and phases of the X-ray modulation by simulation calculations.

$\tilde{B}_\theta / B_0 \leq 10^{-4}$ at the edge, are inferred from the measurements. The reconstructed mode structure from simulations of the X-ray modulation profiles (amplitudes and phases, Fig. 18) is compared in Fig. 19 for the case of an m=3 GAE with predictions of nonlinear model calculations.

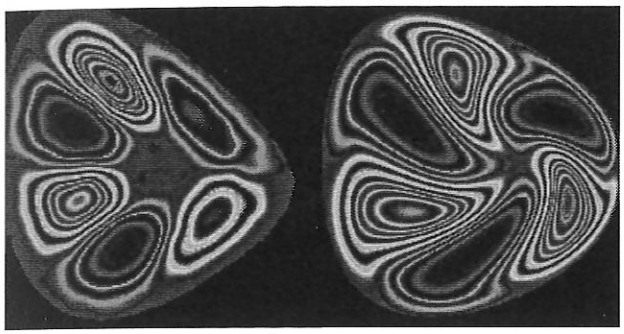

FIG. 19: m=3 mode structure (displacements) as derived from the X-ray simulations (left) and the result of a gyrofluid model calculation (right).

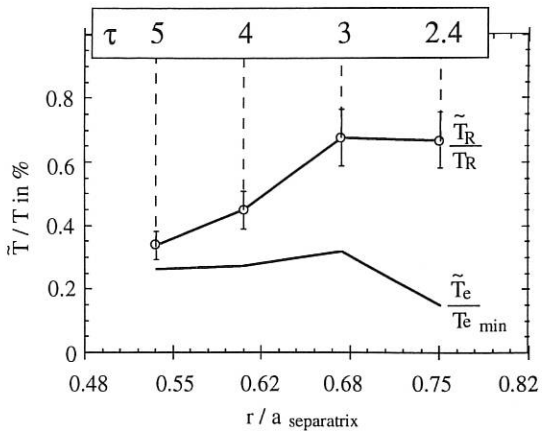

FIG. 21: Measured fluctuation levels at W7-AS at τ_a = 0.53, ECRH heated plasmas at B = 2.5 T, e.g. discharge 23440. The radiation temperature fluctuations (upper curve) are corrected to give the electron temperature fluctuations with a fixed value of density fluctuations and the local value of the optical depth (τ). The corrected values (lower curve) give a minimum value of the electron temperature fluctuations.

2.4.2 *Core temperature fluctuation measurements, method and results*

Turbulent fluctuations of the electron temperature in the plasma core can be relevant to the observed anomalous electron heat conductivity. A relative fluctuation level as low as a few 0.1% could be sufficient to explain a significant amount of the anomalous transport. Standard ECE temperature diagnostics provide the temporal and spatial resolutions, but the sensitivity to small-scale fluctuations is limited by natural fluctuations of the ECE due to the thermal nature of this radiation. The sensitivity to temperature fluctuations is restricted to values above 6%. Smaller fluctuation levels are buried completely under the thermal noise, and correlation techniques must be applied. An intensity interferometer arrangement is applied here (Fig. 20). In this arrangement the thermal noise in both sightlines is uncorrelated if the angle between the crossed lines of sight is above a few degrees, due to the spatial coherence properties of thermal radiation. However, the temperature fluctuations in the common emitting volume remain correlated.

First experiments on W7-AS have been conducted with purely ECRH plasmas at B = 2.5 T characterized by broad, flat density profiles with a central density of 5×10^{19} m^{-3} and peaked temperature profiles with a central temperature of about 1.5 keV. Fluctuations were found in the frequency range up to 150 kHz. The relative level depends on the radial position. In the range $0.5 < r_{eff} / a < 0.75$, accessible in this experiment, the fluctuation level is of the order of 0.5%, as seen in the upper curve of Fig. 21. A main problem of this kind of measurement is the finite optical depth τ of the emitting volume. Only in cases of high optical depth does the radiation temperature T_R measured by the ECE diagnostics approach the electron temperature T_e. Since the optical depth is proportional to the product $n_e T_e$, density fluctuations might increase the measured fluctuation level of the radiation temperature via modulation of the optical depth.

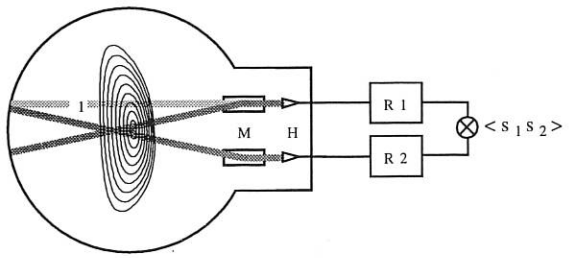

FIG. 20: Experimental arrangement for the ECE correlation experiment. Temperature fluctuations are determined by cross-correlating the signals of the two radiometers R1,R2.

With a density fluctuation level of 2%, as inferred from reflectometry, the measured fluctuation levels of the radiation temperature must be corrected, resulting in clearly lower electron temperature fluctuation values, on the assumption that temperature and density fluctuations are in phase. The resulting minimum level of T_e fluctuations is shown in the lower curve of Fig. 21. With a phase relation between T_e and E fluctuations for maximum transport, the fluctuation levels observed can be transport relevant.

2.4.3 *Density fluctuation measurements from microwave scattering at various rotational transforms*

A new 156 GHz microwave scattering diagnostic went into operation and successfully demonstrated its performance in measuring density fluctuations in the region between the plasma core and plasma edge. It has 4 distinct scattering angles of 6°, 12°, 40° and 50°, corresponding to a scattering wave vector of k_s = 340 - 2800 m^{-1}, and uses heterodyne detection to eliminate oscillator drifts and determine the propagation direction of fluctuation according to k_s.

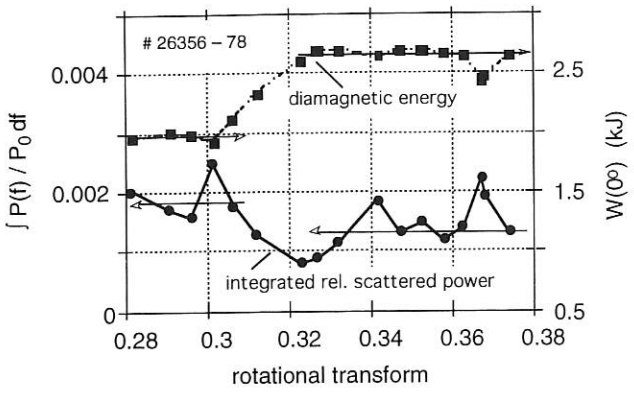

FIG. 22: The integrated relative scattered power and the diamagnetic energy during a scan in rotational transform. The arrows indicate roughly the mean values below and above ι = 0.3. The scattered power shows an anti-correlation with the plasma energy.

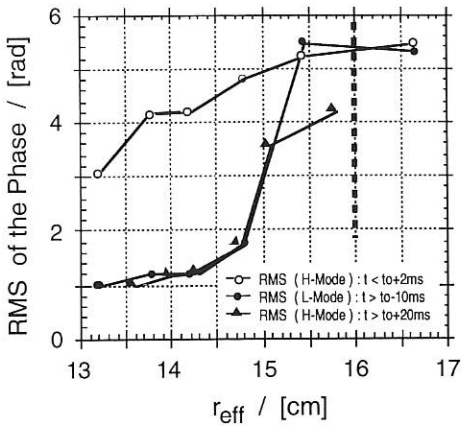

FIG. 23: Radial dependence of the RMS of measured phase fluctuations before (open circles), immediately after (closed circles) and more than 20 ms after (triangles) the L-H transition as indicated by the H_α-drop.

For a series of plasma shots with varying rotational transform ι = 0.28-0.38 the scattered power was measured at an angle of 6°. This chosen scattering wave vector of 340 m^{-1} is the nearest possible to the expected maximum of fluctuations in k-space. The plasma discharges were purely ECR-heated at a magnetic field of 1.27 T and fixed line density. The scattered power was analyzed by integrating the Fourier spectrum in the range of 5 - 200 kHz on both sides of the carrier frequency and related to the undisturbed power of the transmission line. As a first result Fig. 22 shows a variation of more than a factor two in scattered power at different rotational transforms. This anti-correlates with the diamagnetic energy content either below or above ι = 0.3. Nearly all spectra also show coherent mode activity at frequencies around 80 kHz.

2.4.4 *Reflectometry measurements during L- and H-modes*

Density fluctuations in the near edge region of L- and H-mode plasmas were investigated by heterodyne reflectometry. The results obtained with fixed frequency operation in a series of discharges (B = 2.5 T, ι = 0.53, heated with 140 GHz ECRH) are summarized in Fig. 23: The root mean square (RMS) of the measured phase fluctuations is plotted before (○) and immediately after (●) the transition as a function of the effective radius. The limiter position is also included. With the L-H transition an abrupt decrease of phase fluctuations by a factor of about 3 is observed for r_{eff} more than 1 cm inside the limiter position. It corresponds to a decrease of the density fluctuations $\Delta n/n$ from about 9% to 3%. Fig. 23 also includes the RMS data for the H-mode more than 20 ms after the transition (▲). Due to the steepening of the density profile the probed cut-off layer positions are changed. Especially the outermost densities probed shift within the limiter position. They therefore follow the decrease of the fluctuation level with a certain time delay.

With the transition the spectral power decreases in the whole range of fluctuation frequencies investigated (5 to 500 kHz), but this decrease is more pronounced for low frequencies.

During the H-mode bursts (ELMs) appear in the reflectometry phase fluctuations which are also observed in the H_α, soft-X and Mirnov coil signals. The fluctuation spectrum then nearly returns to L-mode conditions, i.e. especially the low frequency component increases as soon as a burst appears.

2.4.5 *Fluctuations in the scrape-off layer*

Fluctuations in the scrape-off layer of tokamaks and stellarators are investigated because of their importance for the transport coefficients in the SOL and hence for the power density at the target plates of a reactor.

In both stellarators and tokamaks the same basic effects seem to work in the scrape-off layer. Measurements with arrays of Langmuir probes and observation of the H_α light from the plasma edge were made on the former ASDEX tokamak and on W7-AS. These provide the experimental basis for a model applicable to both devices.

Because of the high correlation length of the fluctuations in the SOL along the magnetic field, effects at the target plates may not be neglected. With a 2D fluid equation system and the relations between the current density, particle and heat transfer, and sheath potential at the target plate, a linear stability analysis for the SOL was performed. In this model the boundary conditions at the sheath and the pressure gradient together with the magnetic field curvature play the major roles.

Instability is found below a limiting poloidal wavelength in the region of unfavourable magnetic curvature. Experimental observations of characteristic wavelengths and correlation times of the fluctuations agree fairly well with the expectations from this model.

Particle diffusivities were calculated from the dispersion relation using the Kadomtsev-Pogutse estimate ($D \approx \gamma \cdot k^2$). A simplified scrape-off layer model was worked out on the basis of this diffusivity. The predictions of this model are compared

with the measured density and pressure gradients in the SOL of ASDEX in a wide range of parameters. If the SOL temperatures are not too low, good qualitative agreement is found. Quantitative agreement cannot be expected, because of the crude estimate of D. For example, Fig. 24 compares the predicted with the measured density decay lengths.

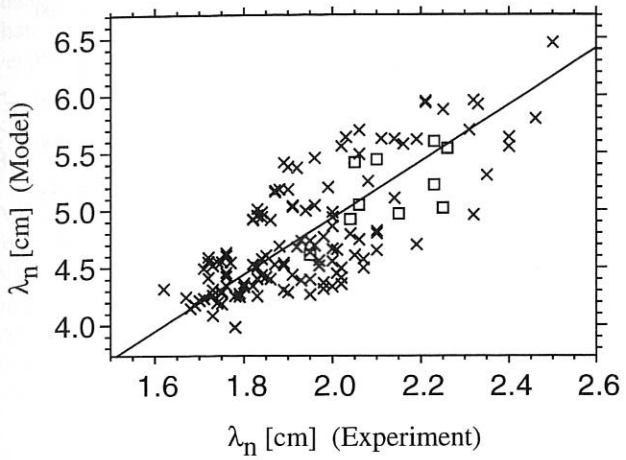

FIG. 24: Comparison of predicted and measured density decay lengths.

Due to the lack of reliable temperature fluctuation diagnostics fluctuations of T_e could not be taken into account in the past. The development of a Langmuir probe with fast sweep of the U-I characteristics now permits first measurements. A radial scan in the vicinity of the last closed flux surface was performed. The measured density, temperature and floating potential fluctuations were of similar normalized magnitude and each decreased with decreasing minor radius. Three probe tips were simultaneously swept to measure the spatial coherence of the fluctuations in the poloidal direction. A decrease in spatial coherence of the fluctuations with increasing tip separation could be demonstrated. A statistically significant coherence of temperature fluctuations between tips was found at frequencies below 50 kHz. However, a higher sweep frequency than the present value of 800 kHz is needed to further reduce spurious temperature fluctuations caused by density fluctuations.

Looking at the raw signals, the observer immediately identifies single events moving with nearly constant velocity rather than waves. In order to numerically analyze measured data as a superposition of events, an algorithm was developed. A set of probe array data is smoothed by a two-dimensional convolution with the estimated shape function of the largest events. Maxima and minima are used as starting points for a fit of individual events. An algorithm minimizing the sum of the absolute value of errors almost ignores smaller structures superimposed on a main structure. By means of an iteration with decreasing size it is attempted to approximate the desired analysis.

3. DIAGNOSTIC DEVELOPMENT

3.1 The High-energy Lithium Beam Diagnostic on W7-AS

During the 1993 campaign, absolute electron density profiles along the beam axis were measured for a wide variety of plasma- and beam- (20, 30, 48, 66 kV) conditions. Limited tests demonstrated the feasibility of determining impurity ion densities as well as the neutral gas density outside the plasma.

Even with maximum plasma aperture, density measurements to the centre of the discharge were possible for n_e below $\sim 4 \times 10^{13}$ cm^{-3} (see Fig. 25). Roughly, n_e-profiles are realizable up to an integrated line density, along the beam, of $n_eL \sim 4 \times 10^{14}$ cm^{-2}, meaning that the gradient region of the profile remains accessible for n_e well in access of 10^{14} cm^{-3}.

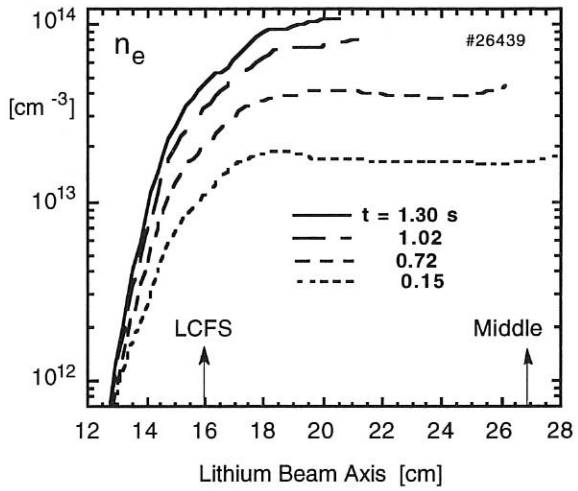

FIG. 25: n_e-profiles for four density levels within one discharge. The n_e-gradients are particularly steep as the beam traverses the plasma at $\phi = -18^o$, i.e. the small side of a nearly standing ellipse. These profiles were obtained solely from the Li[2p-2s] light signals. Comparison with central values of n_e from Thomson scattering shows agreement within 15%. The plasma centre and last closed flux surface LCFS are indicated. $\iota \sim 0.343$, $B_t = 2.54$ T, limiter at $r_{eff} = 0.175$ m. $n_eL(HCN) \sim 1, 2.1, 3.2, 4.2 \times 10^{19}$ m^{-2}.

3.2 Periodic Multichannel Thomson Scattering

The construction of the periodic multichannel Thomson scattering system using a pulsed Nd:YAG laser for W7-AS made considerable progress in the past year. Preliminary investigations necessary for building this diagnostic were reported in Annual Report 1992. This system will enable the measurement of space and time resolved electron temperature and density profiles simultaneously at 16 spatial points every 50 ms. The laser will enter and exit the machine in module 2 through ports 12 and 11, respectively, where the magnetic surfaces have an elliptical cross-section, and the observation will be located in module 3, port 15'. Sixteen equidistant volume elements (4×28

mm) along a 60 cm chord of the scattering plasma between angles 76.6°, and 103.4°, will be imaged by a 4-lens objective (f = 90 cm, diam. = 23 cm, magnification = 2.5) onto the entrance slits of the polychromators. Detection will follow using Si-avalanche diodes.

Most of the components required in order to be able to go into operation with 8 spatial points are completed and the first tests on W7-AS are planned for the coming experimental phase. The distribution of the polychromators in the initial phase will be: 3 for the plasma centre, 3 for the plasma gradient, and 2 for the plasma edge region.

3.3 Diagnostic Developments in the H_α Detection System

The existing H_α detection system consists of 14 single-channel monitors and one linear array mounted in different modules of W7-AS and allows detection of H_α radiation arising from various points within the stellarator. A new set of detectors has been designed which will allow spatially resolved measurements of H_α radiation originating from the new inner limiters. Initially, these detectors will be installed in module 3 in ports 3, 3', 5, and 5'. Each limiter will be viewed by 2 detectors: one multichannel detector for spatially resolved measurements and one single-channel detector for cross-checking purposes.

The multichannel system consists of an objective that images the limiter onto a 4×8 rectangular array of optical fibres. Each fibre is further coupled to individual Si photodiodes for detection purposes. Interference filters placed before the photodiodes select out the desired wavelength and the system has a spatial resolution of 2 cm. The single-channel detector consists of a lens that couples light onto an optical fibre (core Ø = 600 µm). This detector views a circular area of Ø = 7.7 cm at the centre of the limiter and final detection is by means of a Si photodiode. The sampling rate of both the detectors is 5 kHz. Both detection systems will be absolutely calibrated to allow accurate determination of the neutral gas distribution within the machine. The system is expected to go into operation during the next experimental phase starting in early 1994.

3.4 Toroidal Rotation and Viscous Damping

In 1993 toroidal rotation of the W7-AS plasma during neutral beam injection was measured for the first time. The measurements were made in collaboration with K. Ida, NIFS, Japan.

During a series of discharges # 26450 - 57 ECRH (70 + 140 GHz) heating was combined with co-, balanced- and counter-NBI ($H^0 \rightarrow D^+$, 45.5 kV).

By means of the visible spectroscopy scanning mirror system (VISPEC) charge exchange recombination (CXR) of fully ionized carbon was used to measure toroidal rotation (Doppler shift) due to the beam-momentum input and ion temperatures (Doppler broadening) along a line of sight through the plasma centre, intersecting both NBI injectors.

Fig. 26 shows the intensity and NBI power, ion temperature and rotation velocity for shot 26452. The additional input of the second NBI source can be clearly seen on the intensity trace, but no change in ion temperature and rotation velocity was observed.

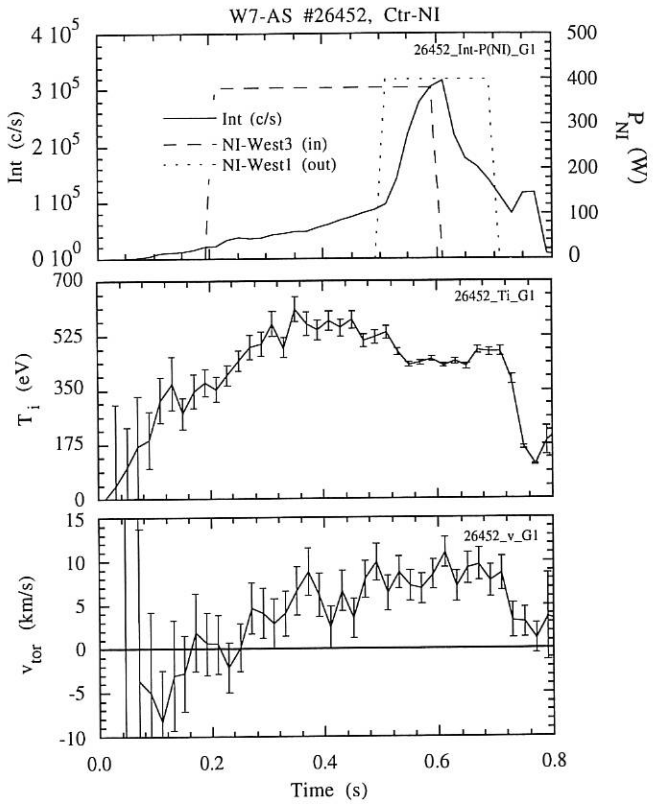

FIG. 26: # 26452, B_0 = 2.52T, ι_a = 0.531

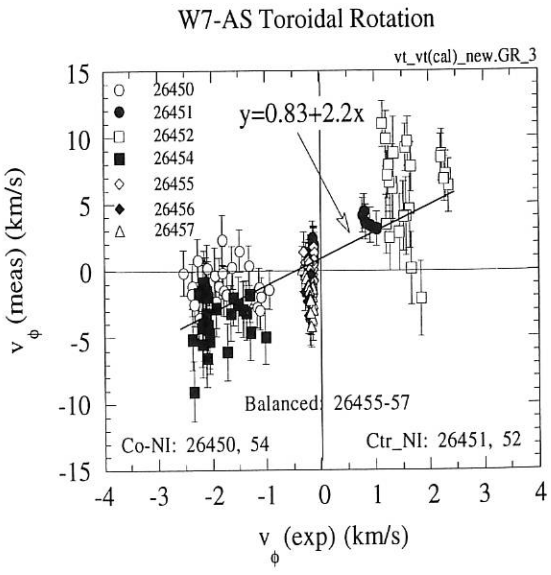

FIG. 27: Measured and expected toroidal rotation

Due to relatively strong toroidal magnetic field ripple in stellarators toroidal rotation should be strongly damped by parallel viscosity (magnetic pumping). A comparison of the expected toroidal rotation, as calculated from the NBI momentum input and neoclassical viscous damping, with the measured toroidal rotation is shown in Fig. 27 for co-, balanced- and counter-injection. In our preliminary results we find that the measured rotation is a factor of about 2 (see fitted line) higher than expected due to neoclassical viscous damping, a result very similar to findings in the CHS heliotron.

3.5 IR Thermography on W7-AS

An infrared camera system (Detector: 120 × 160 Pixels InSb focal plane 2D array, spectral response: 1 to 5.5 μm, spatial resolution: 3 mm/pixel, time resolution: 20 ms/frame, arrangement: viewing one half of the lower limiter, data acquisition: PC based, connected to a MicroVAX) will be put into operation in spring 1994. It is designed to measure the surface temperature of the lower limiter. The IR camera is based on a highly sensitive indium antimonide focal plane array working at liquid nitrogen temperature. The camera is placed inside the magnetic coils to simplify the optical system. It consists of a sapphire window and a multi-element lens. The system characteristics are preliminary.

The camera will be calibrated, and thus the absolute surface temperature can be determined. From the time-dependent surface temperature profile the corresponding distribution of power deposited on the limiter can be calculated by numerically solving the 3D nonlinear heat conduction equation.

3.6 Collective Scattering

The possibility of determining the ion energy distribution by collective scattering is well known from the literature. Due to the lack of sources with sufficient power and pulse length in the far infrared or microwave range of frequencies this method was not applied in present-day fusion devices. The application of this diagnostic method was reconsidered and proposed for the energy distribution measurement of α-particles in JET since high-power gyrotrons with 140 GHz recently became available. We have conducted proof-of-principle experiments at W7-AS with special financial support from the Federal Ministry of Research and Technology in collaboration with IAP Nizhny Novgorod and IPF Stuttgart to demonstrate the applicability of high-power gyrotrons for collective scattering. First spectra were measured (for details see IPF Ann. Report, this volume), which clearly showed that the thermal part of the density fluctuations could be detected with sufficient resolution. After these encouraging results both the 70 and 140 GHz scattering systems are being modified for better spatial and spectral resolution. The measurements will be continued with improved systems in 1994.

3.7 Probes

3.7.1 Polarization electrode

An electrode system for plasma polarization was developed to facilitate H-mode-like conditions by applying radial electric fields. It consists of three coaxially mounted cylindrical components of various graphite materials equipped with thermocouples and constructed such as to avoid plasma contact of insulator surfaces. First experiments indicate successful operation already at relatively small voltages and currents (200 V and 50 A, respectively). A problem to be solved is the gas content of the material.

3.7.2 Combined Langmuir and calorimeter probe

A combined Langmuir and calorimeter probe has been temporarily installed which allows particle and heat flux measurements in the boundary plasma and to the wall at the position were the highest wall loading is expected (outboard midplane with triangular plasma shape).

In addition, the spatial distribution of erosion and deposition phenomena on the wall was measured at this location during selected discharges by applying a new collector probe head system. It allows transfer of collector samples into the chamber which cover a wall area of 8 × 100 mm. After plasma exposure the samples can be retracted for external analysis through a tube of 25 mm diameter.

4. NET/ITER-RELEVANT RESULTS OF W7-AS

W7-AS contributes with eight tasks to the ITER Physics R&D Programme. The results are summarized as follows:

In 1993 W7-AS was very successful in improving global energy confinement. High-power (0.5 MW or 0.9 MW, 0.4 s) ECRH at 140 GHz was performed, and the plasma density was increased up to the cut-off density 1.2×10^{20} m^{-3}. During high-density operation, the H-mode was observed for the first time in a stellarator. The H-phases display all the characteristics known from tokamak H-modes, including ELMs. The achievement of the H-mode in a shear-free stellarator without net toroidal current has consequences on H-mode transition and ELM theories.

ECRH was also used in combination with NBI to control the density despite the beam particle fuelling and for current drive (long-pulse operation). In the description of the ECCD net current as a function of the launch angle, density and trapped particle fraction, excellent agreement with theory was achieved. For optimized stellarators such as W7-X, global Monte Carlo simulation and local analysis show good agreement and demonstrate favourable neoclassical transport and near elimination of the bootstrap current in this configuration.

Pellet ablation, which is important for long-pulse operation, was found to be governed by self-shielding of the pellet by already ablated material, leading to an oscillatory process. The nearly shear-free configuration of W7-AS can uniquely contribute to the role of rational surfaces in the striation formation. Apart from the magnetic axis rational values seem to play a minor role.

Theoretical investigations show that transport in the net-current-free stellarator has gyro-Bohm-like properties; this predicts favourable scaling of the confinement properties when projecting to larger devices. Density limit experiments in W7-AS always led to a smooth thermal collapse without any disruptive instability. At high density, close to the thermal collapse the highest β-values are obtained ($\langle \beta \rangle \leq 1.2\%$). These values are still power limited. MHD fluctuations do not play a limiting role.

Beam driven Alfvén eigenmodes, which can play an important role in the fusion reactor, were clearly demonstrated and studied in W7-AS with NBI. Unlike the tokamak, global Alfvén waves are induced.

In diagnostics higher stability of a conventional reflectometry system was obtained by measuring the phase of the amplitude modulation of a carrier rather than that of the carrier itself.

5. MACHINE OPERATION AND TECHNICAL ACTIVITIES OF W7-AS AND THE AUXILIARY SYSTEMS

The following sections summarize the main technical activities on W7-AS, e.g. machine operation and developments, new installations and repair work as well as developments and technical status of control systems and auxiliary plasma heating systems.

5.1 Main Machine Activities of W7-AS

(W7-AS: R. Allgeyer, W. Andres, J. Bömerl, R. Dunkel. F. Hoffmann, G. Hussong, A. Kellerbauer, B. Moritz, H. Rixner, S. Schraub, R. Semler, J. Stadlbauer, G. Zangl, the W7-AS Technical Team and the W7-AS Assembly Group;

Central Technical Services: B. Brucker, G. Förster, H.-J. Kutsch, E. Maier, J. Perchermeier;

Experimental Plasma Physics Division 1: E. Kaplan, U. Ortner;

Workshops of Experimental Plasma Physics Division 2 and Central Technical Services)

5.1.1 Overview of machine operation and maintenance

In 1993, operation of W7-AS saw three scheduled interruptions. During the long experimentation phase from December 18, 1992, till August 20, 1993, a total of 4,930 discharges were carried out in 79 experimental days. For about 400 discharges the machine was operated at 2.5 T to heat the plasma with the new high-power 140 GHz ECRH system, and for about 205 discharges the experiment was run in mirror configurations (see e.g. Sec. 2.2.6).

During the first two shutdowns, one week in May and two weeks in June, activities on the modular field coils of type 3 were intensified. Electrical modifications for the new fluorine carbon cooling system were installed and a newly constructed support for these coils (see Sec. 5.1.2) was mounted to one coil in module 4. Measurements during the following experimental period yielded coil displacements which were reduced by a factor of 4 at full load (2.5 T). As a consequence, support elements for the remaining nine coils of type 3 were prepared for installation.

During the experimentation phase the preparation work for the installation of the new inner limiters (see Sec. 5.1.3) was continued, a special valve for absolute gas flow measurements was installed and tested, and the boronization system was modified and put into operation for mini-boronization in between discharges. The preparation work for injecting diborane-containing gas mixtures into plasma discharges is under way. To enable glow discharges between pulses an automatic control for the glow discharge power supply in combination with a diagnostic protection system was put into operation. The third and long shut-down started on August 23, 1993, and lasted till the end of February 1994. The main activities during this phase are described in Sec. 5.1.2 to 5.1.4.

5.1.2 The additional support system for the critical modular field coils

For installation of the new additional coil support system nine of the ten vessel port ducts of type 6 located between the modular field coils of types 2 and 3 had to be removed by using a special tool machine developed at IPP. The portholes were closed by welding in a stainless-steel disc provided with an eccentric circular hole to allow installation of new port ducts with reduced diameter. One of the port ducts had already been removed during the shutdown phase in 1992 by the same technique. To insert an additional lateral support element of relatively complicated shape, a multilayer technique was applied. Each support element was radially divided into nine layers of stainless-steel sheet elements, 20 mm thick, each of which had to be divided once. On-site assembly started with the inner layer. Each layer was bolted to the preceding layer. The gaps between the elements and the coils of types 2 and 3 were filled with epoxy resin, layer by layer. A circular hole in the support element provides enough space for a new port duct with reduced diameter welded in place of the removed port duct 6.

5.1.3 The new inner limiter system

At present, W7-AS is equipped with a set of two toroidal bulk-boronized graphite rail limiters, one at the top and one at the bottom of elliptical plasma cross-sections. This system breaks the symmetry of the magnetic configuration, complicating in-

terpretation of physics data, and the power loading capability will be not sufficient for the future upgraded heating systems. These disadvantages and the need of experimental limiter / divertor investigations for W7-X resulted in investigations of a new limiter concept. In a first experimental step nine identical limiter graphite blocks (CC 1000/Fa. Sintec) for protecting the inner vacuum vessel walls of W7-AS were designed and constructed. The old limiter system still acts as main limiter, with the new auxiliary limiters working only in plasma discharges with $\iota = 0.34$ and an inward displacement of 3 cm.

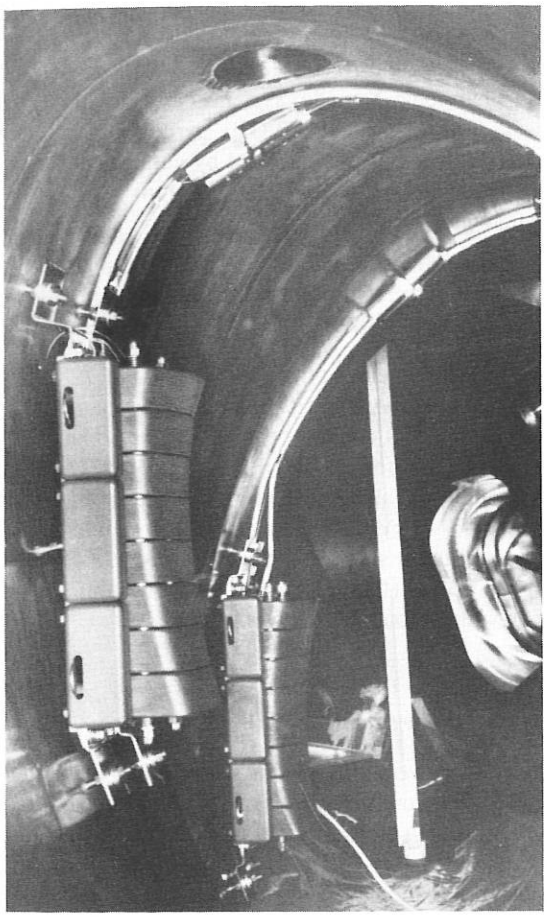

Fig. 28: One pair of the new limiter system arranged in an upside-down symmetry at the inner vessel walls near the triangular plane.

Each of the five modules of W7-AS is now equipped with a pair of the new limiters (Fig. 28); in module 5 only one limiter could be installed because the installed diamagnetic coil interfered with the second limiter position. Every pair of limiters is arranged in upside-down symmetry at the inner vessel walls near the triangular plane. The surface of the graphite limiters, the curvature of which follows the plasma shape, is calculated by 3D CAD. Every graphite block (extending 23 cm in the poloidal and 12 cm in the toroidal direction) is divided into 8 parts mounted on a stainless-steel ground plate. Specially designed and constructed alignment tools were used to attach the new limiters to the inner vessel walls.

Radiation heaters between the ground plates and the graphite permit the limiters to be baked to temperatures of up to 350° C. For the electrical supply a new voltage-regulated heating power system was installed. All limiters are equipped with thermo-couples for investigating temperature rise and possible non-symmetric power loads during plasma discharges. The guiding of the feeding lines to the radiation heaters and thercouples had to be designed by 3D CAD to prevent damage to the conductors by different power loads of various plasma configurations. Additionally the feeding lines were covered by stainless-steel and graphite tiles. The guiding of the conductors inside the vessel thus has a very complex zigzag structure and required time-consuming assembly. Finally the feed-throughs of the feeding lines had to be soldered vacuum-tight into port cups.

5.1.4 Further maintenance, modification and repair work

After the machine was vented in August 1993, the vessel air was investigated by chemical, infrared spectroscopic and radiation measurements to guarantee safety inside the vessel. The various methods are very sensitive to low concentrations, e.g. of toxic gases, but all results were far below every detection level of the investigated materials.

The assembly of the nine additional supports for the coils of type 3 (see Sec. 5.1.2) required extensive dismantling and reassembling of diagnostic elements, the ECRH injection systems and the NBI systems, including the large flanges. Because of the reduced diameter of the new ports of type 6 several diagnostics had to be modified. After inspection and documentation of the machine additional repair work was called for. Damages to one 70 GHz ECRH injection mirror required the construction of a new one. The ICRH antenna had to be dismantled to exchange one of the 3D curved segments of the four high-frequency conductors to the antenna which was considerably melted. Before reinstallation the old and reserve segments were silvered to reduce heat production. Additionally, the antenna was equipped with 3D shaped Faraday cups at the top and the bottom antenna bars which had to be newly designed and constructed. Furthermore, the stainless-steel and graphite shieldings of the insulating gap between module 1 and 2 behind the antenna had to be renewed by a newly constructed, rather complex coverage, because observations of the old shieldings indicated a disturbing influence on the operation of the ICRH antenna.

Further in-vessel work was the replacement of the long-time deposition probes, repair of the old on-line deposition probe and installation of a second one, modification of the glow discharge electrodes and mounting of a newly constructed igniting anode, installation of the ASDEX Bostick gun and new diagnostic elements (e.g. ECE). Various flanges had to be extensively modified for new diagnostic elements, e.g. thermographic observation of the old limiters or D_α measurements of the newly installed auxiliary limiters in module 3. All five turbomolecular pumps and their forepumps had to be dismantled for maintenance work (installation of new ball-bearings) as well as seven sliding flanges for repair work. Complete control

of all screws and fixing bolts of the coil support structure within reach as well as endoscopic control of the machine are standard procedures during every maintenance phase. Installation of the new coils for plasma position control had to be shifted to the next maintenance phase.

In December 1993, the impregnation of the two faulty coils of type 3 was repeated, because the impregnation of coil no. 4.3 in January 1992 had not been completely successful. Nevertheless, the total losses of FC75 from both coils in the period from March 1992 till August 1993 were less than 2 litres (including all leaks of the cooling system). During the experimental period the leak of coil no. 4.3 had been observed with a hand-held halogen leak detector. From the next experimental period on, all coils of type 3 will be cooled with FC77 fluorocarbon fluid by the newly designed and installed cooling system.

5.2 Control Systems

(in collaboration with H. Czich, H. Holitzner and the Electronics Team)

Operation and control of W7-AS plasma parameters are handled by a combination of analog circuits and digital computers. A large number of interlocks and feedback loops are realized with standard electronic circuits. The visualization and input of new control parameters are done by computer. Time-dependent control signals can easily be varied with a Macintosh mouse. The new software allows very fast programming of several modules with up to twelve arbitrary functions each.

A new control hardware has been designed in CAMAC standard for analog output as well as for clusters of time-dependent 16-bit digital signals. A new timer system will be based on this module, where the status of the trigger points can be stored automatically for every experimental shot. In combination with special safety electronics, this module is used for high-precision control of the W7-AS helical field.

Several very different power supplies are in use for the poloidal fields in W7-AS. For feedback control of the plasma current a new electronic facility is available which automatically adapts the regulator to the actual power supply.

The 240 kVA transistor amplifier, which was damaged during critical plasma operation, has been repaired and has a new protection system.

5.3 Electron Cyclotron Resonance Heating

(in collaboration with G. Grünwald, J. Hofner, P. Luttner, U. Weber)

A new 140 GHz prototype gyrotron from the development line at IAP-Nizhny Novgorod generates 0.5 MW for a pulse duration of up to 1.1 s or 0.9 MW for up to 0.4 s. The linearly polarized Gaussian output beam is transmitted to the plasma by an optical mirror system with 10 mirrors. The overall transmission efficiency was measured calorimetrically at high power and is 80%. The main losses (15%) are coupling losses from the gyrotron output to the optical transmission system due to non-Gaussian emission (side lobes) from the gyrotron, because the internal mode converter is not yet fully optimized. An additional 5% are transmission line losses such as spill-over, mirror surface imperfections and resistive losses. The transmission system allows an arbitrary choice of the wave polarization. The microwaves are launched by two movable mirrors inside the vacuum vessel from the low magnetic field side in the equatorial plane of the torus and can be steered with arbitrary toroidal and poloidal launch angles. At a resonant magnetic field of 2.5 T the 70 GHz (1st harmonic O-mode) and 140 GHz (2nd harmonic X-mode) systems can be operated simultaneously. Two of the four 70 GHz gyrotrons, including the transmission lines, were dismantled by autumn 1993 and will be replaced by long-pulse 140 GHz gyrotrons (0.5 MW, 3 s) at the beginning of 1994.

5.4 Neutral Beam Injection into W7-AS

During the experimental phase in 1993 about 728 NI shots were fired into W7-AS in different combinations of the four sources (2 co- and 2 counter-beams). The pulse lengths were varied up to 1.0 s for the INNER and up to 0.65 s for the OUTER sources. In all cases the standard neutral power of 375 kW per source (45 kV, 25 A extracted power) could be reached with a reliability for single sources of between 98.4% (INNER EAST) and 95.5% (OUTER WEST). The reliability of beam operation with all four sources was 90.2%.

5.4.1 3 MW upgrading of NI/W7-AS

The injection power into W7-AS will be doubled by adding four ion sources from the former ASDEX injection to the existing system. A new electric power transformer (2.5 MVA peak power) was installed in October and is now available for 3 MW operation. Installation work for the power supplies and high-voltage valves of the additional ion sources in the new building was continued. Installation of the individual control units for the power supplies is in progress. The extraction grids for the new sources were delivered in 1993 by CEA Grenoble and accepted by IPP. Assembly of these additional four sources is under way.

The maintenance phase of W7-AS, beginning at the end of August, was used to continue upgrading of the mechanical components of the NI boxes. This internal upgrading will be finished before the next experimental phase. The S5 programmable control system was extended to control four sources per box and is now being tested. The hardware extension of the data acquisition is installed and is being put into operation. Extension of the corresponding software is under way.

5.4.2 *NI simulations*

Two versions of the FAFNER code are in routine use. The original code, FAFNER1, is based on spatial coordinates with the advantage of including quantities depending on real-space coordinates (limiter positions, neutral gas density etc.). The second version, FAFNER2, uses magnetic coordinates to take into account the effects of a radial electrical field for arbitrary magnetic structures.

5.4.2.1 *Parametrization of FAFNER1 results*

A fast code was developed to estimate the NI heating power profiles for W7-AS shots. This code, named NIPOR, uses data sets of the local power deposition and analytical fits of the total heating efficiency obtained by previous runs of FAFNER1. To achieve high flexibility, the heating profiles were not stored direct, but in the form of radially deposited heating power as a function of the normalized variable $\xi(r)$, defined as the line-integrated density from the plasma edge to the centre, divided by the volume of the corresponding shell and normalized to $0 < \xi(r) < 1$. The partition of the reconstructed heating profile $p_{heat}(r)$ to the ions $p_i(r)$ and electrons $p_e(r)$ is estimated by using the critical energy $E_{crit}(r)$ as a function of $T_e(r)$. The main input parameters needed for this estimation are the electron density $n_e(r)$, electron temperature $T_e(r)$, toroidal magnetic field B_t and the identifiers of the active NI sources at the corresponding time t_c. These data are routinely read from the ORACLE data set.

5.4.2.2 *Application of FAFNER2*

The FAFNER2 code was applied to the W7-AS, W7-X and TJ-II stellarators. The drift surfaces of collisionless passing particles behave quite differently in these three devices. Due to the optimized B-field structure in W7-X the fast ions move closely to the flux surface, whereas in the helical-axis stellarator, TJ-II, there is a strong shift varying with poloidal angle. This variation explains the better heating efficiency for counter- than for co-injection obtained for TJ-II, in contrast to W7-AS or W7-X, where co-injection is more efficient due to the inward drift. The influence of an assumed radial electric field on the heating efficiencies in these devices was also studied.

5.5 ICRH

Experiments with the broad antenna (installed in 1992) showed that mainly ion Bernstein waves with no heating effect were launched instead of the fast waves wanted. This was obviously caused by parallel currents flowing in the upper and lower horizontal antenna bars. To improve this behaviour, shielding elements were prepared for the next experimental period, which should reduce the effect of these parallel currents.

In order to study ICRH characteristics with different antenna principles at W7-AS, a conventional double loop antenna, fitted to the plasma surface, was designed.

Successful plasma production was achieved with a small loop antenna, fed by a 900 MHz, 30 kW magnetron. The density of 0.8×10^{19} m^{-3} attained was sufficient as NI target, thus allowing plasma operation without ECRH.

WENDELSTEIN 7-X

(Head of Project: Dr. Günter Grieger)

1. WENDELSTEIN 7–X GROUP

C.D. Beidler, E. Harmeyer, N. Jakšić,[1] J. Junker, N. Karulin,[2] J. Kißlinger, F. Rau, H. Renner, J. Simon-Weidner,[1] M. Spada, H. Wobig.

1.1 Wendelstein 7–X Studies

In 1993 the Wendelstein 7-X studies were concentrated on special questions of the coil system, HS 5-10N, and its technical feasibility. Further optimization of the support structure was carried out. Increased attention was given to the divertor structures and plasma boundary physics. Furthermore, neoclassical and anomalous transport were also investigated. The configuration was scaled up to reactor dimensions; the modular coil system and the power balance of a stellarator reactor were investigated.

1.1.1 Force and stress calculations

Magnetic fields and forces and the associated mechanical stresses and strains were calculated for the standard case of HS 5-10N, with improved subdivision of the finite elements in the longitudinal direction of the coils. Each coil owns a coil housing of stainless steel and the mutual intercoil support structure was chosen as a cross-connected framework in order to minimize structural material. Local reinforcements of the structure in the radial and lateral directions were applied.

The ADINA finite-element code was used to compute the stresses and strains of the system applying the orthotropic material data of the ABB conductor. In the calculations the effects of the cooling-down of the coil module and the influence of sliding on stresses were considered. A further optimization of the support scheme was achieved by varying the intercoil structure. This investigation is being done by members of the ZTE division.

1.1.2 Divertor studies

The exhaust in W 7-X under quasi-stationary conditions and the related energy and particle flows at the boundary are dependent on the magnetic structure of the boundary. Within the range of optimization of the W 7-X magnetic configuration, either the formation of a boundary structured by islands (5/6, 5/5, 5/4) for particular values of the rotational transform or of an ergodized boundary layer is possible by shaping the field coils. At present the realization of a configuration with moderate shear seems favourable: Additional small experimental coils and superimposed "resonant" fields ($B^{5,5}$) provide flexibility and allow controlled modification of the boundary and boundary fluxes . The arrangement of the target plates has to reflect the 5-fold symmetry of W 7-X.

As preparation for a detailed divertor design investigations at different fields have been continued:

Modelling of the plasma boundary: The density and temperature profiles can be evaluated on the basis of a geometrical description of the flux bundles and depending on the connection length of the open field lines considering the parallel and perpendicular transport according to experimental data. Additionally, Monte Carlo methods (EIRENE code) are used to calculate the neutral particle distribution. Measures to concentrate the neutrals for efficient pumping and to minimize the impurity reflux can be analyzed.

Analysis of experimental data: The analysis of experimental data on the density, temperature distribution towards the target areas and SOL formation is important

[1] ZTE Division

[2] Guest from Kurchatov Institute, Moscow

to test the theoretical models. In particular, because of the similarities of W 7-AS and TORE-SUPRA ergodized boundary data from these devices can be of specific interest for W 7-X. Consequently, on the basis of the W 7-X concept a new limiter/divertor for W 7-AS has been proposed. Possibilities of close co-operation with TORE-SUPRA have been explored.

Engineering: At present, preliminary design studies combine the individual elements of the divertor for W 7-X inside the vessel and analyze the compatibility with heating and diagnostic requirements: target plates with supporting structure and cooling circuits, installation of "sweep" coils, baffles and integrated pumps. The calculated 3D-target area will be approximated by standardized elements: Flat stripes 5×50 cm^2 consisting of thin C tiles brazed on a water-cooled Cu/Mo structure. Several stripes may be arranged to modules to optimize assembly and maintenance. Stress calculations relating to the properties of the material used are under way to prepare construction of a prototype for testing.

The positioning of target plates is optimized in respect of the following criteria:

- Concentration of the plasma outflow on the target plates and separation of the plasma from the vessel.
- Maximal power load 10 MW/m^2, leading to an angle of incidence of field lines on the target of around 2^o.
- Variation of the magnetic configuration for rotational transform $5/6 \leq \iota \leq 5/4$. Integration of baffles and cryopumps (ceramic TMP) for efficient pumping and stationary operation when dealing with external fluxes of $5 \cdot 10^{21}$ part./s (NBI, pellet, gas feed etc.).

1.1.3 *Island divertor*

The geometrical form of the target plates is based on the island divertor concept described in the Annual Report 1992 and in[3)], which was developed and further refined in 1993. In the previous version, the target plates had to have a certain twist to collect the outstreaming plasma at a small intersection angle at both sides of the islands.

In order to reduce this twist and also the total length of the target plates, they have been split into two parts. Each of them is in contact with one side of the magnetic island and the slot between opens the way for the escaping neutral particles to the cryo-pump installed behind the more horizontal of the two plates. Towards the slot the target plates have an added piece like a collar which is hit by a portion of the plasma particles, especially in a configuration with increased islands. In this case an increased fraction of the neutrals is absorbed at the cryo-pumps and it may be possible that for some special configurations a more closed divertor is practicable. The problem arising from the variation of the rotational transform ι is solved by adjusting parts of the plate to each specific case, as shown in Fig. 1.1. For each of the three cases shown, an ι-domain exists where the separatrix lies between the plasma and the target plates, allowing divertor operation. This domain may be enlarged

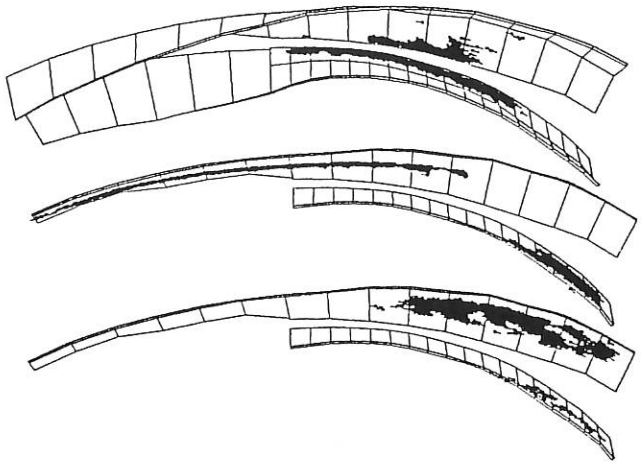

FIG. 1.1: Intersection pattern on the upper target plates, seen at an elevation angle of 45 degree for three configurations: standard case (top), high ι (middle) and low ι case (bottom). The top figure shows, in addition to the target plates, also the baffle plates. The stripes reflect the intersection line of the separatrix with the target plates, broadened by perpendicular diffusion. The maximum power load is about 10 MW/m^2 and the intersection angle in the highly loaded zones is between 1 and 2 ^{o}.

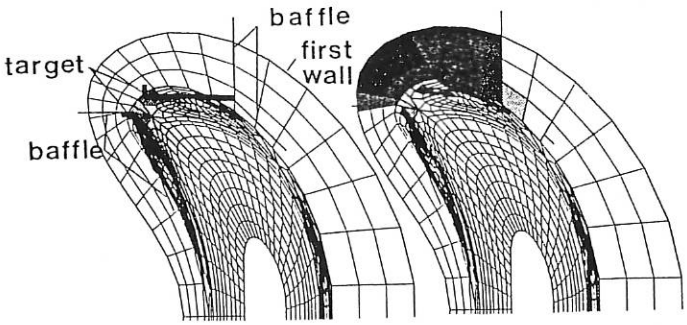

FIG. 1.2: Cross-section of the mesh used for the EIRENE code at the toroidal plane with $\varphi = 0$ (upper part of the up-down symmetric figure). Shown are the radial and poloidal cell boundaries and the positions of the target and baffle plates, which form the pumping chamber. The shaded mesh cells reflect the ion source density from atom-plasma interaction (left) and the neutral particle density (molecules, right) on a logarithmic scale; left: white $< 6 \cdot 10^{15}$ to black $> 5 \cdot 10^{18}$ ions/(sec cm^3); right: white $< 6 \cdot 10^9$ to black $> 4 \cdot 10^{12}$ part./cm^3. The position of the neutral particle source ($6 \cdot 10^{22}$ particles/sec), is defined by the intersection regions of Fig. 1.1 (top, standard case).

[3)] Kißlinger, J., et al., 20^{th} EPS, Lisboa, 1993, 17C, II, 787.

by varying the island size with the sweep coils. In cases without islands at the boundary the target plates act as limiters with about the same values for power loads and intersection angles.

The target plates are located in those regions where the magnetic surfaces and islands have a large radial extent, so that neutral particles reflected by the target plates are re-ionized in the edge plasma. In order to confine the neutral particles in the divertor region, the target plates are combined by baffle plates. These prevent the neutrals from reaching the poloidal regions where the plasma cross-section is of small radial dimension and where neutrals can penetrate more deeply into the hot plasma. Calculations with the EIRENE code show that in the case with baffle plates the neutral particle density outside the plates compared with that in the pumping chamber is reduced by a factor of roughly 1000, see Fig. 1.2, left part.

1.1.4 *Further development of a general solution of the ripple-averaged kinetic equation (GSRAKE)*

A general solution of the ripple-averaged kinetic equation (GSRAKE)[4] using a numerical scheme underwent further development, including complete restructuring to improve its flexibility and efficiency.

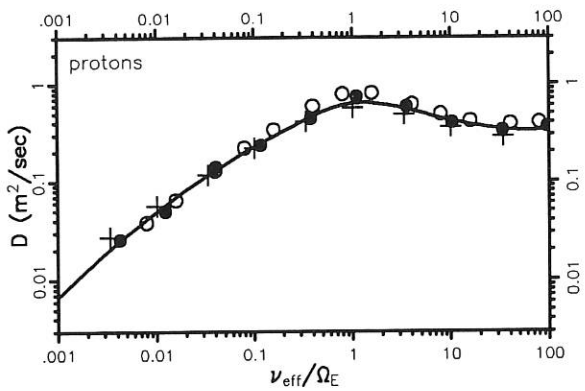

FIG. 1.3: The monoenergetic diffusion coefficient as a function of the normalized collision frequency for an ATF-like configuration with reactor dimensions. Numerical results from GSRAKE are shown by the solid line (composed of 20 data points per decade; total CPU time 85 CRAY-YMP seconds), Monte Carlo estimates are given by the blackened circles (•), DKES (Hirshman, et al., Phys. Fluids 29 (1986) 2951) results by the open circles (o) and FLOCS (D'haeseleer, et al., J. Comput. Phys. 95, (1991) 117) output by crosses (+).

[4] see Annual Report 1991, p. 139.

Subsequent comparisons of GSRAKE results with those of other numerical methods show good agreement in all cases (an example is shown in Fig. 1.3), the computer time required for GSRAKE being only a tiny fraction of that for the other codes.

Extensive studies of the parameter scalings of neoclassical transport in toroidal stellarators were also carried out with GSRAKE. For the most part, the results confirm the expectations of traditional analytic theory. For details see the Proceedings of the IAEA Technical Committee Meeting on Stellarators and Other Helical Confinement Systems, Garching, 10-14 May, 1993, p. 138-145.

1.1.5 *Modification of the ASTRA 1-D transport code for stellarators*

ASTRA[5] is a flexible, time and radius dependent transport code able to assess experimental results and make predictions.

The stellarator version of ASTRA solves three balance equations: for the electron density n_e and temperatures T_e, T_i. The profile of the rotational transform $\iota(r)$ is fixed. Transport properties are described by a matrix including non-diagonal transport cofficients taken from an internal library of formulae. At present the library contains Beidler's neoclassical coefficients for Helias stellarators (Report IPP 2/318, 1993), Kovrizhnykh's coefficients[6] for axially symmetric transport and anomalous electron thermal conductivity. Dependence of the transport on a radial electric field is also added. The right parts of the energy balance equations contain common energy sinks and sources: radiation (bremsstrahlung, synchrotron and impurity), energy exchange between plasma species, and plasma heating.

The principle of programming a task for calculation is to assemble a required model from the library blocks and set up appropriate boundary and initial conditions. The time dependence of values which are not calculated (for example, external heating) can be prescribed.

Calculations by ASTRA for Wendelstein 7-X (see Fig. 1.4) well fit those made with another transport code, TEMPL[7], if the same plasma model is used.

The ASTRA code is suitable for studying plasma transport, analysis of experimental data, scenario assessment, planning of experiments and reactor studies, and, eventually, for modelling of L–H transition.

1.1.6 *Interaction of energetic particles with GAE-like perturbations of magnetic field*

Perturbations of the magnetic field generated by Global Alfvén Eigenmodes modify resonant drift orbits of suprathermal passing particles so that the drift surfaces build island structures.

[5] Pereverzev, G.V., Yushmanov, P.N., et al., Report IPP 5/42, 1991.

[6] Kovrizhnykh, L.M., Nuclear Fusion, **24** (1984) 435.

[7] see Annual Report 1990, p. 131.

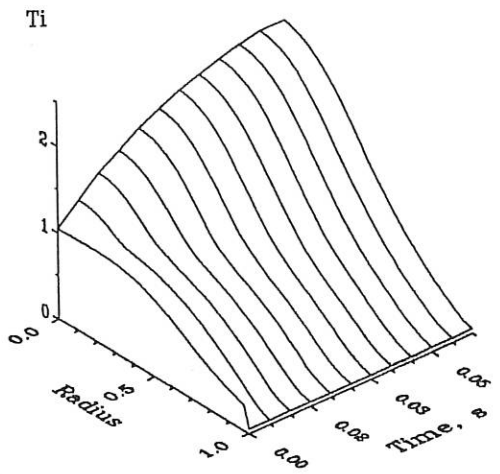

FIG. 1.4: Time development of T_i in Wendelstein 7-X, calculated with ASTRA. ECR power of 10 MW peaked at the axis is switched on at time $t = 0$.

The island width scales as follows:

$$\delta r \propto \sqrt{\frac{R}{a}\frac{\delta B}{B}\frac{r}{m(d\iota/dr)}},$$

where δB is the amplitude of the perturbation and m is the poloidal wave number.

Fulfillment of the resonance conditions depends on the plasma radial electric field and on the profile of the rotational transform $\iota(r)$. If the islands are big enough, this can lead to prompt collisionless losses of passing NBI ions in modern experiments or of thermonuclear alphas in a reactor, even in the case when these particles are well confined in absence of the wave.

1.2 Formulary for Plasma Physics

A collection of formulas frequently used in the field of plasma physics has been compiled and prepared for evaluation by the Microsoft Excel spreadsheet program, which runs on an IBM-compatible PC as well as on a Macintosh computer. The present version of this plasma formulary, a worksheet named FORMEX, comprises 133 formulas depending on 23 variables. The formulas are evaluated numerically and these numerical values are promptly updated whenever any of the input variables is changed. A complete set of input variables can be chosen by the name of an experimental device. Stellarators and tokamaks, 15 altogether, are incorporated in the formula collection. A diagram can be displayed to show how a specific formula depends on any of its input variables. Each formula is extensively annnoted to show its origin and give literature references.

The formula collection is operated with a series of macros, all inside the macro sheet named FORMAK, which are invoked by menu commands from a special menu bar. All the information from the formula collection, the genuine formulas, the table of numerically evaluated plot coordinates, the notes, and the diagrams can be further processed or transfered to any other application with the help of the usual Excel commands.

The formula collection is open to add more formulas and, if needed, variables as well as data of further experimental devices. The two files, FORMEX and FORMAK, are available by ANONYMOUS FTP via the address FTP.IPP-GARCHING.MPG.DE, which allows public access (Lab. Report IPP 2/323, in press).

1.3 Reactor Studies

Helias configurations offer the possibility of a self-consistent reactor concept where plasma losses, stability limits and α-particle losses are not prohibitive to ignition, and where a fusion power of about 3 GW can be produced with reasonable reactor dimensions. A Helias reactor (HSR) is a steady-state reactor with a low amount of recirculating power. To maintain the auxiliary systems, roughly 10% of the electric power is needed. A rough power balance starting from an electric power of 1000 MW shows that on the plasma side a neutron power of 2000-2400 MW has to be delivered; this corresponds to an α-particle heating power of 500-600 MW. This value imposes a lower limit on reactor performance and therefore strongly determines the dimensions and plasma parameters of HSR. Details are given in Report IPP 2/318, 1993.

In the Helias reactor typical data are: $R_0 = 20$ m, $a = 1.6$ m, $B_0 = 5$ T at a stored magnetic energy of 80 GJ. Sufficient space for shield, blanket and divertor systems is necessary, viz. a distance of at least 1.2 m between the first wall and coil winding pack. Fifty modular, non-planar, superconducting NbTi coils generate the magnetic field with a mirror field of about 10% in order to provide better confinement of high-enery α-particles.

A common cryostat surrounds the reactor coil system. It is modulated for maintenance purposes. Magnetic forces on the superconducting modular coils are one of the main technical problems of the reactor. These forces determine the geometry of the coil support system. The maximum net coil force is about 120 MN; and for the whole field period the resulting force amounts to about 350 MN directed towards the torus centre. The inhomogeneous force distribution, the data of the geometry, and the material data of the system are the input data for the stress analysis. A complex stress and strain distribution inside the coils and the structure is evaluated. The magnitude of these values can be kept within technical limits by utilizing an optimized support structure. The detailed results of these computations are given in Report IPP 2/316, 1993.

An optimization procedure was applied to equalize the von Mises stresses in the coil system and minimize the amount of structural material. The result, so far, shows that a reduction of the weight up to 12% is possible.

2. STELLARATOR PHYSICS STUDIES

W. Dommaschk, F. Herrnegger, W. Lotz, P. Merkel, J. Nührenberg, A. Schlüter, C. Schwab, U. Schwenn, E. Strumberger, L.-J. Zheng.
Guests: K. Ichiguchi,[1] J. A. Jimenez,[2] N. Nakajima.[1]

2.1 Introduction

In 1993 the work of the Stellarator Physics Group was concentrated on theoretical preparation of the W7–X phase II – in particular divertor physics studies –, on beginning to augment the level of theoretical description of stellarators, and on introducing the concept of the optimized stellarator to the fusion community /209, 210, 595, 596/. In the latter context it may be noted that i) the HSX project (an approximation of a quasi-helically symmetric stellarator with four periods and modular coils at a rather low aspect ratio) at the Univ. of Wisconsin was approved,[3] ii) joint Japan-US studies were carried out for an approximation of a quasi-helically symmetric device with an $\ell = 1$ continuous torsatron coil,[4] iii) a decision was taken in the US stellarator community on the input for a stellarator reactor study which appears to be a modular quasi-helically symmetric configuration, too, iv) the NESCOIL code was installed at CSCS, the Swiss supercomputer centre, for joint CRPP-IPP-CSCS studies of coils for stellarators.

In Secs. 2.2 and 2.3, examples of advanced levels of theoretical description are given. A nonlocal ballooning mode study investigates the structure of ballooning modes in tokamaks and optimized stellarators. The CAS3D code used for this study was installed at NIFS and is now in use on the supercomputer there. Collaborative test work with RESORM (developed at NIFS) and CAS3D helped to clarify the correct usage of the former and validated both codes for torsatron-type applications.

The well-behavedness of finite-β equilibrium surfaces is the object of advanced equilibrium studies undertaken as collaborative work together with NIFS (HINT code) and PPPL (PIES code).

Finally, in Sec. 2.4, divertor physics work is sketched which is motivated not only by W7–X needs, but also by the question whether material walls can be used as target areas in a stellarator reactor.

2.2 Nonlocal Ballooning Modes

Investigating the ideal MHD non-local ballooning mode structures in optimized stellarators is impeded by their small shear, which restricts the occurrence of resonant 3D mode coupling to very high node-number modes. To facilitate the comparison of tokamak and stellarator ballooning mode structure, a Helias configuration with significantly increased positive shear was used for high-node-number computational mode analysis with the CAS3D ideal MHD stability code /257, 259/. In this Helias case and in the $A = 4.6$ finite-β tokamak case, which is used for comparison, the amount of shear ($|\Delta\iota|/\iota \approx 0.7$), in principle, enables resonant sideband coupling even for low- and medium-node-number modes. Fig. 1 (top part) shows that in the tokamak case a perturbation structure of the ballooning type indeed occurs, the unstable mode being radially extended and composed of many poloidal harmonics with competing amplitudes. This global stability result is in keeping with the local ballooning analysis, which indicates the tokamak case to be locally ballooning unstable. Though the *local* ballooning formalism proves the Helias equilibrium to be also *locally* unstable, the high-node-number mode behaves quite differently. Fig. 1 (bottom part) shows that even for very high node numbers the perturbation Fourier coefficients do not exhibit the tokamak partial mode structure and do not significantly overlap. Thus, in contrast to the tokamak mode, the Helias perturbation may be characterized to be of the Mercier type, a result that has been found before for the low-node-number modes in low-shear stellarator configurations. In addition, the extrapolation to zero radial grid size shows this perturbation to be stable.

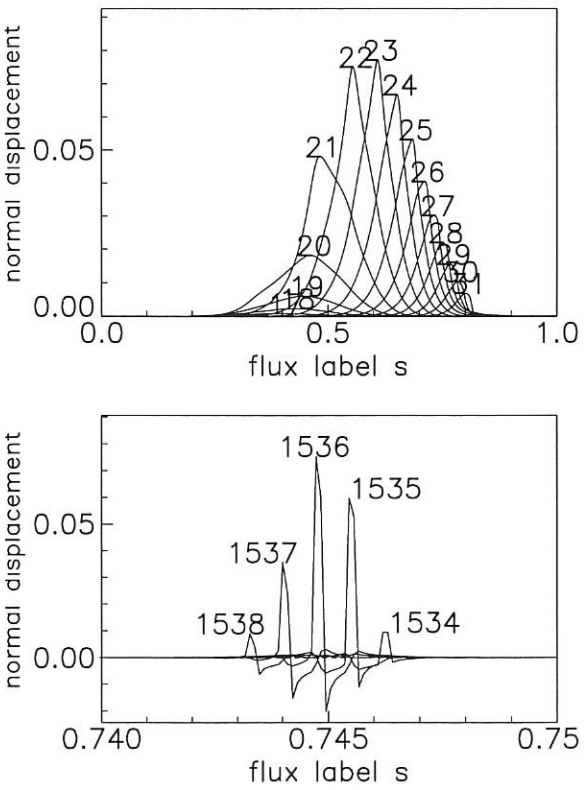

FIG. 1: Fourier coefficients of unstable modes from CAS3D: the $N = 18$ mode in an $A = 4.6$, $\langle\beta\rangle = 0.03$ circular tokamak (top part), the $M = 1536$ perturbation in a high-shear optimized Helias equilibrium (bottom part). Note that the bottom frame covers only approximately 0.01 in plasma radius and that from 89 Fourier coefficients the five leading ones are shown.

[1] National Institute for Fusion Science, Nagoya, Japan.

[2] CIEMAT Madrid.

[3] D.T. Anderson et al., Bull. Am. Phys. Soc. **36** (1991) 2293.

[4] Y. Nakamura et al., Proc. 9th Int. Stell. Workshop (Garching 1993), IAEA, Vienna 1993, p. 548.

2.3 3D MHD Equilibrium Calculations with Advanced Codes

Two 3D equilibrium codes which do not a priori require the existence of regularly nested magnetic surfaces, the HINT[5] and the PIES[6] codes, have been applied to W7–X /115, 191, 261/. Since these codes are built on quite different computational principles – for example, a fourth-order Eulerian grid combined with artificial time evolution in HINT as compared with magnetic-coordinate-based algorithms and β-iteration in PIES – their comparative application will increase confidence in finite-β island-size computations.

Here, two applications are shown. Improvements in the iteration technique of the PIES code have facilitated high-β studies of the W7–X configuration. Fig. 2 shows an example.

With respect to finite-β studies of the sizes of small-scale islands the scale of the radial resolution is of importance. While it is larger than a typical ion gyroradius in Fig. 2, the HINT code structure allows relatively easy access to ion-gyroradius resolution, see Fig. 3. Here, among other features, the change between the zero- and finite-β fine-scale island structures can be appreciated.

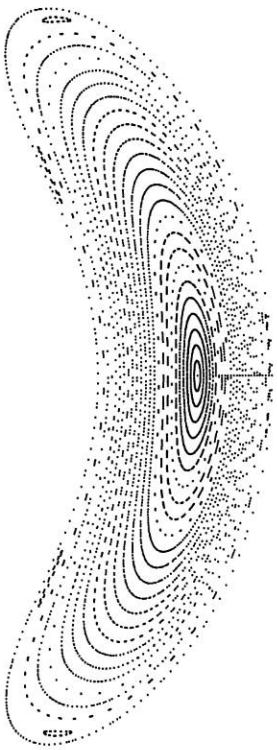

FIG. 2: A $\langle\beta\rangle = 0.04$ equilibrium obtained with the PIES code. Number of radial grid surfaces $k = 25$, $0 \leq m \leq 10$ poloidal, $-6 \leq n \leq 7$ toroidal Fourier modes.

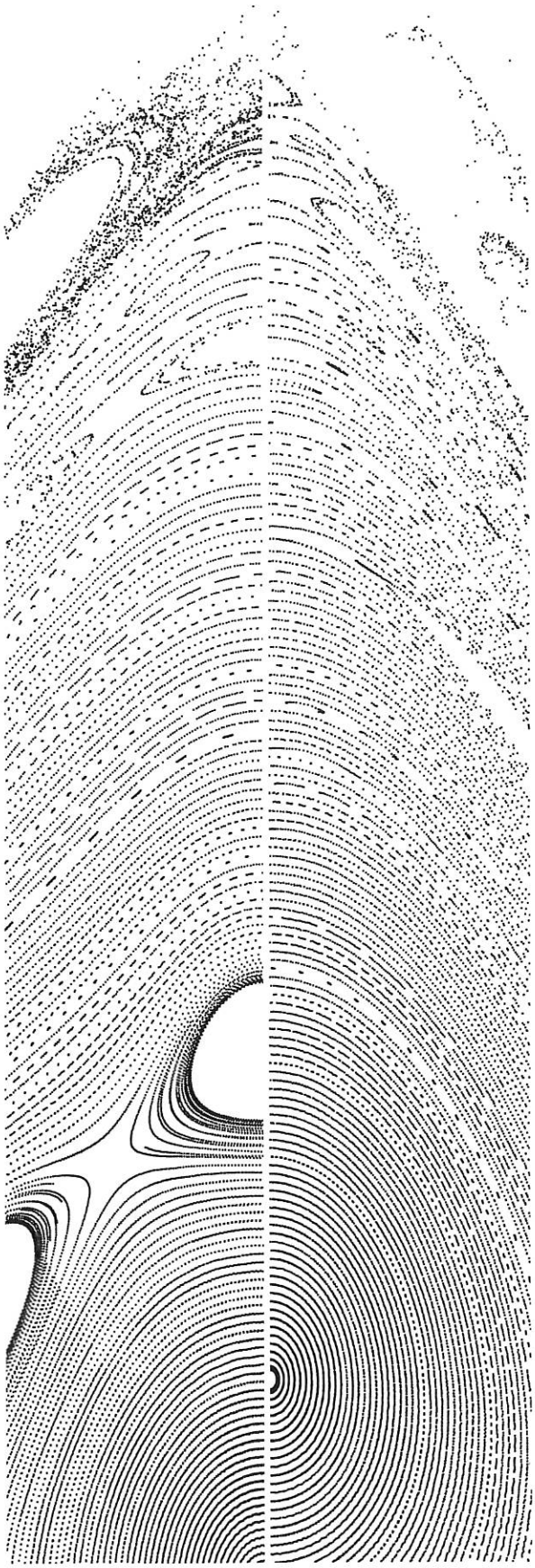

FIG. 3: Parts of the triangular cross-section of a zero-β HINT field (left) and a $\langle\beta\rangle \approx 0.03$ HINT equilibrium.

[5] T. Hayashi, in: *Theory of Fusion Plasmas*, Chexbres, Switzerland (1988), SIF (Bologna 1989) 11.

[6] A. Reiman, H. Greenside, Comp. Phys. Comm. **43** (1986) 157.

2.4 Divertor Physics Studies for W7–X

2.4.1 Geometrical aspects

In order to obtain moderate and uniformly distributed power and particle loads at the divertor plates, small angles of incidence and large wetted areas are needed. The divertor concept[7] developed for W7–X involves so-called troughs as divertor plates which are mapped onto each other by the field lines connecting them. The above goodness parameters can be improved, by varying the geometry of these troughs.

2.4.2 SOL modelling

Tracing magnetic field lines between divertor plates and characterizing them according to their lengths shows that an ordered-layer structure of the field lines in the edge region of Helias stellarators prevails /211, 279, 280/. Because of this layer structure it appears possible to use these field lines as coordinate lines for plasma edge modelling in this part of the edge region: in a first attempt, the temperature, density and velocity along the field lines are calculated by solving simple 1D energy and particle transport equations along 3D field lines[8] /279, 280/. In order to solve these 1D transport equations, a scrape-off layer (SOL) has been defined, i.e. a region in which volume sources of heat and matter – representing the flow of heat and matter from the main plasma – load the field lines. Its thickness is a parameter that has to be determined by particle and energy conservation within the model used here. Together with typical SOL parameters for W7–X (major radius: $R_0 = 5.5$ m, power flow: $P_e = 10$ MW, particle flow: $P_p = 300 \cdot 10^{20}$ s^{-1}) and the information on the field line positions relative to the SOL plasma region, one-dimensional fluid solutions along the field lines have been obtained. The simplest possible choice for a computation corresponding to a high-density situation in front of the targets is energy transport by pure electron heat conduction along the field lines with boundary conditions corresponding to small temperatures at the plates. This approach yields one-dimensional fluid solutions along the field lines. Combining these 1D calculations with complementary Monte Carlo methods which make use of the standard assumptions of SOL modelling, and which have been described in detail,[7] transport across the field lines is simulated by 'diffusion' of the field lines along which the one-dimensional solutions are obtained. The three-dimensional field line structure then leads to three-dimensional distributions of temperature, density (see Fig. 4) and velocity which incorporate effects of cross-field transport. With diffusion taken into account, the foot points of the long field lines, which come close to the last closed magnetic surface and along which a substantial part of the power and particles flows to the divertor troughs, are spread over a larger area on the troughs (approximately twice as large as in the case without diffusion) /279/.

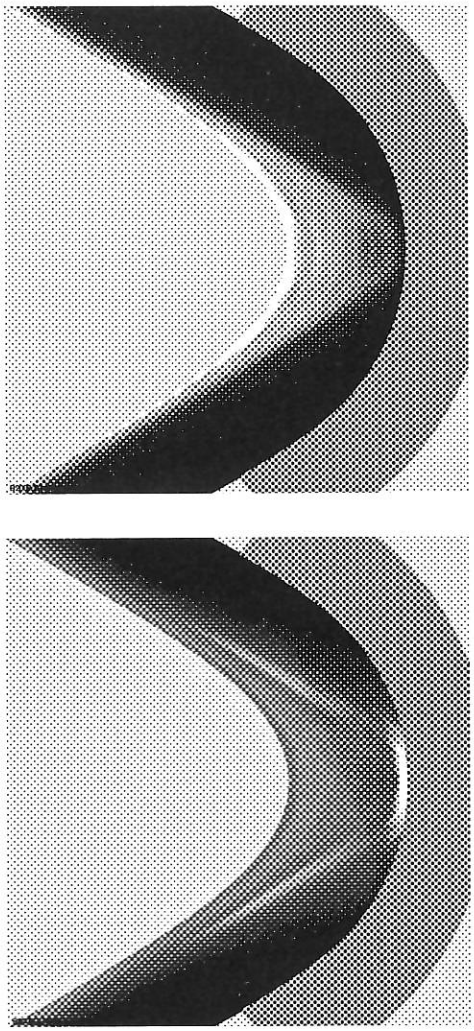

FIG. 4: Characterization of the temperature distribution (above) and density distribution (below) in the SOL taking diffusion across the field lines into account. The plots show part of the triangular cross-section. The white areas mark the regions with the highest temperatures (≥ 300 eV) and the largest densities ($\geq 1 \cdot 10^{20}$ m^{-3}), while the black areas correspond to $T = 0$ and $n = 0$. The inner light grey area shows the plasma inside the last closed magnetic surface and the dark grey area in front of the helical edge marks the helical trough. The SOL width is ≈ 0.025 m.

Furthermore, local structures of the vacuum magnetic field in the edge region, such as remnants of islands, are blurred and the effective field line length of the long field lines on the average is reduced.

---

[7] Strumberger, E., Nucl. Fusion **32** (1992) 737.

[8] Strumberger, E., 4th Int. Workshop on Plasma Edge Theory in Fusion Devices, Varenna 1993, Italy.

3. W 7-X TECHNICAL R & D

W. Bitter[1)], B. Fleischer[1)], H. Greuner, R. Holzthüm[1)], S. Huber[1)], N. Jaksic[1)], S. Kamm[1)], F. Kerl [1)], H. Münch, M. Pillsticker, J. Tretter[1)], J. Sapper, J. Simon-Weidner[1)], B. Sombach[1)], F. Schauer, I. Schoenewolf, F. Werner, A. Wieczorek

R. Heller, K. P. Jüngst, W. Maurer, KfK-ITP

3.1 Outline

The capacity of the technical team in 1993 was again concentrated on two essential tasks: On the one hand, the technical concept of the modular design for the superconducting W 7-X stellarator was presented on tours of further European and American laboratories (NET, PPPL, GA San Diego and UCLA) as well as at specialized conferences (KTG '93, EUCAS '93) in Germany; on the other hand, the design activities for the prototype work and the basic machine were intensified on the drawing boards as well as on the practical side.

First decision-making experimental results could be gained for the CIC superconductor. An extended and time-consuming tendering action aimed at European industry yielded results supporting the feasibility of a full-size nonplanar DEMO coil for W 7-X.

3.2 Basic Machine Design

Last year we reported that a complete CAD assembly from the cold mass and the cryostat was produced. Now we can announce that the cold-mass design could be further optimized in the direction of less structural material and a better understanding of modular assembly conditions.

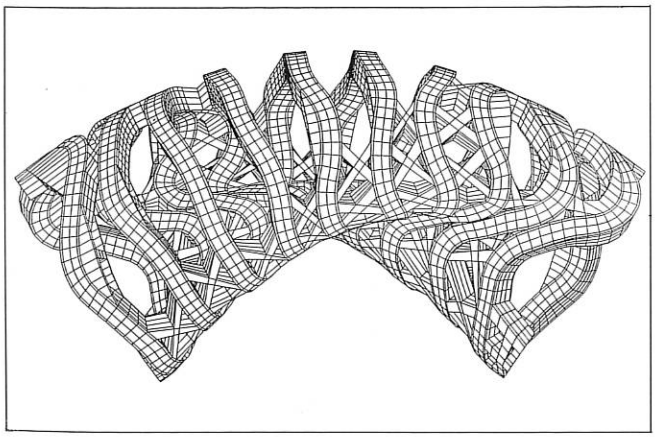

FIG. 1: W 7-X cold mass with structural X-elements

[1)] Central Technical Department

In Fig. 1 the replacement of solid and heavy structural vault elements by optimized X-elements is demonstrated. The gain from such a design is a minimized cold mass and more space between the coil system. Later, the detailed design of the modular dividing planes could be worked out, as shown in Fig. 2.

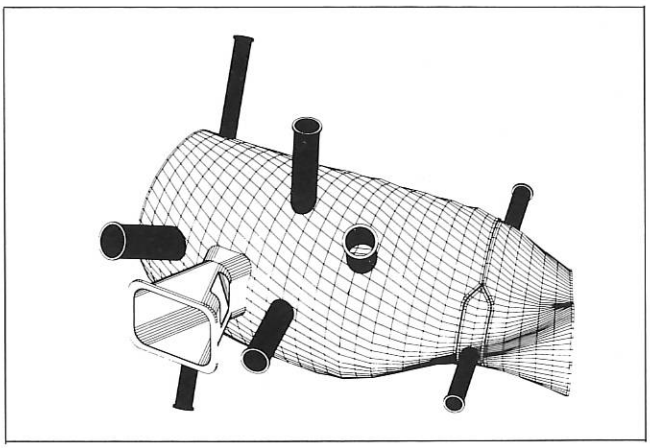

FIG. 2: Modular dividing plane for the vessel

3.3 Prototype Work

As reported last year, two test solenoids to be examined in the STAR test bed at KfK were ordered from TESLA, GB. The first of them was finally delivered with a delay of five months at the end of March last year. After that the coil was prepared at IPP for the test bed (Fig. 3). During commissioning of the LHE cooling circuit in the test plant an impermissibly large oil impurity was detected in the coil. With a chlorine-based solvent - recommended by specialists from the refrigerator manufacturer - solid reaction products were unfortunately generated in the CIC, which could not be dissolved again, using better solvents and the highest possible pressures and temperatures. So the coil could not be used for the envisaged tests.

FIG. 3: STAR-test coil

Together with the cable manufacturer, it was established that the cable had been impaired by an accident during the extrusion process which was not recognized at the time, but which can be safely avoided in future by adequate quality control instructions.

Meanwhile, 200 metres of clean conductor has been shipped to TESLA and the second coil is in production.

To get some more information for the cable before the next test campaign in early summer of 1994, we built a short-length test loop with 5 metres of conductor (see Fig. 4). This short circuit loop was inserted in the STAR test bed at the end of 1993. First reliable results will be available in February 1994. The loop can easily be charged with current by a small flux swing in the background field coils.

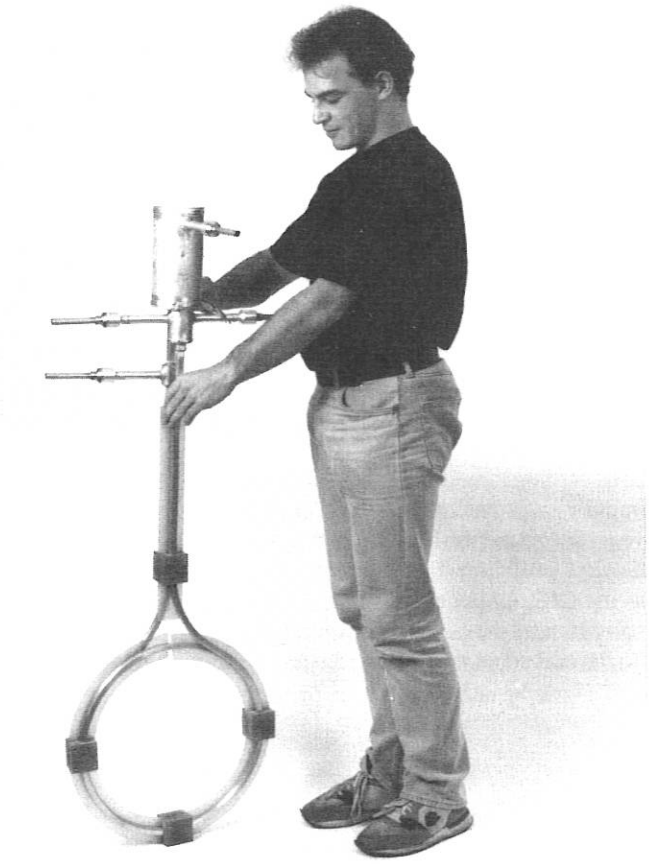

FIG. 4: Test loop from 5 metres cable length

As scheduled, we could issue the call for tenders for the W 7-X DEMO coil in April 1993. The quoted share of the delivery from industry is shown in Fig. 5. Industry was invited to undertake full design and manufacturing responsibility for the whole delivery. Five tenders were submitted, three of them completely fulfilling the specification. The technical and commercial evaluation of the tendering action was ready for contracting at the beginning of November 1993 at IPP. But some EURATOM conditions for preferential support are still blocking release of the contract. A delay of some months or more has unfortunately to be expected in pursuing this urgent development work.

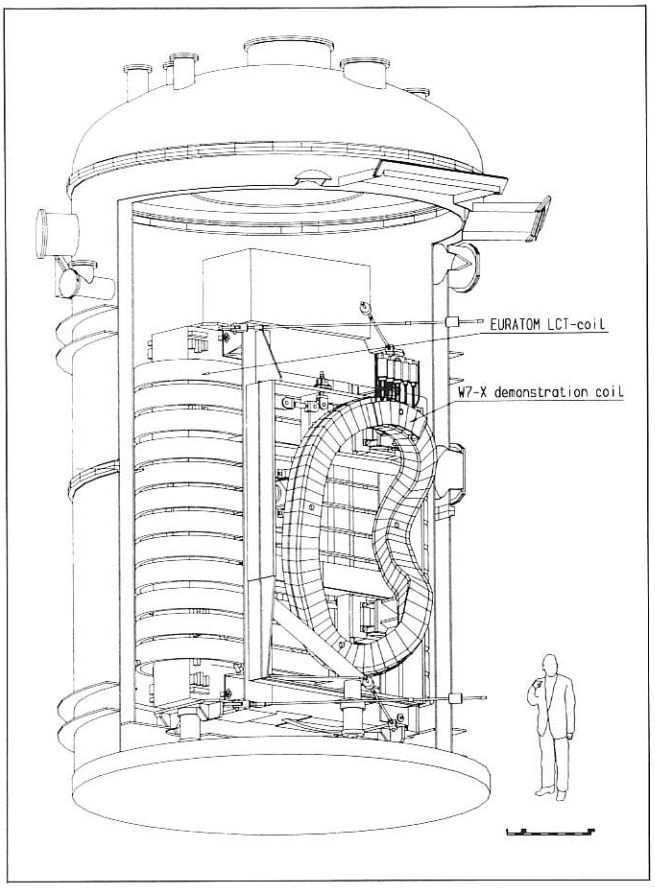

FIG. 5: Assembly of DEMO-coil

3.4 Further Activities

A 1 : 5 scale model for a machine section was ordered from industry using a stereolithographic method for the 3-D production of the components. This model, which will be delivered in February 1994, will serve for in-depth detail design of the magnet and cryostat vessel.

The work for the technical specification of a DEMO cryostat section was continued. The call for tenders for this second essential prototype component of W 7-X will be issued in spring 1994.

In the context of a diploma thesis at the Technical University of Munich transient mechanical disturbances by strand movement in a CIC superconductor were investigated experimentally. It could be shown that small jerky strand motions due to Lorentz forces in the cable can produce significant energy pulses which may reach the dynamic stability margin of the prototype conductor. The results of this work will be integrated in an improved conductor design for the DEMO coil.

IEA IMPLEMENTING AGREEMENT
for Cooperation in Development of the Stellarator Concept
EUROPEAN ATOMIC ENERGY COMMUNITY / US DEPARTMENT OF ENERGY

1. OBJECTIVES OF THE AGREEMENT

The objective of the Implementing Agreement, first concluded in 1985, is to "improve the physics base of the Stellarator concept and to enhance the effectiveness and productivity of research and development efforts related to the Stellarator concept by strengthening co-operation among Agency member countries". To achieve this, it was agreed to exchange information, conduct workshops, exchange scientists, do joint theoretical, design and system studies, coordinate experimental programmes in selected areas, exchange computer codes, and perform joint experiments. In 1990 the Agreement was extended until 1995. The contracting parties are EURATOM, the U.S. DoE, Japan (since October 1992), and Australia (since October 1993).

2. STATUS OF THE AGREEMENT

In 1993 three meetings of the Executive Committee were held. The 16th and the 18th meetings took place in the U.S. (at Princeton on January 6 and St. Louis on November 2), while the 17th meeting was held at Garching on May 11, in conjunction with the IAEA Stellarator Workshop. The main topics of these meetings were the progress of the collaboration, Australia´s request to join the Agreement, the future participation of Russian and Ukrainian laboratories, the status of the experiments, and especially the future of the collaboration. It was agreed to cooperate on reactor studies under the Implementing Agreement. A dialogue was started with that part of the tokamak programme which is oriented towards steady-state operation. A first joint workshop is to take place in 1994. The possibility of exchanging equipment without accompanying personnel will be included in the Agreement.

3. REPORT ON 1993 ACTIVITIES

In 1993, eighteen physicists participated in the exchange of scientists. From Japan K. Ida, K. Ichiguchi, and K. Watanabe (all from Nagoya) and F. Sano and K. Itoh (from Kyoto) visited Garching, their joint effort amounting to more than 6 man-months. They were interested in spectroscopic measurements, discussions on anomalous transport and resistive-MHD nonlocal modes, and the build-up of an International Stellarator Database. From Madrid Mrs. R. Balbin and Mrs. T. Estrada performed temperature and density fluctuation studies on W 7-AS, both staying for about 4 months. Also from CIEMAT, J.A. Jimenez adapted the NEMEC code and a ballooning code to the TJ-II geometry during a 4-week stay, while Mrs. M.A. Ochando was concerned with fluctuations and bolometry on W 7-AS for 2 weeks. During a visit to Madrid, P. Merkel from IPP implemented the NESCOIL code at CIEMAT. T. Luce and R. Waltz (both from San Diego) compared T_e profiles for off-axis ECR heating in stellarators and tokamaks, both staying for 4 weeks at IPP. For 7 weeks R. Isler from Oak Ridge computed plasma impurity compositions from spectroscopic data and undertook a comparison of different codes. M. Murakami (Oak Ridge) contributed to the discussions about an International Stellarator Database during his 5-day visit to IPP in August. L. Gianonne from IPP visited Japan for one month to study edge plasma physics on CHS. During a 2-week stay at Nagoya, Mrs. C. Schwab from IPP implemented the CAS3D code at NIFS. A. Teubel from IPP visited Madrid for 3 months during the summer. W. Mandl from IPP spent 13 months at San Diego to conduct resonant charge exchange spectroscopy on DIII-D.

On May 11, 1993, a contract on cooperation between IPP and the National Institute for Fusion Science, Japan, was signed at Garching to implement the academic collaboration on stellarators, within the framework of the Implementing Agreement.

4. WORKSHOPS

In 1993 the IAEA Workshop on Stellarators took place at Garching on May 10-14. The 5th International Toki Conference on plasma physics and controlled nuclear fusion was held at Toki City from November 16 to 19, 1993, with plasma heating and current drive as the main topics.

Divisions and Groups

THE SCIENTIFIC DIVISIONS OF IPP

Experimental Plasma Physics Division 1
Director: Prof. M. Kaufmann

ASDEX Upgrade
- divertor experiment for investigating the ITER/NET plasma boundary in a reactor-relevant divertor configuration and parameter regime, especially the questions of heat deposition, wall erosion, and particle exaust under good confinement conditions
- investigation of the magnetics of an ITER-type plasma

JET diagnostics
- operation of diagnostics at JET

Experimental Plasma Physics Division 2
Director: Dr. G. Grieger

Wendelstein 7-X
- preparation of construction
- further evolution of numerical and analytical methods of investigating equilibrium, stability and transport in three-dimensional toroidal configurations incl. plasma heating, particle and power exhaust
- engineering, R & D and prototype development

Contributions to stellarator reactor systems studies

Contributions to ITER/NET studies

Experimental Plasma Physics Division 3
Director: Prof. F. Wagner

Wendelstein 7-AS (Advanced Stellarator)
- stellarator with improved confinement conditions
- toroidal plasma confinement in the stellarator
- net-current-free plasmas, plasma production and heating by neutral injection, and high-frequency waves
- plasma stability and impurity effects

Technology Division
Director: Prof. R. Wilhelm

Neutral injection
- development and construction of the injection systems for W 7-AS, ASDEX Upgrade and W 7-X
- implementation of injection experiments

Electron cyclotron resonance heating
- preparation of ECRH for ASDEX Upgrade
- cooperation with ECRH project on W 7-AS

Ion cyclotron resonance heating
- preparation and implementation of ICRH experiments for W 7-AS, ASDEX Upgrade and W 7-X

Plasma technology (see also Surface Physics Division)
- development, characterization and modelling of low-pressure plasma processes for thin-film formation

Surface Physics Division
Directors: Prof. V. Dose
Prof. J. Küppers

Surface physics
- atomistic characterization of surfaces

Plasma wall interactions (analytical)
- interactions of atoms, ions and electrons with solid surfaces
- wall fluxes in the boundary layer of plasma devices
- limiter and wall analyses

Plasma wall interaction (preparative) (see also Technology Division)
- preparation and characterization of thin film coatings for plasma devices

Theory Division
Director: Prof. D. Pfirsch

Theoretical basis of plasma physics
- analytical and numerical MHD computations
- models for anomalous transport
- high-frequency current drive
- turbulence theory

Tokamak Physics
Director: Prof. K. Lackner

Tokamak physics
- experiment-oriented theoretical work for the design and interpretation of tokamak experiments such as ASDEX, ASDEX Upgrade, JET and NET/ITER
- experimental work on plasma edge physics on ASDEX Upgrade

Computer Science Division
Director: Prof. F. Hertweck

Development of the AMOS/D system

Development of data acquisition systems for experiments at IPP

Studies in parallel computer architectures

Berlin Division
Director: Prof. G. Fußmann

Experimental and theoretical investigations on impurities (production, transport, and radiation) in ASDEX Upgrade and W 7-AS

Plasma generator PSI-1
- operation and characterization of a high-current discharge
- plasma interaction with solid surfaces

Arc physics (especially vacuum arcs)

EXPERIMENTAL PLASMA PHYSICS DIVISION 1

(Prof. Dr. Michael Kaufmann)

Division E1 comprises two groups:

1. ASDEX Upgrade Operation and Diagnostics I

Head: W. Köppendörfer
Deputy Head: Streibl, B.

Albrecht, M., Behler, K., Bosch, H.-S., Buchelt, E., Blank, de H.J., Dorn, C., Drube, R., Eberhagen, A., Engstler, J., Finkelmeyer, H., Garcia-Rosales, G., Gehre, O., Gernhardt, J., Goss, H., Gruber, J., Haas, G., Herppich, G., Hohenöcker, H., Hupfloher, H., Jacobi, D., Kass, Th., Klement, G., Kollotzek, H., Kornherr, M., Krause, H., Krüger, P., Mast, K.F., Mattes, K., Meisel, D., Merkel, R., Mertens, V., Neu, G., Raupp, G., Richter, H., Salmon, N., Schilling, H.-B., Schittenhelm, M., Schramm, G., Schneider, H., Schweizer, S., Seidel, U., Söldner, F.X., Streibl, B., Suttrop, W., Treutterer, W., Troppmann, M., Ulrich, M., Vernickel, H., Wieczorek, A., Zasche, D., Zohm, H.,

This group is concerned with the operation of the tokamak experiment ASDEX Upgrade and its peripheral installation. This group also conducts a part of the experimental investigations. ASDEX Upgrade is the follow-up experiment of ASDEX. This work is described under the ASDEX Upgrade project.

2. Diagnostics II

Head: H. Röhr
Deputy Head: Salzmann, H.

Alexander, M., Andelfinger, C., Asmussen, K., Dux, R., Engelhardt, W., Fahrbach, H.-U., Field, A., Fuchs, Ch., Fußmann, G., Götsch, S., Herrmann, W., Jenichen, F., Junker, W., Kallenbach, A., Kurzan, B., Lang, P.T., Lang, R., Lieder, G., Mayer, H.-M., Murmann, H., Neu, R., Sandmann, W., Schönmann, K., Steuer, K.H. Stober, J.

This group is responsible for the development of plasma diagnostics and pellet injectors for ASDEX Upgrade, JET and other experiments. In addition, plasma physics investigations with these diagnostics are conducted by the group. The activities are detailed under the projects ASDEX Upgrade, JET Cooperation and W VII-AS.

EXPERIMENTAL PLASMA PHYSICS DIVISION 2

(Dr. Günter Grieger)

The activity of the Experimental Plasma Physics Division 2 is mainly concentrated on the WENDELSTEIN 7-X Project (see Sec. WENDELSTEIN 7-X Project).

The relevant team is:

W 7-X

D.T. Anderson[1)], S. Anderson[2)], C.D. Beidler, W. Dommaschk, H. Greuner, G. Grieger, E. Harmeyer, F. Herrnegger, K. Ichiguchi[3)], J.A. Jimenez[4)], J. Junker, N. Karulin, J. Kißlinger, W. Lotz, P. Merkel, H. Münch, J. Nührenberg, M. Pillsticker, F. Rau, H. Renner, J. Sapper, F. Schauer, A. Schlüter, I. Schoenewolf, C. Schwab, U. Schwenn, M. Spada, E. Strumberger, D. Sünder, K. Watanabe[5)], A. Wieczorek, H. Wobig, L.-J. Zheng.

---

1) Guest from the University of Wisconsin, Madison (USA)

2) Guest from the University of Wisconsin, Madison (USA)

3) Guest from National Institute for Fusion Science, Nagoya (Japan)

4) Guest from CIEMAT, Madrid (Spanien)

5) Guest from National Institute for Fusion Science, Nagoya (Japan)

EXPERIMENTAL PLASMA PHYSICS DIVISION 3 (W7-AS)

(Prof. Dr. Friedrich Wagner)

Experimental Plasma Physics Division 3 comprises the W7-AS group, the work of which is fully reported in the section "STELLARATOR Project". The members of this group are as follows:

R. Balbin[1], J. Baldzuhn, K. Behringer[15], A. Borschegovsky[5], R. Brakel, R. Buechse, R. Burhenn, G. Cattanei, J. Das, A. Dodhy, D. Dorst, A. Elsner, M. Endler[17], K. Engelhardt, V. Erckmann, T. Estrada[1], Y. Feng, S. Filchenkov[5], U. Gasparino, J. Geiger, T. Geist, S. Geißler, U. Gerstel[17], L. Giannone, P. Grigull, H. Hacker, M. Haese[18], H.J. Hartfuss, O. Heinrich[17], G. Herre[17], C. Hidalgo[1], M. Hirsch, J.V. Hofmann, E. Holzhauer[15], K. Ida[10], V. Il'in[4], V. Isaev[5], R. Isler[8], R. Jaenicke, M. Kaiser, F. Karger, A. Kechriniotis[11], M.A. Kedves[12], M. Kick, A. Kislyakov[2], C. Konrad[17], H. Kroiss, G. Kuehner, K. Kurbatov[6], A. Kus, A.G. Litvak[5], L. Lubyako[5], T. Luce[8] H. Maassberg, C. Mahn, S. Malygyn[6], V. Malygyn[5], W. Mandl, N. Marushchenko[7], K. McCormick, S. Morita[10], M. Murakami[9], H.U. Nickel[16], H. Niedermeyer, M. Ochando[1], W. Ohlendorf, M. Peters[13], V. Plyusnin[7], H. Ringler, A. Rudyj, N. Ruhs, J. Saffert, F. Sardei, S. Sattler[17], F. Schneider, U. Schneider, G. Siller, E. Sizov[3], U. Stroth, E. Suvorov[5], G. Theimer[17], M. Thumm[16], M. Tutter, E. Unger, F. Wagner, R. Waltz[8], A. Weller, E. Würsching, S. Wurdack, H. Yamada[10], M. Zerbini[14], D. Zimmermann, M. Zippe, S. Zöpfel

1) Guest from CIEMAT, Madrid (Spain)
2) Guest from IOFFE Institute, St. Petersburg (CIS)
3) Guest from Gen. Phys. Inst., Moscow (CIS)
4) Guest from Kurchatov Inst., Moscow (CIS)
5) Guest from IAP, Nizhny Novgorod (CIS)
6) Guest from Salut, Nizhny Novgorod (CIS)
7) Guest from Kharkov Inst. (Ukraine)
8) Guest from General Atomics, San Diego (USA)
9) Guest from Oak Ridge National Laboratory (USA)
10) Guest from Nat. Inst. for Science, Nagoya (Japan)
11) Guest from University of Patras (Greece)
12) Guest from KFKI Research Inst., Budapest (Hungary)
13) Guest from FOM-Instituut, Nieuwegein (Holland)
14) Guest from ENEA, Frascati (Italy)
15) Guest from IPF Stuttgart (Germany)
16) Guest from KfK Karlsruhe (Germany)
17) Doctoral fellow
18) Undergraduate

GENERAL THEORY DIVISION

(Prof. Dr. Dieter Pfirsch)

The areas treated in the General Theory Division are: MHD equilibria, linear and nonlinear instabilities, current drive; turbulence, transport. These studies are done in the framework of macroscopic and microscopic theories. Particular topics addressed were: the energy principle of plasma-vacuum systems; the linear stability of various toroidal equilibria and straight equilibria with noncircular cross-sections; nonlinear instability of force-free configurations and of straight tokamaks; Hopf bifurcation; resistive MHD; most probable current sheet profiles; disruptions and ELM's, MHD and drift-wave turbulence; negative-energy waves and corresponding nonlinear instabilities within the framework of quasi-neutral multifluid theory, Maxwell-Vlasov theory and Maxwell-drift kinetic theory, anomalous transport due to, in particular, fusion α-particles. The study of a number of nonlinear phenomena entailed extensive numerical work. With respect to numerical methods, nonlinear systems of ordinary differential equations were investigated.

1. MHD THEORY

1.1 On the Energy Principle for Plasma-Vacuum Systems

D. Lortz

The energy principle of magnetohydrodynamics for plasma-vacuum systems is reconsidered. It is shown that the original formulation of Bernstein et al. (1958) is correct, while that of Lehnert (1993) is not.

1.2 Nonexistence of Some Classes of Nonaxisymmetric MHD Equilibria

A. Salat, R. Kaiser (Univ. Bayreuth) and
J. Tataronis (Univ. of Wisconsin, USA)

The existence of MHD equilibria without toroidal or helical symmetry has long been questioned on theoretical grounds. Proofs of (non)existence, therefore, are highly desirable. We explored this issue for the particular case of magnetic fields whose field lines are plane and poloidally closed around the magnetic axis of a torus. We proved two results: 1) If an axisymmetric configuration, e.g. a corresponding Solovev solution, is perturbed away from axisymmetry either by making the magnetic surfaces "bumpy" with respect to the toroidal angle and/or by bending the magnetic axis away from a circle, there can no longer be an equilibrium with the above-mentioned field configuration. 2) There is no isodynamic equilibrium ($B^2 = const$ on magnetic surfaces) with the above-mentioned field configuration, whether axisymmetric or not.

1.3 Stability of Straight Tokamak Equilibria without Wall Stabilization

D. Lortz and A. Zeiler

A specific straight tokamak equilibrium surrounded by a vacuum and without a conducting wall is proved analytically to be stable to all ideal MHD modes. Stability of axisymmetric modes is proved by solving the eigenvalue problem up to second order in the corrugation amplitude. Whereas elliptical corrugation ($N = 2$) leads to instability for arbitrary current density, an equilibrium with $N \geq 3$ may be stabilized to axisymmetric modes by current reversal. To treat nonaxisymmetric global modes, the potential energy is evaluated by means of tokamak scaling. A sufficient stability criterion is derived according to which the equilibrium is stable to nonaxisymmetric modes if the current density in the outer plasma area is reversed and that in the centre is sufficiently peaked and if the safety factor q at the magnetic axis is greater than unity, increasing monotonically towards the plasma edge.

1.4 Stability of Force-free Plasma-Vacuum Systems

D. Lortz and G. O. Spies

The magnetohydrodynamic stability of plasma-vacuum equilibria with $\nabla \times \mathbf{B} = \mu \mathbf{B}$ in the plasma ($\mu = \text{const}$) is studied in two different geometries: (1) A circular cylinder with identified ends (topological torus) is unstable for all aspect ratios and wall distances unless $|\mu|$ is above the threshold for reversal of the toroidal current density, but below that for reversal of the poloidal one. (2) The classical spheromak (spherical plasma-vacuum interface, homogeneous magnetic field at infinity) is unstable and cannot be wall-stabilized.

1.5 Nonlinear Stability and Hopf Bifurcation

H. Tasso

(a) Nonlinear stability: Nonlinear stability in hydrodynamics and magnetohydrodynamics is discussed especially in

connection with 'unconditional' stability and severe limitations on the Reynolds number. Two examples in magnetohydrodynamics are treated: the case of force-free fields and the case of a straight tokamak. They show that the limitations on the Reynolds numbers can be removed but unconditional stability is preserved. Practical stability needs to be treated for limited levels of perturbation or for conditional stability.
(b) Hopf bifurcation: A special Hopf bifurcation in resistive magnetohydrodynamics can easily be identified by starting from a particularly suitable form of the linearized equations which was previously introduced by the author. This bifurcation is triggered by an increase of density in a plasma otherwise sufficiently stable in the absence of inertia. It is conceivable that the bifurcation may be related to Mirnov oscillations and the density limit for disruption as well as to the onset of MHD or magnetoacoustic turbulence.

1.6 Nonlinear MHD Computations

M. Tippet, D. Biskamp

The XTOR nonlinear MHD code of J. F. Luciani is being used to investigate tokamak phenomena such as major disruptions and ELM's. The code solves the three-dimensional MHD equations in a torus. A recent modification reduces storage requirements by a factor of three, allowing greater resolution.

1.7 Current Sheet Profiles in 2D MHD

D. Biskamp

Numerical simulations of current sheet formation in a two-dimensional, incompressible MHD system reveal that sheets evolve self-similarly with cross-sheet profiles close to $j(\psi) \propto exp\{-2\alpha\psi\}$. This so-called natural profile has previously been derived by several authors as the most probable state in a current-carrying plasma, but the derivation has been subject to some criticism, particularly regarding the strictly 2D case. Using the Elsässer variable formulation, one can, however, show that within a weak, clearly defined approximation the natural profiles have a solid statistical foundation also in 2D.

1.8 Algorithms for Nonlinear Eigenvalue Problems

G. Czapski, R. Meyer-Spasche

Convergence properties of multi-grid approximations of a Grad-Schlüter-Shafranov model equation with free boundary are investigated.

1.9 Numerical Ordinary Differential Equations Versus Dynamical Systems

R. Menzel, R. Meyer-Spasche

Nonlinear systems of ordinary differential equations are investigated: stability of equilibrium points, numerical approximation, comparison of the dynamics in the continuous model with the dynamics in discrete models.

2. TURBULENCE AND TRANSPORT

2.1 Dynamics and Statistics of Inverse Cascade Processes in 2D MHD Turbulence

D. Biskamp, U. Bremer

The inverse cascade for the mean-square potential $A = \int \psi^2 d^2x$ in a 2D magnetofluid randomly forced at small scales is studied. Scaling laws for the initial linear stochastic phase are derived and verified numerically. In the nonlinear cascade phase one finds the spectral behaviour $A_k \simeq 2.6\epsilon_A^{2/3}k^{-7/3}$, where ϵ_A is the injection rate of A. The inverse cascade proceeds by coalescence of current filaments, giving rise to selfsimilar magnetic structures. The coalescence is much faster than in decaying turbulence since the high level of small-scale turbulence generates a large turbulent resistivity. Condensation at $k = 1$ leads to a quasi-static magnetic configuration. The statistics of velocity and magnetic field increments are strictly Gaussian even in the condensation phase, in contrast to the behaviour recently found in the case of 2D Navier-Stokes turbulence.

2.2 Spectral Properties and Statistics of Resistive Drift-Wave Turbulence

D. Biskamp, S. J. Camargo

Resistive drift-wave turbulence is studied by high-resolution numerical simulations in the limit of small viscosity (high Reynolds numbers), such that the adiabaticity parameter C is the only relevant parameter. For $C > 1$ the particle flux is equal to the quasilinear value, while for $C < 1$ the latter is larger. Energy, enstrophy and density fluctuation spectra exhibit a maximum at some wavenumber k_o, and a power law behaviour for $k > k_o$. The statistics of vorticity and density fluctuations are non-Gaussian for $k > k_o$, indicating strong small-scale intermittency, but are perfectly Gaussian for $k \sim k_o$, which is consistent with the absence of large-scale long-living coherent structures, in contrast to the behaviour of the highly viscous system previously studied.

2.3 Drift-Wave Spectra in 1D and 2D

H. Tasso

Equilibrium statistics of model Hamiltonians for 1D and 2D nonlinear drift wave equations are considered. While in 1D the energy spectrum is Lorentzian (see previous work of the author), it has the shape $(\mu^2 + k^2)^{-3/2}$ in 2D, i.e. $\sim k^{-3}$ for large k, in agreement with measurements on tokamaks.

2.4 LH Waves Absorption

R. Croci, E. Canobbio

Study of LH wave absorption has yielded a useful approximation for the space-dependent Quasi Linear Diffusion Coefficient. The nonlinear interaction between the electric field and QLDC (through the dependence of the plateau limits on the gradient of the electric field modulus) and its

role in the successful explanation of the experimental LH current drive results (absorption and density limits) have been clarified.

2.5 Reflection and Absorption of Ordinary Waves in an Inhomogeneous Plasma

R. Croci

The solution of the Vlasov-Maxwell equations for confined plasma slabs with field sources in vacuum when the electric field is parallel to the external magnetic field (ordinary waves) was reduced to the solution of a singular integral equation in k space. The asymptotic solution of this equation when the inhomogeneity length is larger than the Larmor radius was deduced. Since the solution does not involve restrictions on the field wavelength, it was then possible to derive the reflection and absorption coefficients of the waves from the source in vacuum.

2.6 Plasma Rotation in Ohmic Plasmas

D. F. Düchs, H. Morsi (CEU, Brussels)

Plasma rotation was measured for ohmically heated JET plasmas through highly resolved Doppler-shifted X-ray lines from nickel impurities. A large data base was collected. The various existing theoretical models were reviewed and found to be unsuitable. It seems that toroidal momentum can be picked up by the impurities during the influx phase in the boundary layer, and transported inwards through several stages of ionization.

2.8 Anomalous Transport Due to Finite Ion Gyroradii

D. F. Düchs, G. Kamelander (ÖFZ Seibersdorf, Austria), F. Pohl

In an ignited magnetized fusion plasma the density of α-particles is not negligible. During most of their cooling-down period their gyroradii considerably exceed the Debye shielding lengths. This leads to the creation of electric fields in the case of spatial gradients. Mechanisms of the viscosity type can lead to a redistribution of the electrons corresponding to (gradient-dependent) anomalous transport. Similar effects can occur for fast ions produced by neutral beam injection or RF wave heating, or in plasma boundary layers with steep gradients.

2.8 Diffusion of Magnetic Field Lines

D. F. Düchs, A. Montvai, (CRIP Budapest)
Ch. Sack (CEU Brussels), Graf Finck v. Finckenstein (TH Darmstadt)

Realistic perturbation levels of tokamak magnetic fields can hardly ever lead to fully stochastic field line distributions. The "stochastic" appearance of puncture maps ("Poincare plots") usually masks underlying structures and can also easily be produced by using unsuitable numerical methods to solve the (nonlinear) field line equations. Mapping procedures for the field line equations in Hamiltonian form were developed and have turned out to be much more adequate.

3. THEORY OF NEGATIVE-ENERGY WAVE PERTURBATIONS

3.1 Negative-Energy Perturbations in a Magnetically Confined Plasma in the Framework of Maxwell-Drift Kinetic Theory

G. N. Throumoulopoulos (Univ. of Ionia, Greece), and D. Pfirsch

1) Plane equilibria: For tokamak- and shearless stellarator-like analytic cold-ion equilibria the fraction of thermal electrons associated with negative-energy perturbations (active particles) is determined. Negative-energy perturbations exist for $\eta_e < 0$ and $\eta_e > 2/3$, $\eta_e = d\ln T_e/d\ln N_e$. In both cases it is found that a substantial fraction α of thermal electrons are active, in particular $\alpha \sim 1/3$ for linearly stable equilibria with $\eta_e = 1$. For all equilibria considered the phase space occupied by active electrons increases as one proceeds from the centre to the plasma edge region. 2) Cylindrically symmetric equilibria: The perturbation energy is obtained by evaluating the general expression derived by Pfirsch and Morrison.[1] The conditions for the existence of negative-energy perturbations which must hold in the minimum-energy frame of reference are derived for vanishing initial field perturbations and found to be in general similar to the plane case. The implications for tokamak equilibria are now being examined.

3.2 Negative-Energy Perturbations in General and in Arbitrary One-dimensional Vlasov-Maxwell Equilibria

D. Correa-Restrepo, D. Pfirsch

The expression for the free energy of arbitrary perturbations of general Vlasov-Maxwell equilibria derived by Morrison and Pfirsch[1] is put in a concise form, which is subsequently evaluated for the case of internal perturbations in arbitrary equilibria, e.g. plane or circularly cylindrical configurations. With the single exception of configurations in which the equilibrium distribution functions are everywhere isotropic and monotonically decreasing functions of the particle energy, these equilibria allow negative-energy perturbations without requiring a large spatial variation of the perturbation across the equilibrium magnetic field.

3.3 Nonlinear Instabilities Relating to Negative-Energy Modes

D. Pfirsch

The nonlinear instability of general linearly stable systems allowing linear negative-energy perturbations is investigated with the aid of a multiple time scale formalism. It is shown that the basic equations thus obtained imply resonance conditions and possess inherent symmetries which lead to the existence of similarity solutions of these equations. These solutions can be of an explosive type, while oscillatory and static solutions are normally linearly unstable.

---

[1] D. Pfirsch and P. J. Morrison, Phys. Fluids B **3**, 271, 1991.

TOKAMAK PHYSICS

(Prof. Dr. Karl Lackner)

The main task of this division is theoretical and experimental support of IPP tokamak activities. Consequently, the major part of its work is reported in the sections regarding ASDEX Upgrade, JET and ITER/NET. The activities described below concern either more basic aspects of fusion plasma physics or the development of models and codes not exclusively linked to one particular experiment.

Head: K. Lackner, Deputy: J. Neuhauser
Team: G. Becker, A. Bergmann, M. Bessenrodt-Weberpals, M. Brambilla, K. Büchl, A. Carlson-Rubner, R. Chodura, D. Coster, W. Feneberg, S. Fiedler, O. Gruber, O. Kardaun, K. Lackner, L. Lengyel, P. Martin, J. Neuhauser, G. Pautasso, T. Richter, M. Schlüter, R. Schneider, W. Schneider, J. Schweinzer, B. Scott, P. Spathis, M. Weinlich, H. Werthmann, R. Wunderlich, H.-P. Zehrfeld.

Guests: A. Boozer, College of William & Mary, Williamsburg, B. Braams, New York University, Yu. Igitkhanov, Kurchatov Institute, Moscow, S. Jardin, PPPL, Princeton, E. Kakoulidis, Demokritos, Athens, C. Kessel, PPPL, Princeton, G. Kristof, Technical University, Budapest, A. Kukushkin, Kurchatov Institute, Moscow, G. Kyriakakis, Demokritos, Athens, P. Lalousis, IESF, FORTH, Heraklion, P. McCarthy, University of Cork, H. O'Callaghan, University of Cork, S. Pitcher, Institute for Aerospace Studies, Toronto, P. Platzer, Institut für Allgemeine Physik, Vienna, D. Reiter, KFA, Jülich, V. Rozhansky, Kalinin Polytechnical Institute, Leningrad, N. Tsois, Demokritos, Athens, R. Zanino, Politecnico Torino.

1. PLASMA TRANSPORT AND TURBULENCE STUDIES

1.1 Computational Studies of Electron Drift Dynamics in Two Dimensions

The principal difficulty in this type of simulation is the electron dynamics parallel to the magnetic field. The interaction of this with the main $E \times B$ drift perpendicular to the field is the point of focus, but it involves only the component with very small gradient parallel to the field. Much larger parallel gradients are involved in the parallel ion dynamics, but a simulation which has to resolve parallel electron dynamics with these gradients would be inordinately expensive. To circumvent this problem, one develops implicit algorithms able to take large time steps while leaving fast but physically uninteresting dynamics in equilibrium. Such schemes are accurate only to $O(\tau)$. Recently, however, a new scheme which retains stability for all τ but extends accuracy to second order was developed, following its successful implementation in the field of finite-element MHD computation.[1] The scheme, called DIRK2, breaks the time step into three parts: implicit-explicit-implicit, with step fractions chosen to give accuracy to $O(\tau^2)$. By allowing larger values of τ, the time needed for computation of one saturated state has been reduced by a factor of about seven.

The electron fluid drift model has been extended to low collisionality: specifically, the long mean-free path regime, which usually holds in tokamak plasmas, and the "transcollisional regime" (collision and fluctuation frequencies comparable), which is particularly relevant to the L-to-H mode transition while still faithfully treating the electron dynamics. The model has passed comparison tests against a drift-kinetic computation in the linear regime. The results show that thermal conduction is most strongly affected by the long mean-free path, but since the resistivity is unaffected the turbulence retains the mode structure it has in the collisional regime, and is actually strengthened by the reduction in dissipation. The implication is that the drift wave turbulence emerging from these studies[2] is not restricted to the collisional regime, and it is certainly relevant to L-to-H transitions observed in the ASDEX and D-III-D tokamaks.

The process of electron production by ionization of neutrals has been incorporated into the model. If such terms are important in the equations, the time scale ordering separating profile adjustment and fluctuation evolution will break down. When the ionization source term is included in two dimensions, the density of neutrals needed to alter the fluctuations' structure is found to be about ten times larger than that actually present.

---

[1] A.H. Glasser, J. Comput. Phys. 85 (1989) 159
[2] B.D. Scott, Phys. Fluids B 4 (1992) 2468

1.2 Computational Studies of Electron Drift Dynamics in Three Dimensions

Motivated by the desire to properly treat the variation of the background on flux surfaces, work on an electron fluid numerical tokamak has been accelerated. Although the ions and trapped electrons must eventually be incorporated, the basic interaction between the plasma and the external discharge is through the parallel current. So a system bringing fluid electron drift dynamics and two-dimensional MHD together is a necessary step.
The present effort is proceeding in axisymmetric flux-coordinate geometry, so that tokamaks of arbitrary cross-section may be addressed. This work uses a system in which only one of the coordinates has a nonvanishing gradient parallel to the field; this becomes the "parallel" direction, and only a few grid points in it are needed even if several thousand are used in the other two.

1.3 A General Transport Simulation

To incorporate the predictions of turbulence model into 1- or 1 1/2-D transport simulations, a numerical scheme has been developed allowing for arbitrary dependence of the fluxes on the transported quantities and their gradients. This same treatment is used to compute the parallel dynamics in the three-dimensional computations outlined above, allowing full nonlinear stepping of the axisymmetric background. In addition, a simple one-dimensional numerical tokamak has been developed which incorporates the new transport model with a finite-element treatment of the MHD equilibrium maintenance, including the external Ohmic circuitry. This same method will be used to incorporate two-dimensional MHD with the turbulence in flux coordinates, building the fluid numerical tokamak.

1.4 Neoclassical Transport with Surface Variation of the Macroscopic Quantities

Including into neoclassical theory the variation of temperature, flow velocity and density along the magnetic field leads to the so-called gyrokinetic equation, which was solved by a moment expansion about a local Maxwellian. Use was made of a model collision operator correctly describing a plasma consisting of electrons and high Z-impurities and introducting an error <2 into the coefficients of a pure plasma. This method yielded results for the up-down asymmetry of the temperature, the poloidal variation of viscous forces, the electrical resistivity and the bootstrap current in the low-collisionality regime that showed strong deviation from the present neoclassical calculation, where these effects of surface variation of the macroscopic quantities were neglected. The temperature variation found so far is large enough to predict via the drift term a factor of 10 in the electron thermal transport over the theory of trapped particles. In the region of mean free path representative of present experiments the asymmetry of the temperature scales with the square root of collisionality and does not follow the asymptotic behaviour of the usual perturbation theory. To obtain precise results for the bootstrap current depending on a balance between viscous and friction forces, a further improvement of the collision model is required.

1.5 Transport Simulations of the Ignited ITER with High Helium Fraction

Computer simulations with special versions of the one dimensional BALDUR predictive transport code were carried out to investigate the particle confinement of helium and hydrogen, the energy confinement and the burn control in the high-density scenario of the ITER CDA physics phase. The code uses empirical transport coefficients for ELMy H-mode plasmas, an improved model of the scrape-off layer (SOL), an impurity radiation model for helium and iron and fast burn control by neutral beam injection feedback. Self-sustained thermonuclear burn is achieved for hundreds of seconds. The necessary energy confinement time τ_E is found to be 4.2 s, which is attainable according to the ITER H-mode scaling. In the ignited ITER, a significant dilution of the DT fuel by helium takes place. Steady-state helium fractions of up to 8 % are obtained, which are found to be compatible with self-sustained burn. The SOL model yields self-consistent electron densities and temperatures at the separatrix ($n_e = 5.8 \cdot 10^{19}\ m^{-3}, T_e = 80\ eV$). Small helium Mach numbers cause a high helium density pedestal, a steady-state helium content of 7% and a ratio $\tau_p^{He}/\tau_E = 4.9$ in the baseline case. Variation of the diffusion coefficient D at fixed electron heat diffusivity χ_e results in $\tau_p^{He}/\tau_E = 0.5\chi_e/D + 4.1$, the high offset being due to the helium density pedestal. The radiation loss required for halving the divertor heat load is reached with 0.2 % iron. Simulations further show that efficient burn control is achieved in the sawtooth-free case and also with sawteeth (see Fig. 1). Heating up to ignition and burn control are found to be also possible at small injection energies such as 0.5 MeV and even 0.2 MeV. Computer experiments with current and density ramps and an extended burn duration of 410 s were conducted.

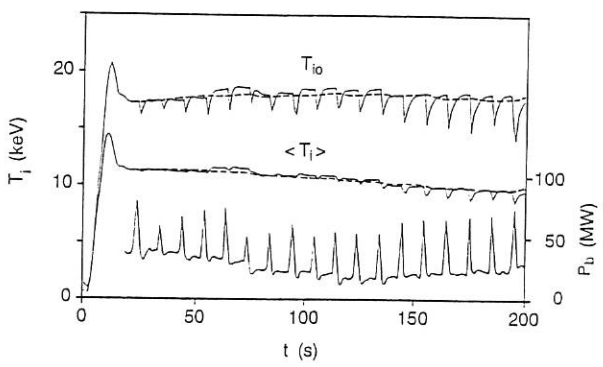

FIG. 1: Performance of burn control in the presence of sawteeth. Time development of ion temperatures and neutral beam power of the feedback system. The ion temperatures from the run without sawteeth are shown for comparison (dashed curves).

Special versions of the 1.5-D BALDUR transport code have been developed on the basis of the PPPL-BALDUR code. They include empirical scalings of transport coefficients, separate treatment of heat conduction and convection in the SOL, flux limit for parallel electron heat conduction, non-equidistant grid for modelling the steep gradient zone and SOL and burn control by NBI feedback. The code will be applied in transport simulations of ITER and ASDEX Upgrade.

1.6 Modelling of Neutral Beam Power Deposition Profiles

A statistically well-designed database of 48 electron and ion power deposition profiles, generated with the FREYA Monte Carlo code using the fixed beam geometry and circular plasma cross-section of ASDEX, was analyzed in order to investigate the direct recovery of the beam power deposition profiles $p_t(r)$ from the following plasma profiles, which are assumed to be known: electron density $n_e(r)$, electron temperature $T_e(r)$, impurity $Z_{eff}(r)$ and background neutral density $n_o(r)$. An algorithm has been developed, which succeeds in the recovery of $p_t(r)$ with a typical fractional error of $< 5\%$ over most of the plasma rising to $\approx 10\%$ at the edge. These error levels are very close to the inherent Monte Carlo scatter in the FREYA profiles. It is envisaged that this analysis will be extended to ASDEX Upgrade once the FREYA code is adapted for non-circular geometry and peaked toroidal current profiles.

1.7 Discriminant Analysis to Predict the Occurrence of ELMs in H-mode Discharges *

The application of discriminant analysis to a standard dataset from ASDEX, JET, and JFT-2M discharges (see Annual Report 1992) was extended to cover, for ASDEX and JET, the influences of the distance between the plasma and wall, the elapsed time since the L-H transition, and the ohmic, instead of the instantaneous electron density ('plasma memory'). Linear and quadratic boundaries in plasma parameter space where small ELMs are expected to occur are estimated from the data, together with their uncertainties, and their performance is compared with that of more flexible non-parametric boundaries, which are more complicated to describe.

2. DIVERTOR AND LANGMUIR PROBE PHYSICS

2.1 Fluid Boundary Conditions at a Divertor Target

Although fluid models are widely used for the description of plasma flow in the scrape off layer, the question of boundary conditions at the divertor target for the flow components along magnetic field lines is not yet satisfactorily settled. If the plasma consists of N viscous, heat-conducting ion fluids, then for the 2N parabolic momentum and energy equations 2N boundary values for the ion velocities and temperatures have to be prescribed. These boundary values have to be compatible with the requirements of the kinetic theory of the electrostatic sheath in front of the target. This theory yields only one condition for a combination of all ion boundary velocities (Bohm condition), i.e. there is a deficiency of boundary conditions for ion velocities for N>1 and there are no boundary conditions for the ion temperatures.
A way out of this situation would be to neglect ion viscosity and ion heat conduction or to treat them as small corrections iteratively. In this case the ion equations become hyperbolic. If the target is assumed to absorbions, than the boundary conditions on the ion equations would be that all fluid characteristics should point out of the plasma region, which means that no boundary conditions whatever may be imposed on ion velocities and temperatures. From the conditions of outgoing characteristics at the boundary follows a necessary condition on the flow velocities which is identical with the Bohm condition if the ion thermalforces are set to zero and the ion adiabatic constant γ_i is set to 3. Thus a solution of the inviscid ion fluid equations without boundary conditions at the target automatically fulfill the Bohm condition. It includes the presheath region, where the plasma adjusts to the conditions of the sheath. The inviscid ion fluid solution may then be used as a starting point for iteratively taking into account the ion viscosity.

2.2 2D Particle Simulation of the Sheath in Front of a Flat Langmuir Probe in a Magnetic Field

The sheath in front of a flat Langmuir probe oriented obliquely to a strong magnetic field was studied by performing two-dimensional particle simulations with a 2D-3V PIC code (see Annual Report 1992) calculating the full ion and electron orbits. The Poisson equation is solved in a plane parallel to the magnetic field. The dependences of the sheath structure and the probe current on the angle between the magnetic field and probe surface, and on the size and voltage of the probe, were determined.
The gross structure of the sheath is similar to that in 1D simulations, i.e. a quasi-neutral magnetic sheath with a thickness of some ion Larmor radii and a Debye sheath with a large space charge. The extent of the Debye sheath is strongly dependent on the probe voltage, and therefore the Debye sheath and the adjacent part of the magnetic sheath are essentially two-dimensional. The Debye sheath thickness strongly increases when the incidence angle of the magnetic field is decreased or the probe voltage increased. The dependence on the probe voltage is similar to the well-known Child-Langmuir law, whereas that on the angle is due to the increase of the local Debye length at the sheath entrance owing to the density drop inside the magnetic sheath, which is connected to the acceleration of

* In cooperation with S.-I. Itoh, K. Itoh, and J.W.P.F. Kardaun.

the ions perpendicular to the probe surface.
Non-saturation of the ion current, as observed in recent measurements with Langmuir probes flush-mounted into divertor target plates in ASDEX Upgrade, is seen in the simulations when the thickness of the Debye sheath is no longer small compared with the projection of the probe width along the field lines. Then more ions are drawn by the strong electric field onto the probe than are collected when the probe is at plasma potential. The current-voltage characteristics obtained from the 2D simulations have the same form as those from experiments, although in the experiment the angle is much smaller and the probe size is much larger. Scaling relations for the sheath thickness and the current to the probe were obtained and confirmed by additional 1D simulations with very small incidence angles.

3. THEORY OF HEATING AND WAVES IN TOROIDAL PLASMAS

3.1 Ion Distribution Function during Ion Cyclotron Heating

A new, very fast code, SSFPQL, solving the steady-state quasilinear kinetic equation for the ion distribution function in two velocity variables during IC heating has been written. It omits toroidal trapping of energetic ions, but includes finite Larmor radius effects to all orders. It can be used to take into account quasilinear effects in the description of wave propagation and absorption with reasonable numerical effort. Applications of SSFPQL to ASDEX Upgrade and ITER have been made. At the power levels to be expected in ITER, quasilinear self-boosting of first-harmonic heating of tritium is not sufficient to overcome the rather low absorption efficiency at ohmic temperatures: a reduction of the density or a low concentration of the 3 He minority might be required at the beginning of the heating pulse. Above 15 keV on the other hand the quasilinear increase of the fusion reactivity by suprathermal tritium ions is not negligible and might lower the ignition temperature by a few keV.

3.2 Effects of Collisionless and Collisional Damping on the Launching Efficiency of Ion Bernstein Waves

The code which solves the integral wave equation for ion Bernstein waves in slab geometry was extended by coding the local power balance and including collisional losses. Bernstein waves are found to be very sensitive to ion cyclotron damping, and the slow cold-plasma wave to electron Landau damping. Thus for efficient launching the frequency should not be close to an ion cyclotron harmonic in the plasma periphery, and the average $k_{||}$ of the antenna should not be too large. It is also found that collisional damping can dissipate a non-negligible fraction of the launched power and could be made prohibitive by even a modest anomalous increase of the effective collision frequencies.

3.3 Drift Waves in Toroidal Geometry

The kinetic wave equation for electrostatic drift waves was rederived, starting from the formal solution of the Vlasov equation in toroidal geometry. No a-priori assumption (ballooning, radial localization) is made about the form of the solutions. It is assumed, however, that the collisionality is sufficiently large to make toroidal trapping negligible (plateau regime), and an expansion in the ion Larmor radius is made to transform the integral wave equation into a set of second-order differential equations for the components of the poloidal Fourier spectra of the wave field. A preliminary scheme for the solution of these equation has been worked out.

4. PELLET ABLATION IN REACTOR-GRADE PLASMAS

4.1 A Self-consistent MHD Ablation Model

A time-dependent quasi-two-dimensional ablation model has been developed. The ablation of a pellet injected into a magnetically confined plasma and the temporal variation of the properties of the cloud surrounding it are calculated in a self-consistent manner. The energy deposition in the shielding cloud is determined by stopping length calculations applied along the magnetic field lines with allowance for electrostatic shielding effects. The stopping length calculations are supplemented by thermal diffusion calculations, thus redistributing the energy deposited in the discrete energy group approximation. The neutral cloud is allowed to expand also in the direction perpendicular to the magnetic field. Finite rate equations are used for determining the time history of the ionization state of the ablated substance. The deceleration and full stopping of the cross-field motion is calculated by means of an MHD model, thus determining the transient variation of the lateral cloud dimension and the corresponding modifications of the field-aligned density and temperature distributions used in the stopping length calculations. The expulsion of the magnetic field lines by the expanding and ionized ablatant and their rediffusion into the partial magnetic cavity thus formed are also calculated. The variation of the ablation rate along the pellet path is calculated at a sequence of flux surfaces, thus determining the particle deposition profile. The results of penetration depth calculations were compared with values derived from experiment and from other ablation models. Good correspondence was found at moderate plasma temperatures. Predictive calculations performed for a reactor-grade plasma yielded, owing to magnetic shielding effects, substantially larger penetration depths than those obtained with the standard NGS ablation models.

SURFACE PHYSICS DIVISION

(Prof. Dr. Volker Dose
Prof. Dr. Jürgen Küppers)

Scientific activities in the Surface Physics Division proceed via three routes, which we call plasma wall interaction (analytical), plasma wall interaction (preparative) and surface science. Our work on analytical problems of plasma wall interaction is for the purpose of this report further divided into two categories. Those activities which take place in intimate collaboration with fusion devices are included in the respective chapters on tokamaks and stellarators. Additional laboratory work described in this chapter is grouped under the title plasma wall interaction processes. Contributions to the field of plasma wall interaction (preparative) are described in a separate section entitled plasma technology. This project is a joint venture with the IPP Technology Division. More fundamental studies, summarized under the heading of surface science, comprise a continuation of previous activities in magnetism and contributions to the Sonderforschungsbereich 338. The latter concentrates on adsorption at solid surfaces and integrates work at the Munich Universities and IPP and MPQ.

Head: V. Dose, Deputy Head: E. Taglauer,

V. Alimov[4], A. Annen[1], R. Behrisch, E. Bertel, J. Biener[1], J. Cramer[2], T. Detzel[1], M. Donath, W. Eckstein, K. Ertl, Th. Fauster, P. Franzen[3], A. Friedl[3], Y. Furuyama[5], C. Garcia-Rosales[3], S. Grudeva-Zotova[6], B. Gubanka[2], P. Hanesch[1], D. Hildebrandt[7], R. Hytry[3], W. Jacob, C. Jandl[1], M. Kaiser[3], A. v. Keudell[1], K. Krieger, J. Krumrey[2], S. Labich[2], A. Niehof[3], K. Lange[1], M. Langhoff[1], W. von der Linden, C. Linsmeier[1], C. Lutterloh[1], A.P. Martinelli, M. Mayer[1], N. Memmel, W. Möller, D. Naujoks[3], J. Onsgaard[8], F. Passek[1], P. Pecher[1], H. Plank[3], J. du Plessis[9], W. Poschenrieder, A. Rabe[2], G. Ramos-Lopez[1], J. Reinmuth[2], S. Reiter[1], P. Roos[1], J. Roth, P. Sandl[3], A. Schenk[1], B. Scherzer, A. Schiavi[3], S. Schömann[2], U. Schubert[1], R. Schwörer[1], G. Staudenmaier, A. Steltenpohl[2], I.S.T. Tsong[10], P. Varga[11], E. Viljoen[9], G. Venus, H. Verbeek, M. Vonbank[3], W. Wang[12], B. Winter[3].

1 Doctoral Candidate
2 Undergraduate Student
3 Post Doc
4 Guest, Academy of Science, Moscow, USSR
5 Guest, Kobe University of Mercantile Marine, Japan
6 Guest, Bulgarian Academy of Sciences, Sofia, Bulgaria
7 Berlin Division of IPP
8 Guest, Odense University, Denmark
9 Guest, Orange Free State, Bloemfontein, SA
10 Guest, Arizona State University, USA
11 Guest, Technical University Vienna, Austria
12 Guest, Academia Sinica, Shanghai, China

1. PLASMA WALL INTERACTION

1.1 Recycling

The plasma density control in fusion experiments and the helium dilution of the plasma strongly depend on the recycling behaviour of the first wall for incident hydrogen and helium ions. The main recycling processes for hydrogen are kinetic reflection of low energy ions, reemission after recombination to molecules in the implanted surface layer or atomic hydrogen reemission at high temperatures. Radiation damage in the crystalline material may act as trapping centre for hydrogen and helium ions. These processes were investigated with strong emphasis on graphite and carbon based materials.

1.1.1 Angular dependence of kinetic scattering of low energy deuterium ions from carbon surfaces
(M. Mayer, W. Eckstein, B.M.U. Scherzer)

Trapping and particle reflection coefficients for 50-500 eV deuterium on graphite have been measured for angles of incidence between 0 and 75 degrees by determining the increase of the areal density of trapped deuterium with implantation fluence using the D(^{3}He, p)α nuclear reaction. The particle reflection from a smooth (HOPG) and a rough (EK98) surface is compared in Fig. 1.

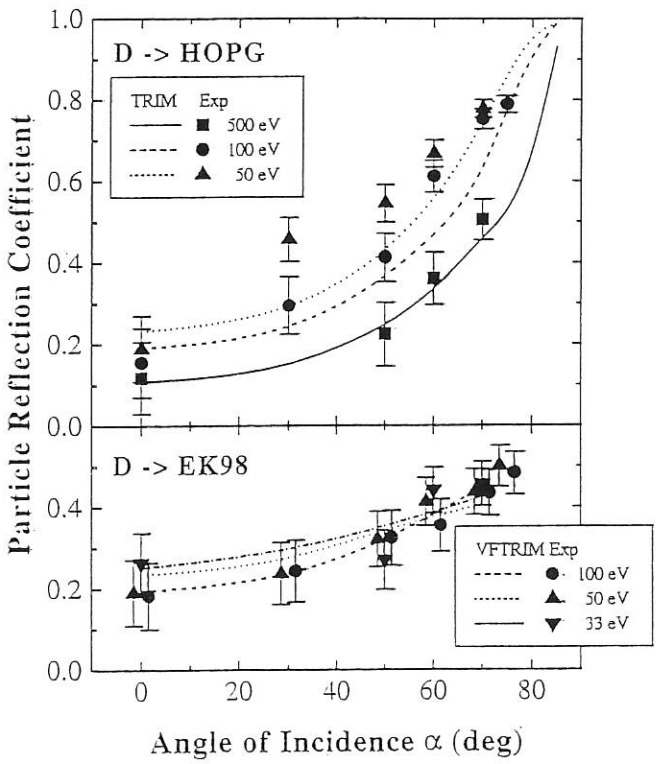

FIG 1: Dependence of the reflection coefficient for deuterium ions on the angle of incidence for smooth HOPG and rough EK 98 graphite surfaces.

The experimental results were compared with computer calculations using the TRIM.SP- and the VFTRIM-program. For a smooth surface there is good agreement between experiment and computer simulation. Surface roughness accounts for a decrease of 50% of particle reflection at oblique incidence and low energies. Surface roughness as determined by scanning-tunnel microscopy can be simulated with fractal surfaces in VFTRIM. Quantitative agreement between experiment and simulation can be achieved.

1.1.2 High temperature reemission from graphite
(P. Franzen)

The model of Möller and Scherzer for trapping and reemission of hydrogen from graphite was extended to include the effects observed during implantation above 1000 K. It is assumed that atomic hydrogen is released if a hydrogen atom reaches the geometrical surface without recombination. The emitted flux J of atomic hydrogen is then given by

$$J = D \cdot \left. \frac{\delta c}{\delta x} \right|_{x=0},$$

where D is the atomic diffusion constant, c is the concentration of atomic hydrogen in solution, and the boundary condition at the surface is c(0)=0. With this ansatz the atomic re-emission from graphite and USB15 as well as the dependence of the re-emitted atomic flux in the stationary state on the ion energy could be correctly reproduced. The model predicts, however, a larger dependence of the implanted flux density than observed experimentally. These calculations were performed with the PIDAT package (a computer Program for Implant Diffusion and Trapping), which is now available at the IBM RISC6000 workstation.

1.1.3 Hydrogen retention and reemission in impure graphite
(M. Langhoff, B.M.U. Scherzer)

Hydrogen retention and reemission in graphite is investigated with respect to the mobile inventory of hydrogen in the first wall of fusion devices. Deuterium is implanted to high fluences into graphite by a RF discharge with a mean energy of 150 eV. An energetic He beam (2.6 MeV) allows in-situ measurements of the hydrogen inventory by means of ERD (elastic recoil detection). Simultaneously the beam is used for RBS (Rutherford backscattering spectrometry) to monitor impurities on the target arising from erosion of the surrounding chamber walls.

Time-resolved measurements show no mobile hydrogen at room temperature. The induced desorption by ions in the MeV range, however, is enhanced by Fe_2O_3 impurities on the graphite. This is not the case for tungsten impurities. These impurities also lead to a surface topology consisting of spikes about 1μm long and 0.4μm in diameter. This is thought to be the reason for a much higher hydrogen inventory than that

observed in pure graphite. Carbon walls, on the other hand, lead to build-up of a plain hydrogenous film that exhibits extremely low ion-induced desorption. Measurements of the hydrogen inventory at elevated temperatures (600 K) similar to conditions in fusion devices are in progress.

1.1.4 *Annealing of radiation damage due to implantation of helium and deuterium in HOPG graphite and diamond*

(G. Ramos, B.M.U. Scherzer)

The formation and annealing of radiation damage due to the implantation of helium (20 keV) and deuterium (8 keV) in basal-oriented HOPG graphite and diamond <100> was investigated by Rutherford backscattering spectroscopy in channeling geometry (RBS-c). About 500 carbon atoms per incoming ion were displaced in HOPG due to the implantation of ^{3}He ions at 300 K and about 70 in diamond. These values are greater than those predicted by model calculations (60 and 40, respectively) with TRIM.SP.

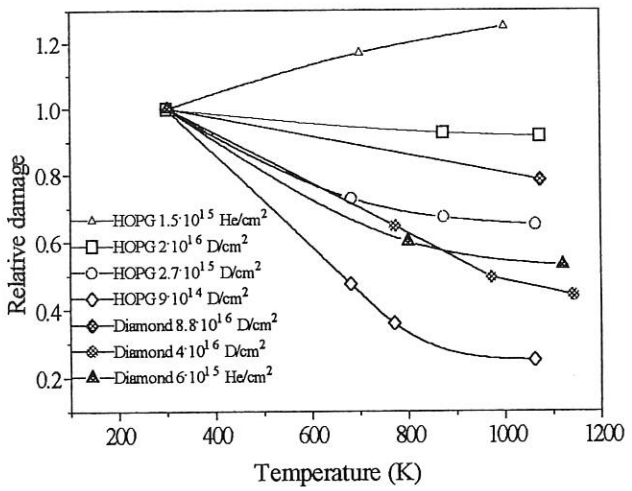

FIG. 2: Thermal annealing of radiation damage due to implantation of helium and deuterium at 300 K with different fluences in HOPG-graphite and diamond <100>.

Upon heating up to 950-1150 K, low fluence deuterium induced damage showed between 50% and 70% annealing in HOPG and diamond (see Fig. 2). Low fluence helium induced damage, however, showed annealing in diamond and an increase of disorder in HOPG. Only little desorption of the low fluence implanted helium due to the annealing was observed in both materials. The increase of disorder in HOPG is attributed to the formation of blisters during heating.

The desorption of helium from basal-oriented HOPG showed a dependence on the defect concentration produced during implantation at 300 K. For high fluence implanted helium ($\phi > 10^{16}$ He/cm^2), for which crystalline twin growth is observed at the surface, helium starts to desorb already at 500 K, while for low fluences ($\phi < 10^{16}$ He/cm^2), for which no twins are detectable, little desorption is observed up to the highest annealing temperature (950 K).

1.2 Erosion and Surface Composition Changes due to Ion Bombardment

Incident plasma ions will erode plasma-facing surfaces by kinetic ejection of surface atoms. The threshold energy for these ejection processes depends on the ion-target atom combination and increases for light ions with the atomic mass of the target material. A systematic comparison for a large variety of ion-target combinations leads to a new empirical description of the energy dependence of sputtering and of the threshold energy. Fundamental understanding was improved in extensive computer simulations of the sputtering process, including isotope effects, temperature dependences and aspects of crystalline texture of the material.

Most newly developed plasma-facing materials are compounds of different elements. In these materials compositional changes of the surface layer occur due to ion-induced diffusion and segregation, preferential sputtering of components as well as deposition or implantation of incident ions. These processes are difficult to study by computer simulation and constitute the emphasis of the experimental investigations.

1.2.1 *Revised formulae for sputtering data*

(C. García-Rosales, W. Eckstein , J. Roth)

In the last three decades a large number of sputtering yield data measured and/or calculated at IPP have accumulated, which include the energy and angular dependence of the sputtering yield for a large number of projectile-target combinations. All these data were collected in a recent IPP Report (IPP 9/82), where the data for normal incidence as a function of ion energy have been fitted by the Bohdansky equation

$$Y\left(E_0, a = 0^\circ\right) = Q\, S_n^{KrC}\left(1 - \left(\frac{E_{th}}{E_0}\right)^{2/3}\right)\left(1 - \frac{E_{th}}{E_0}\right)^2$$

where E_0 is the projectile energy, α the angle of incidence, E_{th} the threshold energy where sputtering becomes zero and S_n the nuclear stopping cross-section based on the Kr-C potential. The values Q and E_{th} are used as fit parameters. Q determines the maximum of the yield curve. The large number of fitting values obtained for Q and E_{th} on the basis of the collected data allows the derivation of analytic expressions for Q and E_{th}. The analytic scaling for Q is based on Sigmund's theory for sputtering and is given by

$$Q\,E_s^{2/3} = 1.633\left(Z_1 Z_2\right)^{2/3}\left(Z_1^{2/3} + Z_2^{2/3}\right)^{1/3}\frac{M_1^{5/6} M_2^{1/6}}{M_1 + M_2}\,\frac{3 + M_2/M_1}{20 + \left(M_2/M_1\right)^{1.6}}$$

where E_s is the surface binding energy (heat of sublimation) and Z_1, Z_2, M_1, M_2 the projectile and target atomic numbers and masses, respectively. This equation leads to a good fit of the Q values obtained by fitting the experimental and calculated sputtering data. For E_{th} the best fit equation based on the large number of fitted parameters of the threshold energy is given by

$$\frac{E_{th}}{E_s} = 7.0\left(\frac{M_2}{M_1}\right)^{-0.54} + 0.15\left(\frac{M_2}{M_1}\right)^{1.12}$$

This fit is shown in Fig. 3. These two fit equations give a good guess for the parameters Q and E_{th} of the Bohdansky equation for a given projectile-target combination at normal incidence and for all energies. However, in cases where data are available it is preferable to use the specific fit values given in the figures of the report mentioned above.

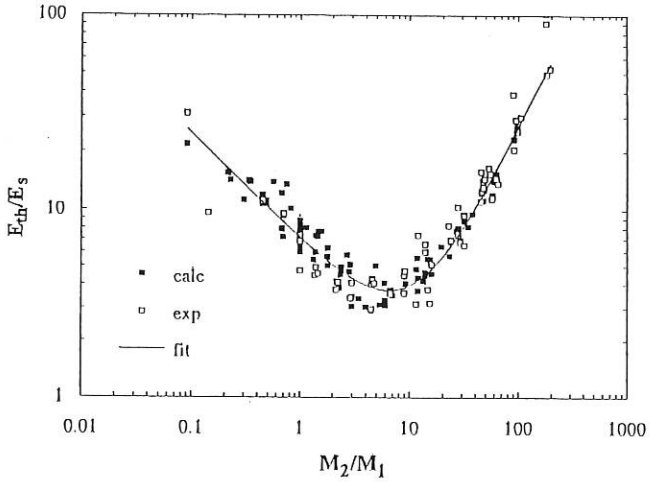

FIG. 3: The relative threshold energy, E_{th}/E_s, versus the ratio of target to projectile mass. Solid squares represent calculated data, open squares experimental data. The solid line is a fit to all available data, due to the formula given above.

1.2.2 *Threshold sputtering*
(W. Eckstein, C. Garcia-Rosales, J. Roth, J. Laszlo)

Due to the large fluxes of particles to walls and divertors (limiters) in fusion plasma machines it may be important to have information on the behaviour of sputtering near the threshold. The sputtering yield was determined by computer simulation as a function of the angle of incidence for the examples D on Cu, Au, Ar on Cu, Cu on Cu and Xe on C to cover the important mass ratio range. It is found that for light ion bombardment (large mass ratio) the threshold is nearly independent on the angle of incidence which is not the case for heavy ion bombardment (mass ratios ϕ lower than 10). A further result is that the widely used Bohdansky formula is too steep near threshold energies. A simple analytic model makes clear that the inelastic energy loss plays an important role to explain the lower threshold and the dependence on the angle of incidence for small mass ratios.

1.2.3 *Fundamental aspects of sputtering*
(W. Eckstein, R. Behrisch, M. Hou, M.T. Robinson, E.S. Mashkova, V.A. Molchanov)

The sputtering of an isotope mixture of 50% ^{92}Mo and 50% ^{100}Mo was investigated by computer simulation. The energy and angular distribution were studied and found to be in good agreement with recent experimental data. Also the fluence needed to reach equilibrium agrees with experimental findings.

Temporal aspects of the sputtering of copper single crystals were studied by computer simulation in the binary collision approximation with the MARLOWE code. The self-sputtering of a Cu(100) crystal with incident energies from 1 to 100 keV was selected as a case study. At normal incidence most atoms are ejected at the beginning of cascade development. Time correlations in the energy and momentum transported by the atoms through the surface are studied and an important contribution of the surface refraction by the binding potential is found. Analysis of the relative emission energies within limited delays reveals that the fraction of quasi-simultaneously ejected first neighbours is not sufficient to explain experimental results on cluster emission.

The angular distribution of sputtered W is investigated experimentally and by computer simulation. Differences between the two results can be attributed to the effect of surface topography either initially or subsequently during ion bombardment.

The sputtering yield depends on the surface binding energy (heat of sublimation), which decreases slightly with increasing dependence on temperature. There also exist a few cases where the heat of sublimation increases with temperature, e.g. tungsten. The final effect on the sputtering yield for bombardment of silver with deuterium is studied by computer simulation. The increase in the yield can be appreciable but is usually smaller than the thermal evaporation.

1.2.4 *Sputtering and surface composition modifications of Ti doped graphite RG-Ti*
(C. García-Rosales, J. Roth, R. Behrisch)

Carbon materials containing about 2 at % Ti, such as the Russian material RG-Ti, exhibit a very high thermal conductivity, thus making them candidates for high heat flux components in fusion devices. The RG-Ti material was investigated in respect of its thermal stability, sputtering behaviour, chemical erosion, surface composition modifications as well as trapping and release of hydrogen due to D^+ bombardment at energies between 50 and 1000 eV and at temperatures of up to 2000 K. The results of this study can be summarized as follows: a major fraction of Ti in RG-Ti forms TiC precipitates. The Ti is stable up to temperatures $\leq$2000 K, as can be seen from the Ti depth profiles after heating to 2000 K as measured with RBS. The energy dependence of the sputtering yield of RG-Ti at room temperature

due to D^+ bombardment is very similar to pure graphite, showing also the absence of a threshold energy due to hydrocarbon formation at energies below 100 eV. The chemical reactivity of pure carbon with energetic hydrogen leads to enhanced erosion yields due to methane formation with a maximum at temperatures around 800 K. The presence of Ti in RG-Ti reduces the maximum of the methane formation of pure graphite by a factor of 3. This may be due to a small fraction of Ti in solid solution with graphite (≤0.6 at %). No Ti enrichment at the surface could be detected after 1 keV D^+ sputtering at 770 K. D^+ bombardment of RG-Ti at temperatures >1200 K leads to the development of a columnar structure, because the TiC grains, which are not eroded by radiation enhanced sublimation (RES) but only by physical sputtering, shield the underlying graphite from erosion. After long-time sputtering at high temperatures steady-state Ti enrichment at the surface will be found, which amounts to about 9 at % Ti at 1700 K. Thermal desorption spectra of D_2 and CD_4 molecules from RG-Ti after D^+ implantation at 400 K showed that a small Ti addition to graphite does not significantly alter the deuterium retention and reemission behaviour of pure graphite.

1.2.5 *Surface segregation during ion bombardment of alloys*

(J. du Plessis, G. van Wyk, E. Taglauer)

The surface composition of Pd/Pt alloys was investigated after irradiation with ions as a function of ion energy using AUGER and ion scattering spectroscopy. Preferential sputtering of Pd is most pronounced for light ions (He^+) and low ion energies; for heavy ions (Xe^+) only a weak energy dependence was observed. Depletion of the second and consecutive layers, indicative of a segregation process, was found and the results were used to determine segregation energies and radiation-enhanced diffusion coefficients.

The equilibrium composition at the surface of Au_3Cu was determined as a function of temperature. Pronounced segregation of Au was seen and the kinetics was studied by sputtering and thermal annealing.

1.2.6 *Boron segregation and chemical binding in ion-bombarded USB15 graphite*

(R. Schwörer, J. Roth)

Boronized USB15 graphite containing 15 wt.-% boron was bombarded with 1keV D^+-ions at different temperatures. The structural change at the surface was detected by in situ Auger Electron Spectroscopy (AES) and the fine structure of the carbon Auger-signal was investigated by Chemical Factor Analysis (CFA). With CFA it is possible to calculate the chemical state of the carbon atoms by assuming that carbon exists either in the graphitic or carbidic state. The CFA results in much more carbidic carbon than is expected from the measured boron-carbon concentration at the surface (Fig. 4). According to the boron-carbon phase diagram, up to 2.3% boron dissolves in the graphite matrix at lattice sites. This leads to distortions of the sp2-binding structure of the hexagonal carbon rings and a more carbidic electronic structure of the carbon atoms. Thus the low chemical erosion of boronized graphites could be a chemical effect, e.g. by lowering the binding energy between carbon and hydrogen atoms, thus reducing the production of precursors of hydrocarbon molecules. The observed boron maximum and minimum when changing the sample temperature from 300 K to 1000 K during sputtering (Fig. 4) is due to diffusion of displaced boron atoms within the ion range and subsequent surface segregation.

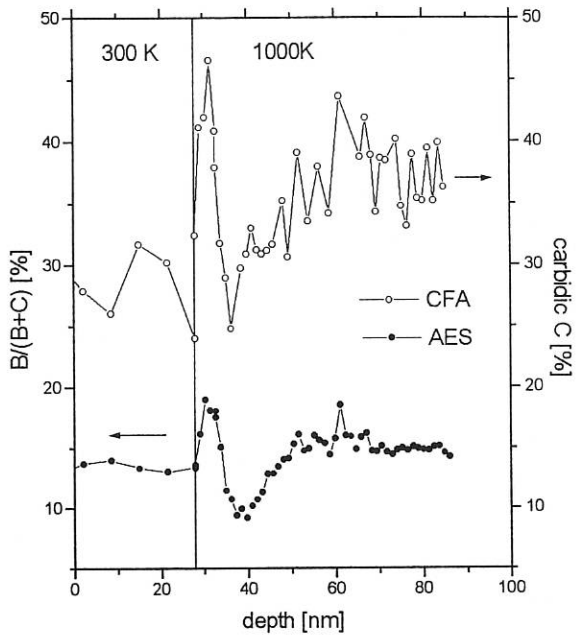

FIG. 4: Boron and carbidic carbon concentrations vs. eroded depth. Filled circles: concentration of boron at the surface calculated from the Auger signal heights. Open circles: carbidic carbon calculated by CFA.

1.2.7 *Carbon film growth due to low energy beams*

(Y. Lifshitz, C.D. Roux, K. Boyd, W. Eckstein, J.W. Rabalais, W. Wang, H. Plank, J. Roth, J. Steffen)

The development of carbon films on Li, Si, Ni and Au due to 30-300 eV carbon bombardment is studied experimentally (Auger spectroscopy) and by computer simulation with the dynamic program, TRIDYN. Both results are in good agreement and are in accord with the subplantation model. For carbon and hydrocarbon ions the deposition behaviour on Si and graphite was studied as a function of temperature in the energy range 90 to 6000 eV. The analysis was done by weight change, ion beam analysis and AES. While at room temperature the deposition coefficient for carbon and hydrocarbon ions is the same, at elevated temperatures the deposition coefficient drastically decreases for hydrocarbon ions (Fig. 5). Taking into account the erosion of deposited carbon atoms by self-sputtering and chemical sputtering by the hydrogen ions, a net

deposition coefficient can be calculated in general agreement with the experiments.

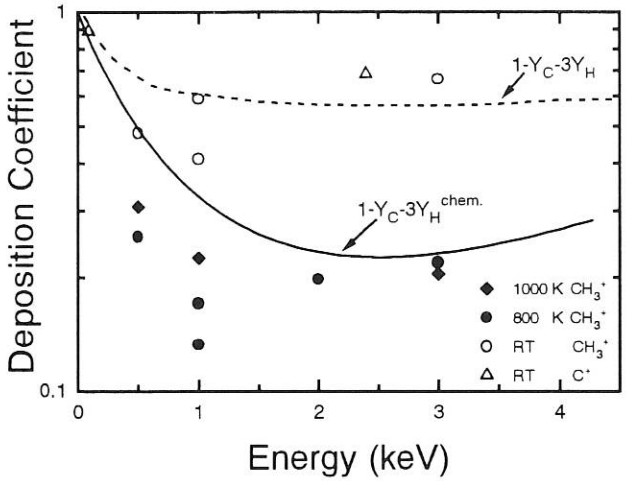

FIG. 5: Deposition coefficient of carbon and hydrocarbon ions onto Si and graphite for different temperatures. The curves are estimates taking self-sputtering and hydrogen sputtering into account.

1.3 Plasma Edge Studies in Fusion Experiment

Most of the investigations of the plasma-wall interaction group constitute direct investigations of the plasma-facing surfaces in plasma experiments as well as observation of the boundary plasma. The results from experiments which conducted in close collaboration with ASDEX Upgrade or W7-AS are included in the respective sections.

1.3.1 Soft X-ray tomography at W7-AS based on MaxEnt reconstruction

(K. Ertl, W. v. d. Linden, V. Dose)

The reconstruction of emissivity profiles from soft X-ray chord measurements poses a highly underdetermined and ill-posed inversion problem. Particularly suited to such problems is the Maximum Entropy method, which quantifies in a consistent probability-theory-based approach the information gain due to experimental data. It provides unbiased results for the most probable local emissivity along with confidence intervals. No model assumptions are necessary to obtain a unique solution of the underdeterminded inversion problem. Moreover, it is possible to take additional prior knowledge into account and improve the results in a systematic and controlled way. The Maximum Entropy method was applied to reconstruct the time development of SX-emissivity profiles to study mode activities in W7-AS discharge. The results were visualized in a movie.

1.3.2 CH_4 and CO fuelling studies in ASDEX

(K. Krieger, J. Roth, V. Dose)

On ASDEX, the fuelling behaviours of CH_4 and CO were investigated by means of sinusoidally modulated gas puffing. Depending on the gases used, quite different penetration behaviours of the carbon impurity were observed. It turned out that the penetration probability of carbon atoms produced by dissociation of CO molecules is a factor of approximately two higher than the penetration probability for carbon atoms produced by the dissociation of CH_4 molecules. These are attributed to the different fragmentation processes of the CO and CH_4 molecules and the corresponding losses of neutral radicals and atoms to the vessel walls, which are higher for CH_4. From the greater penetration probability of carbon originating from CO fragmentation, more serious carbon impurity fuelling by oxygen induced chemical erosion is inferred as compared with that by hydrogen induced chemical erosion.

1.3.3 Erosion/redeposition

(D. Naujoks, R. Behrisch, J. Roth)

The ERO computer program for describing erosion/redeposition at the vessel walls of high-temperature plasma experiments was extended from limiter to divertor geometry. It was further applied to divertor as well as limiter probes from ASDEX Upgrade and TEXTOR. These investigations show that deposition of impurities present in the SOL plasma largely determine the net erosion of plasma-exposed tiles, especially for high-density low-temperature plasmas.

2. SURFACE SCIENCE

In the last two years the activities of the surface science group converged mainly on two subjects: Epitaxial growth of metal films on metal substrates and electronic states in reduced dimension (surface states, quantum wells and quantum wires). Both research areas are highly relevant to the understanding of surface and thin film magnetism. The expertise in structure sensitive methods on the one hand and in (spin-resolved) electron spectroscopies on the other allows one to relate structural parameters to electronic and magnetic properties of surfaces and epitaxial thin films.

The role of surface states in surface reconstruction and adsorbate bonding, the investigation of surface phase transitions and the characterization of supported metal-oxide catalysts are subjects of a collaboration within Sonderforschungsbereich (SFB) 338.

2.1 SFB 338

(E. Bertel, J. Cramer, P. Hanesch, P. Roos, P. Sandl in collaboration with G. Hörmandinger, Imperial College, London; S. Labich, C. Linsmeier, N. Memmel, A. Rabe, S. Reiter, S. Schömann, A. Steltenpohl. E. Taglauer in collaboration with H. Knözinger and J. Peisl, University of Munich)

Quantum-well-states in ultrathin Na films on Cu(110) were investigated by photoemission and inverse photoemission spectroscopy. Good agreement was found with layer-resolved

multiple-scattering calculations (G. Hörmandinger, Imperial College, London). The coverage dependence of the spectra reflects disturbed layer-by-layer growth for the first few monolayers.

The growth structure and stability of ultrathin cobalt films on Cu(111) were studied with low-energy ion scattering. At room temperature growth proceeds via formation of three-dimensional cobalt islands, accompanied by diffusion of copper substrate atoms onto these islands. The copper diffusion continues after the cobalt evaporation, thereby leading to the formation of a copper overlayer on the cobalt islands. In the initial stage of growth the cobalt films mainly continue the fcc structure of the copper substrate. However, with increasing coverage more and more stacking faults occur, as expected for the transition into the stable hcp structure of cobalt.

By studying Cu(115) surfaces by scanning tunnel microscopy (STM) it was possible to visualize the stepped surface structure which can be deduced from the bulk crystallinity (see Fig. 1). Geometric relaxation of surface atoms was found within the terraces and will be further studied. The formation of (104) facets on these surfaces upon oxygen adsorption was deduced from ion scattering measurements.

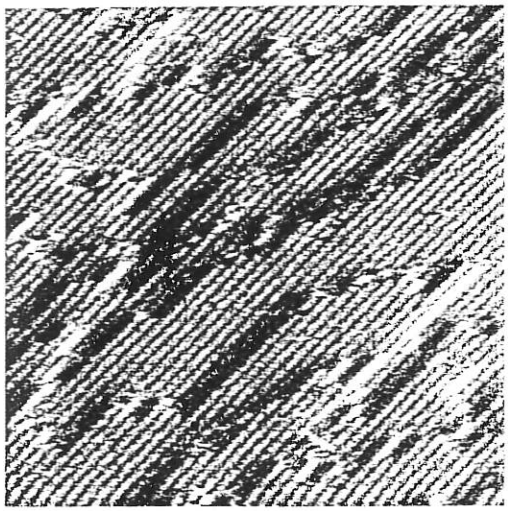

FIG. 6: Analog-differentiated STM picture of a Cu(115) surface, 313Åx313Å, showing (110) step edges running from the lower left to upper right corner.

An investigation of surface states on the one-dimensionally disordered system H/Ni(110) ("streaky phase") led to the discovery of one-dimensional Shockley surface states.

A general symmetry analysis of surface states on fcc low-index surfaces was carried out. From the results a method was derived for adsorbate site determination. Application to inverse photoemission results from the molecular adsorbate system C_2H_4/Ni(110) indicates an adsorbate position in the troughs for the saturated monolayer.

Continued studies on supported metal oxide catalysts showed by ion scattering (ISS) and thermal desorption spectroscopies that for the model system Rh/TiO_2 encapsulation ("strong metal support interaction") occurs for calcination temperatures above 750 K. XPS measurements showed no concomitant reduction of the support oxide, in contrast to current interpretations. Reduction was observed as a consequence of ion bombardment.

2.2 Surface Magnetism

(Th. Detzel, M. Donath, V. Dose, K. Ertl, B. Gubanka, W. von der Linden, F. Passek, M. Vonbank in collaboration with A. Hubert, University of Erlangen, J. Noffke, TU Clausthal, and W. Nolting, University of Valladolid, Spain)

The study of the spin-dependent electronic structure of magnetic systems was extended from surfaces to ultrathin films. A Kerr microscope was added to the experimental equipment to characterize the magnetic domain structures of the samples.

Spin-resolved inverse photoemission measurements of bcc Fe on W(110) as a function of film thickness demonstrate the development of the spin-split Fe band structure. Spin-dependent interface states are characteristic of overlayer films with a thickness of less than 4 monolayers (ML). Strong hybridization effects with substrate states are observed. For thicker films the electronic states of bulk Fe appear. A study of the spin-dependent attenuation of emission features from tungsten with increasing overlayer thickness reveals a short and spin-dependent inelastic mean free path of low-energy electrons (kinetic energy about 10 eV) in ferromagnetic iron of 3.4 and 5.4 ML for minority and majority electrons, respectively. The image-potential-induced surface state on "thick" Fe films (more than 15 ML) exhibits an exchange splitting of 57±5 meV and, in addition, a spin-dependent linewidth, indicative of spin-dependent decay channels being responsible for the lifetime.

The structural and magnetic information gained by spin-resolved appearance potential spectroscopy of Fe films on Cu(001) leads to remarkable conclusions. Below 2 ML, where the growth is dominated by island formation and copper diffusion, no ferromagnetic order is detected. For a thickness between 2 and 4 ML, the Fe film adopts the fcc structure of the Cu substrate and shows ferromagnetic behaviour with out-of-plane anisotropy. 5 to 10 ML of fcc Fe are nonferromagnetic except the uppermost surface layer. The experimental spin asymmetry is consistent with the signal of one ferromagnetic surface layer on top of nonmagnetic fcc Fe. In addition, it is sensitive to adsorbates. The peculiar behaviour is presumably due to expansion of the outermost iron layer. For a thickness larger than 10 ML a structural transition to bcc Fe occurs, which exhibits ferromagnetic behaviour with in-plane anisotropy. The data show the critical influence of growth mode and lattice parameters on magnetic properties.

TECHNOLOGY DIVISION

(Prof. Dr. Rolf Wilhelm)

IPP activities in plasma heating, viz. neutral beam injection (NBI), ion cyclotron resonance heating (ICRH), both on ASDEX Upgrade and W7-AS, and electron cyclotron resonance heating (ECRH) on ASDEX Upgrade, are concentrated in the Technology Division. More detailed descriptions of these projects are given in the pertinent sections of this report. The following presents further information on specific technical development and theoretical work within the plasma heating programme or in connection with general reactor aspects.
For the further joint activity of the Technology Division and Surface Physics Division, namely the Plasma Technology project, the reader is referred to the section under that heading

1. NEUTRAL INJECTION HEATING

Group leader: E. Speth
Deputy: W. Ott

M. Ciric, J.-H. Feist, K. Freudenberger, B. Heinemann, W. Kraus, H. Lohnert[1], W.Melkus[1], F.-P. Penningsfeld, F. Probst, R. Riedl, W. Schärich, B. Sombach[1], A. Stäbler, R. Süss, A. Teubel, O. Vollmer, K. Wittenbecher
[1] ZTE

1.1 Results from the RF Source Developement

W. Kraus, J.-H. Feist, E. Speth

The RF source has been tranferred to the ASDEX Upgrade testbed for testing the long-pulse capability, and measurements of the beam properties have been started with a more reliable diagnostic than at the short-pulse teststand.

In the source version used for these experiments, an internal antenna of five turns is electrically insulated from the plasma by quartz tubing. The inner diameter of the tube (7 mm) is smaller than that of the metallic lead (4.5 mm), so that the quartz coil can be cooled internally with compressed air.

Compared with the design based on an external RF antenna, the plasma volume is enlarged by the interspace between the antenna and the metal side walls. Because of the resulting reduction of the power efficiency, the extracted beam current did not exceed 82 A, obtained at 100 kW, which is close to the maximum output power of the RF generator.

In order to reach the design value of 85 A without working at the maximum load of the power supply, additional copper side walls were mounted 2 cm outside the antenna.

By this means the source volume was reduced from 50 l to 39 l. In addition, the permanent magnets previously needed outside the side walls to reduce the wall losses have been rendered superfluous. The extraction measurements showed a reduction of 15 % of the RF power required for the same beam current. At the chosen distance between the antenna and side walls the reduction of the antenna inductance caused by the eddy currents is restricted to 25 %, and ohmic losses to less than one per cent.

The first results of the beam extraction and diagnostic showed some inconsistencies with the previous measurements on the short-pulse teststand. Clarifying these questions will be the subject of the work in the immediate future.

2. ION CYCLOTRON RESONANCE HEATING

Group Leader: F. Wesner
Deputy: F. Hofmeister

M. Ballico, W. Becker, F. Braun, R. Fritsch, F. Hofmeister, C. Hoffmann, J.-M. Noterdaeme, S. Puri, Ph. Verplancke[1], H. Wedler, F. Wesner
[1] Aspirant of the Belgian N.F.W.O.

2.1 Stability of ICRH Operation

F. Braun

To study the interaction between the resonant circuits of generators, lines and antenna, calculations were made including the antenna coupling, the whole feeding line and matching system and the power amplifier stage of the generator with its nonlinear valve charcteristics. The calculations show that self-

oscillations occur in the event of transients such as load variations or switching-on of the power, if both a sufficiently large impedance and phase differences > $|90^0|$ between forward and reflected power are seen by the power tetrode. Power amplitudes at frequencies just beside the nominal one can be large enough for safety switching off or even to cause damage. By varying the impendance, e.g. via the load or generator output matching systems or the transforming line length (frequency), the unstable behaviour can be avoided. This could be confirmed by tests.

2.2 Analysis of Heat Modulation Experiments with ICRH

C. Hoffmann

Modulating the heating power flowing into the plasma by one of the major RF-heating methods (ion or electron resonance) has the advantage that no additional density modulation is introduced. Yet ICRH and ECRH also have important differences. ICRH has a much broader deposition profile and, in general, delivers power to both electrons and ions. Interpretation for the envisaged modulation experiments with ICRH on AUG is under preparation. Apart from subjecting the expected data to a linear analysis in terms of extracting the coefficients of the transport matrix, the nonlinear response of the plasma has to be taken into account. One nonlinearity specifically caused by ICRH heating is the generation of a non-Maxwellian particle distribution. The less collisional fast particles deliver power to the plasma when the external power is decreased during the modulation cycle, smearing out the power modulation in time and thus altering the phase lag and amplitude of the corresponding temperature signals. This has been investigated with the FPSOLV kinetic code, which was equipped with energy loss terms. Simulated charge exchange signals show qualitatively different behaviour in different energy ranges. Corresponding measurements will put these dynamics to the test. For further investigation of the minority heating scenario a simplified fast-particle model has been developed, which will now be inserted into the transport code ASTRA. The interaction of modulated RF power with other nonlinear plasma responses, such as the sawtooth instability, the L-H transition and edge-localized modes will in future be investigated.

A different ICRH modulation scenario is to choose the frequency such that any ion resonance is avoided. Good electron absorption is achieved if the electron temperature profile is sufficiently peaked in the centre. This scenario was prepared in comparison with experiments performed on DIII-D.

2.3 Langmuir Probes at Frequencies in the Ion Cyclotron Range

Ph. Verplancke, Aspirant of the Belgian N.F.W.O.

In order to study sheath effects in an RF-heated machine, the behaviour of a Langmuir probe at RF frequencies is investigated. Possibly, this will also allow us to measure ion quantities with such a probe.

The results of 1-D particle-in-cell simulations, presented in the Annual Report 1992, showed strong changes of the Langmuir characteristic at sweep frequencies in the ion cyclotron range. These results have been refined to determine the underlying mechanisms. Basically, in the presence of a grazing incidence magnetic field, the plasma density falls off towards the wall in a sheath with a thickness of the order of the ion Larmor radius r_{Li}. Together with the reduction of the saturation current with a factor of sin α, this explains that the sheath displacement current becomes important at frequencies as low as ω_{ci} sin α (ω_{ci} = ion cyclotron frequency, α = angle of magnetic field to the wall). The amplitude of this displacement current contains information about r_{Li} and thus about the ion temperature.

An electronic circuit has been developed to measure probe currents of up to 200 MHz. It was tested in an experiment with existing probes at the W7-AS stellarator. The Langmuir characteristics show strong hysteresis on the electron saturation side, which might be explained by the effect of polarization current perpendicular to the probe's flux tube. Only in the neighbourhood of ω_{ci} itself does ion saturation disappear, probably because the angle of the magnetic field is not well defined on the cylindrical probes with diameters as small as r_{Li}.

Six flat, flush-mounted probes, which should allow better comparison with the theory, were built into the lower outer divertor plate in segment 3 of ASDEX Upgrade in September. The data acquisition system will be put into operation soon.

3.0 ECRH ON ASDEX UPGRADE

(ECRH Group, in cooperation with IPF Stuttgart and IAP Nizhny Novgorod)

Group leader : F. Leuterer
Deputy: M. Münich

F. Brandl, H. Brinkschulte, F. Monaco, F. Ryter, C. Wharton[1], M. Zouhar

[1] Guest, Cornell University, Ithaca, N.Y.

3.1 Operation of Gyrotrons in the Poloidal Stray Field of a Tokamak

Tokamaks with an air core transformer and with vertical field coils outside the toroidal magnetic field coils, such as ASDEX Upgrade and ITER, have a far-reaching poloidal magnetic field. Although this field decreases approximately as r^{-3}, in the case of ASDEX Upgrade there is still a field of up to 35 G at a distance of 15 m from the tokamak centre. For ITER with higher currents, and much larger major radius, such a situation will exist at a distance of close to 75 m. Heating systems with high-power electron tubes will have to work in this environment. We investigated this problem for the ECRH system to be installed at ASDEX Upgrade.

Calculations of the electron beam trajectory in the gyrotron showed that the perpendicular (to the beam axis) component of a stray magnetic field, although very much smaller than the resonator field, strongly affects the beam position in the gyrotron cavity and also the beam deposition in the collector.

For ASDEX Upgrade we originally intended to install the tubes on the upper floor of the gyrotron hall. However, there the perpendicular component of the field is too large and cannot be tolerated. It also turned out that its compensation only in the collector region is not sufficient.

Consequently, it was decided to install the gyrotrons on the ground floor of the gyrotron hall. The cavity region of the tube is then in the midplane of the torus, where the radial component of the stray field goes through zero. However, high-current leads under the floor create additional intolerable magnetic fields. In order to screen them, we covered the floor with a layer of 2 cm of soft iron.

The influence of such an iron floor on the ASDEX Upgrade stray field was studied with the PROFI code. It turned out that the field distribution was slightly changed. The radial component is now zero at the floor and increases continuously with height, i.e. along the tube.

With an additional iron plate of about 2 x 2 m above the gyrotron at a height of up to 2.5 m, this field can be straightened again, resulting in a radial component of < 5 G all along the tube. Fig. 1 shows this radial component at the most

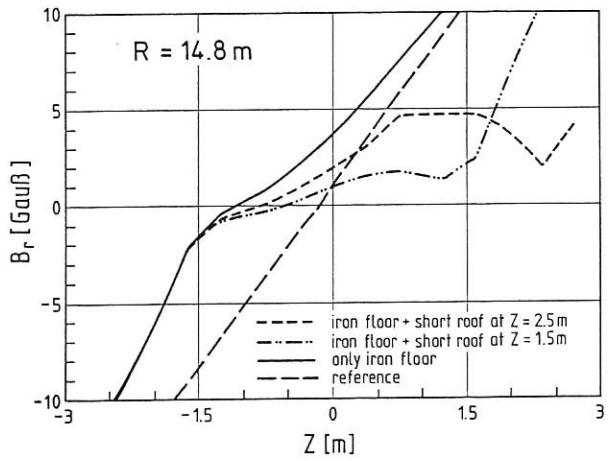

Fig. 1 Variation of the radial component of the stray magnetic field due to iron floor and roof

critical gyrotron position (R = 14.8 m) for the cases of the bare stray magnetic field, the case with only the iron floor, and with an additional iron roof above the most critical gyrotron.

The vertical component may also require some compensation. This can be done with Helmholtz coils in the collector region whose parameters are about I = ±10 A, n = 100, D = 50 cm. Such a coil has a time constant of the order of 20 ms and can follow the time variation of the stray field.

4. THEORETICAL STUDIES OF TOKAMAK CURRENT DRIVE

S. Puri

We discuss the possibility of realizing steady-state tokamak operation via a combination of bootstrap current, and an efficient ($\gamma \sim 2$) current drive using low-phase-velocity Alfvén waves.

4.1 Bootstrap Current in a Tokamak

An examination of the sources for bootstrap current in an axisymmetric toroidal geometry reveals that in a steady-state reactor plasma, the bootstrap current is determined principally by the temperature gradient and not by the density or the pressure gradients (as currently believed). Thermal gradients give rise not only to a primary bootstrap current but to a still larger secondary contribution due to the induced particle pinch with its associated bootstrap current under steady-state conditions. Assuming that the alpha-particle heating can sustain a parabolic temperature profile, up to 80 % of the total plasma current could be delivered through the ∇T-driven bootstrap current for the SSTR tokamak parameters.

Assuming $T_e = T_i$, $E_{|8} = 0$, and $\Gamma = 0$, the total neoclassical ∇T-driven steady-state bootstrap current contribution obtained from the Hinton-Hazeltine large-aspect-ratio neoclassical theory is given by

$$j^{bs}_{\nabla T} = -\frac{\varepsilon^{1/2} nT}{B_\theta}\left[\frac{1.35}{T}\frac{dT}{dr} + \frac{0.27}{T}\frac{dT}{dr}\right]$$

$$= -\frac{\varepsilon^{1/2} nT}{B_\theta}\frac{1.62}{T}\frac{dT}{dr},$$

where the two terms in the brackets are contributed by the secondary and the primary ∇T bootstrap current contributions, respectively. The total ∇T-driven bootstrap current for the SSTR reactor parameters may amount to as much as 58 % of the plasma current.

Inclusion of the finite-aspect-ratio (Hirshman-Sigmar) corrections increases the ∇T-driven bootstrap current contribution to an even more impressive figure of over 80 % of the total plasma current for the SSTR tokamak parameters.

In conclusion, sustaining a steady-state tokamak reactor primarily through bootstrap current appears eminently plausible. However, contrary to existing beliefs, the bootstrap current originates, principally, from the gradients of temperature. The source for maintaining the temperature profile is assumed to be the alpha-particle heating in a reactor plasma.

4.2 Alfvén-Wave Current Drive

In cylindrical geometry, high current-drive efficiences are obtainable both for (i) the low and (ii) the high (compared to electron thermal speed) phase-velocity waves[1]; because of the large momentum input per unit energy expenditure in the first case, and low plasma collisionality in the second case.

In toroidal geometry, however, the slow waves couple momentum initially to the trapped electrons with no resultant primary current drive. However, the toroidal momentum given to the trapped particles is conserved via radial Ware pinch. In steady state, the trapped particles return to their original positions, transferring in the process the stored canonical angular momentum to the passing electrons via collisions. The resulting current-drive efficiency[2,3] of $\gamma \sim 2$ would suffice for the realization of a high-Q tokamak reactor.

Coupling geometry for the Alfvén waves is identical to that of the ion-cyclotron waves using poloidal current-carrying antennas. However, unlike the ion-cyclotron waves, good coupling to Alfvén waves is possible only using high (n = 6 - 8) toroidal wave numbers[4], with antenna coupling efficiencies approaching $\eta_A \sim 1$.

An experimental study of Alfvén-wave currrent drive would be feasible (and desirable) in ASDEX Upgrade with the present ICRH antennas in conjunction with additional loops, so as to obtain a toroidal wave number n = 6. Although the lower electron temperature would allow a current-drive efficiency of only $\gamma \sim 0.1$, a significant toroidal current would be generated with about 6 - 8 MW of RF power at around 2.5 MHz. Logical stages in the experimental programme would consist of:

1. RF breakdown tests at 2.5 MHz using a single existing ICRH loop
2. Coupling tests at low power
3. Full power current drive.

5. REACTOR ORIENTED STUDIES

A. F. Knobloch

In continuing ongoing tokamak reactor studies, particular emphasis was placed on the accessible configurations and additionally on the overall efficiency.

For the respective operating points the assumption was made that a fixed enhancement factor on a respective L-mode energy confinement power scaling would be required in keeping with the desired ELMy H-mode operation (e.g., f_{HGO} = 1.6 for Goldston and f_{H89P} = 1.9 for ITER 89P scaling). With fixed input assumptions on the specific plasma properties and the reactor radial build, parameters of possible consistent reactor configurations can be derived preferably as a function of the respective optimum aspect ratio. The optimum is defined (independently of the energy confinement scaling) such that for any given fusion power level the pertaining average neutron wall load is a maximum vs. the toroidal field utilization (B/B_{max})[5].

When expressing the reactor parameters vs. the optimum or a defined non-optimum aspect ratio, one generally obtains relations including a reference parameter value (defined by the governing relations and the input data), and a function of the aspect ratio only. This form is convenient for structured evaluation of the accessible parameter range.

For pulsed reactor concepts inductive current drive is assumed (roughly characterized by infinite Q). The desired steady-state operating mode would also specify infinite Q. Steady-state operation at finite Q, however, means reduced performance.

Since the inclusion of any specific energy confinement scaling in the configuration optimization does not lead to relevant modifications, and in view of the present situation, in which only some approximations for a possible "ultimate" confinement scaling relation are available, the purely geometric optimization approach has been maintained. It turns out that a number of recent reactor design studies of the so-called advanced type (SSTR, SSTR-Ua, ECadv.) arrive at almost exactly the same aspect ratio as defined by that approach. Others (ITER, ITER-SSTR, SSTR-Uc1, SSTR-Uc2) that are termed conventional are considerably below the optimum aspect ratio and very large in fusion power. Design studies for long-pulse operation lead to large aspect ratios (PULSE, IDLT). Since a larger maximum toroidal field leads to strong reduction in inductive burn time, pulsed reactor designs have typically a lower B_{max} level.

The two conditions imposed on the plasma current by the current-q relation and by the energy confinement scaling based on a fixed enhancement factor (f_{HGO} = 1.6 was taken as a first option) strongly limit the accessible parameter domain for any assumed maximum toroidal field within a range $q_{min} < q(A) < q_{max}$. This limitation excludes both the very low and very large aspect ratio domains, depending on the respective combination of B_{max} and the input assumptions for the operating point.

There are very rigid domains of accessible reactor parameters and configurations within the q range mentioned which are further restricted by geometrical constraints. The possible inductive burn duration varies particularly strongly with the aspect ratio. For a high stationary Q-value both the minimization of the current-drive power and the desired increase of the bootstrap current fraction favour q_{max}, which implies large B_{max}.

Low aspect ratio leads to short burn duration or low Q, a very high fusion power level at the Troyon beta limit for low q, and moderate B_{max}. The operating temperature is about 10 keV and is in the thermally unstable domain. Optimum aspect ratio leads to longer burn duration or larger Q, a moderate fusion power level at the Troyon beta limit for higher q and B_{max}. The operating temperature is about 17 keV and is in the thermally stable domain.

The quantitative results are sensitive to the assumptions with possible consequences for a future power reactor.

Some relations with the overall efficiency η were evaluated. It was found that the improvement of Q is of interest up to the largest attainable level, since η gradually still improves with increasing Q for Q > 100, for example /528/.

---

1) D. J. H. Wort, Plasma Phys. **13** (1971) 258.
2) S. Puri, R. Wilhelm, APS Conf. Proc. **190** (1989) 458.
3) A. G. Elfimov, S. Puri, Nucl. Fusion **30** (1990) 1215.
4) S. Puri, Nucl. Fusion **27** (1987) 1091.
5) A. F. Knobloch: Mit welchen Parametern könnte ein stationärer Tokamak-Fusionsreaktor realisiert werden? IPP Garching, 1992.

PLASMA TECHNOLOGY

(Prof. Dr. Wolfhard Möller
until 30.09.93)

The Plasma Technology group is concerned with three tasks: Surface coatings are produced by means of plasma-enhanced chemical vapour deposition (PECVD) for special applications, mainly in fusion plasma devices. New or improved PECVD procedures or devices are being developed for this purpose. As the scientific part of the activity, plasma, plasma edge, and thin film diagnostics are employed in order to correlate the discharge parameters with the properties of the resulting coatings and improve understanding of the basic mechanisms of plasma deposition. The third goal is a modelling of the deposition process which allows the discharge conditions to be adjusted in a predictable way in order to optimize a desired property of the growing film.

V. Dose (Division Head)[1], M. Engelhard[2] (until 30.04.93), A. Friedl[2] (until 14.11.93), W. Fukarek[2], S. Grudeva-Zotova[4], F. Höhn[2], R. Hytry[1], W. Jacob[1], A. v. Keudell[1], J. Krumrey[1], K. Lange[1], P. Pecher[1], J. Perchermeier[3], J. Reinmuth[1], R. Wilhelm (Division Head)[2].

1 Surface Physics Division
2 Technology Division
3 Central Technical Services
4 Short-term visitor (University of Sofia, Bulgaria)

1. INVESTIGATION OF MULTIPACTOR DISCHARGES

(Cooperation with ICRH Group)

Multipactor discharges in the frequency range between 30 and 80 MHz were investigated in a new vacuum system. Total chamber pressure and residual gas mass spectroscopy were used as analytical techniques. In preliminary experiments increase of the chamber pressure during the discharge was generally found. This increase depends on several experimental factors such as the gas type and gas load of the electrodes. To improve the analytical potential of the experiment, the addition of an Auger electron spectrometer was planned and commissioned. This will allow surface changes induced by multipactor discharges to be investigated.

2. IN-SITU PLASMA DIAGNOSTICS

2.1 Microwave Interferometry

The performance of a home built microwave interferometer was substantially improved. The former transmitter, a klystron, was replaced by a "Gunn" diode. Further improvement of the phase detection circuit and the measuring electronics results in satisfactory long-term stability and a detection limit of 0.6 deg, which corresponds to a mean electron density of $2.4*10^9$ cm^{-3}.

2.2 Ion and Radical Fluxes onto the Substrate from a DC Glow Discharge in Methane

Absolute neutral, radical, and ion fluxes from a DC glow discharge in methane onto a negatively biased substrate were measured. The species were detected after passing through a small orifice in the substrate electrode by means of an energy and mass analyzer consisting of an electrostatic sector field followed by a quadrupole mass spectrometer. C_2H_5 radical fluxes were investigated by conventional mass spectrometry at fixed electron impact energy. The CH_3 fluxes were determined by ionization threshold mass spectrometry (ITMS). ITMS is based on the approx. 4 eV difference between the threshold energies for direct ionization of CH_3 and dissociative ionization of CH_4 parent molecules to distinguish between CH_3^+ ions produced by the two reactions in the built-in electron impact ion source. In the case of radical and neutral analysis, hydrocarbon gases of known pressure in the discharge vessel were used for calibration. The measured ion fluxes were calibrated and normalized by comparison with the results of a retarding field analyzer which allows reliable measurement of absolute mass-integrated energy distributions. Furthermore, growth rates and H/C ratios of amorphous hydrogenated carbon films (C:H) deposited in this discharge were determined by means of high-energy ion scattering analysis. Results are shown in Fig.1. The carbon growth rate R_C rises from about $0.5*10^{13}$ $cm^{-2}s^{-1}$ to $1.3*10^{15}$ $cm^{-2}s^{-1}$ in the pressure range investigated. The corresponding particle fluxes are shown in the right-hand panel of Fig.1.

In the whole pressure range the ion flux to the sample contributes only about 30% to the total carbon growth rate . Consequently, other species have to contribute at least 70% to the measured growth rates. This growth is carried by the incoming flux of C_xH_y radicals. In general, it is assumed that CH_3 radicals make the dominant contribution to the film growth. However, it turned out that in our case C_2H_5 radicals are the most prominent radicals in the discharge. For example, for a DC bias of -710 V and a methane pressure of 10 Pa a C_2H_5 flux of $2.0*10^{16}$ cm^{-1} has to be compared with a CH_3 flux of $1.3*10^{15}$ $cm^{-1}s^{-1}$. A possible explanation for this flux ratio is the production of C_2H_6 from CH_3 on the chamber surfaces. C_2H_6 turned out to be the most abundant C_2-hydrocarbon in the plasma and leads mainly to C_2H_5 by electron impact.

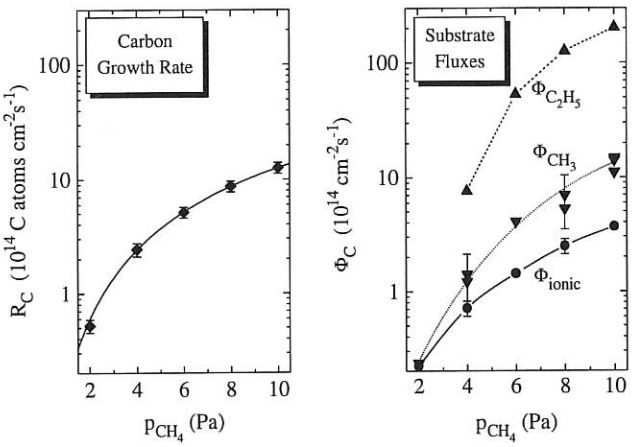

FIG.1: Carbon growth rate (left) and ion and radical fluxes to the substrate (right) from a DC plasma in methane at a bias voltage of -710 V as a function of the discharge pressure.

The growth rates and a-C:H film compositions measured as a function of the particle fluxes may be rationalized on the basis of an empirical surface growth model. This model includes adsorption and desorption of radical species, ion-induced deposition of radicals, ion-induced release of hydrogen, and direct incorporation of the energetic hydrocarbon ions. On the assumption that every incoming ion is incorporated in the growing film, the measured ion flux accounts for about 30% of the carbon growth rate. Ion-induced deposition of radicals is, therefore, the dominant growth mechanism and accounts for about 70% of the film growth. The effective sticking coefficient, defined as the probalitity of an incoming radical to establish a chemical binding to the growing film, depends on the ion flux, ion energies, and the flux of the radicals themselves. In addition, an independent experiment showed that the effective sticking of CH_3 radicals on non-activated surfaces (in particular, surfaces without ion bombardment) is negligible.

3. SURFACE MECHANISMS DURING C:H GROWTH

For in-situ investigation of surface mechanisms during the growth of C:H films, an in-situ spectroscopic ellipsometer in the visible spectral range was constructed. In an ellipsometric experiment, changes in the state of light polarization upon reflection from the sample can be determined and expressed by the two ellipsometric angles Ψ and Δ. In combination with an optical modelling of the experimental results, the thickness and the complex index of refraction of the film can be determined with high accuracy. As a light source a xenon lamp is used in combination with a glass fibre optic and a monochromator for wavelengths from 450 nm to 700 nm. The incident light is polarized by a prism polarizer and the change in the state of polarization upon reflection on the sample is determined by a rotating analyzer. An ECR plasma source is used to generate a plasma beam for depositing C:H films on silicon substrates. As the film properties are mainly determined by the energy of the ions impinging on the surface and by the substrate temperature during deposition, the substrates can be heated and a DC or RF bias voltage can be applied to the substrate holder. In addition, optical spectroscopy can be performed to monitor the plasma composition.

For characterization of the plasma source and evaluation of the deposition parameters, in-situ experiments were performed in which the application of RF and DC bias voltages during deposition was compared. As C:H films are insulating, the plasma potential is determined rather by the charge state of the film surface than by the underlying conducting wall. By applying a DC voltage a decrease in the growth rate and a decrease in the index of refraction are observed with increasing film thickness during growth. This is attributed to a change in the sheath potential between the plasma and film surface. With increasing film thickness the resistance of the C:H-layer increases, so that the potential of the film surface shifts and approaches the floating potential of the plasma. As a consequence, the sheath potential and accordingly the ion energies decrease with increasing film thickness. This is consistent with the observed change in the optical properties and growth rate. When an RF voltage is applied, an increase in the growth rate and index of refraction is observed with increasing film thickness, which points to a changing sheath potential. In an RF discharge the sheath potential between the plasma and film surface is determined by the amplitude of the RF field. As the substrates are capacitively coupled to the RF generator, direct current to the subtrate has to be zero during deposition. In view of this, it is not yet clear how the sheath potential can change.

The contribution of neutrals and ions to the deposition of C:H films is of particular interest. To investigate this, masking experiments were performed to separate the ions from the neutrals. This separation is easily obtained by means of a mask. The ions, which in our pressure range are guided by the magnetic field lines and accelerated by the sheath potential, hit the sample surface more or less perpendicularly. Consequently, they cannot reach the substrate underneath a mask is mounted several mm above the film surface. Neutrals, on the other hand, reach also the region shaded by the mask. These experiments have clearly shown that the activation of the film surface by ions appreciably increases the growth rate.

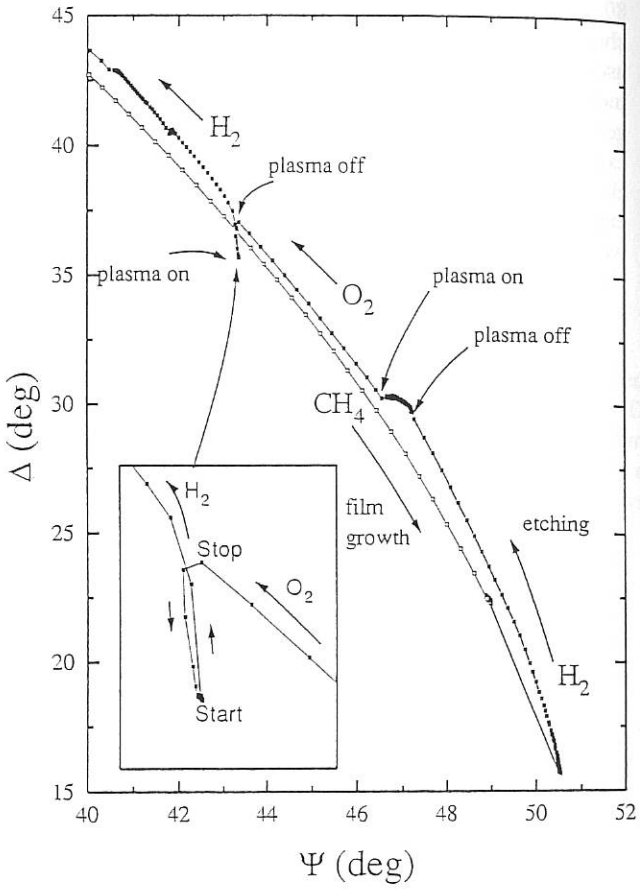

FIG. 2: Ellipsometric response during deposition and etching of C:H films. The deposition process yields in the curve shown by the open squares. Etching of the film either in hydrogen or in oxygen does not follow this curve in the reverse direction, contrary to expectation when simply the film thickness is decreased. The inset shows the complicated dynamic of the surface after the oxygen plasma is switched off.

The influence of ions on the erosion of plasma-deposited C:H films was investigated in oxygen and hydrogen plasmas. It was observed that the influence of oxygen ions during etching in an oxygen plasma is much larger than that of hydrogen ions in a hydrogen plasma. This is attributed to the higher mass of oxygen and the higher reactivity of oxygen on the film surface in forming carbon monoxide during etching. Changes in the actual state of the film surface were observed in situ by ellipsometry. The results are shown in Fig. 2. As the optical response of the C:H film during etching does not follow the optical response during growth of the identical film, the surface morphology and coverage have to be different during etching and deposition. This change in the optical response of the film

surface may also be observed in plasma shutdown experiments, where a substantial shift occurs when the plasma is switched on or off. This might be related to the adsorption or desorption of molecules from the plasma or a change in the charge state of the surface, but requires further detailed investigation.

4. RUNNING WAVEGUIDE DISCHARGE

A plasma-enhanced chemical vapour deposition process by means of a so-called running discharge has been developed. C:H films were deposited over a length of 2.5 m on the inner wall of an assembled waveguide system without any mechanical movement of the system. Such C:H layers deposited from a methane plasma on the inner wall of a copper waveguide exhibit a secondary electron emission coefficient below unity and can therefore suppress multipactor discharges in high-power microwave launchers of fusion experiments. For a basic understanding of the running discharge process, breakdown of the discharge in the metallic waveguide was studied in argon plasmas as a function of the magnetic field, microwave power and gas pressure. A sharp transition between a magnetically enhanced localized discharge and a running discharge was observed at increasing pressure in the range of a few pascal at a microwave power of 100 W. As can be seen in Fig. 3, the magnetically enhanced breakdown as well as the transition from a localized discharge to a running discharge were investigated as functions of the argon pressure in the waveguide (0.3...130 Pa) at a fixed gas flow of 3.5 sccm. In order to achieve breakdown at a microwave power input of 100 W below a pressure of 130 Pa, enhanced confinement by means of a magnetic field is needed. Breakdown occurs if the current through the magnetic field coils is increased. Experimental results for magnetically enhanced breakdown are shown in Fig. 3 as black circles. At increasing gas pressure breakdown occurs at a lower magnetic field. At 0.3 Pa breakdown requires an ECR (electron cyclotron resonance) magnetic field, while at 130 Pa plasma ignition occurs at a microwave power of 100 W without applying any magnetic field at the microwave entrance window.

If the coil current is decreased after plasma ignition, the plasma extinguishes at a certain magnetic field. This behaviour is denoted in Fig. 2 by black triangles. At 0.3 Pa at least half of the ECR field is necessary for sustaining the once ignited localized discharge. This magnetic field decreases again with increasing pressure until at 4 Pa the plasma can be sustained without any magnetic field. In this case, the plasma no longer remains localized near the magnetic field coils after magnetically enhanced breakdown, but moves through the waveguide towards the microwave entrance window. That point marks the transition from the magnetically enhanced localized discharge to the running discharge. In the range from 4 Pa to 130 Pa a magnetically ignited running discharge was obtained at a constant microwave power of 100 W. The plasma motion of the running discharge can be explained as a continuous secondary gas breakdown at the plasma boundary facing the microwave entrance.

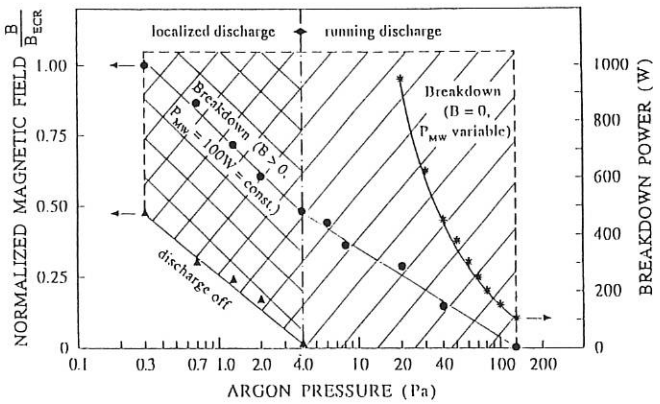

FIG. 3: Magnetic field for breakdown (black circles) and extinction of the discharge (black triangles) in a magnetically enhanced argon plasma with constant microwave input power of 100 W (left-hand scale of the figure) as well as microwave input power for breakdown at the microwave entrance window (asterisk) in a microwave discharge without any applied magnetic field (right-hand scale of the figure) as a function of the argon gas pressure in the evacuated waveguide system. Around 4 Pa the transition from a magnetically enhanced localized discharge to a running discharge is observed.

Above 130 Pa a conventional microwave discharge breaks down at the microwave entrance window. If no magnetic field is applied, but the microwave power is increased, breakdown of the microwave discharge at the entrance window (asterisks in Fig. 3) is already achieved at lower gas pressure, e.g. at 20 Pa with a power of 1000 W. Local breakdown of the discharge and formation of a running discharge do not necessarily require a local magnetic field, but can also be obtained by a locally enhanced electric field. This local enhancement can be managed by means of a metallic needle in the simplest case. Indeed, such a type of running discharge was obtained at an argon pressure of 50 Pa.

BERLIN DIVISION

(Head of Division: Prof. Dr. G. Fussmann)

The research activities of the Berlin Division of the IPP cover independent investigations in Berlin as well as joint work with the experimental and theoretical groups in Garching. They are devoted to several aspects of edge plasma physics, impurity transport and plasma-wall interaction in both types of fusion experiments at IPP, the tokamak and the stellarator.
The current cooperation with the ASDEX Upgrade team includes spectroscopic investigations of the divertor region, IR thermography of divertor plates, Langmuir probe measurements in the divertor and Hα measurements. The Berlin Division is supporting the Wendelstein W7-AS project with Langmuir probe measurements, collector probes of different kinds and a sniffer probe. Contributions to these IPP projects are presented in the relevant sections of this report.
Additionally, a large probe manipulator as part of the SOL diagnostics of ASDEX Upgrade is nearly completed and an IR camera to measure the surface temperature of a W7-AS limiter is under construction. Both devices will be installed in spring 1994.
The boundary layer spectrometer is undergoing final tests and the system will be installed at ASDEX Upgrade in March 1994 for observation of the boundary and divertor regions in the VUV and visible spectral range.
A plasma generator is being operated in Berlin for studying the plasma behaviour near material surfaces, physics of materials under high particle and heat flux conditions and plasma-wall interaction, and to develop diagnostics.
A surface analysis laboratory equipped with a SIMS-AES device primarily designed to handle large probes from fusion experiments was put into operation.
The theory group is involved in various studies of edge physics problems, e.g. the effect of neutral particles on density limits in tokamaks, modelling of marfes, the electron temperature in the high-recycling regime.
Plasma polarization experiments in W7-AS and arcing investigations in AUG are being conducted in close cooperation with a WIP (Scientists Integration Programme) group from Humboldt University, Berlin, which is dealing with fundamental problems of arc cathode spots in vacuum.

P. Bachmann, M. Behnke, H. Behrendt, W. Bohmeyer, E. Dietrich, L. Dietrich, H. Greuner, H. Grote, K. Günther, E. Hantzsche[4], S. Hesse, A. Herrmann, D. Hildebrandt, B. Jüttner[4], M. Kammeyer, H. Kastelewicz, P. Kornejew[1], M. Laux, B. Napiontek, E. Pasch[2], P. Pech, R. Radtke, H.-D. Reiner, J. Sachtleben, W. Schneider[3], A. Stareprawo, D. Sünder, U. Wenzel, H. Wolff

1 Seconded from Experimental Division 1

2 Seconded from KFA Jülich

3 Funded by Labour Recruitment Office

4 Funded by the „Scientists Integration Programme" (WIP)

1. PLASMA GENERATOR PSI-1

The PSI-1 facility was set up to study the plasma behaviour near material surfaces, plasma-wall interaction, materials physics under high particle and heat flux conditions and to develop and test new diagnostics. Fig. 1 shows the basic layout.

A steady-state plasma is generated between a heated cylindrical LaB_6 cathode (heating power 7.5 kW, 1650° C) and a hollow anode. The plasma, confined by an axial magnetic field (0.1 T in the target chamber), streams through the differential pumping stage into the diagnostic and target chamber and is neutralized at a plasma dump. The typical diameter of the plasma column is about 120 mm in the target chamber. The design current and voltage values of 1000 A and 200 V could be realized. The plasma parameters in the target chamber achieved so far are $n_e \leq 4 \cdot 10^{19}$ m^{-3}, $T_e = 5$ - 30 eV.

The main aim in 1993 was to reach the design parameters of the machine, to study the dependences of the plasma parameters on the external control parameters (discharge current, magnetic configuration, neutral pressure of the working gases argon and hydrogen) and reduce plasma impurities.

Fig. 2 shows the dependence of the floating potential of the neutralizer plate on the discharge current. This floating potential gives a rough measure of the electron temperature. The figure demonstrates the large influence of the neutral pressure in the cathode region, whereas the current is seen to be less important. There are significant differences for operation in hydrogen and argon. The maximum electron temperatures determined were 30 eV in H and 10 eV in Ar; the respective electron densities attained were $3 \cdot 10^{18}$ m^{-3} and $4 \cdot 10^{19}$ m^{-3}.

First spectroscopic measurements indicated contamination of the plasma by copper from the anode. The effect can be observed in argon as well as in hydrogen. It has a weak dependence on the discharge current and is very strongly dependent on the pressure in the cathode region. The contamination can be strongly reduced by lowering the magnetic field in the anode region. Fig. 3 demonstrates this dependence for an argon discharge at 400 A. A reduction of the current of the magnetic coil leads to a decrease of the Cu resonance line at 327.4 nm, with the intensities of the ArIII lines increasing simultaneously. The magnetic field configuration was routinely evaluated.

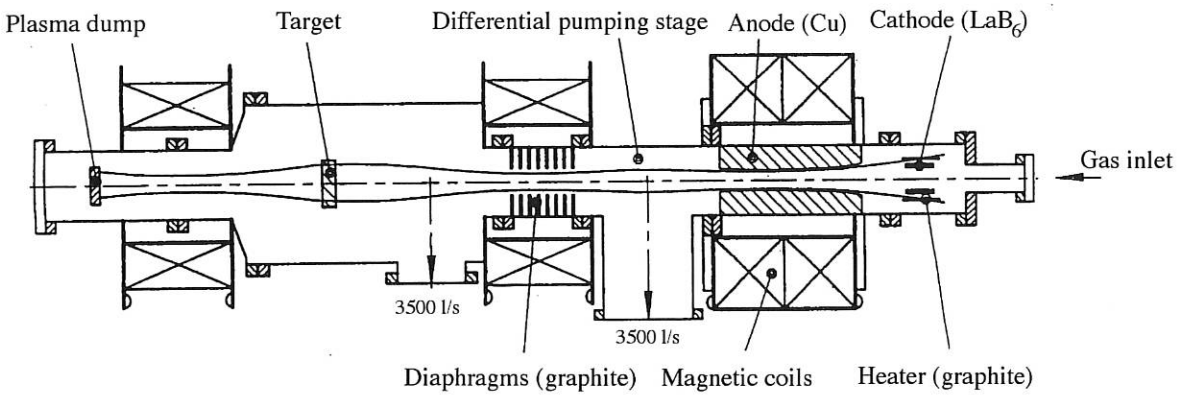

FIG. 1: Schematic side view of the plasma generator PSI-1 (total length ≈ 2.5 m) with magnetic field line contour shown.

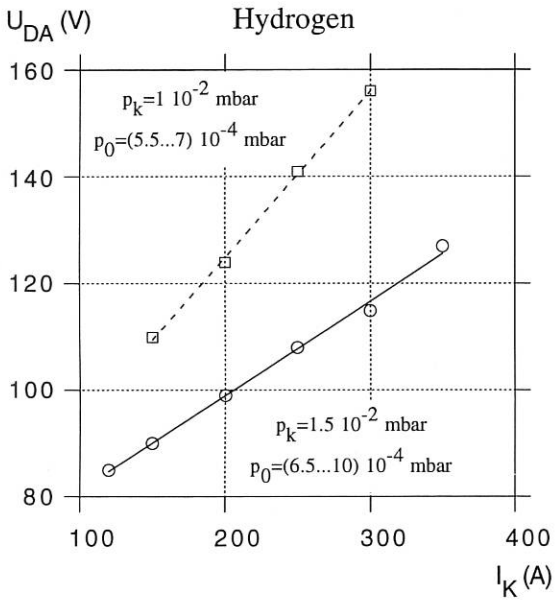

FIG. 2: Floating potential of the plasma dump (U_{DA}) as a function of the discharge current (I_K) for two different sets of neutral gas pressure in the cathode (p_K) and t arget chamber (p_0)

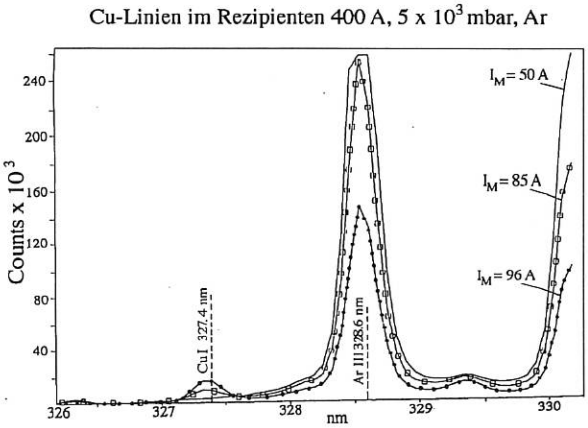

FIG. 3: Spectral lines of Cu and Ar in the target chamber (showing the reduction of copper with increasing current in the magnet coil at the anode).

New diagnostics:
On the basis of a *Nd-YAG laser* (P = 100 MW, τ = 9 ns) a Thomson scattering experiment was put into operation to determine the local electron density and temperature. First experiments were carried out to determine these values in the centre of the plasma beam. Measurements of the radial profiles are planned for 1994.

A *fast scanning Langmuir probe* allows radial plasma profiles to be determined. First measurements in the plasma centre show good agreement with Thomson scattering data.

A thermal *He beam* was injected into the edge of a hydrogen plasma with an electron temperature of about 10 eV. Several relative line intensities were recorded in order to determine T_e and n_e from the line ratios of HeI to HeII. The electron densities obtained in this way are in good agreement with those determined by microwave interferometry.

Calorimetry was completed to set up the power balance of the discharge as well as the power input into a target.

IR thermography was used to measure the surface temperature of the target with high temporal and spatial resolution.

A two-photon-Lyman$_\alpha$ experiment for determining the relative number density of H- and O-atoms is prepared.

2. PROBE MANIPULATOR FOR ASDEX UPGRADE

As part of the SOL diagnostics, the manipulator was designed for probe measurements in the main chamber of ASDEX Upgrade. The system allows a variety of probe heads (collector probe, Langmuir probes, heat flux probes, retarding field probes etc.) to be exposed to the plasma boundary.

The objectives of the scientific programme are to determine radial profiles of impurity deposition and of plasma parameters in the boundary plasma and compare these data with those obtained by means of divertor probes, and code calculations.

The system can transfer the probe heads from a magazine to the plasma boundary over a distance of two metres and position them with an accuracy of better than 1 mm. Probe heads can be replaced between discharges. The magazine can hold up to six probe heads. Each probe head has eight electrical connections which allow biasing, voltage and current measurements.

The central part of the probe heads can be rotated. In this way the inclination of the probe surface to the direction of the magnetic field can be varied.

In collector probe measurements this rotation is used to achieve time resolution (up to 20 ms). This can be performed by rotating a central cylindrical collector sample behind a fixed shield with an exposure slit.

In addition, a reciprocating probe can be adapted to the manipulator. For this purpose the rotational mechanism is replaced by a pneumatic high-speed linear drive system. The maximum stroke of the probe head is 10 cm in the radial direction within 150 ms for full travel forth and back. This allows radial profiles of plasma edge parameters to be measured from the wall to just inside the separatrix.

Transfer of the complete system to IPP Garching and installation are planned for March 1994.

3. UHV LABORATORY

The surface analysis laboratory was furnished with new equipment and put into operation. The main analysis device is an Auger electron spectrometer in conjunction with a static SIMS. An additional X-ray source will be installed to carry out XPS using the hemispherical electron energy analyzer of the Auger spectrometer. The whole system is specially designed to introduce and handle large samples (divertor or limiter tiles up to 140 x 140 x 25 mm^3 and cylindrical collector probes 32 mm in diameter and 88 mm hight, as commonly used in ASDEX Upgrade and W7-AS) without breaking the vacuum and cutting samples. The sample positioning and analysis can be carried out in programmed mode. The ion gun for SIMS and sputter etching operated with oxygen or rare gases can be focused down to 1 µm and special etching patterns can be chosen.

Additionally, an optical profilometer (depth resolution 20 nm) is used for calibrating sputter etched depth profiles.

The expertises of the surface lab are mainly used for investigating collector probes, limiter and divertor tiles etc. exposed in the fusion machines of IPP. As an example, the depth profile obtained with the Auger spectrometer of a layer deposited on a long-term aluminium sample in W7-AS is shown in Fig. 4. Two experimental periods with repeated boronization separated by an experimental period

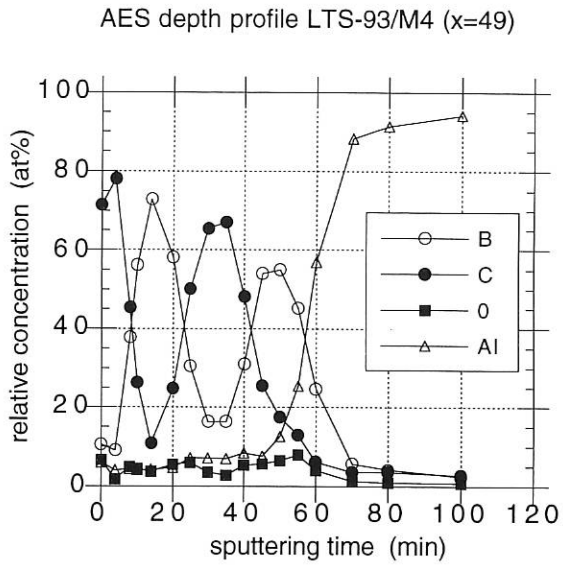

FIG. 4: Depth profile of a long-term collector probe surface

without boronization are clearly reflected by the variation of the relative boron and carbon concentrations with the depth (represented by the sputtering time). This indicates that, despite boronization, carbon remains the main impurity in the plasma of W7-AS.

4. THE BOUNDARY LAYER SPECTROMETER

In 1993 the manufacture of the boundary layer spectrometer was continued. This spectrometer system was designed in the joint effort between ASDEX Upgrade and IPP Berlin. The system collimates light from a common line of sight into two spectrometers:

- 1 m visible spectrometer covering the wavelength region λ = 200 nm to 700 nm

- 1 m normal incidence VUV spectrometer covering λ = 30 nm to 200 nm

The imaging system for the visible radiation is a Cassegrain optics, whereas the VUV radiation is imaged to the spectrometer by an elliptic mirror. By means of a swivel mirror wide parts of the plasma edge and the full divertor region can be observed. It is also possible to measure radial intensity distributions of impurities when the swivel mirror looks in the toroidal direction.

The spectrometer system will be installed at ASDEX Upgrade in 1994 and will be used initially in combination with a divertor gas inlet system for investigations of the impurity transport in the divertor and boundary plasma. Future topics are the impurity retention of the divertor, the development of marfes and cx reactions of impurities, as well as rotation and T_i measurements.

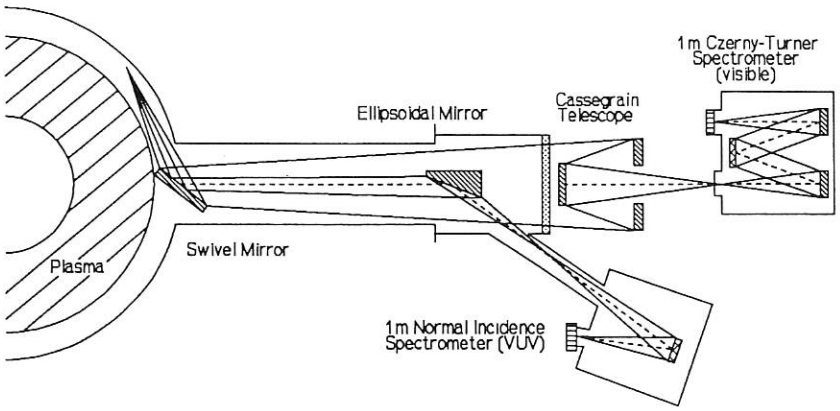

FIG. 5: The boundary layer spectrometer for impurity investigations in ASDEX Upgrade.

5. THEORY

5.1 Bifurcation of Electron Temperature in the High-Recycling Regime

Multiple solutions and bifurcation of the electron temperature along a magnetic flux tube bounded by target plates on two sides are obtained. The heat flow into the high-recycling layer in the front of the target plates must balance the ionization losses and the thermal flux onto the wall. If one solves the heat equation with a source term, describing the power input into the flux tube, and these nonlinear boundary conditions, a system of two coupled polynomials of 8th order for the boundary values of the temperature is derived. An essential result is the existence of two asymmetric solutions above a critical power input although the boundary conditions and the source term are symmetric with respect to the midplane of the flux tube.

5.2 Effect of Neutral Particles on Thermal Instabilities and Density Limits in Tokamak Plasmas

The onset of density disruption, which limits the maximum plasma density, is triggered by impurity radiation in the edge plasma and can be connected with the radiative thermal instability (RTI). Its increment strongly depends on the impurity (carbon) profile, which is significantly affected by charge exchange between impurity ions and hydrogen atoms. Analytical and numerical calculations show that with increasing hydrogen density both the threshold of the RTI and the plasma density limit decrease.

5.3 Elastic Processes in Hydrogen-Helium Plasmas

Classical methods are employed to calculate deflection functions, cross-sections and collision rates for elastic collisions between neutral atoms or molecules and ions. The algorithm for deriving all relevant data needed for a kinetic description of such processes in a background plasma with Maxwellian ion velocity distribution is presented. Data fits for these quantities are calculated for hydrogenic and helium species. Furthermore, data fits for the Ω integrals needed in a hydrodynamic description are given. The implementation of such processes in kinetic Monte Carlo neutral gas transport models is described.

5.4 Numerical Marfe Studies for ASDEX Upgrade

Marfes - as precursors of the density limit in high-density discharges - may serve as reliable criteria for discharge controlling in order to avoid disruption. Calculations were made with the B2-EIRENE code package to study the formation and temporal development of marfes and get information about the discharge parameter regime for the existence of marfes .

The stand-alone version of the B2 code was used to determine the density limit for Marfe onset as a function of the input power, the safety factor and the impurity concentration. Good qualitative agreement with available experimental data was obtained. Time-dependent calculations with the full coupled multifluid code (deuterium, helium, carbon) show highly dynamic Marfe behaviour. "Steady-state" Marfes can be dynamically sustained by appropriately controlling the plasma density or impurity concentration. The impurity radiation pattern of Marfes is usually dominated by C^{3+}-line radiation, which should therefore be suitable for optical monitoring.

COMPUTER SCIENCE DIVISION

(Prof. Dr. Friedrich Hertweck)

F. Hertweck, Ch. Brosig, G. Czapski, R. Dohmen, H. Fisser, H. Friedrich, K.-H. Goihl, P. Heimann, A. Jülich (on leave), J. Maier, A. Müller, M.G. Pacco-Düchs, I. Precht, Ute Schneider, D. Stolz, R. Strunz, Ch. Tichmann, R. Tisma, M. Zilker

The major activities of the division are related to the development and maintenance of the data acquisition system for ASDEX Upgrade, the AMOS/D System developed in close collaboration with the ASDEX Upgrade project. It is a distributed system of workstations connected to a central computer. Activities in the field of parallel processing encompass both transputer systems for the acquisition and processing of large amounts of data and the execution of programs on commercial parallel machines.

1. The AMOS/D System

The activities in 1993, as in the previous years, were concerned with the commissioning of the AMOS/D System, in particular to include more diagnostics and to adapt to the increasing amounts of data. Towards the end of the year, nearly 50 diagnostics, altogether producing about 60 MB of raw data per shot were in operation. In 1993, about 1600 discharges were made. As the system is now fully operational, a considerable amount of work is required for maintenance of software and hardware.

1.1 The AMOS/2 Central System

The central part of the AMOS/D System is a virtual machine, known as AMOS/2, which runs on an IBM 3090/150 mainframe with 64 MByte real storage. The disk capacity of AMOS/2 was extended from 8 GBytes to 14 GBytes in the past year.

Tuning the system again was an important task. The I/O subsystem was improved and a new scheduling class for priority jobs, like the shot file monitor, was introduced. Roll out/roll in of jobs and a new interjob synchronization method provide a better environment for shotfile analysis jobs. The FORTRAN environment was enhanced as well. The emergency procedures for the recovery of data after a severe disk malfunction were revised and tested.

As the UNIX workstations become more powerful, it is to be expected that all data analysis can be performed on a UNIX compute server. Planning has started to implement some of the AMOS/2 services, like the shotfile monitor, on a UNIX machine.

1.2 AMOS/2 Archive System

Now level 0 shot files are saved on special tapes to improve fetching of files belonging to the same shot. To speed up tape fetches, a second fetch queue has been installed. A new priority scheduling of fetch requests guarantees a fair response time. The tape capacity has been doubled (from 1000 tapes to 2000 tapes). 'Salt mine files' are removed from SILO tapes and moved to external tapes. By the end of 1993, a total of 143,764 files have been archived. This includes 110,531 AUGD shotfiles comprising 109 GByte data.

1.3 Shot File Dependence Data Base

By the end of 1993, a preliminary version of the Shot File Dependence Data Base (DDB) has been put into operation under the AMOS/2 System. The main purpose of the DDB is to record the functional dependence of shot files on each other, and to keep the whole set of shot files consistent. Each time a new shot file of level > 0 has been produced, the DDB is notified. In case a shot file is declared invalid later, the information recorded in the data base is used to invalidate all shot files derived from it.

1.4 AMOS/D Network

The performance of the originally installed fiberoptic network, designed for data of 8-12 MBytes per shot, has reached its limits. Today the network has to transfer more than 60 MBytes per shot to the archiving mainframe computer, in addition to the standard network load, caused by the TCP/IP traffic. On shot days, a traffic of 4 GByte of data has been measured between the central AMOS/2 system and the workstations in a period of 24 hours.

In the past years, FDDI has become a widely accepted technology for local area networks. It is now available on nearly every computer platform for a reasonable price. The transfer rate is 10 times higher than that of the previously used Ethernet technology. The revised AMOS/D network, based on an FDDI backbone ring, is shown in FIG. 1.

The FDDI ring is integrated into the existing network and consists of two concentrators linked by two fiber pairs to form a double ring topology. Now all subnets of desktop workstations connect to the FDDI ring and therefore most of the TCP/IP traffic is passed through the ring. A new VMEbus node computer was designed that houses a CPU, an FDDI VMEbus Interface and several old style fiberoptic network interfaces for the VMEbus data acquisition workstations. Data acquisition workstations, based on VMEbus SPARCengines, are connected to the FDDI ring with an Ethernet FDDI router. Shot data is transferred to the IBM mainframe through a newly designed FDDI/IBM Channel-Interface router. This ASDEX Upgrade FDDI ring is connected to the backbone FDDI ring of the computer center, to gain access to the general services.

1.5 Shot Program Editor SPED

The SPED tool is used to define data for the forward control of an ASDEX Upgrade discharge (a "shot"). It was originally designed to run on the proprietary window system of ISI workstations. Since SUN workstations with X11 and OPENWIN desktops are widely used now with the ASDEX Upgrade experiment, SPED was adapted to these interfaces.

1.6 Andrew File System (AFS)

AFS is a distributed file system and provides the possibility to organize all the files of IPP in one hierarchical file tree. Files are stored on different machines in the computer network. Every machine in the network has access to all the files as if they were on a local disk. AFS has been tested and installed in cooperation with the computer center and ASDEX Upgrade.

1.7 Solaris 2.x

The UNIX version, currently running on all workstations is based on Berkeley 4.2. SPARC center machines delivered by SUN will only be supported by the Solaris operating system, so the move from Berkeley 4.2 to System V Release 4 will be necessary. To gain experience with this operating system, Solaris 2.3 has been installed on a few workstations.

1.8 Fortran 90

In 1991/1992 the ISO/ANSI Technical Committees approved a new standard of FORTRAN, FORTRAN 90, which is a significant extension of old FORTRAN 77. The NAGWare FORTRAN 90 compiler and several utilities have been tested extensively and have been made available to the users. Lectures and courses on the new features of FORTRAN 90 have been given and were widely appreciated.

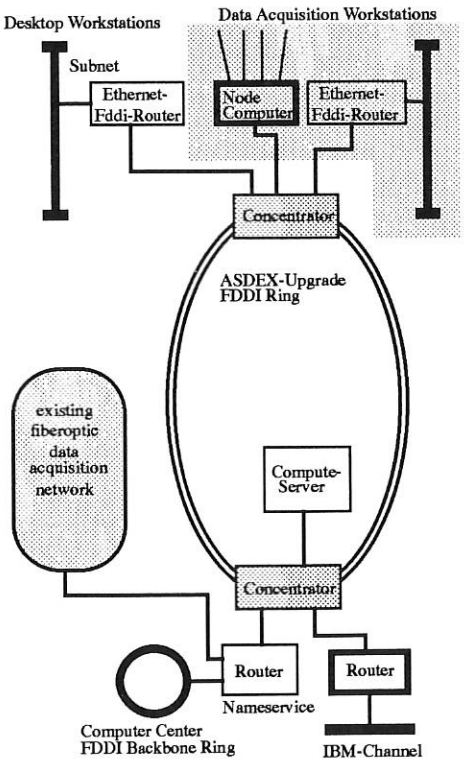

FIG. 1: FDDI Network

2. Parallel Processing

2.1 Parallelization of User Programs

The investigations concerning the applicability of parallel computers to typical plasma codes have been continued. In particular, a Monte-Carlo program which was originally developed by Lotz and Nührenberg for a CRAY vector computer, was parallelized and implemented on the nCUBE2 system. The parallel program is structured in a way that the main program and all subroutines are essentially preserved. This feature guarantees that changes in the code can be made likewise easily in the parallel program as in the original code. The performance of the parallel implementation is quite satisfactory, the speedup reaches 90-100% of what can be expected according to Amdahl's Law. Compared to the CRAY Y/MP, the nCUBE2 system with 64 processors is by the factor 1.5 slower.

The parallel code was ported to the KSR1 parallel machine (LRZ München, GWDG Göttingen), which is based on the global shared memory conception, while the nCUBE2 system is of message passing type. The speedup of the KSR1 program is even slightly better than that of the nCUBE2 program. By porting the program, we had the possibility to compare the two different architectures. We found that the work necessary to implement the parallel algorithm on each of the machines is of comparable complexity and even of similar kind. Furthermore, a recipe has been derived how to proceed when porting programs from the nCUBE2 to the KSR1. This recipe should be applicable to quite a lot of nCUBE2 programs.

2.2 A Transputer Multiprocessor System for Plasma Diagnostics

The Mirnov and Soft-Xray diagnostics have been put into operation on ASDEX Upgrade. Both diagnostics collect massive amounts of data that must be processed both in real time and between shots. A host system integrates the diagnostics into the UNIX environment. A transputer, subsystem is responsible for the acquisition of the data.

The subsystem is realized with a transputer multiprocessor network with a switchable topology. The network is based on building blocks, where one block can accept 8 input channels with a maximum data rate of 1 MByte/sec per channel. A block consists of two input boards (8 fifo-buffered channels), one transputer board (4 modules with a T800 and 4 MByte dynamic memory), and a backplane to interconnect the VMEbus compatible boards (see Fig. 2). One transputer handles two input channels with an online storage capacity of 1.6 MBytes per channel. All the interconnections between the blocks and to the host system use differential signals to increase the reliability and to allow physical distribution of the network.

The control software running on the subsystem enables the user to sample the data of the various channels with a predefined sample rate in certain windows of the time axis. The total amount of data that can be acquired is 200 MBytes. Further processing and reduction of the raw measurement data must be done on the transputer network with a peak performance rate of 96 MFLOPS. With this design it is guaranteed that only the interesting and necessary data will be transferred from the subsystem to the host and later to the archive file system.

Soft-Xray Diagnostics: a 64 processor system

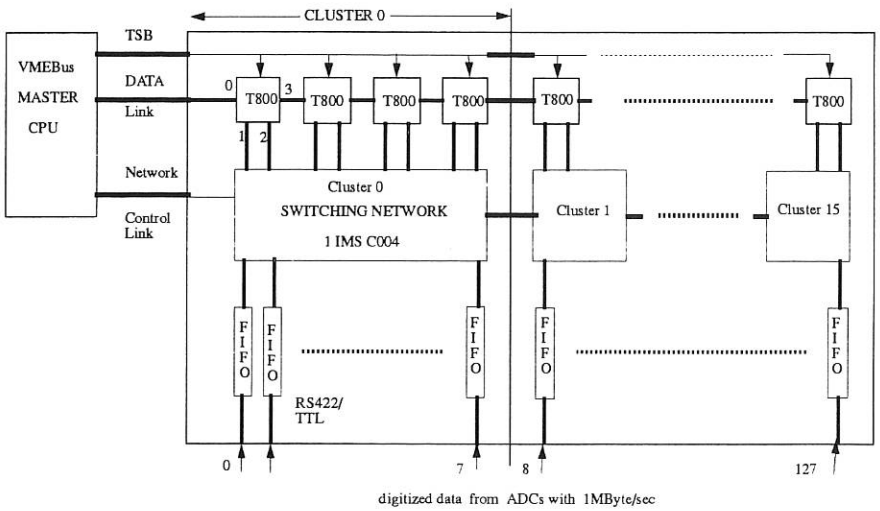

FIG. 2: Soft-Xray Diagnostics

CENTRAL TECHNICAL SERVICES

(Dr.-Ing. Harald Rapp)

The Central Technical Services (ZTE) of Max-Planck-Institut für Plasmaphysik support the experimental divisions with the design, construction and operation of experiments and their diagnostics. They also provide and run all kinds of utilities for facility operation. They are subdivided into six departments and employ approximately 170 workers, technicians and engineers. Detailed knowledge of the experimental conditions and the appropriate techniques and tools is decisive for meeting the requirements of the research divisions. Task-sharing between the research groups, industry and the Central Technical Services is standard practice for minimizing costs and manpower. In 1993 replacement of personnel and equipment was a major concern.

1. MECHANICAL DESIGN AND CALCULATION

(J. Simon-Weidner)

The group comprises about 25 technicians and engineers. Calculations deal with mechanical stresses in coils, vacuum vessels and supports and with the thermomechanical loads on the walls and limiters. The department is equipped with a network of workstations and a link to Garching Computer Centre. A variety of programs for CAD as well as finite-element computation are available. In 1993 group members participated in the calculation of stress due to halo currents in the ASDEX Upgrade tokamak and continued designing the W7X stellerator experiment as well as the prototype components. Other tasks of the department mainly concern the design of experimental equipment such as high-power and high-frequency components and plasma diagnostics.

2. ELECTRONICS DEVELOPMENT

(D. Arz)

The department consist of 3 groups, one of which develops and constructs the switching equipment for operating the neutral-beam and high-frequency plasma heating systems. There are presently 16 switch boxes running and being maintained, with another 4 under construction. An electronic service group maintains and repairs all kinds of electronic equipment. A third group develops analogue and digital electronic equipment such as special amplifiers and converters for signal matching, interfaces between different computers and control systems, microprocessor-based controllers and high-power DC and AC power supplies.

3. MATERIALS TECHNOLOGY

(E. Trcka)

The department offers a variety of technical services for materials testing and processing. These comprise surface preparation such as galvanic or vapour deposition, soldering and welding for vacuum applications, testing and investigation of materials, chemistry and vacuum services. Surface coating of high-frequency components and manufacture of galvano-plastics are part of the approved special services. Waste management has assumed an important role.

4. ELECTRIC POWER SUPPLY

(W.R. McGlaun)

The department is responsible for the electric power supply of IPP and the experiments. Furthermore, it provides support with the design and construction of controls for machines and experimental systems. The staff operates 4 flywheel generators, with a total power of 580 MVA and an available energy of 2.6 GJ . The energy is transmitted via a modular system of thyristor-controlled converters (462 MVA in total) and diode rectifiers to the experiments and loads. Also the high-voltage supply for the plasma heating systems is prepared and operated by the department. In 1993 the 10 kV input cables with switch and control installations from the electric power supplier to IPP were renewed.

5. FACILITY OPERATION

(H. Rapp)

A small group is involved in planning and supervising installations for heating, air conditioning, water and cranes or elevators. Cooling of the magnet field coils of the experiments is provided by two water circuits, one of them a closed loop with a cooling tower and the other using ground water. During the report period a couple of tasks for renewing heating stations, fuel oil tanks and cooling-water pipes could be settled.

6. WORKSHOPS

(M. Keiner)

About half of the ZTE personnel work in workshops and with supporting groups. The capacity meets the basic needs for constructing and assembling experimental setups. If necessary, additional capacity is purchased from industry. There are several groups for mechanical fabrication and joinery, electrical and electronic manufacturing, maintainance of utility installations and apprentice training. Some of the craftsmen routinely participate in construction or repair work during shut-down phases of experiments. The costs and capacity of the Central Technical Services are permanently controlled and accounted. Work for nuclear fusion projects can be supported by EURATOM. The annual budget is typically 20 million DM. Without facility operation and powersupply, 135,000 man-hours were expended on fabrication and engineering in 1993.

ADMINISTRATION

(Dr. Thomas Köstlin)

The administration and general services of Max-Planck-Institut für Plasmaphysik are organized in departments. Six of them are presented here:

PERSONNEL DEPARTMENT

The personnel department is responsible for administrative matters relating to personnel. The personnel figures of the institute for 1993 were as follows:

Total personnel	1002
Scientists	291
Technicians	436
Directorate and Staff Representative Council	21
General Services	76
Administration	69
Other personnel	109

PURCHASING AND CONTRACTS DEPARTMENT

The purchasing and contracts department is responsible for all contracts and orders carried out by IPP, Garching and Berlin This year, nearly 9,500 purchase orders were placed. Included were complex contracts, many of them having been signed after a European-wide call for tenders. Furthermore, all export and import formalities are handled within this department: about 150 international and European shipments were made in 1993.

LEGAL AND PATENT DEPARTMENT

The legal department attends to patent applications and supervision, contracts of cooperation, and licensing of patents in cooperation with Garching Innovation GmbH, a subsidiary of the Max Planck Society. In 1993 the division supervised 135 patents and similar rights.

FINANCE DEPARTMENT

The finance department is responsible for financial planning and all financial transactions and fiscal matters of IPP.

Total budget in 1993:	151.0 MDM
This budget was financed as follows:	
Federal Republic of Germany through Federal Ministry of Research and Technology (BMFT)	89.3 MDM
Bavaria	9.1 MDM
Berlin	0.7 MDM
EURATOM	32.0 MDM
Other income	19.9 MDM

SITE AND BUILDINGS DEPARTMENT

The site and buildings department is in charge of planning, construction, structural alteration and reconditioning of buildings and main service facilities. Building maintenance is also provided for the neighbouring Max Planck Institutes of Astrophysics and Extraterrestrial Physics, the European Southern Observatory and the Berlin Division of IPP.

SOCIAL DEPARTMENT

The social department gives assistance to employees seeking housing, provides accommodation for guests in IPP residences, and runs the transport pool, bus and cleaning services.

Publications

Publications and Conference Reports

1. *Abanese*, R.; Bottura*, L.; Ciochio*, S.; Gernhardt, J.; Gruber, O.; Seidel, U.; et al.:* Validation of Numerical Codes for the Analysis of Plasma Discharges. Fus. Eng. Des. **23**, 299-322 (1993).

2. *Abramov*, V.A.; Bachmann, P.; Morozov*, D.K.; Sünder, D.:* Effect of Neutral Particles on Density Limits in Tokamaks. In: Proc. 20th EPS Conf. Control. Fusion and Plasma Phys., Lisbon 1993, Eds. J.A.C.Cabral, M.E.Manso, F.M.Serra, et al. ECA 17C. Europ. Phys. Soc., Geneva 1993, 823-826.

3. *Ambrosino*, G. ; Celentano*, G.; Garofalo*, F.; McCarthy, P.; Gernhardt, J.; Schneider, W.; et al.:* A Novel On-Line Shape Identification Code for Use in Fast Control Systems. In: Proc. 17th Symp. Fusion Technol., Rome 1992, Eds. C.Ferro, M.Gasparotto, H.Knöpfel. North-Holland Publ., Amsterdam 1993, 423-426.

4. *Andelfinger, C.; Buchelt, E.; Cierpka, P.; Kollotzek, H.; Lang, P.; Lang, R.; Prausner, G.; Söldner, F.X.; Ulrich, M.; Weber, G.:* A New Centrifuge Pellet Injector for Fusion Experiments. Rev. Sci. Instrum. **64**, 983-989 (1993).

5. *Baldzuhn, J.; Ohlendorf, W.; Weller, A.; Burhenn, R.; Kick, M.; WVII-AS-Team:* CXRS-Measurement and Code-Calculation of Impurity Profiles. In: Proc. 20th EPS Conf. Control. Fusion and Plasma Phys., Lisbon 1993, Eds. J.A.C.Cabral, M.E.Manso, F.M.Serra, et al. ECA 17C. Europ. Phys. Soc., Geneva 1993, 1207-1210.

6. *Baldzuhn, J.; Sandmann, W.; WVII-AS-Team:* Analysis of Luminescence Signals Observed During Pellet Injection. Plasma Phys. Control. Fusion **35**, 1413-1431 (1993).

7. *Ballico, M.; Cattanei, G.; Plyusnin*, V.; WVII-AS-Team; ICRH-Team:* First Experimental Results Using a Toroidally Broad ICRH Antenna on the W7-AS Modular Stellarator. In: Proc. 9th Int. Workshop on Stellarators, Garching 1993. IAEA, Wien 1993, 413-419.

8. *Ballico, M.; Cattanei, G.; Plyusnin*, V.; WVII-AS-Team; ICRH-Team:* ICRF Heating Experiments in the W7-AS Stellarator Using a Narrow K Spectrum Antenna. In: Proc. 20th EPS Conf. Control. Fusion and Plasma Phys., Lisbon 1993, Eds. J.A.C.Cabral, M.E.Manso, F.M.Serra, et al. ECA 17C. Europ. Phys. Soc., Geneva 1993, 949-951.

9. *Bartels, H.-W.:* Impact of Runaway Electrons. Fusion Eng. Des. **23**, 323-328 (1993).

10. *Bartiromo*, R.:* Transport Properties of Current Driven Tokamak Plasmas. Plasma Phys. Contr. Fusion **35**, 167-179 (1993).

11. *Bartiromo*, R.; Barbato*, E.; Gabellieri*, L.; Leuterer, F.; Söldner, F.X.; Gehre, O.; Murmann, H.; et al.:* Fast Electron Confinement During Lower Hybrid Experiments in ASDEX. Nucl. Fusion **33**, 1483-1492 (1993).

12. *Becker, G.:* Investigation of Transport in the Ignited ITER Plasma by Computer Simulations. Nucl. Fusion **33**, 1435-1443 (1993).

13. *Becker, G.:* Thermal Energy and Bootstrap Current Fusion Reactor Plasmas. In: Proc. 20th EPS Conf. Control. Fusion and Plasma Phys., Lisbon 1993, Eds. J.A.C.Cabral, M.E.Manso, F.M.Serra, et al. ECA 17C. Europ. Phys. Soc., Geneva 1993, 1403-1406.

14. *Beckschulte, M.; Taglauer, E.:* Influence of Work Function Changes on the Charge Exchange in Low-Energy Ion Scattering. Nucl. Instrum. Methods Phys. Res. B **78**, 29-37 (1993).

15. *Behrendt, H.; Bohmeyer, W.:* Komplettierung einer Anlage zur Simulation der Plasma-Wand-Wechselwirkung in einem Fusionsreaktor (ZIE 9001). Bericht an das BMFT. MPI Plasmaphysik, Berlin 1993, 13 S.

16. *Behrisch, R.; Eckstein, W.:* Sputtering Yield Increase with Target Temperature for Ag. Nucl. Instrum. Methods Phys. Res. B **82**, 255-258 (1993).

17. *Behrisch, R.; Venus, G.:* Heat Removal by the Divertor Plate and Limiter Materials in Fusion Reactors. J. Nucl. Mater. **202**, 1-9 (1993).

18. *Beidler, C.:* Neoclassical Transport Scalings Determined from a General Solution of the Ripple-Averaged Kinetic Equation (GSRAKE). In: Proc. 9th Int. Workshop on Stellarators, Garching 1993. IAEA, Wien 1993, 138-145.

19. *Beidler, C.; Gasparino, U.; Geiger, J.; Harmeyer, E.; Kißlinger, J.; Kühner, G.; Rau, F.; Ringler, H.; Wobig, H.; WVII-AS-Team; ECRH-Group:* Wendelstein 7-AS Configurations at Various Mirror Ratios and iota-Values. In: Proc. 20th EPS Conf. Control. Fusion and Plasma Phys., Lisbon 1993, Eds. J.A.C.Cabral, M.E.Manso, F.M.Serra, et al. ECA 17C. Europ. Phys. Soc., Geneva 1993, 341-344.

20. *Beidler, C.; Gasparino, U.; Geiger, J.; Harmeyer, E.; Kißlinger, J.; Kühner, G.; Rau, F.; Ringler, H.; Wobig, H.; WVII-AS-Team; ECRH-Group:* Wendelstein 7-AS Configurations at Various Mirror Ratios and iota-Values. In: Proc. 9th Int. Workshop on Stellarators, Garching 1993. IAEA, Wien 1993, 84-95.

21. *Beidler, C.; Grieger, G.; Harmeyer, E.; Karulin, N.; Kißlinger, J.; Lotz, W.; Nührenberg, J.; Rau, F.; Wobig, H.:* Reactor Studies on Advanced Stellarators. In: Proc. 14th Conf. on Plasma Phys. and Control. Nucl. Fusion Res., 3, Würzburg 1992. IAEA, Wien 1993, 327-337.

22. *Beidler, C.; Harmeyer, E.; Kißlinger, J.; Karulin, N.; Rau, F.; Wobig, H.:* Power Balance in a Helias Reactor. In: Proc. 20th EPS Conf. Control. Fusion and Plasma Phys., Lisbon 1993, Eds. J.A.C.Cabral, M.E.Manso, F.M.Serra, et al. ECA 17C. Europ. Phys. Soc., Geneva 1993, 421-424.

23. *Beidler, C.; Harmeyer, E.; Kißlinger, J.; Rau, F.; Renner, H.; Wobig, H.:* Island Divertor Concept for the Stellarators Wendelstein 7-X and Wendelstein 7-AS. In: Proc. 9th Int. Workshop on Stellarators, Garching 1993. IAEA, Wien 1993, 385-390.

24. *Beidler, C.; Harmeyer, E.; Kißlinger, J.; Rau, F.; Renner, H.; Wobig, H.:* Island Divertor Concept for the Stellarator Wendelstein 7-X. In: Proc. 20th EPS Conf. Control. Fusion and Plasma Phys., Lisbon 1993, Eds. J.A.C.Cabral, M.E.Manso, F.M.Serra, et al. ECA 17C. Europ. Phys. Soc., Geneva 1993, 787-790.

25. *Beidler, C.; Kißlinger, J.; Maaßberg, H.; Nührenberg, J.; Rau, F.; Wobig, H.; et al.:* Progress in Physics Studies for URAGAN-2M Torsatron. In: Proc. 9th Int. Workshop on Stellarators, Garching 1993. IAEA, Wien 1993, 164-193.

26. *Bergmann, A.:* 2D Particle Simulation of the Magnetized Sheath of a Flush-Mounted Langmuir Probe. In: Proc. 20th EPS Conf. Control. Fusion and Plasma Phys., Lisbon 1993, Eds. J.A.C.Cabral, M.E.Manso, F.M.Serra, et al. ECA 17C. Europ. Phys. Soc., Geneva 1993, 803-806.

27. *Bergmann, A.; Mulser*, P.:* Breaking of Resonantly Excited Electron Plasma Waves. Phys. Rev. E **47**, 3585-3598 (1993).

28. *Bertel, E.; Memmel, N.; Rangelov, G.; Bischler*, U.:* Compressed CO Adsorption Layers on the (110) Surfaces of Ni, Pd, and Pt: An Inverse Photoemission Study of the Unoccupied Electronic Band Structure. Chem. Phys. **177**, 337-348 (1993).

29. *Bessenrodt-Weberpals, M.:* Experimental Results in Tokamak Physics. In: IPP Summer University for Plasma Phys., Garching 1993, Ed. H.-W.Bartels. MPI Plasmaphysik, Garching 1993, 69-81.

30. *Bessenrodt-Weberpals, M.:* Leuchte heller als die Sonne. Schweizer Maschinenmarkt **13**, 36-39 (1993).

31. *Bessenrodt-Weberpals, M.; Wagner, F.; ASDEX-Team; ICRH-Team; NI-Team(ASDEX); PSI-Group; Gehre, O.; Giannone, L.; Hofmann, J.V.; Kallenbach, A.; McCormick, K.; Mertens, V.; Murmann, H.; Ryter, F.; Scott, B.; Siller, G.; Söldner, F.X.; Stäbler, A.; Steuer, K.-H.; Stroth, U.; Tsois*, N.; Verbeek, H.; Zohm, H.:* The Isotope Effect in ASDEX. Nucl. Fusion **33**, 1205-1238 (1993).

32. *Biener, J.; Schenk, A.; Winter, B.; Küppers, J.:* HREEL Spectroscopy of Thin Ion Beam Deposited C:H(D) Films. J. Electron Spectrosc. Relat. Phenom. **64/65**, 331-339 (1993).

33. *Biener, J.; Schenk, A.; Winter, B.; Lutterloh, C.; Schubert, U.A.; Küppers, J.:* The Mechanism of Chemical Erosion of C:H Films: a HREELS and TDS Study. In: Proc. 3rd Seminar on Surface Science, Kaprun 1993, Eds. G.Betz, P.Varga. Inst. f. Allg. Physik, Univ. Wien 1993, 203-208.

34. *Biener, J.; Schenk, A.; Winter, B.; Lutterloh, C.; Schubert, U.A.; Küppers, J.:* Spectroscopic Identification of C-H Species in C:H Films Using HREELS. Surf. Sci. **291**, L725-L729 (1993).

35. *Biener, J.; Schenk, A.; Winter, B.; Lutterloh, C.; Schubert, U.A.; Küppers, J.:* A Surface Reaction with Atoms: Hydrogenation of sp and sp^2-Hybridized Carbon by Thermal H (D) Atoms. J. Chem. Phys. **99**, 3125-3128 (1993).

36. *Biener, J.; Schubert, U.A.; Schenk, A.; Winter, B.; Lutterloh, C.; Küppers, J.:* Modeling the Elementary Steps of Low-Pressure Diamond Deposition. Adv. Mater. (Weinh.) **5**, 639-643 (1993).

37. *Bischler*, U.; Bertel, E.:* One-Dimensional Surface States (Chain States) on a Metal Surface: H on Ni(110). Phys. Rev. Lett. **71**, 2296-2299 (1993).

38. *Bischler*, U.; Bertel, E.:* Simple Source of Atomic Hydrogen for Ultrahigh Vacuum Applications. J. Vac. Sci. Technol. A **11**, 458-460 (1993).

39. *Bischler*, U.; Sandl, P.; Bertel, E.; Brunner*, T.; Brening*, W.:* Sticking, Adsorption, and Absorption of Atomic H on Cu(110). Phys. Rev. Lett. **70**, 3603-3606 (1993).

40. *Biskamp, D.:* Current Sheet Profiles in Two-Dimensional Magnetohydrodynamics. Phys. Fluids B **5**, 3893-3896 (1993).

41. *Biskamp, D.:* Geometric Properties of Level Surfaces in MHD Turbulence. Europhys. Lett. **21**, 563-567 (1993).

42. *Biskamp, D.:* Nonlinear Magnetohydrodynamics. Cambridge Univ.Press, Cambridge 1993. 378 S.

43. *Bosch, H.-S.; Schneider, R.; Pitcher*, C.S.; Haas, G.; Neuhauser, J.; Poschenrieder, W.; Braams*, B.; Büchl, K.; Field, A.; Gehre, O.; Herrmann, A.; Kaufmann, M.; Laux, M.; Lieder, G.; Meisel, D.; Reiter*, D.; Richter, T.; Wenzel, U.; ASDEX-Upgrade-Team:* 2D Model Validation of ASDEX-Upgrade Scrape-Off Layer Plasmas. In: Proc. 20th EPS Conf. Control. Fusion and Plasma Phys., Lisbon 1993, Eds. J.A.C.Cabral, M.E.Manso, F.M.Serra, et al. ECA 17C. Europ. Phys. Soc., Geneva 1993, 795-798.

44. *Brakel, R.; Burhenn, R.; Grigull, P.; Hartfuß, H.-J.; Jänicke, R.; Kühner, G.; Sardei, F.; Stroth, U.; Weller, A.; WVII-AS-Team; NI-Group; et al.:* Dependence of Transport on Rotational Transform in the Stellarator W7-AS. In: Proc. 20th EPS Conf. Control. Fusion and Plasma Phys., Lisbon 1993, Eds. J.A.C.Cabral, M.E.Manso, F.M.Serra, et al. ECA 17C. Europ. Phys. Soc., Geneva 1993, 361-364.

45. *Brakel, R.; Grigull, P.; Sardei, F.; Burhenn, R.; Herre, G.; Maaßberg, H.; Wolff, H.; WVII-AS-Team; PSI-Group; ECRH-Group:* Boundary Topology, Edge Transport and Impurity Control in the Wendelstein 7-AS Stellarator. In: Proc. 14th Conf. on Plasma Phys. and Control. Nucl. Fusion Res., 2, Würzburg 1992. IAEA, Wien 1993, 501-506.

46. *Brakel, R.; WVII-AS-Team; ECRH-Group:* Recycling Studies in the Wendelstein 7-AS Stellarator. In: Proc. 9th Int. Workshop on Stellarators, Garching 1993. IAEA, Wien 1993, 369-374.

47. *Brambilla, M.:* Modeling Loop Antennas for HF Plasma Heating in the Ion Cyclotron Frequency Range. Plasma Phys. Control. Fusion **35**, 41-62 (1993).

48. *Brambilla, M.:* Modelling Heating and Current Drive in the Ion Cyclotron Frequency Range. Plasma Phys. Control. Fusion **35**, Suppl.A, 141-165 (1993).

49. *Brambilla, M.; Hoffmann, C.:* Self-Consistent Modeling of IC Minority Heating. In: Proc. 20th EPS Conf. Control. Fusion and Plasma Phys., Lisbon 1993, Eds. J.A.C.Cabral, M.E.Manso, F.M.Serra, et al. ECA 17C. Europ. Phys. Soc., Geneva 1993, 957-960.

50. *Büchse, R.; Gasparino, U.; Hartfuß, H.-J.; Jänicke, R.; Weller, A.; ECRH-Group; WVII-AS-Team:* Temperature Relaxations During Current Drive Experiments in the W7-AS Stellarator. In: Proc. 20th EPS Conf. Control. Fusion and Plasma Phys., Lisbon 1993, Eds. J.A.C.Cabral, M.E.Manso, F.M.Serra, et al. ECA 17C. Europ. Phys. Soc., Geneva 1993, 365-368.

51. *Cappello*, S.; Biskamp, D.:* MHD Studies of Stationary Turbulent Dynamics in a Reversed-Field Pinch. In: Proc. 20th EPS Conf. Control. Fusion and Plasma Phys., Lisbon 1993, Eds. J.A.C.Cabral, M.E.Manso, F.M.Serra, et al. ECA 17C. Europ. Phys. Soc., Geneva 1993, 487-490.

52. *Carlson, A.; Grigull, P.; Günther, K.; Hildebrandt, D.; Laux, M.; Pech, P.; Reiner, H.-D.; Weinlich, M.; Wolff, H.:* Langmuir Probes in Strong Magnetic Fields. In: Proc. 20th EPS Conf. Control. Fusion and Plasma Phys., Lisbon 1993, Eds. J.A.C.Cabral, M.E.Manso, F.M.Serra, et al. ECA 17C. Europ. Phys. Soc., Geneva 1993, 1103-1106.

53. *Chatelier, M.; Engelmann, F.; Wagner, F.; Watkins, M.L.:* Steady State Operation of Fusion Plasmas. Plasma Phys. Control. Fusion **35**, 1451-1477 (1993).

54. *Coad,* J.P.; Behrisch, R.; De Kock*, L.; Koch, A.; Weschenfelder*, F.; Wienhold*, P.; Wilhelm, R.:* Assessment Techniques for Measurement of Target Erosion/Redeposition in Large Tokamaks. J. Nucl. Mater. **200**, 360-365 (1993).

55. *Correa-Restrepo, D.; Pfirsch, D.:* Negative-Energy Waves in an Inhomogeneous Force-Free Vlasov Plasma with Sheared Magnetic Field. Phys. Rev. E **47**, 545-563 (1993).

56. *Croci, R.:* Reflection and Absorption of Ordinary Waves in an Inhomogeneous Plasma. J. Plasma Phys. **50**, 109-123 (1993).

57. *D'Haeseleer, W.D.; Beidler, C.:* An Efficient Physics-Based Monte-Carlo Algorithm for Simulating Alpha-Particle Orbits in Tokamak Fusion-Reactor Plasmas with Toroidal-Field Ripple. Comput. Phys. Commun. **76**, 41-62 (1993).

58. *Detzel, Th.; Memmel, N.; Fauster, Th.:* Growth of Ultrathin Iron Films on Cu(001): An Ion-Scattering Spectroscopy Study. Surf. Sci. **293**, 227-238 (1993).

59. *Donath, M.:* Recent Developments in Surface and Thin Film Magnetism Probed by Spin-Polarized Electrons. Surf. Sci. **287/288**, 722-731 (1993).

60. *Donath, M.:* Spin-Dependent Empty Electronic States at Magnetic Surfaces. In: Magnetism and Structure in Systems of Reduced Dimension, Eds. R.F.C.Farrow, B.Dieny, M.Donath, et al. Plenum Pr., New York 1993, 243-255.

61. *Donath, M.; Passek, F.; Dose, V.:* Surface State Contribution to the Magnetic Moment of Ni(111). Phys. Rev. Lett. **70**, 2802-2805 (1993).

62. *Dose, V.:* Multivariate Analysis of PECVD Data. Appl. Phys. A **56**, 471-477 (1993).

63. *Du Plessis, J.; Taglauer, E.:* Contour Mapping as an Interpretive and Calculative Tool in Alloy Sputtering Measurements. Nucl. Instrum. Methods Phys. Res. B **78**, 212-216 (1993).

64. *Eckstein, W.:* Comment on 'Isotopic Fractionation in the Sputtering of ^{92}Mo - ^{100}Mo Targets' by D.L.Weathers, S.J.Spicklemire, T.A.Tombrello, I.D.Hutcheon and H.Gnaser. Nucl. Instrum. Method Phys. Res. B **83**, 329-333 (1993).

65. *Eckstein, W.; Garcia-Rosales, C.; Roth, J.; Laszlo*, J.:* Threshold Energy for Sputtering and its Dependence on Angle of Incidence. Nucl. Instrum. Methods Phys. Res. B **83**, 95-109 (1993).

66. *Eckstein, W.; Mashkova*, E.S.; Molchanov*, V.A.; et al.:* The Effect of Target Texture and Target Topography on the Spatial Distributions of Material Sputtered from Tungsten. Appl. Phys. A **57**, 271-277 (1993).

67. *Endler, M.; Giannone, L.; Niedermeyer, H.; Rudyj, A.; Theimer, G.; ASDEX-Team:* Experimental and Theoretical Investigation of Density and Potential Fluctuations in the Scrape-Off Layer of ASDEX. In: Proc. 20th EPS Conf. Control. Fusion and Plasma Phys., Lisbon 1993, Eds. J.A.C.Cabral, M.E.Manso, F.M.Serra, et al. ECA 17C. Europ. Phys. Soc., Geneva 1993, 583-586.

68. *Engelhard, M.; Jacob, W.; Möller, W.; Koch, A.:* Absolute CH Radical Density Measurements in a Methane ECR Plasma. In: Proc. ISPC-11, Loughborough 1993, Ed. J.Harry. Int. Union Pure and Appl. Chem., Loughborough 1993, 1392-1397.

69. *Erckmann, V.; Brakel, R.; Burhenn, R.; Grigull, P.; Hartfuß, H.-J.; Hofmann, J.V.; Jänicke, R.; Maaßberg, H.; Niedermeyer, H.; Ohlendorf, W.; Ringler, H.; Rudyj, A.; Wagner, F.; Weller, A.; WVII-AS-Team; Baldzuhn, J.; Bomba, B.; Cattanei, G.; Dodhy, A.; Dorst, D.; Elsner, A.; Endler, M.; Engelhardt, K.; Gasparino, U.; Geissler, S.; Geist, T.; Giannone, L.; Hacker, H.; Heinrich, O.; Herre, G.; Hildebrandt, D.; Karger, F.; Kick, M.; Kroiss, H.; Kubo*, S.; Kühner, G.; Lazaros, A.; Mahn, C.; McCormick, K.; Pech, P.; Ruhs, N.; Saffert, J.; Sardei, F.; Sattler, S.; Tutter, M.; Unger, E.; Wenzel, U.; Wolff, H.; Würsching, E.; Zimmermann, D.; Zippe, M.; Zöpfel, S.; et al.:* H-Mode Like Transitions in the W7-AS Stellarators with High Power 140 GHz ECRH. In: Proc. 14th Conf. on Plasma Phys. and Control. Nucl. Fusion Res., 2, Würzburg 1992. IAEA, Wien 1993, 469-481.

70. *Erckmann, V.; Burhenn, R.; Geist, T.; Hartfuß, H.-J.; Kick, M.; Maaßberg, H.; WVII-AS-Team; Kasparek*, W.; Müller, G.; Schüller, P.G.; Il'in, V.I.; Kurbatov, V.I.; Malygin, S.; Malygin, V.I.:* High Power 140 GHz ECRH Experiments at the W7-AS Stellarator. In: Radio Frequency Power in Plasmas, Eds. M.Porkolab, J.Hosea. AIP Conf. Proc. 289, AIP, New York 1993, 137-148.

71. *Erckmann, V.; Burhenn, R.; Hartfuß, H.-J.; Kick, M.; Maaßberg, H.; WVII-AS-Team; NI-Team(WVII-AS); et al.:* Recent Results with 140 GHz ECRH at the W7-AS Stellarator. In: Proc. 20th EPS Conf. Control. Fusion and Plasma Phys., Lisbon 1993, Eds. J.A.C.Cabral, M.E.Manso, F.M.Serra, et al. ECA 17C. Europ. Phys. Soc., Geneva 1993, 345-348.

72. *Erckmann, V.; Gasparino, U.; Maaßberg, H.; WVII-AS-Team:* Study of EC Current Drive Efficiency and Bootstrap Current by Power Modulation Experiments. In: Proc. 20th EPS Conf. Control. Fusion and Plasma Phys., Lisbon 1993, Eds. J.A.C.Cabral, M.E.Manso, F.M.Serra, et al. ECA 17C. Europ. Phys. Soc., Geneva 1993, 1021-1024.

73. *Erckmann, V.; Suvorov, E.V.; Holzhauer, E.; Kasparek*, W.:* Status of Collective Thomson Scattering Experiments at 70 GHz and 140 GHz on W7-AS. In: Proc. 5th Joint Russian-German Meeting on ECRH and Gyrotrons, Karlsruhe 1993. Kernforschungszentrum Karlsruhe, 1993, 207-229.

74. *Erckmann, V.; Wagner, F.; Baldzuhn, J.; Brakel, R.; Burhenn, R.; Gasparino, U.; Grigull, P.; Hartfuß, H.-J.; Hofmann, J.V.; Jänicke, R.; Niedermeyer, H.; Ohlendorf, W.; Rudyj, A.; Weller, A.; Bomba, B.; Cattanei, G.; Dodhy, A.; Dorst, D.; Elsner, A.; Endler, M.; Geist, T.; Giannone, L.; Hacker, H.; Heinrich, O.; Herre, G.; Hildebrandt, D.; Karger, F.; Kick, M.; Lazaros, A.; Mahn, C.; McCormick, K.; Pech, P.; Sardei, F.; Sattler, S.; Schneider, F.; Schneider, U.; Siller, G.; Stroth, U.; Tutter, M.; Unger, E.; Wolff, H.; Würsching, E.; Zöpfel, S.; et al.:* The H-Mode of the W7-AS Stellarator. Phys. Rev. Lett. **70**, 2086-2089 (1993).

75. *Erckmann, V.; WVII-AS-Team; et al.:* Recent Results with 140 GHz ECRH at the W7-AS Stellarator. In: Proc. 8th Joint Workshop on Electron Cyclotron Emission and Electron Cyclotron Resonance Heating, Gut Ising 1992. MPI Plasmaphysik, Garching 1993, 481-495.

76. *Erckmann, V.; WVII-AS-Team; ECRH-Group; KfK-Gyrotron-Group; IAP-Gyrotron-Group; KIAE-ECRH-Group:* Overview on W7-AS Results with 140 GHz ECRH. In: Proc. 5th Joint Russian-German Meeting on ECRH and Gyrotrons, Karlsruhe 1993. Kernforschungszentrum Karlsruhe, 1993, 111-140.

77. Erckmann, V.; WVII-AS-Team; NI-Team(WVII-AS); et al.: Status and Prospects of 140 GHz ECRH. In: Proc. 9th Int. Workshop on Stellarators, Garching 1993. IAEA, Wien 1993, 602-610.

78. Ertl, K.; Vonbank, M.; Dose, V.: Spin-Resolved Soft X-Ray Appearance Potential Spectroscopy on Iron and Nickel. Solid State Commun. **88**, 557-561 (1993).

79. Estrada, T.; Sanchez*, J.; Hartfuß, H.-J.; Hirsch, M.; Geist, T.:* Density Fluctuation Measurements by Broadband Heterodyne Reflectometry on the W7-AS Stellarator. In: Proc. 20th EPS Conf. Control. Fusion and Plasma Phys., Lisbon 1993, Eds. J.A.C.Cabral, M.E.Manso, F.M.Serra, et al. ECA 17C. Europ. Phys. Soc., Geneva 1993, 369-372.

80. Estrada, T.; Sanchez*, J.; Hartfuß, H.-J.; Hirsch, M.; Geist, T.:* Fluctuation Studies in Wendelstein 7-AS by Reflectometry. In: Proc. 9th Int. Workshop on Stellarators, Garching 1993. IAEA, Wien 1993, 292-297.

81. Feist, J.-H.; Stäbler, A.; Dunne, J.-L.; Freudenberger, K.; Heinemann, B.; Riedl, R.; Sielanko, J.; Speth, E.: Performance of the Ion Removal System for the ASDEX-Upgrade Neutral Beam Injectors. In: Proc. 17th Symp. Fusion Technol., Rome 1992, Eds. C.Ferro, M.Gasparotto, H.Knöpfel. North-Holland Publ., Amsterdam 1993, 486-490.

82. Feist, J.-H.; Stäbler, A.; Ertl, W.; Heinemann, B.; Speth, E.: Large Scale Titanium Getter Pumps for the ASDEX-Upgrade Neutral Beam Injectors. In: Proc. 17th Symp. Fusion Technol., Rome 1992, Eds. C.Ferro, M.Gasparotto, H.Knöpfel. North-Holland Publ., Amsterdam 1993, 262-266.

83. Fiedler, S.: Lithium Beams for Fusion Plasma Diagnostics. In: Proc. Int. Workshop on Plasma Phys., Pichl 1993, Eds. M.F.Heyn, et al. dbv-Verl., Graz 1993, 163-167.

84. Field, A.; Büchl, K.; Fuchs, J.C.; Fußmann, G.; Herrmann, A.; Lieder, G.; Napiontek, B.; Radtke, R.; Wenzel, U.; Zohm, H.; ASDEX-Upgrade-Team: Spectroscopic Investigation of ELM Phenomena in the ASDEX-Upgrade Divertor with High Time Resolution. In: Proc. 20th EPS Conf. Control. Fusion and Plasma Phys., Lisbon 1993, Eds. J.A.C.Cabral, M.E.Manso, F.M.Serra, et al. ECA 17C. Europ. Phys. Soc., Geneva 1993, 575-578.

85. Fu, G.Y.; Cooper*, W.A.; Gruber*, R.; Schwenn, U.; Anderson*, D.V.:* Fully Three-Dimensional Ideal Magnetohydrodynamic Stability Analysis of Low-n Modes and Mercier Modes in Stellarators. Phys. Fluids B **4**, 1401-1411 (1993).

86. Gärtner, K.; Nitschke*, M.; Eckstein, W.:* Computer Simulation Studies of Low Energy B Implantation into Amorphous and Crystalline Silicon. Nucl. Instrum. Methods Phys. B **83**, 87-94 (1993).

87. Gasparino, U.: Summary of ECE and ECRH Theory-Sessions. In: Proc. 8th Joint Workshop on Electron Cyclotron Emission and Electron Cyclotron Resonance Heating, Gut Ising 1992. MPI Plasmaphysik, Garching 1993, 5-7.

88. Gasparino, U.: Theoretical Aspects of Electron Cyclotron Emission, Heating and Current Drive. In: Proc. 8th Joint Workshop on Electron Cyclotron Emission and Electron Cyclotron Resonance Heating, Gut Ising 1992. MPI Plasmaphysik, Garching 1993, 19-44.

89. Geiger, J.; WVII-AS-Team: W7-AS Equilibria with Toroidal Current. In: Proc. 9th Int. Workshop on Stellarators, Garching 1993. IAEA, Wien 1993, 222-226.

90. Geiger, J.; Kühner, G.; Maaßberg, H.; Ringler, H.; WVII-AS-Team: Effects of Plasma Currents and Pressure on the Magnetic Configuration of the W7-AS Stellarator. In: Proc. 20th EPS Conf. Control. Fusion and Plasma Phys., Lisbon 1993, Eds. J.A.C.Cabral, M.E.Manso, F.M.Serra, et al. ECA 17C. Europ. Phys. Soc., Geneva 1993, 353-356.

91. Geist, T.: 70 and 140 GHz Notch-Filters. In: Proc. 8th Joint Workshop on Electron Cyclotron Emission and Electron Cyclotron Resonance Heating, Gut Ising 1992. MPI Plasmaphysik, Garching 1993, 417-422.

92. Giannone, L.; Balbin, R.; Hidalgo*, C.; Niedermeyer, H.:* Spatial Correlation of Density, Potential and Temperature Fluctuations in Wendelstein 7-AS. In: 20th EPS Conf. on Control. Fusion and Plasma Phys., Lisbon 1993, Eds. J.A.C.Cabral, M.E.Manso, F.M.Serra, et al. ECA 17C. Europ. Phys. Soc., Geneva 1993, 735-738.

93. Giannone, L.; Balbin, R.; Niedermeyer, H.; Endler, M.; Hidalgo*, C.; Theimer, G.; Rudyj, A.; Verplancke, P.; WVII-AS-Team:* Temperature, Density and Potential Fluctuations by a Swept Langmuir Probe in Wendelstein 7-AS. In: Proc. 9th Int. Workshop on Stellarators, Garching 1993. IAEA, Wien 1993, 286-291.

94. Giannone, L.; Balbin, R.; Niedermeyer, H.; Endler, M.; Hidalgo*, C.; Theimer, G.; Rudyj, A.; Verplancke, P.; WVII-AS-Team:* Temperature, Density and Potential Fluctuations by a Swept Langmuir Probe in Wendelstein 7-AS. In: Proc. 20th EPS Conf. Control. Fusion and Plasma Phys., Lisbon 1993, Eds. J.A.C.Cabral, M.E.Manso, F.M.Serra, et al. ECA 17C. Europ. Phys. Soc., Geneva 1993, 735-738.

95. Gieler, M.; Aumayr*, F.; Schweinzer, J.; et al.:* Electron Capture by Doubly Charged Ions from Laser-Excited Alkali Atoms I. He^{2+} - Na*(3p) Collisions. J. Phys., B (London). **26**, 2137-2151 (1993).

96. Gieler, M.; Aumayr*, F.; Weber*, M.; Schweinzer, J.; et al.:* Electron Capture by Doubly Charged Ions from Laser-Excited Alkali Atoms II. He^{2+} - Na*(3p) Collisions. J. Phys., B (London). **26**, 2153-2164 (1993).

97. Goedbloed, J.P.; Huysmans*, G.T.A.; Poedts*, S.; Schwarz, E.; et al.:* Computation of Resistive MHD Modes in Thermonuclear and Astrophysical Plasmas. In: Proc. IAEA Techn. Comm. Meeting on Advances in Simulation and Modelling of Thermonuclear Plasmas, Montreal 1992. IAEA, Wien 1993, 316-337.

98. Graß, M.; Braun*, J.; Borstel*, G.; Fauster, Th.; Dose, V.; et al.:* Unoccupied Electronic States and Surface Barriers at Cu Surfaces. J. Phys. Condens. Matter **5**, 599-614 (1993).

99. Grieger, G.: Comparison of Recent Fusion Reactor Studies Based on Toroidal Magnetic Confinement. Fusion Eng. Des. **22**, 99-106 (1993).

100. Grieger, G.: Comparison of Recent Fusion Reactor Studies Based on Toroidal Magnetic Confinement. In: Proc. 17th Symp. Fusion Technol., Rome 1992, Eds. C.Ferro, M.Gasparotto, H.Knöpfel. North-Holland Publ., Amsterdam 1993, 99-106.

101. Grieger, G.: Fusionsreaktor nach dem Stellaratorkonzept. In: Proc. Jahrestagung Kerntechnik, Köln 1993. Dt. Atomforum e.V., Bonn 1993, 5-11.

102. Grieger, G.: A Stellarator Reactor of the Wendelstein 7-Line. In: Proc. Int. Workshop on Steady State Tokamaks, Princeton 1993. PPPL, Princeton 1993, Vol. 1, ohne Pag.

103. Grieger, G., Milch, I.: Das Fusionsexperiment Wendelstein 7-X. Phys. Bl. **11**, 1001-1005 (1993).

104. Grigull, P.; Herre, G.; Kißlinger, J.; Sardei, F.; Hildebrandt, D.; Pech, P.; Wolff, H.; WVII-AS-Team; ECRH-Group; NI-Team(WVII-AS): Boundary Layer Studies on W7-AS. In: Proc. 9th Int. Workshop on Stellarators, Garching 1993. IAEA, Wien 1993, 526-529.

105. Grigull, P.; Herre, G.; Kißlinger, J.; Sardei, F.; Hildebrandt, D.; Pech, P.; Wolff, H.; WVII-AS-Team; NI-Team(WVII-AS); et al.: Edge Plasma Profile and Particle Transport Study on the Wendelstein 7-AS Stellarator. In: Proc. 20th EPS Conf. Control. Fusion and Plasma Phys., Lisbon 1993, Eds. J.A.C.Cabral, M.E.Manso, F.M.Serra, et al.ECA 17C. Europ. Phys. Soc., Geneva 1993, 739-742.

106. Gruber, O.; ASDEX-Upgrade-Team: Overview on Vertical Displacement Investigations on ASDEX Upgrade. In: Proc. Workshop on Electromagnetic Forces and Related Effects on Blankets and Other Structures Surrounding the Plasma Torus, Karlsruhe 1992. EUR 14820 EN. CEC, Brussels 1993, 30-43.

107. Gruber, O.; Gernhardt, J.; McCarthy, P.; Lackner, K.; Seidel, U.; Schneider, W.; Woyke, W.; Zehrfeld, H.P.: Position and Shape Control on ASDEX-Upgrade. In: Proc. 17th Symp. Fusion Technol., Rome 1992, Eds. C.Ferro, M.Gasparotto, H.Knöpfel. North-Holland Publ., Amsterdam 1993, 1042-1046.

108. Gruber, O.; Lackner, K.; Pautasso, G.; Seidel, U.; Streibl, B.: Vertical Displacement Events and Halo Currents. Plasma Phys. Control. Fusion **35**, Suppl.B, 191-204 (1993).

109. Grudeva-Zotova, S.: Deposition and Characterization of Anti-Multipactoring Coatings. Final Report CEC COST Project No. ERB-CIPA-CT-92-2040, 1993, 15 S.

110. Hansen, J.P.; Nielsen*, S.E.; Schweinzer, J.:* Electron Capture Cross Sections from Initially Aligned p-state Atoms. J. Phys., B (London). **26**, L471-L475 (1993).

111. Harmeyer, E.; Kißlinger, J.; Rau, F.; Wobig, H.: The Modular Coil System of a Helias Reactor. In: Proc. 9th Int. Work-shop on Stellarators, Garching 1993. IAEA, Wien 1993, 471-476.

112. Härtel, T.; Strüber*, U.; Küppers, J.:* Growth and Properties of Thin Ag Films on Pt(111) Surfaces. Thin Solid Films **229**, 163-170 (1993).

113. Hartfuß, H.-J.; Erckmann, V.; Gasparino, U.; Giannone, L.; Maaßberg, H.; Tutter, M.: Heat Wave Experiments on the W7-AS Stellarator. In: Proc. 8th Joint Workshop on Electron Cyclotron Emission and Electron Cyclotron Resonance Heating, Gut Ising 1992. MPI Plasmaphysik, Garching 1993, 211-221.

114. Hartfuß, H.-J.; Erckmann, V.; Gasparino, U.; Giannone, L.; Maaßberg, H.; WVII-AS-Team: Heat Wave Studies on W7-AS. In: Proc. 9th Int. Workshop on Stellarators, Garching 1993. IAEA, Wien 1993, 340-344.

115. Hayashi, T.; Sato*, T.; Lotz, W.; Merkel, P.; Nührenberg, J.; Schwenn, U.; Strumberger, E.:* 3-D MHD Study of Helias and Heliotron. In: Proc. 14th Conf. on Plasma Phys. and Control. Nucl. Fusion Res., 2, Würzburg 1992. IAEA, Wien 1993, 29-34.

116. Heinemann, B.; Sombach., B.; Dunne, J.-L.; Ertl, W.; Feist, J.-H.; Freudenberger, K.; Riedl, R.; Speth, E.; Stäbler, A.; Vollmer, O.: Manufacturing and Assembly of the Neutral Beam Injector for ASDEX-Upgrade. In: Proc. 17th Symp. Fusion Technol., Rome, 1992, Eds. C. Ferro, M. Gasparetto, H. Knöpfel. Elsevier Publ., Amsterdam 1993, 524-528.

117. Herre, G.; Grigull, P.; Sardei, F.; Kißlinger, J.; WVII-AS-Team: Connection Length Studies and SOL Parameters for the Limiter and Separatrix Dominated Configurations in W7-AS. In: Proc. 9th Int. Workshop on Stellarators, Garching 1993. IAEA, Wien 1993, 375-378.

118. Herrmann, A.; Junker, W.; Günther, K.; Kaufmann, M.; Neuhauser, J.; Richter, T.; Schneider, R.; ASDEX-Upgrade-Team: Asymmetric Energy Flux to the ASDEX-Upgrade Divertor Plates Determined by Thermography and Calorimetry. In: Proc. 20th EPS Conf. Control. Fusion and Plasma Phys., Lisbon 1993, Eds. J.A.C.Cabral, M.E.Manso, F.M.Serra, et al. ECA 17C. Europ. Phys. Soc., Geneva 1993, 567-570.

119. Herrnegger, F.; Dommaschk, W.: Stochasticity of Magnetic Field Lines in Analytical and Coil Fields. In: Current Research on Fusion, Laboratory and Astrophysical Plasmas, Eds. S.Kuhn, K.Schöpf, R.Schrittwieser. World Scientific Publ., Singapore 1993, 69-79.

120. Hildebrandt, D.; Burhenn, R.; Brakel, R.; Grigull, P.; Pech, P.; Rau, F.; Roth, J.; Wolff, H.; WVII-AS-Team: Studies on Impurity Production and Transport in W7-AS. In: Proc. 9th Int. Workshop on Stellarators, Garching 1993. IAEA, Wien 1993, 379-384.

121. Hoffmann, C.; Hofmeister, F.; Noterdaeme, J.-M.; Brambilla, M.; Fuchs, J.C.; Gehre, O.; ASDEX-Upgrade-Team; ICRH-Team: Comparison of Theoretical and Calculated ICRH Antenna Resistance on ASDEX Upgrade. In: Proc. 20th EPS Conf. Control. Fusion and Plasma Phys., Lisbon 1993, Eds. J.A.C.Cabral, M.E.Manso, F.M.Serra, et al. ECA 17C. Europ. Phys. Soc., Geneva 1993, 953-956.

122. Hofmann, J.V., Milch, I., Wagner, F.: Stand der Fusionsforschung. Vakuum Praxis **4**, 237-248 (1993).

123. Hofmann, J.V.; WVII-AS-Team; ECRH-Group; NI-Group: Impurity Fluxes and Profiles in Wendelstein 7-AS. In: Proc. 20th EPS Conf. Control. Fusion and Plasma Phys., Lisbon 1993, Eds. J.A.C.Cabral, M.E.Manso, F.M.Serra, et al. ECA 17C. Europ. Phys. Soc., Geneva 1993, 1203-1206.

124. Hofmeister, F.; Braun, F.; Grimm, R.; Wesner, F.; ICRH-Team: Acquisition of Technical Data and Matching Procedures for the ICRH System on ASDEX Upgrade. In: Proc. 17th Symp. Fusion Technol., Rome 1992, Eds. C.Ferro, M.Gasparotto, H.Knöpfel. North-Holland Publ., Amsterdam 1993, 1047-1051.

125. Hou, M.; Eckstein, W.; Robinson*, M.T.:* Computer Simulation of Temporal Aspects of the Copper Single Crystal Sputtering. Nucl. Instrum. Methods Phys. Res. B **82**, 234-241 (1993).

126. Hughes, I.G.; Behrisch, R.; Martinelli, A.P.:* Depth Profiling of Deuterium Using Nuclear Reaction Analysis. Nucl. Instrum. Methods Phys. Res. B **79**, 487-49 (1993).

127. Hytry, R.; Möller, W.; Wilhelm, R.; Keudell, A. von: Moving-Coil Waveguide Discharge for Inner Coating of Metal Tubes. J. Vac. Sci. Technol. A **11**, 2508-2517 (1993).

128. Jäckel, H.J.; Chankin*, A.; Falter*, H.; Janeschitz, G.; Lingertat, J.:* Accountability of the Divertor Power in JET. In: Proc. 20th EPS Conf. Control. Fusion and Plasma Phys., Lisbon 1993, Eds. J.A.C.Cabral, M.E.Manso, F.M.Serra, et al. ECA 17C. Europ. Phys. Soc., Geneva 1993, 287-290.

129. Jacob, W.; Möller, W.: On the Structure of Thin Hydrocarbon Films. Appl. Phys. Letters **63**, 1771-1773 (1993).

130. Jacob, W.; Reinke, P.; Möller, W.: Ion Energy Distributions from Electron Cyclotron Resonance Methane Plasmas. Diamonds and Related Materials **2**, 378-382 (1993).

131. Jaksic, N.; Simon-Weidner, J.; Harmeyer, E.: On Mechanical Boundary Conditions in Large Helias Coil Systems and the Influence of Sliding on Stresses. In: Proc. 17th Symp. Fusion Technol., Rome 1992, Eds. C.Ferro, M.Gasparotto, H.Knöpfel. North-Holland Publ., Amsterdam 1993, 877-881.

132. Janeschitz, G.; Lesourd, M.; Lingertat, J.; Vlases, G.:* The Importance of the Ion Grad Drift Direction for the Divertor Plasma at JET. In: Proc. 20th EPS Conf. Control. Fusion and Plasma Phys., Lisbon 1993, Eds. J.A.C.Cabral, M.E.Manso, F.M.Serra, et al. ECA 17C. Europ. Phys. Soc., Geneva 1993, 559-562.

133. Janev, R.K.; Smith*, J.J.; Schweinzer, J.; et al.:* Collision Database for Lithium Beam Interaction with Fusion Plasmas. IAEA, Wien 1993. 87 S.

134. Jänicke, R.; Ascasibar, E.; Grigull, P.; Lakicevic, I.; Zippe, M.; Hailer*, H.; Schwörer*, K.:* Detailed Investigation of the Vacuum Magnetic Surfaces on the W7-AS Stellarator. Nucl. Fusion **33**, 687-704 (1993).

135. Jänicke, R.; Weller, A.; Hartfuß, H.-J.; Lazaros, A.; Sattler, S.; Zohm, H.; WVII-AS-Team; NI-Team(WVII-AS); et al.: Fluctuations and Transport in the W7-AS Stellarator. In: Proc. 14th Conf. on Plasma Phys. and Control. Nucl. Fusion Res., 2, Würzburg 1992. IAEA, Wien 1993, 483-491.

136. Jänicke, R.; WVII-AS-Team; ECRH-Group; NI-Group: Overview of W7-AS Results. In: Proc. 9th Int. Workshop on Stellarators, Garching 1993. IAEA, Wien 1993, 18-23.

137. Jannussis, A.: New Deformed Heisenberg Oscillator. J. Phys. (London) A **26**, L233-L237 (1993).

138. Kaiser, R.; Lortz, D.: On the Existence of Plasma Corners. ZAMM **73**, 165-171 (1993).

139. Kaiser, R.; Tasso, H.: Three-Dimensional Toroidal Magneto-hydrodynamics Equilibria with 'Canal' Surface Currents. Phys. Fluids B **5**, 1030-1031 (1993).

140. Kaiser, R.: Resistive Ballooning in W7-AS and W7-X. Nucl. Fusion **33**, 1281-1291 (1993).

141. Kallenbach, A.; Fußmann, G.; Kiemer, K.; Mayer, H.-M.; Pitcher, C.S.; ASDEX-Upgrade-Team:* The Influence of Spatially and Temporally Varying Edge Conditions on the Interpretation of Spectroscopic Particle Flux Measurements. In: Proc. 20th EPS Conf. Control. Fusion and Plasma Phys., Lisbon 1993, Eds. J.A.C.Cabral, M.E.Manso, F.M.Serra, et al. ECA 17C. Europ. Phys. Soc., Geneva 1993, 571-574.

142. Kallenbach, A.; Mayer, H.-M.: Characteristics of a Freely Programmable ICCD Detector for Multichord Particle Influx Measurements on the ASDEX Upgrade Tokamak. Rev. Sci. Instrum. **64**, 1257-1262 (1993).

143. Kardaun, O.; H-Mode-Database-Working-Group: ITER: Analysis of the H-Mode Confinement and Threshold Databases. In: Proc. 14th Conf. on Plasma Phys. and Control. Nucl. Fusion Res., 3, Würzburg 1992. IAEA, Wien 1993, 251-270.

144. Karulin, N.; Wobig, H.: Alpha Particle Confinement in a Helias Reactor under the Influence of GAE's. In: Proc. 9th Int. Workshop on Stellarators, Garching 1993. IAEA, Wien 1993, 425-429.

145. Kastelewicz, H.; Schneider, R.; Neuhauser, J.; Reiter, D.; Braams*, B.; Wenzel, U.; Büchl, K.; Laux, M.; Mertens, V.:* Numerical Marfe Simulations at ASDEX and ASDEX-Upgrade. In: Proc. 20th EPS Conf. Control. Fusion and Plasma Phys., Lisbon 1993, Eds. J.A.C.Cabral, M.E.Manso, F.M.Serra, et al. ECA 17C. Europ. Phys. Soc., Geneva 1993, 807-810.

146. Kaufmann, M.; Bosch, H.-S.; Field, A.; Fußmann, G.; Gruber, O.; Herrmann, A.; Junker, W.; Kallenbach, A.; Köppendörfer, W.; Krieger, K.; Lackner, K.; Laux, M.; Mertens, V.; Napiontek, B.; Naujoks, D.; Neuhauser, J.; Poschenrieder, W.; Roth, J.; Ryter, F.; Zohm, H.; Albrecht, M.; Alexander, M.; Asmussen, K.; Becker, G.; Behler, K.; Bergmann, A.; Bessenrodt-Weberpals, M.; Brambilla, M.; Braun, F.; Büchl, K.; Carlson, A.; Chodura, R.; De Barbieri, O.; De Blank, H.J.; De Pena Hempel, S.; Dorn, C.; Drube, R.; Eberhagen, A.; Engelhardt, W.; Engstler, J.; Fahrbach, H.-U.; Feist, J.-H.; Feneberg, W.; Fuchs, J.C.; Garcia-Rosales, C.; Gehre, O.; Gernhardt, J.; Götsch, S.; Gruber, J.; Günther, K.; Haas, G.; Heinemann, B.; Herppich, G.; Herrmann, W.; Hofmeister, F.; Hohenöcker, H.; Jacobi, D.; Jüttner, B.; Kardaun, O.; Kass, T.; Kiemer, K.; Kollotzek, H.; Kornherr, M.; Kurzan, B.; Lang, P.; Lang, R.; Lengyel, L.; Leuterer, F.; Lieder, G.; Mast, K.-F.; Mayer, H.-M.; Meisel, D.; Merkel, R.; Münch, M.; Murmann, H.; Neu, G.; Neu, R.; Noterdaeme, J.-M.; Pautasso, G.; Raupp, G.; Richter, H.; Richter, T.; Röhr, H.; Salmon, N.; Salzmann, H.; Sandmann, W.; Schilling, H.-B.; Schittenhelm, M.; Schneider, H.; Schneider, R.; Schneider, W.; Schönmann, K.; Schramm, G.; Schweinzer, J.; Scott, B.; Seidel, U.; Söldner, F.X.; Speth, E.; Stäbler, A.; Steuer, K.-H.; Streibl, B.; Suttrop, W.; Treutterer, W.; Troppmann, M.; Ulrich, M.; Venus, G.; Vernickel, H.; Vollmer, O.; Wedler, H.; Weinlich, M.: Edge Physics and H-Mode Studies in ASDEX Upgrade. Plasma Phys. Control. Fusion **35**, Suppl.B, 205-214 (1993).

147. Keudell, A. von; Möller, W.; Hytry, R.: Deposition of Dense C:H Films at Elevated Substrate Temperature. Diamond and Related Materials **2**, 251-254 (1993).

148. Keudell, A. von; Möller, W.; Hytry, R.: Deposition of Dense Hydrocarbon Films from a Nonbiased Microwave Plasma. Appl. Phys. Lett. **62**, 937-939 (1993).

149. Kick, M.; Baldzuhn, J.; Ballico, S.D.; Bomba, B.; Brakel, R.; Büchse, R.; Burhenn, R.; Cattanei, G.; Dodhy, A.; Dorst, D.; Elsner, A.; Endler, M.; Engelhardt, K.; Erckmann, V.; Gasparino, U.; Geiger, J.; Geissler, S.; Geist, T.; Giannone, L.; Grigull, P.; Hacker, H.; Hartfuß, H.-J.; Heinrich, O.; Herre, G.; Hofmann, J.V.; Jänicke, R.; Karger, F.; Konrad, C.; Kroiss, H.; Kühner, G.; Lazaros, A.; Maaßberg, H.; Mahn, C.; Mandl, W.; McCormick, K.; Niedermeyer, H.; Ohlendorf, W.; Renner, H.; Ringler, H.; Rudyj, A.; Ruhs, N.; Saffert, J.; Sardei, F.; Sattler, S.; Schneider, F.; Schneider, U.; Siller, G.; Stroth, U.; Theimer, G.; Tutter, M.; Unger, E.; Verbeek, H.; Wagner, F.; Weller, A.; Würsching, E.; Wurdack, S.; Zimmermann, D.; Zippe, M.; Zöpfel, S.:* Experimental Status of the "Advanced Stellarator" W7-AS. In: Proc. Jahrestagung Kerntechnik, Köln 1993. Dt.Atomforum e.V., Bonn 1993, 25-28.

150. Kick, M.; Erckmann, V.; Junker, J.; Kislyakov, A.; Kühner, G.; Maaßberg, H.; Penningsfeld, F.-P.; Sardei, F.; WVII-AS-Team; NI-Team(WVII-AS); et al.:* Ion Energy Confinement at the W7-AS Stellarator. In: Proc. 20th EPS Conf. Control. Fusion and Plasma Phys., Lisbon 1993, Eds. J.A.C.Cabral, M.E.Manso, F.M.Serra, et al. ECA 17C. Europ. Phys. Soc., Geneva 1993, 357-360.

151. Kick, M.; Erckmann, V.; Junker, J.; Kislyakov, A.; Kühner, G.; Maaßberg, H.; Penningsfeld, F.-P.; Sardei, F.; WVII-AS-Team; NI-Team(WVII-AS); ECRH-Group; Gyrotron-Group:* Ion Energy Confinement at the W7-AS Stellarator. In: Proc. 9th Int. Workshop on Stellarators, Garching 1993. IAEA, Wien 1993, 304-308.

152. Knözinger, H.; Taglauer, E.:* Toward Supported Oxide Catalysts via Solid-Solid Wetting. Catalysis **10**, 1-40 (1993).

153. Koch, A.: Diagnostik von Plasmastrahlen mittels Laserstreuverfahren. VDI Reihe 8, Nr. 356, VDI Verl., Düsseldorf 1993, 121 S.

154. Koch, A.: In situ - Charakterisierung von plasmaunterstützten Beschichtungsprozessen. VDI Reihe 8, Nr. 357, VDI-Verl., Düsseldorf 1993., 155 S.

155. Konrad, C.; Bartels, H.-W.; Andritsos, F.:* Passive Removal of Afterheat in the Next Step Fusion Device. In: Proc. 17th Symp. Fusion Technol., Rome 1992, Eds. C.Ferro, M.Gasparotto, H.Knöpfel. North-Holland Publ., Amsterdam 1993, 1734-1738.

156. Köppendörfer, W.; Andelfinger, C.; Ballico, M.; Becker, W.; Behler, K.; Bessenrodt-Weberpals, M.; Bosch, H.-S.; Braun, F.; Büchl, K.; Carlson, A.; Cha, S.; Chu, C.-C.; Dorn, C.; Drube, R.; Eberhagen, A.; Fahrbach, H.-U.; Fieg, D.; Field, A.; Fuchs, J.C.; Fußmann, G.; Gehre, O.; Gernhardt, J.; Götsch, S.; Gruber, J.; Gruber, O.; Hass, G.; Herrmann, W.; Hofmeister, F.; Jacobi, D.; Jenichen, F.; Junker, W.; Jüttner, B.; Kallenbach, A.; Kardaun, O.; Kaufmann, M.; Kornherr, M.; Krause, H.; Kurzan, B.; Lackner, K.; Lang, R.; Laux, M.; Lieder, G.; Mast, K.-F.; Mayer, H.-M.; McCarthy, P.; Meisel, D.; Merkel, R.; Mertens, V.; Murmann, H.; Neuhauser, J.; Noterdaeme, J.-M.; Oswald, J.; Poschenrieder, W.; Puri, S.; Raupp, G.; Richter, H.; Richter, T.; Röhr, H.; Roth, J.; Ryter, F.; Salmon, N.; Salzmann, H.; Schittenhelm, M.; Schneider, R.; Schneider, W.; Schramm, G.; Schumacher, U.; Schweinzer, J..; Seidel, U.; Söldner, F.X.; Steuer, K.-H.; Streibl, B.; Troppmann, M.; Ulrich, M.; Venus, G.; Vernickel, H.; Wedler, H.; Wenzel, U.; Wesner, F.; Wieczorek, A.; Woyke, W.; Zasche, D.; Zehrfeld, H.P.; Zohm, H.: Results of the First Operational Phase of ASDEX Upgrade. In: Proc. 14th Int. Conf. on Plasma Phys. and Control. Nucl. Fusion Res., 1, Würzburg, 1992. IAEA, Wien 1993, 127-140.

157. Köppendörfer, W.; Milch, I.: ASDEX Upgrade - Aufbau eines Kernfusionsexperimentes. Film C 1789. Publ. Wiss. Film. Techn. Wiss./Naturw. **11**, 113-128 (1993).

158. Krasheninnikov, S.I.:* On Nonlocal Electron Heat Conduction. Phys. Fluids B **5**, 74-76 (1993).

159. Kratochwil, Th.; Wittmann*, M.; Küppers, J.:* Adsorption of Ethanol on Ni(100) Surfaces. J. Electr. Spec. and Rel. Phenom. **64/65**, 609-617 (1993).

160. Kraus, W.; Feist, J.-H.; Lochter, M.; Speth, E.:* A High Power RF Plasma Generator for Neutral Beam Injection. In: Proc. 17th Symp. Fusion Technol., Rome 1992, Eds. C.Ferro, M.Gasparotto, H.Knöpfel. North-Holland Publ., Amsterdam 1993, 549-553.

161. Krieger, K.; Roth, J.; Dose, V.; Hofmann, J.V.: CH_4 and CO Fuelling Studies in the ASDEX Tokamak, Nucl. Fusion **33**, 1591-1598 (1993).

162. Kutsch, H.-J.; Wesner, F.; Noterdaeme, J.-M.; et al.: Insulating Al_2O_3 Layers in ICRH Antennas for ASDEX Upgrade. In: Proc. 17th Symp. Fusion Technol., Rome 1992, Eds. C.Ferro, M.Gasparotto, H.Knöpfel. North-Holland Publ., Amsterdam 1993, 569-573.

163. Lackner, K.; Schneider, R.: The Role of Edge Physics and Confinement Issues in the Fusion Reactor. Fusion Eng. Des. **22**, 107-116 (1993).

164. Lackner, K.; Schneider, R.: The Role of Edge Physics and Confinement Issues in the Fusion Reactor. In: Proc. 17th Symp. Fusion Technol., Rome 1992, Eds. C.Ferro, M.Gasparotto, H.Knöpfel. North-Holland Publ., Amsterdam 1993, 107-116.

165. Lang, P.; Mast, K.-F.; et al.: Photoresponse of a Miniaturized Metal Film Bolometer to Ultrashort Mid- and Far-Infrared Laser Pulses. Infrared Phys. **34**, 481-486 (1993).

166. Lang, P.; Mast, K.-F.; et al.: Photoresponse of a Miniaturized Metal Film Bolometer to Ultrashort Mid- and Far-Infrared Laser Pulses. In: Conf. Digest 8th Int. Conf. on IR and mm Waves, Essex 1993, Eds. J.R.Birch, T.J.Parker. SPIE Proc. 2104. SPIE, Bellingham 1993, 116-117.

167. Lange, K.; Jacob, W.; Möller, W.: Ion and Neutral Fluxes onto the Substrate from a DC Discharge in Methane. In: Proc. ISPC-11, Loughborough 1993, Ed. J.Harry. Int. Union Pure and Appl. Chem., Loughborough 1993, 1266-1271.

168. Laurence, P.; Lortz, D.; Spies, G.O.; Soria*, F.:* Some Monotonicity and Convexity Results for Integral Means. Z. Naturforsch. A **48**, 841-843 (1993).

169. Lauterbach, J.; Wittmann*, M.; Küppers, J.:* A FTIRAS Study of CO Adsorbed at Ni(100) Surfaces. Ber. Bunsenges. Phys. Chem. **97**, 326-328 (1993).

170. Lazaros, A.: The Fast Ion Resonant Effect in Low Shear, NBI Heated Plasmas. Nucl. Fusion **33**, 1515-1521 (1993).

171. Lederer, H.; Hertweck, F.: Erfahrungen bei der Portierung realer Programme. In: Parallelrechner für die Grundlagenforschung, Ed. H.Weberpals. GWDG-Bericht Nr. 36. GWDG, Göttingen 1993, 3-10.

172. Lederer, H.: Ein Jahr nCUBE Parallelrechner am IPP. In: DV-Notizen Nr. 29, Eds. F.Hertweck, F.Zite-Ferency, S.Maurmann. MPG, München 1993, 19-30.

173. Lengyel, L.: Pellet Ablation and Wall Erosion: Physics and Modelling. In: Proc. Workshop on the Use of Atomic Beams in Plasma Experiments, Budapest 1993. Hungarian Acad. of Sciences, Budapest 1993, 75-82.

174. Lengyel, L.; Spathis, P.: A Time-Dependent, Self-Consistent, Slab-Symmetric Ablation Model with Allowance for Transverse Expansion and Magnetic Confinement Effects. In: Proc. 20th EPS Conf. Control. Fusion and Plasma Phys., Lisbon 1993, Eds. J.A.C.Cabral, M.E.Manso, F.M.Serra, et al. ECA 17C. Europ. Phys. Soc., Geneva 1993, 1447-1450.

175. Lieder, G.; Napiontek, B.; Radtke, R.; Field, A.; Fußmann, G.; Kallenbach, A.; Kiemer, K.; Mayer, H.-M.; ASDEX-Upgrade-Team: Interpretation of Low Ionized Impurity Distributions in the ASDEX

Upgrade Divertor. In: Proc. 20th EPS Conf. Control. Fusion and Plasma Phys., Lisbon 1993, Eds. J.A.C.Cabral, M.E.Manso, F.M.Serra, et al. ECA 17C. Europ. Phys. Soc., Geneva 1993, 579-582.

176. Lifshitz, Y.; Roux*, C.D.; Boyd*, K.; Eckstein, W.; Rabalais*, J.W.:* Analysis of Carbon Film Growth from Low Energy Ion Beams Using Dynamic Trajectory Simulations and Auger Electron Spectroscopy. Nucl. Instrum. Methods Phys. Res. B **83**, 351-356 (1993).

177. Linden, W. von der; Donath, M.; Dose, V.: Unbiased Access to Exchange Splitting of Magnetic Bands Using the Maximum Entropy Method. Phys. Rev. Lett. **71**, 899-902 (1993).

178. Lortz, D.; Haimerl, W.:* Axisymmetric Magnetohydrodynamic Equilibria without a Wall. Z. Naturforsch. A **48**, 1131-1150 (1993).

179. Lortz, D.: Hydrodynamik. B.I. Hochschultaschenbuch 696. B.I. Wissenschaftsverl., Mannheim 1993. 135 S.

180. Lortz, D.: On Rayleigh's Stability Criterion for Couette Flow. Z. Naturforsch. A **48**, 703-704 (1993)

181. Lossev, V.; Küppers, J.: Adsorption of Hydrogen on Be(0001) Surfaces. Surf. Sci. **284**, 175-185 (1993).

182. Lotz, W.: Neoclassical Transport of Impurities in Stellarators. In: Proc. 9th Int. Workshop on Stellarators, Garching 1993. IAEA, Wien 1993, 577-582.

183. Maaßberg, H.; Brakel, R.; Burhenn, R.; Gasparino, U.; Grigull, P.; Kick, M.; Kühner, G.; Sardei, F.; Ringler, H.; Stroth, U.; Weller, A.: Transport in Stellarators. Plasma Phys. Control. Fusion **35**, Suppl.B, 319-332 (1993).

184. Maaßberg, H.; Burhenn, R.; Dyabilin, K.S.; Gasparino, U.; Kühner, G.; Ringler, H.:* Experimental and Neoclassical Electron Heat Transport in the LMFP Regime for the Stellarators W7-A, L-2, and W7-AS. Phys. Fluids B **5**, 3627-3640 (1993).

185. Maaßberg, H.; Dyabilin, K.S.:* Simulation of the Potential Rotation Shear Layer for Stellarators. In: Proc. 20th EPS Conf. Control. Fusion and Plasma Phys., Lisbon 1993, Eds. J.A.C.Cabral, M.E.Manso, F.M.Serra, et al. ECA 17C. Europ. Phys. Soc., Geneva 1993, 409-412.

186. Maaßberg, H.; Lotz, W.; Nührenberg, J.: Neoclassical Bootstrap Current and Transport in Optimized Stellarator Configurations. Phys. Fluids B **5**, 3728-3736 (1993).

187. Mandl, W.; Wade, M.R.; Burrell, K.H.: Absolute Measurement of Ion Density Profiles as a Function of Time with Charge Exchange Spectroscopy at DIII-D. In: Proc. 35th APS Div. of Plasma Phys. Annual Meeting, St. Louis 1993. APS, New York 1993, 7T36.

188. McCormick, K.; Fiedler, S.; Kyriakakis, G.; Neuhauser, J.; Schneider, R.; et al.:* Particle and Energy Transport in the ASDEX Scrape-Off Layer. In: Proc. 20th EPS Conf. Control. Fusion and Plasma Phys., Lisbon 1993, Eds. J.A.C.Cabral, M.E.Manso, F.M.Serra, et al. ECA 17C. Europ. Phys. Soc., Geneva 1993, 587-590.

189. Memmel, N.: Spectroscopy of Metal Surface States by Inverse Photoemission. Prog. Surf. Sci. **42**, 75-88 (1993).

190. Memmel, N.; Rangelov, G.; Bertel, E.: Influence of the Substrate on the Band Structure of Alkali Metal Monolayers. Surf. Sci. **285**, 109-116 (1993).

191. Merkel, P.; Johnson, J.L.; Monticello*, D.A.; Reiman*, A.H.:* Equilibrium Studies with the PIES Code. In: Proc. 9th Int. Workshop on Stellarators, Garching 1993. IAEA, Wien 1993, 132-137.

192. Mertens, V.; Büchl, K.; Junker, W.; Mast, K.-F.; Schittenhelm, M.; Bessenrodt-Weberpals, M.; Field, A.; Fuchs, J.C.; Gehre, O.; Gruber, O.; Herrmann, A.; Haas, G.; Kallenbach, A.; Kastelewicz, H.; Kaufmann, M.; Köppendörfer, W.; Laux, M.; Lieder, G.; Neuhauser, J.; Ryter, F.; Salzmann, H.; Sandmann, W.; Steuer, K.-H.; Stäbler, A.; Zohm, H.; ASDEX-Upgrade-Team: Experimental Investigation and Interpretation of Marfes and Density Limit in ASDEX Upgrade. In: Proc. 20th EPS Conf. Control. Fusion and Plasma Phys., Lisbon 1993, Eds. J.A.C.Cabral, M.E.Manso, F.M.Serra, et al. ECA 17C. Europ. Phys. Soc., Geneva 1993, 267-270.

193. Milch, I.: Erfolg in der Fusionsforschung. Techn. Rundschau **85**, 20-21 (1993).

194. Milch, I.: Feuer und Eis. Erste Pellet-Experimente an ASDEX Upgrade. Schweizer Maschinenmarkt **41,** 76-77 (1993).

195. Milch, I.: Heißer als die Sonne. Techn. Rundschau **85**, 38-39. (1993).

196. Milch, I.: Wendelstein 7-AS. Ein neuer Käfig für das Sonnenfeuer. In: AGF-Jahresheft 1993, AGF. Petersberg Verl., Bonn 1993, 8-10.

197. Möller, W.: Modelling and Computer Simulation of Ion-Beam and Plasma-Assisted Film Growth. Thin Solid Films **228**, 319-325 (1993).

198. Möller, W.: Plasma and Surface Modeling of the Deposition of Hydrogenated Carbon Films from Low-Pressure Methane Plasmas. Appl. Phys. A **56**, 527-546 (1993).

199. Möller, W.; Keudell, A. von; Engelhard, M.: Simultaneous Plasma and Surface Modeling of Hydrogenated Carbon Films from Methane. In: Proc. ISPC-11, Loughborough 1993, Ed. J.Harry. Int. Union Pure and Appl. Chem., Loughborough 1993, 1662-1667.

200. Naujoks, D.; Behrisch, R.; Coad, J.P.; De Kock*, L.:* Material Transport by Erosion and Redeposition on Surface Probes in the Scrape-off Layer of JET. Nucl. Fusion **33**, 581-590 (1993).

201. Naujoks, D.; Behrisch, R.; Philipps, V.; Schweer*, B.:* Erosion and Redeposition on Carbon Probes in TEXTOR. In: Proc. 20th EPS Conf. Control. Fusion and Plasma Phys., Lisbon 1993, Eds. J.A.C.Cabral, M.E.Manso, F.M.Serra, et al. ECA 17C. Europ. Phys. Soc., Geneva 1993, 651-654.

202. Neumann, G.; Bänziger, U.; Kammeyer, M.; Lange, M.: Plasma-Density Measurements by Microwave Interferometry and Langmuir Probes in an RF Discharge. Rev. Sci. Instrum. **64**, 19-25 (1993).

203. Niedermeyer, H.; Balbin, R.; Carlson, A.; Endler, M.; Giannone, L.; Hidalgo*, C.; Rudyj, A.; Theimer, G.; Weinlich, M.; WVII-AS Team:* Edge Turbulence in ASDEX and W7-AS. In: Proc. 9th Int. Workshop on Stellarators, Garching 1993. IAEA, Wien 1993, 357-362.

204. Niehus, H.; Heiland*, W.; Taglauer, E.:* Low-Energy Ion Scattering at Surfaces. Surf. Sci. Rep. **17**, 213-303 (1993).

205. Nolting, W.; Geipel, G.; Ertl, K.:* Magnetic Phase Transitions and Correlation Effects in Two-Particle Spectroscopies. Z. Phys. B **92**, 75-89 (1993).

206. Noterdaeme, J.-M.; Hoffmann, C.; Brambilla, M.; Büchl, K.; Eberhagen, A.; Fuchs, J.C.; Gehre, O.; Gernhardt, J.; Gruber, O.; Kallenbach, A.; Köppendörfer, W.; Poschenrieder, W.; Salmon, N.; Schneider, W.; Wesner, F.; ICRH-Team; ASDEX-Upgrade-Team: Combination of Fundamental and Second Harmonic Minority Ion Cyclotron Resonance Heating on ASDEX Upgrade. In: Proc. 20th EPS Conf. Control. Fusion and Plasma Phys., Lisbon 1993, Eds. J.A.C.Cabral, M.E.Manso, F.M.Serra, et al. ECA 17C. Europ. Phys. Soc., Geneva 1993, 945-948.

207. Noterdaeme, J.-M.; Hoffmann, C.; Brambilla, M.; Büchl, K.; Eberhagen, A.; Field, A.; Fuchs, J.C.; Gehre, O.; Gernhardt, J.; Gruber, O.; Haas, G.; et al.: First Results of Ion Cyclotron Heating on ASDEX-Upgrade. In: Radio Frequency in Plasmas, Eds: M.Porkolab, J.Hosea. AIP Conf. Proc. 289, AIP, New York 1993, 12-24.

208. Noterdaeme, J.-M.; Van Oost, G.: The Interaction between Waves in the Ion Cyclotron Range of Frequencies and the Plasma Boundary. Plasma Phys. Control. Fusion **35**, 1481-1511 (1993).

209. Nührenberg, J.: Computational Optimization of Stellarators: The Computational Stellarator. In: Proc. IAEA Techn. Comm. Meeting on Advances in Simulation and Modelling of Thermonuclear Plasmas, Montreal 1992. IAEA, Wien 1993, 412-425.

210. Nührenberg, J.; Merkel, P.; Schwab, C.; Schwenn, U.; et al.: MHD-Theoretical Aspects of Stellarators. Plasma Phys. Control. Fusion **35**, Suppl.B, 115-128 (1993).

211. Nührenberg, J.; Strumberger, E.; Sünder, D.; Reiter, D.:* Development of Divertor Concept for Optimized Stellarators. In: Proc. 14th Conf. on Plasma Phys. and Control. Nucl. Fusion Res., 2, Würzburg 1992. IAEA, Wien 1993, 449-460.

212. Nührenberg, J.; Zheng, L.-J.: Influence of an Energetic-Particle Component on Ballooning Modes in an Optimized Stellarator. In: Proc. 20th EPS Conf. Control. Fusion and Plasma Phys., Lisbon 1993, Eds. J.A.C.Cabral, M.E.Manso, F.M.Serra, et al. ECA 17C. Europ. Phys. Soc., Geneva 1993, 413-416.

213. Passek, F.; Donath, M.: Magnetic Surface State Becomes Nonmagnetic by Oxygen Adsorption. Phys. Rev. Lett. **71**, 2122-2125 (1993).

214. Pautasso, G.; Gruber, O.; Köppendörfer, W.; Lackner, K.; Richter, T.; Schneider, W.; Seidel, U.; Streibl, B.; ASDEX-Upgrade-Team: Experimental Investigation and Modeling of Vertical Displacement Events in ASDEX Upgrade. In: Proc. 20th EPS Conf. Control. Fusion and Plasma Phys., Lisbon 1993, Eds. J.A.C.Cabral, M.E.Manso, F.M.Serra, et al. ECA 17C. Europ. Phys. Soc., Geneva 1993, 199-202.

215. Pautasso, G.; Herrmann, A.; Lackner, K.; ASDEX-Upgrade-Team: Energy Balance During Disruption Associated with Vertical Displacement Events. In: Proc. 20th EPS Conf. Control. Fusion and Plasma Phys., Lisbon 1993, Eds. J.A.C.Cabral, M.E.Manso, F.M.Serra, et al. ECA 17C. Europ. Phys. Soc., Geneva 1993, 199-202.

216. Pereverzev, G.V.: On the Applicability of the Eikonal Description of LH Waves. In: Proc. 20th EPS Conf. Control. Fusion and Plasma Phys., Lisbon 1993, Eds. J.A.C.Cabral, M.E.Manso, F.M.Serra, et al. ECA 17C. Europ. Phys. Soc., Geneva 1993, 885-888.

217. Pfirsch, D.: Negative-Energy Modes in Collisionless Kinetic Theories and their Possible Relation to Nonlinear Instabilities. In: Current Research on Fusion, Laboratory and Astrophysical Plasmas, Eds. S.Kuhn, K.Schöpf, R.Schrittwieser. World Scientific Publ., Singapore 1993, 9-23.

218. Pfirsch, D.: Nonlinear Instabilities Relating to Negative-Energy Modes. Phys. Rev. E **48**, 1428-1435 (1993).

219. Pfirsch, D.; Correa-Restrepo, D.: Energy of Linear Quasi-neutral Electrostatic Drift Waves. Phys. Rev. E **47**, 1947-1959 (1993)

220. Pfirsch, D.; Sudan, R.:* Nonlinear Ideal Magnetohydrodynamics Instabilities. Phys. Fluids B **5**, 2052-2061 (1993).

221. Pinkau, K.: Energie war die Währung der Vergangenheit, Energie ist die Währung der Zukunft - was können und wollen wir uns dafür kaufen? In: Fortschritt und Gesellschaft, Ed. E.-L.Winnacker. Hirzel, Stuttgart 1993, 77-79.

222. Pinkau, K.: Fusionsforschung - Stand der Forschung und Perspektiven. Freiburger Universitätsblätter Heft **120**, 69-82 (1993).

223. Pinkau, K.: Science and Politics. In: Final Report 28th Int. Congr. of History of Science, Hamburg - Munich 1989, Eds. F.Krafft, C.J.Scriba. Steiner Verl., Stuttgart 1993, 19-25.

224. Pitcher, C.S.; Bosch, H.-S.; Carlson, A.; Dorn, C.; Field, A.; Herrmann, A.; Neuhauser, J.; Richter, T.; Schneider, W.; ASDEX-Upgrade-Team:* First Results with the In-Vessel Probe on ASDEX-Upgrade. In: Proc. 20th EPS Conf. Control. Fusion and Plasma Phys., Lisbon 1993, Eds. J.A.C.Cabral, M.E.Manso, F.M.Serra, et al. ECA 17C. Europ. Phys. Soc., Geneva 1993, 291-294.

225. Poschenrieder, W.; ASDEX-Upgrade-Team; ICRH-Team: Gaseous Impurity Production in ASDEX Upgrade Discharges. In: Proc. 20th EPS Conf. Control. Fusion and Plasma Phys., Lisbon 1993, Eds. J.A.C.Cabral, M.E.Manso, F.M.Serra, et al. ECA 17C. Europ. Phys. Soc., Geneva 1993, 591-594.

226. Puri, S.: Plasma Dielectric Tensor in a Tokamak. In: Proc. 20th EPS Conf. Control. Fusion and Plasma Phys., Lisbon 1993, Eds. J.A.C.Cabral, M.E.Manso, F.M.Serra, et al. ECA 17C. Europ. Phys. Soc., Geneva 1993, 1471-1474.

227. Puri, S.: Resolution of the Lower-Hybrid Current Drive Spectral-Gap Anomaly via Enhanced Toroidal Landau Damping. Czech. J. Phys. **43**, 631-645 (1993).

228. Radtke, R.; Lieder, G.; Napiontek, B.; Field, A.; Fußmann, G.; Kallenbach, A.; Kiemer, K.; Mayer, H.-M.; ASEDX-Upgrade-Team: The Multichord Divertor Spectrometer System of the ASDEX Upgrade Tokamak. In: Proc. 21st Int. Conf. on Phen. in Ionized Gases (ICPIG), Bochum 1993, Eds. G.Ecker, U.Ahrendt, J.Böseler. Arbeitsgem. Plasmaphysik, Bochum 1993, 466-467.

229. Raupp, G.; Aubanel, C.; Neu, G.; Pirsch, T.; Richter, H.; Trzinski, T.; Zasche, D.: Discharge Information Management for ASDEX Upgrade. In: Conf. Record of the 8th Conf. on Real-Time Computer Applications in Nuclear, Particle and Plasma Phys., Eds. D.Axen, R.Poutissou. TRIUMF, Vancouver 1993, 162-173.

230. Raupp, G.; Bruhns, H.; Förster, K.; Hertweck, F.; Huber, R.; Jülich, A.; Neu, G.; Richter, H.; Schneider, U.; Streibl, B.; Woyke, W.; Zasche, D.; Zehetbauer, T.:* ASDEX-Upgrade Discharge Control and Shot Management. In: Proc. 17th Symp. Fusion Technol., Rome 1992, Eds. C.Ferro, M.Gasparotto, H.Knöpfel. North-Holland Publ., Amsterdam 1993, 1072-1076.

231. Reinke, P.; Jacob, W.; Möller, W.: The Influence of the Ion Energy on the Growth and Structure of Thin Hydrocarbon Films. J. Appl. Phys. **74**, 1354-1361 (1993).

232. Reinke, P.; Jacob, W.; Möller, W.: Investigation of the Growth Mechanism of C:H Films from an ECR Plasma. In: Proc. ISPC-11, Loughborough 1993, Ed. J.Harry. Int. Union Pure and Appl. Chem., Loughborough 1993, 823-828.

233. Richter, H.; Cole, R.; Fitzek*, M.; Förster, K.; Neu, G.; Raupp, G.; Woyke, W.; Zasche, D.; et al.:* Overview of the ASDEX-Upgrade Experiment Management Software. In: Proc. 17th Symp. Fusion Technol., Rome 1992, Eds. C.Ferro, M.Gasparotto, H.Knöpfel. North-Holland Publ., Amsterdam 1993, 1077-1081.

234. Richter, H.; Neu, G.; Raupp, G.; Zasche, D.: System Integration of the ASDEX-Upgrade Timing System. In: Conf. Record of the 8th Conf. on Real-Time Computer Applications in Nuclear, Particle and Plasma Phys., Eds. D.Axen, R.Poutissou. TRIUMF, Vancouver 1993, 267-269.

235. Roth, J.: Impurity Generation Processes in Particle-Surface Interaction: Data Status and Needs. In: Atomic and Plasma-Material Interaction Processes in Control. Thermonuclear Fusion, Eds. R.K.Janev, H.W.Drawin. Elsevier Science Publ., Amsterdam 1993, 381-401.

236. Ryter, F.; et al.: H-Mode Thermal Confinement Time under ELM-free Conditions in Deuterium, Nucl. Fusion **33**, 979-990 (1993).

237. Ryter, F.; Gruber, O.; Büchl, K.; Field, A.; Fuchs, J.C.; Gehre, O.; Herrmann, A.; Kaufmann, M.; Köppendörfer, W.; Mast, K.-F.; Murmann, H.; Noterdaeme, J.-M.; Pereverzev, G.V.; Zohm, H.; ASDEX-Upgrade-Team; ICRH-Team: Ohmic H-Mode and H-Mode Power Threshold in ASDEX Upgrade. In: Proc. 20th EPS Conf. Control. Fusion and Plasma Phys., Lisbon 1993, Eds. J.A.C.Cabral, M.E.Manso, F.M.Serra, et al. ECA 17C. Europ. Phys. Soc., Geneva 1993, 23-26.

238. Ryter, F.; H-Mode-Database-Working-Group: An Examination of the ITER H-Mode Power Threshold Database. In: Proc. 20th EPS Conf. Control. Fusion and Plasma Phys., Lisbon 1993, Eds. J.A.C.Cabral, M.E.Manso, F.M.Serra, et al. ECA 17C. Europ. Phys. Soc., Geneva 1993, 15-18.

239. Salmon, N.: First Electron Temperature Edge Measurements on the ASDEX Upgrade Tokamak Using a Heterodyne Radiometer. In: Conf. Digest 8th Int. Conf. on IR and mm Waves, Essex 1993, Eds. J.R.Birch, T.J.Parker. SPIE Proc. 2104. SPIE, Bellingham 1993, 254-255.

240. Sandl, P.; Bischler, U.; Bertel, E.:* The Interaction of Atomic Hydrogen with Cu(110). Surf. Sci. **291**, 29-38 (1993).

241. Sapper, J.; WVII-X-Technical-Group: Superconducting Coil Development for the Wendelstein 7-X Stellarator. Fusion Eng. Des. **20**, 23-32 (1993).

242. Sapper, J.; WVII-X-Technical-Group: The Wendelstein 7-X Project, a Next Step Towards a Stellarator-Reactor. In: Proc. Jahrestagung Kerntechnik, Köln 1993. Dt. Atomforum e.V., Bonn 1993, 29-32.

243. Sardei, F.; Grigull, P.; Herre, G.; Kißlinger, J.; Richter-Glötzl, M.; WVII-AS-Team: Open Magnetic Surfaces and Resonant Topology for Modelling Plasma Edge Transport in W7-AS. In: Proc. 9th Int. Workshop on Stellarators, Garching 1993. IAEA, Wien 1993, 530-535.

244. Sardei, F.; Grigull, P.; Herre, G.; Kißlinger, J.; Richter-Glötzl, M.; WVII-AS-Team; et al.: Open Magnetic Surfaces and Resonant Topology in the Separatrix-Dominated Boundary Region of the W7-AS Stellarator. In: Proc. 20th EPS Conf. Control. Fusion and Plasma Phys., Lisbon 1993, Eds. J.A.C.Cabral, M.E.Manso, F.M.Serra, et al. ECA 17C. Europ. Phys. Soc., Geneva 1993, 405-408.

245. Sattler, S.; Hartfuß, H.-J.: Intensity Interferometry for Measurement of Electron Temperature Fluctuations in Fusion Plasmas. Plasma Phys. Control. Fusion **35**, 1285-1306 (1993).

246. Sattler, S.; Hartfuß, H.-J.: Laboratory Test of an Intensity Interferometer for Measurement of Electron Temperature Fluctuations on Wendelstein 7-AS. In: Proc. 8th Joint Workshop on Electron Cyclotron Emission and Electron Cyclotron Resonance Heating, Gut Ising 1992. MPI Plasmaphysik, Garching 1993, 175-189.

247. Sattler, S.; Hartfuß, H.-J.: Temperature Fluctuations in the Core of Wendelstein 7-AS. In: Proc. 9th Int. Workshop on Stellarators, Garching 1993. IAEA, Wien 1993, 298-303.

248. Schauer, F.; WVII-X-Technical-Group: R&D Activities for the Wendelstein 7-X Superconducting Coil System. In: Proc. 17th Symp. Fusion Technol., Rome 1992, Eds. C.Ferro, M.Gasparotto, H.Knöpfel. North-Holland Publ., Amsterdam 1993, 922-926.

249. Schauer, F.; WVII-X-Technical-Group: Status of W7-X Technical Developments. In: Proc. 9th Int. Workshop on Stellarators, Garching 1993. IAEA, Wien 1993, 194-199.

250. Schissel, D.P.; H-Mode-Database-Working-Group:* Analysis of the ITER H-Mode Confinement Database. In: Proc. 20th EPS Conf. Control. Fusion and Plasma Phys., Lisbon 1993, Eds. J.A.C.Cabral, M.E.Manso, F.M.Serra, et al. ECA 17C. Europ. Phys. Soc., Geneva 1993, 103-106.

251. Schneider, F.; ASDEX-Team; WVII-AS-Team: Optimum Plasma Control Using Thyristor Power Converters. In: Proc. 17th Symp. Fusion Technol., Rome 1992, Eds. C.Ferro, M.Gasparotto, H.Knöpfel. North-Holland Publ., Amsterdam 1993, 927-931.

252. Schneider, R.; Reiter, D.; Neuhauser, J.; Lackner, K.; Igitkhanov, Yu.L.; Kastelewicz, H.; et al.:* Analysis of Cold Divertor Concepts by 2-D Simulations Neutral Models and Influence on Convergence. In: Proc. 20th EPS Conf. Control. Fusion and Plasma Phys., Lisbon 1993, Eds. J.A.C.Cabral, M.E.Manso, F.M.Serra, et al. ECA 17C. Europ. Phys. Soc., Geneva 1993, 775-778.

253. Schneider, R.; Reiter, D.; Neuhauser, J.; Lackner, K.; Igitkhanov, Yu.L.; Kastelewicz, H.; et al.:* On the Feasibility of Gastargets. In: Proc. 9th Int. Workshop on Stellarators, Garching 1993. IAEA, Wien 1993, 510-515.

254. Schneider, U.; ASDEX-Team: Ten Years of Operating Experience with ASDEX. In: Proc. 17th Symp. Fusion Technol., Rome 1992, Eds. C.Ferro, M.Gasparotto, H.Knöpfel. North-Holland Publ., Amsterdam 1993, 742-746.

255. Schneider, U.; Förster, K.: The ASDEX Upgrade Shot Program Editor. In: Proc. 17th Symp. Fusion Technol., Rome 1992, Eds. C.Ferro, M.Gasparotto, H.Knöpfel. North-Holland Publ., Amsterdam 1993, 1082-1085.

256. Schneider, U.; Stadlbauer, J.; WVII-AS-Team: Boronization on Wendelstein 7-AS. In: Proc. 17th Symp. Fusion Technol., Rome 1992, Eds. C.Ferro, M.Gasparotto, H.Knöpfel. North-Holland Publ., Amsterdam 1993, 376-380.

257. Schwab, C.: Comparison of Tokamak and Stellarator Ballooning Mode Structures. In: Proc. 20th EPS Conf. Control. Fusion and Plasma Phys., Lisbon 1993, Eds. J.A.C.Cabral, M.E.Manso, F.M.Serra, et al. ECA 17C. Europ. Phys. Soc., Geneva 1993, 417-420.

258. Schwab, C.: Computation of Stable MHD TAE Modes with CAS3D. In: Proc. 9th Int. Workshop on Stellarators, Garching 1993. IAEA, Wien 1993, 227-232.

259. Schwab, C.: Ideal Magnetohydrodynamics: Global Mode Analysis of Three-Dimensional Plasma Configurations. Phys. Fluids B **5**, 3195-3206 (1993).

260. Schweinzer, J.; Fiedler, S.; McCormick, K.: Lithium Beam Diagnostics at ASDEX Upgrade and W7-AS. In: Proc Workshop on the Use of Atomic Beams in Plasma Experiments, Budapest 1993. Hungarian Acad. of Sciences, Budapest 1993, 570-574.

261. Schwenn, U.: Application of the HINT Code to W7-X. In: Proc. 9th Int. Workshop on Stellarators, Garching 1993. IAEA, Wien 1993, 108-113.

262. Schwenn, U.: Computer Simulation of Plasmas. In: IPP Summer University for Plasma Phys., Garching 1993, Ed. H.-W.Bartels. MPI Plasmaphysik, Garching 1993, 179-194.

263. Schwörer, R.; Garcia-Rosales, C.; Roth, J.: Dynamics of B Sublimation from Boron Doped Graphite USB15. Nucl. Instrum. Methods Phys. Res. B **80/81**, 1468-1471 (1993).

264. Scott, B.: Drift Wave Turbulence in the Transcollisional Regime. In: Proc. 20th EPS Conf. Control. Fusion and Plasma Phys., Lisbon 1993, Eds. J.A.C.Cabral, M.E.Manso, F.M.Serra, et al. ECA 17C. Europ. Phys. Soc., Geneva 1993, 1411-1414.

265. Scott, B.: Finite Larmor Radius Kinetic Effects in Collisionless Fluid Equations. In: Current Research on Fusion, Laboratory and Astrophysical Plasmas, Eds. S.Kuhn, K.Schöpf, R.Schrittwieser. World Scientific Publ., Singapore 1993, 137-142.

266. Scott, B.: Self-Consistent Models of Drift Wave Turbulence: Implications for Transport Scenarios. In: Proc. 14th Conf. on Plasma Phys. and Control. Nucl. Fusion Res., 2, Würzburg 1992. IAEA, Wien 1993, 203-211.

267. Siegele, R.; Roth, J.; Scherzer, B.; et al.: Damage and Deuterium-Trapping in HOPG-Graphite. J. Appl. Phys. **73**, 2225-2233 (1993).

268. Silva, A.; Cupido*, L.; Manso*, M.E.; Söldner, F.X.; ASDEX-Upgrade-Team; et al.:* Fast Sweep Multiple Broadband Reflectometer for ASDEX Upgrade. In: Proc. 17th Symp. Fusion Technol., Rome 1992, Eds. C.Ferro, M.Gasparotto, H.Knöpfel. North-Holland Publ., Amsterdam 1993, 747-750.

269. Silva, A.; Manso*, M.E.; Varela*, P.; Albrecht, M.; Söldner, F.X.; et al.:* First Density Measurements with Microwave Reflectometry on ASDEX Upgrade. In: Proc. 20th EPS Conf. Control. Fusion and Plasma Phys., Lisbon 1993, Eds. J.A.C.Cabral, M.E.Manso, F.M.Serra, et al. ECA 17C. Europ. Phys. Soc., Geneva 1993, 1107-1110.

270. Söldner, F.X.; Bartiromo, R.; Leuterer, F.; Zarnstroff*, M.C.; Bosch, H.-S.; Fahrbach, H.-U.; Müller, E.R.; Murmann, H.; Steuer, K.-H.; Vollmer, O.:* Combined Operation of Lower Hybrid and Neutral Beam Injection on ASDEX. Nucl. Fusion **33**, 333-347 (1993).

271. Söldner, F.X.; Pereverzev, G.V.; Bartiromo, R.; Fahrbach, H.-U.; Leuterer, F.; Murmann, H.; Stäbler, A.; Steuer, K.-H.:* Electron and Ion Heat Transport with Lower Hybrid Current Drive and Neutral Beam Injection Heating in ASDEX. Nucl. Fusion **33**, 795-803 (1993).

272. Spathis, P.; Lengyel, L.: Simulation of Vapor Shield Evolution at Carbonized Target Plates. In: Proc. 20th EPS Conf. Control. Fusion and Plasma Phys., Lisbon 1993, Eds. J.A.C.Cabral, M.E.Manso, F.M.Serra, et al. ECA 17C. Europ. Phys. Soc., Geneva 1993, 1443-1446.

273. Stäbler, A.; Burhenn, R.; Grigull, P.; Hofmann, J.V.; McCormick, K.; Müller, E.R.; Neuhauser, J.; Niedermeyer, H.; Reiter, D.; Schneider, R.; Steuer, K.-H.; Weller, A.; Würsching, E.; Zohm, H.; ASDEX-Team; WVII-AS-Team:* Comparison of Density Limit Physics on the ASDEX Tokamak and the Wendelstein 7-AS Stellarator. In: Proc. 14th Conf. on Plasma Phys. and Control. Nucl. Fusion Res., 2, Würzburg 1992. IAEA, Wien 1993, 523-529.

274. Streibl, B.; Behler, K.; McCarthy, P.; Drube, R.; Ernesti, J.; Finkelmeyer, H.; Gernhardt, J.; Gruber, O.; Herppich, G.; Hupfloher, H.; Jacobi, D.; Klement, G.; Kollotzek, H.; Köppendörfer, W.; Lackner, K.; Mattes, K.; Mertens, V.; Neu, G.; Noterdaeme, J.-M.; Oswald, J.; Poschenrieder, W.; Raupp, G.; Richter, H.; Richter, T.; Schneider, H.; Schramm, G.; Schweizer, S.; Seidel, U.; Vernickel, H.; Wieczorek, A.; Wesner, F.; Woyke, W.; Zasche, D.: ASDEX-Upgrade-Team: The First Period of Operation. In: Proc. 17th Symp. Fusion Technol., Rome 1992, Eds. C.Ferro, M.Gasparotto, H.Knöpfel. North-Holland Publ., Amsterdam 1993, 751-755.

275. Stroth, U.; Giannone, L.; Erckmann, V.; Geist, T.; Hartfuß, H.-J.; Jänicke, R.; Kühner, G.; Ringler, H.; Sardei, F.; WVII-AS-Team: On the Diffusive Nature of W7-AS Transport. In: Proc. 20th EPS Conf. Control. Fusion and Plasma Phys., Lisbon 1993, Eds. J.A.C.Cabral, M.E.Manso, F.M.Serra, et al. ECA 17C. Europ. Phys. Soc., Geneva 1993, 349-352.

276. Stroth, U.; Giannone, L.; Erckmann, V.; Geist, T.; Hartfuß, H.-J.; Jänicke, R.; Kühner, G.; Ringler, H.; Sardei, F.; WVII-AS-Team: On the Diffusive Nature of W7-AS Transport. In: Proc. 9th Int. Workshop on Stellarators, Garching 1993. IAEA, Wien 1993, 319-323.

277. Stroth, U.; Kühner, G.; Maaßberg, H.; Ringler, H.; WVII-AS-Team: Dimensionally Similar Discharges in the W7-AS Stellarator. Phys. Rev. Lett. **70**, 936-939 (1993).

278. Strüber, U.; Küppers, J.:* Spectroscopic Confirmation of STM Derived Ag/Pt Mixing in Annealed Ag Submonolayers at Pt(111) Surfaces. Surf. Sci. **294**, L924-L928 (1993).

279. Strumberger, E.: Sol Modeling for the W7-X Ergodic Divertor Concept. In: Proc. 20th EPS Conf. Control. Fusion and Plasma Phys., Lisbon 1993, Eds. J.A.C.Cabral, M.E.Manso, F.M.Serra, et al. ECA 17C. Europ. Phys. Soc., Geneva 1993, 791-794.

280. Strumberger, E.: Topology of Field Line Mapping in the Ergodic Region of Optimized Stellarators and Divertor Design. In: Proc. 9th Int. Workshop on Stellarators, Garching 1993. IAEA, Wien 1993, 536-541.

281. Sünder, D.; Wobig, H.: Bifurcation of Electron Temperature in the High Recycling Regime. In: Proc. 20th EPS Conf. Control. Fusion and Plasma Phys., Lisbon 1993, Eds. J.A.C.Cabral, M.E.Manso, F.M.Serra, et al. ECA 17C. Europ. Phys. Soc., Geneva 1993, 819-822.

282. Sünder, D.; Wobig, H.: Electron Temperature Bifurcation in the High Recycling Regime. In: Proc. 9th Int. Workshop on Stellarators, Garching 1993. IAEA, Wien 1993, 521-525.

283. Taglauer, E.: Sputtering and Surface Science. Mat.-Fys. Medd. **43**, 643-657 (1993).

284. Taglauer, E.; Du Plessis, J.: Surface Segregation and Preferential Sputtering in Binary Systems. In: Proc. Symposium on Surface Science, Kaprun 1993, Eds. G.Betz, P.Varga. Inst. f. Allg. Physik, Univ. Wien 1993, 59-62.

285. Taglauer, E.; Knözinger, H.:* Investigation of Catalyst Systems by Means of Low-Energy Ion Scattering. In: Surface Science: Principles and Applications, Eds. R.F.Howe, R.N.Lamb, K.Wandelt. Proc. in Phys. 73, Springer, Berlin 1993, 264-278.

286. Tasso, H.: Lyapunov Stability of Large Systems of van der Pol-Like Oscillators and Connection with Turbulence and Fluctuations Spectra. Phys. Lett. A **183**, 165-168 (1993).

287. Tasso, H.: A Manifest Hopf Bifurcation in Resistive Magnetohydrodynamics. Phys. Lett. A **80**, 257-258 (1993).

288. Tasso, H.: Remarks on Non-Linear Stability in Dissipative Magnetohydrodynamics. Nuovo Cim. B **108**, 827-830 (1993).

289. Teubel, A.; Penningsfeld, F.-P.: Collisionless Fast Ion Confinement and Computed NBI Heating Efficiency in Stellarators - A Comparitive Study of W7-A, W7-AS, and W7-X. In: Proc. 20th EPS Conf. Control. Fusion and Plasma Phys., Lisbon 1993, Eds. J.A.C.Cabral, M.E.Manso, F.M.Serra, et al. ECA 17C. Europ. Phys. Soc., Geneva 1993, 401-404.

290. Throumoulopoulos, G.N.; Pfirsch, D.: Negative Energy Waves in a Magnetically Confined Guiding Center Plasma. In: Proc. 20th EPS Conf. Control. Fusion and Plasma Phys., Lisbon 1993, Eds. J.A.C.Cabral, M.E.Manso, F.M.Serra, et al. ECA 17C. Europ. Phys. Soc., Geneva 1993, 1467-1470.

291. Tsui, H.Y.W.; Wootton, A.J.; Bengston, R.D.; Rudyj, A.; et al.:* Edge Turbulence and Transport Studies. In: Proc. 14th Conf. on Plasma Phys. and Control. Nucl. Fusion Res., 2, Würzburg, 1992. IAEA, Wien 1993, 673-678.

292. Verbeek, H.; Heinrich, O.; WVII-AS-Team: Low Energy Neutral Particle Analysis at the Stellarator W7-AS. In: Proc. 20th EPS Conf. Control. Fusion and Plasma Phys., Lisbon 1993, Eds. J.A.C.Cabral, M.E.Manso, F.M.Serra, et al. ECA 17C. Europ. Phys. Soc., Geneva 1993, 727-730.

293. Verplancke, P.: Measuring Neutral Beam Profiles in TEXTOR. Physicalia Mag. **15**, 233-238 (1993).

294. Vollmer, O.; Stäbler, A.; Feist, J.-H.; Klaster, K.; Obermayer, S.; Speth, E.; Wittenbecher, K.: Control and Data Acquisition of the Neutral Beam Injection for ASDEX-Upgrade. In: Proc. 17th Symp. Fusion Technol., Rome 1992, Eds. C.Ferro, M.Gasparotto, H.Knöpfel. North-Holland Publ., Amsterdam 1993, 1106-1110.

295. Wagner, F.; Erckmann, V.; Estrada, T.; Grigull, P.; Hartfuß, H.-J.; Hirsch, M.; Herre, G.; Hofmann, J.V.; Rudyj, A.; Weller, A.; WVII-AS-Team:* H-Mode Studies on W7-AS. In: Proc. 9th Int. Workshop on Stellarators, Garching 1993. IAEA, Wien 1993, 330-339.

296. Wagner, F.; Stroth, U.: Transport in Toroidal Devices-Experimentalist's View. Plasma Phys. Control. Fusion **35**, 1321-1371 (1993).

297. Weller, A.; Spong, D.A.:* Global, Toroidal and Helical-Induced Shear Alfvén Instabilities in Stellarators. In.: Proc. 9th Int. Workshop on Stellarators, Garching 1993. IAEA, Wien 1993, 554-557.

298. Weller, A.; Spong, D.A.; Hartfuß, H.-J.; Jänicke, R.; Lazaros, A.; Penningsfeld, F.-P.; Sattler, S.; WVII-AS-Team; NI-Team(WVII-AS):* Stability of Neutral Beam Driven Alfven Eigenmodes in the Wendelstein W7-AS Stellarator. In: Proc. 20th EPS Conf. Control. Fusion and Plasma Phys., Lisbon 1993, Eds. J.A.C.Cabral, M.E.Manso, F.M.Serra, et al. ECA 17C. Europ. Phys. Soc., Geneva 1993, 337-340.

299. Werthmann, H., Brambilla, M.: Solution of the Nonlocal Wave Equation. In: Proc. Int. Workshop on Plasma Phys., Pichl 1993, Ed. M.F.Heyn, et al. dbv-Verl, Graz 1993, 228-232.

300. Werthmann, H.; Brambilla, M.: Solution of the Nonlocal Wave Equation of an IBW Mode Conversion Problem. In: Proc. 20th EPS Conf. Control. Fusion and Plasma Phys., Lisbon 1993, Eds. J.A.C.Cabral, M.E.Manso, F.M.Serra, et al. ECA 17C. Europ. Phys. Soc., Geneva 1993, 961-964.

301. Wesner, F.; Kutsch, H.-J.; Noterdaeme, J.-M.; Fritsch, R.; et al.: Protecting Limiters for the ASDEX Upgrade ICRH Antennae. In: Proc. 17th Symp. Fusion Technol., Rome 1992, Eds. C.Ferro, M.Gasparotto, H.Knöpfel. North-Holland Publ., Amsterdam 1993, 406-409.

302. Wilhelm, R.: Application of Fusion High-Power RF Techniques to the Non-Fusion Field. Plasma Phys. Control. Fusion **35**, Suppl.A, 199-210 (1993).

303. Wilhelm, R.: Characterization of Plasma Near Surfaces. J. Nucl. Mater. **200**, 273-281 (1993).

304. Wilhelm, R.: ECR Plasma Sources. In: Proc. of a NATO Advanced Res. Workshop on Microwave Discharges, Eds. C.M.Ferreira, M.Moisan. NATO ASI Series 302, Plenum Press, New York 1993, 161-179.

305. Wilhelm, R.: Industrial Applications of Plasma Physics. In: Int. School of Plasma Phys., Piero Caldirola, Industrial Applications of Plasma Phys., Varenna 1993, Eds. G.Bonizzoni, W.Hooke, E.Sindoni. ISPP-13, SIF, Bologna 1993, 577-579.

306. Wilhelm, R.: Microwave Plasmas for Surface Treatment and Thin-Film Production. In: Int. School of Plasma Phys., Piero Caldirola, Industrial Applications of Plasma Phys., Varenna 1993, Eds. G.Bonizzoni, W.Hooke, E.Sindoni. ISPP-13, SIF, Bologna 1993, 185-197.

307. Winters, H.F.; Coufal*, H.J.; Eckstein, W.:* Influence of Energy Reflected from the Target on Thin Film Characteristics. J. Vac. Sci. Technol. A **11**, 657-663 (1993).

308. Wobig, H.: Introduction to Stellarator Physics. In: IPP Summer University for Plasma Phys., Garching 1993, Ed. H.-W.Bartels. MPI Plasmaphysik, Garching 1993, 82-100.

309. Wobig, H.: Optimisation of Stellarators for Fusion Reactors. In: Proc. Jahrestagung Kerntechnik, Köln 1993. Dt. Atomforum e.V., Bonn 1993, 12-24.

310. Wobig, H.: The Theoretical Basis of a Drift-Optimized Stellarator Reactor. Plasma Phys. Control. Fusion **35**, 903-917 (1993).

311. Wolf, R.C.; Eriksson*, L.-G.; Von Hellermann*, M.; Mandl, W.; et al.:* Motional Stark Effect Measurements of the Local ICRH Induced Diamagnetism in JET Plasmas. In: Proc. 20th EPS Conf. Control. Fusion and Plasma Phys., Lisbon 1993, Eds. J.A.C.Cabral, M.E.Manso, F.M.Serra, et al. ECA 17C. Europ. Phys. Soc., Geneva 1993, 91-94.

312. Wyk, G.N. van; Roos, W.D.; Du Plessis*, J.; Taglauer, E.:* Sputter Induced Concentration Profiles in Binary Alloys. Inst. Phys. Conf. Ser. **130**, 435-438 (1993).

313. Zasche, D.; Bruhns, H.; Cole*, R.; Förster, K.; Huber, R.; Lüddecke*, K.; Jülich, A.; Neu, G.; Raupp, G.; Richter, H.; Schneider, U.:* Tokamak Discharge Description at ASDEX-Upgrade. In: Conf. Record of the 8th Conf. on Real-Time Computer Applications in Nuclear, Particle and Plasma Phys., Eds. D.Axen, R.Poutissou. TRIUMF, Vancouver 1993, 264-266.

314. Zheng, L.-J.: Ideal-MHD and Kinetic Ballooning Mode Equations in Low-Shear Configurations. In: Proc. 9th Int. Workshop on Stellarators, Garching 1993. IAEA, Wien 1993, 233-238.

315. Zheng, L.-J.: Stability Criteria for Edge Flute Modes in the Two-Fluid Regime. Phys. Fluids B **5**, 1402-1407 (1993).

316. Zheng, L.-J.: Two-Fluid Equations for Low-n Singular Modes in the Low-Frequency Regime. Phys. Fluids B **5**, 1962-1970 (1993).

317. Zohm, H.; Büchl, K.; Field, A.; Fuchs, J.C.; Gehre, O.; Herrmann, A.; Kaufmann, M.; Lieder, G.; Ryter, F.; Schittenhelm, M.; ASDEX-Upgrade-Team; ICRH-Team: Characterization of ELMS on ASDEX-Upgrade. In: Proc. 20th EPS Conf. Control. Fusion and Plasma Phys., Lisbon 1993, Eds. J.A.C.Cabral, M.E.Manso, F.M.Serra, et al. ECA 17C. Europ. Phys. Soc., Geneva 1993, 19-22.

318. Zohm, H.; Lackner, K.; Ludescher, C.:* Statistical Analysis of Disruptions in ASDEX. Nucl. Fusion **33**, 655-662 (1993).

Diploma Theses

319. Gubanka, B.: Aufbau eines Kerrmikroskops zur Untersuchung magnetischer Strukturen an Oberflächen. Techn. Univ. München 1993.

320. Kiemer, K.: Untersuchung von Wasserstofflinienstrahlung in der Plasmarandschicht. Techn. Univ. München 1993.

321. Labich, S.: Thermische Desorptionsspektroskopie an Rh/TiO_2-Modellkatalysatoren. Univ. München 1993.

322. Rabe, A.: Wachstum und Struktur ultradünner Kobaltfilme auf Cu (111). Techn. Univ. München 1993.

Doctoral Theses

323. Dietrich, E.: Mathematische Modellierung des Randschichtplasmas (russ.). Moskau 1993.

324. Engelhard, M.: Messung und Modellierung absoluter Radikaldichten in einem ECRH-Methanplasma. Techn. Univ. München 1993.

325. Feng, Y.: Formulation and Application of the Neutral Particle Beam Deposition Code SINBAD. Heidelberg 1993.

326. Franzen, P.: Hochtemperaturreemission von Wasserstoff aus Graphit. Techn. Univ. München 1993.

327. Friedl, A.: Aufbau eines in-situ-IR-Spektralellipsometers zur Charakterisierung plasmadeponierter C:H-Schichten. Techn. Univ. München 1993.

328. Geipel, G.: Manifestation magnetischer Phasenübergänge in Auger Elektronen und Auftrittspotential-Spektroskopie. Bayreuth 1993.

329. Hytry, R.: Innenbeschichtung eines Hohlleiters mit Hilfe einer ECR-Laufentladung. Techn. Univ. München 1993.

330. Jandl, C.: Untersuchung des dynamischen Inventars von Wasserstoff in Graphit unter Beschuß aus einem RF-Plasma. Techn. Univ. München 1993.

331. Passek, F.: Untersuchungen zur Spinabhängigkeit der elektronischen Struktur von Eisen- und Nickel-Systemen mit reduzierter Dimension. Bayreuth 1993.

332. Sattler, S.: Fluktuationen der Elektronentemperatur gemessen durch Intensitätsinterferometrie am Stellarator W7-AS. Univ. Düsseldorf 1993.

333. Zeiler, A.: Stabile Tokamaks ohne Wand. Univ. München 1993.

Habilitation

334. Donath, M.: Spin-Dependent Electronic Structure at Magnetic Surfaces: the Low-Miller-Index Surfaces of Nickel. Bayreuth 1993.

Patents

335. Braun, F.: "Koaxialleitungswiderstand für hohe Leistungen" (AZ: 13443). Deutschland P 43 01 583.2, Patentanmeldung: 21.1.1993.

336. Derfler, H.; Perchermeier, J.; Spitzer, H.: "Beschichtung geringer Sekundäremission" (AZ: 11383). USA 4,559,281, Freigabe: 27.4.1993.

337. Fukarek, W.: "Schnelles spektroskopisches Ellipsometer" (AZ: 13654). Deutschland P 43 43 490.8, Patentanmeldung: 20.12.1993.

338. Haas, G.: "Heißkathoden-Ionisationsmanometer II" (AZ: 13035). Japan 4-95639, Auslandsanmeldung: 15.4.1992. Deutschland G 93 05 441, Gebrauchsmustereintragung: 22.7.1993.

339. Koch, A.; Langlotz, M.; Marlier, S.: "Mikrowelleninterferometer" (AZ: 13400). Deutschland P 43 00 949.2, Patentanmeldung: 15.1.1993.

340. Kraus, W.: "Zur Anordnung in einem Vakuumgefäß geeignete selbsttragende isolierte Leiteranordnung, insbesondere Antennenspule für einen Hochfrequenz-Plasmagenerator" (AZ: 13438). Deutschland P 42 41 927.1. Europa (DE, FR, GB, IT, CH) 93119967.3, Auslandsanmeldungen: 10.12.1993. USA Nr. noch unbekannt am 13.12.1993.

341. Liebl, H.: "Kontaktionisations-Ionenstrahlquelle" (AZ: 12304). Großbritannien 2,212,654 , Freigabe: 6.7.1993. Frankreich 8808931, Freigabe: 6.7.1993. USA 4,983,845, Freigabe: 6.7.1993. Japan 1764884, Freigabe: 6.7.1993.

342. Liebl, H.: "Doppelfokussierendes Massenspektrometer hoher Eingangsapertur" (AZ: 9115-73). USA 3,949,221, erloschen 1993.

343. Liebl, H.: "Quadropolfeld-Massenanalysator hoher Eingangsapertur" (AZ: 9163-73). USA 3,935,453, erloschen 1993.

344. Liebl, H.; Senftinger, B.: "Elektronenmikroskop" (AZ: 12537). Deutschland 39 04 032, Patenterteilung: 15.7.1993. Großbritannien 2,230,643, Patenterteilung: 27.10.1993.

345. Müller, G.; Wilhelm, R.: "Mikrowellenfenster" (AZ: 11951). Japan 62-128491, Freigabe: 23.11.1993. Irland 1216/87, Freigabe: 23.11.1993. Portugal 84939, Freigabe: 3.5.1993.

346. Mukherjee, S.B.: "Wärmeschutzschild" (AZ: 12437). Deutschland 38 28 902.4, Weiterführung durch den Erfinder Oktober 1993. Europa (DE, GB, FR, IT) 89115024, Weiterführung durch den Erfinder Oktober 1993.

347. Richter, H.: "Modulares Koppelnetz" (AZ: 12521). USA 5,175,539, Patenterteilung: 29.12.1992.

348. Schneider, F.: "Synchronisierter Meßverstärker" (AZ: 12032). Japan 5649.5, Offenlegung 1993. Europa (DE, FR, GB, IT, CH, LI, NL) 0257200 B 1, Patenterteilung: 28.4.1993. Deutschland P 36 27 610, Freigabe: 30.7.1993.

349. Schneider, F.: "Hybrider Regler" (AZ: 12606). Deutschland P 39 31 133, Patenterteilung: 6.5.1993. USA 5,184,292, Patenterteilung: 2.2.1993.

350. Weber, G.: "Vakuumdichte Stromdurchführung" (AZ: 13303). Deutschland DE 42 12 859 A 1, Offenlegung: 21.10.1993. Europa (DE, FR, GB, IT, CH) 93106254.1, Auslandsanmeldungen: 16.4.1993.

351. Wilhelm, R.: "Mikrowellen-Plasmaverfahren" (AZ: 12418). Europa (DE, FR, GB, IT) 0346738, Freigabe: 17.5.1993. USA 4,897,285, Freigabe: 17.5.1993.

352. Wilhelm, R.; Möller, W.; Hytry, R.: "Verfahren und Einrichtung zur PECVD-Innenbeschichtung eines Hohlkörpers mittels eines Mikrowellenplasmas" (AZ: 13308 und 13444). Deutschland P 42 14 401 und P 42 42 324, Europa (DE, FR, GB, IT, CH, LI) 93106914.0, Auslandsanmeldungen: 28.4.1993. Deutschland P 42 14 401, Patenterteilung: 11.3.1993.

353. Vollmer, O.: "Digitales Dosierventil" (AZ: 13333). Deutschland P 42 17 577.1, Aufgabe: 1993.

Lectures

354. Abramov, V.A.; Bachmann, P.; Morozov*, D.K.; Sünder, D.:* The Influence of Neutral Particles on the Radiative Thermal Instability in SOL Plasmas. 4th Int. Workshop "Plasma Edge Theory in Fusion Devices", Varenna 1993.

355. Albrecht, M.; Manso, M.E.; Serra*, F.; Söldner, F.X.; et al.:* Dichteprofilbestimmung durch Mikrowellenreflektometrie an ASDEX Upgrade. Verhandl. DPG (VI) **28**, 113, P14.75 (1993).

356. Andelfinger, C.; Buchelt, E.; Cierpka, P.; Kollotzek, H.; Lang, P.; Lang, R.; Prausner, G.; Söldner, F.X.; Ulrich, M.; Weber, G.: A New Centrifuge Pellet Injector for Fusion Experiments. Verhandl. DPG (VI) **28**, 96-97, P14.17 (1993).

357. Baldzuhn, J.: H-Mode und H-Mode ähnliche Erscheinungen bei NI. W7-AS Workshop, IBZ Garching 1993.

358. Baldzuhn, J.: He-Gaspuff - Experimente am W7-AS mit CXRS. W7-AS Seminar, Garching 1993.

359. Ballico, M.: A Self-Consistent Calculation of the Current Distribution in an ICRH Antenna. Technologie Seminar "Heizung", Schloß Ringberg, Tegernsee 1993.

360. Ballico, M.: ICRH: W7-AS Stellarator and Stellarators Worldwide. Technologie Seminar "Heizung", Schloß Ringberg, Tegernsee 1993.

361. Becker, W.: Konditionieren der ICRH-Vakuumleitungen und Antennen. Technologie Seminar "Heizung", Schloß Ringberg, Tegernsee 1993.

362. Becker, W.: PC-Datenerfassung für "langsame" Vorgänge (Temperatur, Vakuum, usw.). Technologie Seminar "Heizung", Particle Balance in Fusion Experiments. Plasma Boundary Physics Phenomena in Tokamaks and Stellarators. Santander 1993.

363. Behrisch, R.; Eckstein, W.: The Importance to Understand the Interaction of Low Energy Light Ions with Solids for the Control of the Plasma Wall Interaction in Fusion Research. Hahn-Meitner-Inst., Berlin 1993.

364. Behrisch, R.: Contribution of the Vessel Walls to the Hydrogen, Schloß Ringberg, Tegernsee 1993.

365. Behrisch, R.: Impurity Production due to Plasma Wall Interaction in Fusion Experiments. Plasma Boundary Physics Phenomena in Tokamaks and Stellarators. Santander 1993.

366. Behrisch, R.: Modification of the Carbon and Beryllium Walls in JET by Erosion, Redeposition and Deuterium Trapping after the 1991 Discharge Period. JET-Seminar, Abingdon 1993.

367. Behrisch, R.; Naujoks, D.: Boundary Conditions at the Vessel Walls Being in Contact with a Hot Plasma. 4th Int. Workshop "Plasma Edge Theory in Fusion Devices", Varenna 1993.

368. Behrisch, R.; Naujoks, D.; Coad, J.P.:* Materialtransport an Gefäßwänden magnetisch eingeschlossener Plasmen. Verhandl. DPG (VI), **28**, 91, P13.2 (1993).

369. Bergmann, A.: 2d-PIC-Simulation der Debye-Schicht vor einer Langmuirsonde im Magnetfeld. Verhandl. DPG (VI) **28**, 99, P14.26 (1993).

370. Bertel, E.: Adsorbatplatz-Bestimmung mit Hilfe von Oberflächenzustands-Spektroskopie? Seminar Physik Dept., Techn. Univ. München 1993.

371. Bertel, E.: Adsorption of Atomic Hydrogen on Cu(110): Sticking, Reconstruction and Electronic Surface States. Int. Workshop on Hydrogen Adsorption, Techn. Univ. München 1993.

372. Bertel, E.: Eindimensionale Oberflächenzustände an H/Ni(110). Workshop Oberflächenphysik, Erlangen 1993.

373. Bertel, E.: Oberflächenzustände: Lokale Bindungen und Rekonstruktion. Kolloquium, Univ. Bochum 1993.

374. Bessenrodt-Weberpals, M.: Diagnostik heißer Laborplasmen. Univ. Düsseldorf, SS 1993.

375. Bessenrodt-Weberpals, M.: Plasma-Material-Bearbeitung. Univ. Düsseldorf, WS 1993/94.

376. Bessenrodt-Weberpals, M.: Plasmaphysik in technischen Anwendungen. Univ. Düsseldorf, WS 1992/93.

377. Bessenrodt-Weberpals, M.: Symbiose von Hoch- und Niedertemperatur-Plasmaphysik in Tokamakentladungen. Physikal. Kolloquium, Ruhr-Univ. Bochum 1993.

378. Beyer, H.; Gündel, H.; Kornejew, O.; Kornejew, P.; Rudolph, R.: Spektroskopische Messung der Neutralgastemperatur an diffusionsgekühlten Hf-Entladungen. Verhandl. DPG (VI) **28**, 110, P14.66 (1993).

379. Biener, J.; Schenk, A.; Winter, B.; Küppers, J.: HREEL Spectroscopy of Thin Ion Beam Deposited C:H(D) Films. Vibrations at Surfaces VII, Santa Margherita 1993.

380. Biener, J.; Schenk, A.; Winter, B.; Lutterloh, C.; Schubert, U.A.; Küppers, J.: Hydrogenation of Amorphous C:H Surfaces by Thermal H(D) Atoms. 13th Europ. Conf. Surface Science, Warwick 1993.

381. Biener, J.; Schenk, A.; Winter, B.; Lutterloh, C.; Schubert, U.A.; Küppers, J.: Structure and Thermal Decomposition of Thin Ion-Beam Deposited C:H Films. Verhandl. DPG (VI) **28**, 1616, SF29.4 (1993).

382. Bischler, U.; Bertel, E.:* One Dimensional Surface States on a Metal Surface: H on Ni(110). 13th Europ. Conf. Surface Science, Warwick 1993.

383. Bischler, U.; Bertel, E.:* One-Dimensional Surface States: Chain States and the Streaky H/Ni(110) Phase. Verhandl. DPG (VI) **28**, 1515, SF9.7 (1993).

384. Biskamp, D.: Examples of Systems with Fast Reconnection. Spring Coll. on Plasma Physics, Int. Centre Theoret. Physics, Trieste 1993.

385. Biskamp, D.: MHD Turbulence and Turbulent Reconnection. Spring Coll. on Plasma Physics, Int. Centre Theoret. Physics, Trieste 1993.

386. Biskamp, D.: Scaling Properties and Small-Scale Current Structures in MHD Turbulence. Invited Talk. 5th Europ. Fusion Theory Conf., Madrid 1993.

387. Biskamp, D.: Stationary Models of Magnetic Reconnection. Spring Coll. on Plasma Physics, Int. Centre Theoret. Physics, Trieste 1993.

388. Bohmeyer, W.; Herrmann, A.; Kammeyer, M.; Kornejew, P.; Pasch, E.; Reiner, H.-D.; Behrendt, H.; Dietrich, L.; Greuner, H.; Grote, H.: Erste Ergebnisse zu einer Hochstrom-Bogenentladung zur

Simulation des Randplasmas einer Fusionsanlage. Verhandl. DPG (VI) **28**, 80, P8.3 (1993).

389. Boozer, A.H.: Changes in the Tokamak Current During MHD Activity. Int. Sherwood Fusion Theory Conf., Newport 1993.

390. Bosch, H.-S.: Kernfusion - Stand der Forschung. EVS-Seminar: Energie und Umwelt heute - Zukunftsperspektiven, Höfen/Enz 1993.

391. Bosch, H.-S.: Plasmaphysik und Fusionsforschung I. Univ. Augsburg, WS 1993/94.

392. Bosch, H.-S.; Haas, G.; Meisel, D.: Erste Ergebnisse der Helium Neutralgasmessung im Divertor von ASDEX-Upgrade. Verhandl. DPG (VI) **28**, 83-84, P9.6 (1993).

393. Bosch, H.-S.; Schneider, R.; Neuhauser, J.; Herrmann, A.; et al.: Model Validation at IPP: ASDEX and ASDEX-Upgrade. EC Meeting on Edge Modelling of ITER Conditions, Garching 1993.

394. Bosch, H.-S.; Schneider, R.; Reiter, D.; Neuhauser, J.; Baelmans, T.; Kastelewicz, H.; Wunderlich, R.; Lackner, K.; Kaufmann, M.; et al.:* 2-D Modellierung der Plasmarandschicht im Tokamak: von ASDEX bis zu ITER. Verhandl. DPG (VI) **28**, 82, P.9.2 (1993).

395. Brakel, R.; Burhenn, R.; Grigull, P.; Hartfuß, H.-J.; Kühner, G.; Stroth, U.; WVII-AS-Team; ECRH-Group: Isotopeneffekt in W7-AS. Garching 1993.

396. Brakel, R.; WVII-AS-Team; ECRH-Group: Vergleich von He-Glimmentladung und Borierung zur Wandkonditionierung in W7-AS. Garching 1993.

397. Brambilla, M.: H.F. Wave Equations in Non-Homogeneous Plasmas and FEL Techniques for their Numerical Solution. Univ. Bochum 1993.

398. Braun, F.: ICRH Generatoren. Technologie Seminar "Heizung", Schloß Ringberg, Tegernsee 1993.

399. Brinkschulte, H.: HF-Konditionieren, HF-Vakuumfenster. Technologie Seminar "Heizung", Schloß Ringberg, Tegernsee 1993.

400. Büchse, R.: Kernfusion - Reale Option oder ewiger Traum. Hannover 1993.

401. Burhenn, R.: Iota Abhängigkeit des Transports. Garching 1993.

402. Burhenn, R.; Brakel, R.; Grigull, P.; Hartfuß, H.-J.; Jänicke, R.; Kühner, G.; Sardei, F.; Stroth, U.; Weller, A.; WVII-AS-Team; ECRH-Group; NI-Group: Dependence of Transport on Rotational Transform in W7-AS. Garching 1993.

403. Camargo, S.J.: Renormalization Group in Magnetohydrodynamic Turbulence. Univ. Sao Paulo 1993.

404. Carlson, A.: Langmuir Probes in Strong Magnetic Fields. Austin 1993.

405. Chodura, R.: Boundary Conditions of a Multifluid Plasma at an Absorbing Target. Varenna 1993.

406. Chodura, R.; Igitkhanov, Yu.L.: Boundary Conditions for Fluid Equation with Non-Local Transport. Verhandl. DPG (VI) **28**, 79, P7.6 (1993).

407. Ciric, M.: Generatoren für HF-Plasmaquellen. Technologie Seminar "Heizung", Schloß Ringberg, Tegernsee 1993.

408. Cramer, J.; Bertel, E.: Die unbesetzte Bandstruktur von Ethylen auf Ni(110). SFB-Seminar, Filzmoos 1993.

409. Detzel, Th.; Fauster, Th.; Memmel, N.: Growth and Stability of Ultrathin Iron Films on Cu(001) Studied by LEIS. Verhandl. DPG (VI) **28**, 1598, SF24.6 (1993).

410. Detzel, Th.; Fauster, Th.; Memmel, N.: Growth of Ultrathin Iron Films on Cu(001) Studied by LEIS. 3rd Conf. Analysis by a Combination of Ion Beam and Surface Specific Techniques, Namur 1993.

411. Dietrich, E.: Mathematical Studies on 1-D Hydrodynamical SOL Models with Non-Local Boundary Conditions. 4th Int. Workshop "Plasma Edge Theory in Fusion Devices", Varenna 1993.

412. Donath, M.: Surface and Thin Film Magnetism Probed by Spin-Polarized Electrons. Seminaire IPCMS, Strasbourg 1993.

413. Dose, V.: Inverse Photoemission. Stellenbosch 1993.

414. Dose, V.: Maximum Entropy Advanced Data Reduction. Univ. Pretoria 1993.

415. Dose, V.: Multivariate Analysis of PECVD Data. Atomic Energy Commission, Pretoria 1993.

416. Dose, V.: Neues von der Röntgenbremsstrahlung. Kolloquium, Kiel 1993.

417. Dose, V.: Nuclear Fusion - Concepts and Perspectives. Inst. of Physics, Budapest; Nat. Accelerator Center, Kapstadt; Univ. Bloemfontein; Univ Pretoria 1993.

418. Du Plessis, J.; Taglauer, E.: Surface Concentration Modification of PtPd Alloys by Noble Gas Ion Sputtering. 5th Europ. Conf. on the Application of Surface and Interface Analysis, Catania 1993.

419. Düchs, D.: Gleichgewichte magnetisierter Plasmen und deren (numerische) Berechnung. Univ. Bochum, SS 1993.

420. Düchs, D.: Status of Fusion Theory in Europe. Special Session. 5th Europ. Fusion Theory Conf., Madrid 1993.

421. Düchs, D.: Transporteigenschaften magnetisierter Fusionsplasmen. Univ. Bochum, WS 93/94.

422. Eckstein, W.: Computer Simulation of Ion-Solid Interactions I and II. Univ. Nova de Lisbon, 1993.

423. Eckstein, W.: Data Collection at IPP. IAEA Advisory Group Meeting, Vienna 1993.

424. Eckstein, W.: Threshold Behaviour of Sputtering. IAEA, Vienna 1993.

425. Eckstein, W.; Behrisch, R.; Scherzer, B.; Roth, J.: Properties of Beryllium as a Plasma Facing Material. Workshop on Beryllium for Fusion Applications, Karlsruhe 1993.

426. Ekedahl, A.; Baranov*, Y.; Bhatnagar* S.; Söldner, F.X.; et al.:* Analysis of ICRF-Enhanced Lower Hybrid Current Drive on JET and Mode Conversion of the Fast Wave. Bull. Am. Phys. Soc. **38**, 2055, 7R 12 (1993).

427. Endler, M.; Giannone, L.; Niedermeyer, H.; Rudyj, A.; Theimer, G.: Fluktuationen in der Abschälschicht von toroidalen Plasmaeinschlußexperimenten. Verhandl. DPG (VI) **28**, 82, P9.1 (1993).

428. Erckmann, V.: ECRH and ECCD with 70 and 140 GHz at the W7-AS Stellarator. Nizhny Novgorod 1993.

429. Erckmann, V.: Heizung und Stromtrieb bei der Elektronen Zyklotron Resonanz am W7-AS. Stuttgart 1993.

430. Erckmann, V.: Overview on W7-AS Results with 140 GHz ECRH. Garching 1993.

431. Erckmann, V.: Recent Results from the W7-AS Stellarator. Princeton 1993.

432. Erckmann, V.: Recent Results with 140 GHz ECRH at the W7-AS Stellarator. Naka 1993.

433. Erckmann, V.: Status of Collective Thomson Scattering Experiments at 70 GHz and 140 GHz on W7-AS. Garching 1993.

434. Faugel, H.: Phasenmessung und Regelung. Technologie Seminar "Heizung", Schloß Ringberg, Tegernsee 1993.

435. Feist, J.-H.: First Results from the RF Source on the Large Testbed. Joint Development Comm. Meeting, Culham 1993.

436. Feist, J.-H.: High-Heat Flux Panels und ihre Kühlsysteme. Technologie Seminar "Heizung", Schloß Ringberg, Tegernsee 1993.

437. Feist, J.-H.: NBI-Systeme im IPP, Vergleich JET, DIII-D, JT-60 U etc. Technologie Seminar "Heizung", Schloß Ringberg, Tegernsee 1993.

438. Feist, J.-H.: Negative Ionen: Notwendigkeit, Probleme, derzeitiger Entwicklungsstand. Technologie Seminar "Heizung", Schloß Ringberg, Tegernsee 1993.

439. Feist, J.-H.: Results from the AUG-NI Testbed. Joint Development Comm. Meeting, Garching 1993.

440. Feist, J.-H.: Simulation of Space Charge Effects in the AUG-NI Reflection Magnet. Joint Development Comm. Meeting, Culham 1993.

441. Feist, J.-H.: Zwei Jahre Teststandbetrieb: Erfahrungen und Empfehlungen. Technologie Seminar "Heizung", Schloß Ringberg, Tegernsee 1993.

442. Feng, Y.; Kißlinger, J.; Sardei, F.: Implementierung des EIRENE Code für Teilchenbilanz und Randschichttransport am W7-AS. Garching 1993.

443. Fiedler, S.: Lithium Beams for Fusion Plasma Diagnostics. Pichl 1993.

444. Field, A.; Fußmann, G.; Lieder, G.; Pitcher, C.S.; Schumacher, U.; ASDEX-Upgrade-Team:* Interpretation of the Line Emission from the Divertor Region of ASDEX-Upgrade in Terms of Divertor Plate Erosion. Verhandl. DPG (VI) **28**, 88, P9.3 (1993).

445. Friedl, A.; Fukarek, W.; Möller, W.: Real Time in-situ Ellipsometric Investigation of C:H Film Growth. Verhandl. DPG (VI) **28**, 1591, SF22.76 (1993).

446. Fritsch, R.: Vakuumdichte Keramikverbindungen in ICRH-Elementen. Technologie Seminar "Heizung", Schloß Ringberg, Tegernsee 1993.

447. Fuchs, J.C.: Bolometer Tomography at ASDEX Upgrade. JET Symposium, Culham 1993.

448. Fuchs, J.C.; Lackner, K.; Mast, K.-F.: Zweidimensionale Entfaltung von Bolometersignalen an ASDEX-Upgrade. Verhandl. DPG (VI) **28**, 116, P14.86 (1993).

449. Fukarek, W.: In-situ Ellipsometrie bei der Schichtabscheidung aus Plasmen. Forschungszentrum Rossendorf 1993.

450. Garcia-Rosales, C.: Erosion Processes in Plasma Wall Interaction. Invited Talk. 6th Int. Conf. on Fusion Reactor Materials, Stresa 1993.

451. Garcia-Rosales, C.: Sputtering and Surface Composition Modifications of Ti Doped Graphite RG-Ti at Temperatures up to 2000 K. 6th Int. Conf. on Fusion Reactor Materials, Stresa 1993.

452. Garcia-Rosales, C.: Surface Near Depletion of Dopants. 6th Int. Workshop on Carbon Materials, Jülich 1993.

453. Garcia-Rosales, C.: Technisch einsetzbare niedrig Z Materialien für den Divertor II. ASDEX-Upgrade Seminar, Schloß Ringberg, Tegernsee 1993.

454. Gasparino, U.: Electron Cyclotron Current Drive and Bootstrap Current. Madrid 1993.

455. Gasparino, U.: Response of ECRH/ECCD to Power Modulation and Trapped/Passing Particle Coupling. 5th Joint Russian-German Meeting on ECRH and Gyrotrons, Garching 1993.

456. Geiger, J.: Gleichgewichtsrechnungen mit freiem Rand für W7-AS mittels VMEC. Garching 1993.

457. Geiger, J.; WVII-AS-Team; NI-Team: 3-dim. Magnetohydrodynamische Gleichgewicht mit freiem Rand für W7-AS. Verhandl. DPG (VI) **28**, 98, P14.21 (1993).

458. Geist, T.: Gyrotron Stray Radiation Suppression Filters for ECE Radiometers. Garching 1993.

459. Giannone, L.: Measurements of Electron Thermal Conductivity Using ECRH Power Modulation in W7-AS. Technologie Seminar "Heizung", Schloß Ringberg, Tegernsee 1993.

460. Grieger, G.: Evolution of Toroidal Magnetic Confinement. Jülich 1993.

461. Grieger, G.: Fusion Power Coordinating Committee-Report to CERT. Paris 1993.

462. Grieger, G.: Introduction - Status of the W7-X Project - Goals of the Meeting - Approval of the Agenda. W7-X Stellarator Meeting, Schloß Ringberg, Tegernsee 1993.

463. Grieger, G.: Lunar Mining for ^{3}He, Power Generation by Thermonuclear Fusion. Dijon 1993.

464. Grieger, G.: Overview on Expected Reactor Properties and Tasks for W7-X - Summary and Conclusions of the EURATOM Ad-Hoc Group. Presentation of the Wendelstein 7-X Stellarator Project. NET, Garching; PPPL, Princeton; GA, San Diego 1993.

465. Grieger, G.: Stellarator Reactor Studies (Wendelstein 7-Line). UCLA, Los Angeles 1993.

466. Grieger, G.: Thermonukleare Fusion, ein Beitrag zur langfristigen Energieversorgung?! "Saterra - Zurück zur Vernunft". Mittweida 1993.

467. Grieger, G.: Wendelstein 7-X - An Integrated Concept Test on the Reactor Potential of Advanced Stellarators. Workshop on Physics Issues to be Investigated in Parallel with ITER and Required Devices. Cadarache 1993.

468. Grieger, G.: Wendelstein 7-X. Joint Working Group II, Brussels 1993.

469. Grieger, G.: What a Wendelstein Stellarator Reactor Looks Like. Workshop on Physics Issues to be Investigated in Parallel with ITER and Required Devices. Cadarache 1993.

470. Grieger, G.; Nührenberg, J.; Renner, H.; Sapper, J.; Wobig, H.: Stellarator Reactor Studies and Related Technology Activities in the European Community. UCLA, Los Angeles 1993.

471. Grigull, P.: Besonderheiten der Randschicht in Stellaratoren unter Berücksichtigung neuerer W7-AS Resultate. Berlin 1993.

472. Grigull, P.: The Scrape-Off Layer in Stellarators: Topological Features and Experimental Results. Santander 1993.

473. Grigull, P.; Herre, G.; Sardei, F.: Neuere Randschicht-Untersuchungen am W7-AS. Garching 1993.

474. Grote, H.; Behrendt, H.; Bohmeyer, W.; Dietrich, L.; Greuner, H.: Aufbau einer Hochstrom-Bogenentladungsanlage zur Simulation des Randplasmas einer Fusionsanlage. Verhandl. DPG (VI) **28**, 108, P14.57 (1993).

475. Gruber, O.: Anforderungen des Tokamak Programms an die Heizung. Schloß Ringberg, Tegernsee 1993.

476. Gruber, O.: Diagnostics for Plasma Control: ASDEX Upgrade --> ITER. Naka 1993.

477. Gruber, O.: Magnetische Topologie in Phase II und Phase III. Schloß Ringberg, Tegernsee 1993.

478. Gruber, O.: Untersuchungen zum Energieeinschluß. Schloß Ringberg, Tegernsee 1993.

479. Gruber, O.; et al.: Heating (Status and Prospects) and H-Mode Results in ASDEX Upgrade. Toki-City 1993.

480. Gruber, O.; et al.: PF Coils, Equilibrium and Vertical Stability of the ITER EDA Design. Naka 1993.

481. Gruber, O.; ASDEX-Upgrade-Team: Plasma Control on ASDEX Upgrade and Possible Extension to ITER. Naka 1993.

482. Gruber, O.; Lackner, K.; Pautasso, G.; Seidel, U.; Streibl, B.: Vertical Displacement Events and Halo Currents. Lisbon 1993.

483. Hacker, H.; Burhenn, R.; W7-AS-Team; ECRH-Group; NI-Team: Radial aufgelöste Messungen der VUV-Linienstrahlung als Beitrag zum Verunreinigungstransport in W7-AS Plasmen. Greifswald 1993.

484. Hantzsche, E.: Plasmaexpansionsmodell mit variablem Coulomblogarithmus und mit Neutralkomponente. Verhandl. DPG (VI) **28**, 96, P14.15 (1993).

485. Harmeyer, E.; Kißlinger, J.; Rau, F.; Wobig, H.: Magnetic Field and Force Distribution in Modular Stellarator Coil Configurations. 9th COMPUMAG Conf. on the Computation of Electromagnetic Fields, Miami 1993.

486. Hartfuß, H.-J.: Störexperimente zur Bestimmung der Elektronenwärmeleitung an W7-AS. Garching 1993.

487. Hartfuß, H.-J.: Transport Studies Using ECRH Power Modulation on W7-AS. Garching 1993.

488. Hartfuß, H.-J.; Erckmann, V.; Gasparino, U.; Giannone, L.; Maaßberg, H.; WVII-AS-Team: Heat Wave Studies on W7-AS. Varenna 1993.

489. Hartfuß, H.-J.; Sattler, S.; WVII-AS-Team: Evidence for Temperature Fluctuations in the W7-AS Stellarator. Varenna 1993.

490. Hartfuß, H.-J.; W7-AS-Team: Experimente zu Einschluß und Transport am Stellarator W7-AS. Greifswald 1993.

491. Heinrich, O.; Schneider, R.; Verbeek, H.; Reiter, D.; Neuhauser, J.; ASDEX-Team; W7-AS-Team:* Ionentemperaturen am Plasmarand von ASDEX und Wendelstein 7-AS. Greifswald 1993.

492. Herre, G.; Rudyj, A.; Endler, M.; Giannone, L.; Niedermeyer, H.; WVII-AS Team: Fluktuationsuntersuchungen am Stellarator Wendelstein 7-AS. Greifswald 1993.

493. Hildebrandt, D.: Ergebnisse von Depositionsproben W7-AS. W7-AS-Workshop, Garching 1993.

494. Hirsch, M.: Neue Ergebnisse der Reflektometrie. Garching 1993.

495. Hoffmann, C.: Chaotische Dynamik schwingender Systeme. Technologie Seminar "Heizung", Schloß Ringberg, Tegernsee 1993.

496. Hoffmann, C.: Plasmaheizung mit Radiowellen. Technologie Seminar "Heizung", Schloß Ringberg, Tegernsee 1993.

497. Hofmann, J.V.; WVII-AS-Team; ECRH-Group; NI-Group: Poloidale und Toroidale Rotation in Wendelstein 7-AS. Garching 1993.

498. Hofmeister, F.: Anpassung bei ICRH: Möglichkeiten, Stand, Weiterentwicklung. Technologie Seminar "Heizung", Schloß Ringberg, Tegernsee 1993.

499. Hofmeister, F.: Verzahnung zwischen Steuerung und Datenerfassung. Technologie Seminar "Heizung", Schloß Ringberg, Tegernsee 1993.

500. Igitkhanov, Yu.L.: Implication of Kinetic Effects for Fluid Codes. Varenna 1993.

501. Igitkhanov, Yu.L.: Impurity Transport in the Edge Tokamak Plasma. Santander 1993.

502. Igitkhanov, Yu.L.: Kinetic Effects in the Tokamak Plasma. Santander 1993.

503. Igitkhanov, Yu.L.; Kukushkin A.S.; Runov, A.M.; Chodura, R.:* Application of BGK Collision Operator for Kinetic Correction of Fluid Models. Varenna 1993.

504. Igitkhanov, Yu.L.; Mikhailov, M.I.; Feneberg, W.:* Fluid Description of Edge Plasma Transport in a Non-Orthogonal Coordinate System. Varenna 1993.

505. Igitkhanov, Yu.L.; Naujoks, D.: Selfconsistent Description of Sputtering in the Edge Boundary Plasma. Verhandl. DPG (VI) **28**, 123, P15.22 (1993).

506. Jänicke, R.: Iota Scan vom 17.8.93: Unterschiede, Profile, Fluktuationen. Garching 1993.

507. Jänicke, R.: Überlegungen zum H-Mode Arbeitspunkt. Garching 1993.

508. Junker, J.: Diagnostics at W7-AS and W7-X. W7-X Stellarator Meeting, Schloß Ringberg, Tegernsee 1993.

509. Jüttner, B.; Büchl, K.; Weinlich, M.; ASDEX-Upgrade-Team: Arcing in ASDEX-Upgrade. 4th Int. Workshop "Plasma Edge Theory in Fusion Devices", Varenna 1993.

510. Kallenbach, A.; Endler, M.; Fußmann, G.; Kiemer, K.; Lieder, G.: Über die Messung von Elektronendichteschwankungen aus der

Strahlungsemission ionisierender Teilchen. Verhandl. DPG (VI) **28**, 97, P14.18 (1993).

511. Kardaun, O.; Kus, A.: Density Dependence of the Confinement Time According to the H-Mode Database ITERH.DB2. H-Mode Database Working Group Meeting, JET, Abingdon 1993.

512. Kardaun, O.; Kus, A.: Interaction and Residual Analysis of the H-Mode Confinement Database. H-Mode Database Working Group Meeting, JET, Abingdon 1993.

513. Kardaun, O.; Kus, A.: Offset-Linear Scalings Based on ITERH.DB2. H-Mode Database Working Group Meeting, Naka 1993.

514. Kardaun, O.; Stroth, U.; Gruber, O.; Martin, P.: On ASDEX's Contribution of the Profile Database. H-Mode Database Working Group Meeting, Naka 1993.

515. Kardaun, O.; Stroth, U.; Gruber, O.; Martin, P.: Profile Data Based on TRANSP at ASDEX. H-Mode Database Working Group Meeting, JET, Abingdon 1993.

516. Kasparek, W.:* Übersicht über ECRH-Systeme, Energieübertragung und Antennen. Technologie Seminar "Heizung", Schloß Ringberg, Tegernsee 1993.

517. Kasparek, W.; Brinkschulte, H.; Leuterer, F.; Münich, M.; Zouhar, M.:* The ASDEX-Upgrade ECRH Transmission System. 5th Joint Russian-German Meeting on ECRH and Gyrotrons, Garching, Stuttgart, Karlsruhe 1993.

518. Kastelewicz, H.; Schneider, R.; Neuhauser, J.; Reiter, D.; Braams*, B.; Wenzel, U.; Büchl, K.:* Marfe-Rechnungen für ASDEX-Upgrade. Verhandl. DPG (VI) **28**, 98, P14.23 (1993).

519. Kaufmann, M.: ASDEX Upgrade Results. Report to the Fachbeirat, Garching 1993.

520. Kaufmann, M.: Edge Physics, H-Mode, and Other Studies in ASDEX Upgrade. PPPL, Princeton 1993.

521. Kaufmann, M.: Erzeugung sehr hoher Temperaturen. Bad Honnef 1993.

522. Kaufmann, M.: IPP Tokamak Programme: Medium and Long Term. Brussels 1993.

523. Kaufmann, M.: Temperatur in Plasmen/Fusionsreaktor. Bad Honnef 1993.

524. Kaufmann, M.: Wo steht die Fusionsforschung? Garching 1993.

525. Keudell, A. von: Das Wachstum von amorphen C:H-Filmen. Forschungszentrum Rossendorf 1993.

526. Keudell, A. von; Fukarek, W.; Möller, W.: On the Temperature Dependent Growth of Hydrocarbon Layers. Verhandl. DPG (VI) **28**, 1510, SF8.4 (1993).

527. Kick, M.: Experimental Status of the "Advanced Stellarator" W7-AS. Köln 1993.

528. Knobloch, A.F.: Reaktoraspekte (Konfiguration, Wirkungsgrad etc.). Technologie Seminar "Heizung", Schloß Ringberg, Tegernsee 1993.

529. Konrad, C.: Erste Meßergebnisse der Mikrowellenstreuung am Wendelstein 7-AS. Garching 1993.

530. Konrad, C.; Hartfuß, H.-J.; Siller, G.: Kohärente Mikrowellenstreuung am Fusionsexperiment Wendelstein 7-AS. Verhandl. DPG (VI) **28**, 133, P15.60 (1993).

531. Kratochwil, Th.; Wittmann*, M.; Küppers, J.:* Adsorption of Ethanol on Ni(100) Surfaces. Vibrations at Surfaces VII, Santa Margherita 1993.

532. Kratochwil, Th.; Wittmann*, M.; Küppers, J.:* Adsorption of Ethanol on Ni(100) Surfaces. Verhandl. DPG (VI) **28**, 1616, SF29.6 (1993).

533. Kraus, W.: A High Power RF Plasma Source for Neutral Beam Injection Systems. 2nd German-Russian Conference on Electric Porpulsion Engines and their Technical Applications. Moscow 1993.

534. Kraus, W.: Erzeugung und Neutralisation von negativen Wasserstoff-Ionen durch HF-Plasmen. Technologie Seminar "Heizung", Schloß Ringberg, Tegernsee, 1993.

535. Krieger, K.: Divertor Retention Studies by Means of Impurity Gas Puffing. GA, San Diego 1993.

536. Krieger, K.: Plasma Wall Interaction in Nuclear Fusion Devices. IPP Summer Univ. for Plasma Physics, Garching 1993.

537. Krieger, K.; Roth, J.; Hofmann, J.V.: Untersuchung des Kohlenstoff- und Sauerstoffzuflusses am Tokamak ASDEX. Verhandl. DPG (VI) **28**, 83, P9.5 (1993).

538. Kühner, G.: Thomsonstreuung bei nichtthermischer Elektronenverteilung. Garching 1993.

539. Kühner, G.: Vergleich und Zuverlässigkeit von Profilmessungen. Garching 1993.

540. Küppers, J.: Die chemische Erosion von Graphit durch H. Univ. Bochum 1993.

541. Labich, S.: Thermische Desorptionsspektroskopie TDS, CO-Desorption am Rh/TiO_2-Modellkatalysator. Seminar Oberflächenchemie und Katalyse, Univ. München 1993.

542. Lang, P.: Quasicontinuous Refuelling of the Tokamak ASDEX Upgrade with a Centrifuge Pellet Injector. First Carolus Magnus Summer School on Plasma Physics, Vaals 1993.

543. Lang, P.: Status and Recent Results of the AUG Centrifuge Pellet Injector. Techn. Univ. St. Petersburg 1993.

544. Lang, P.: Status of the ASDEX-Upgrade Diagnostics System. Techn. Univ. St. Petersburg 1993.

545. Lang, P.; Andelfinger, C.; Cierpka, P.; Lang, R.; Söldner, F.X.: Erste Testergebnisse der neuentwickelten Pellet-Zentrifuge für ASDEX-Upgrade. Verhandl. DPG (VI) **28**, 73-74, P.3.7 (1993).

546. Lang, R.: First Results of Pellet Injection into ASDEX Upgrade Plasmas. Techn. Univ. St. Petersburg 1993.

547. Laux, M.: Detachment of the Divertor Plasma in ASDEX-Upgrade. JET Seminar, Abingdon 1993.

548. Laux, M.: Probe Measurements in the Divertor Plates of ASDEX-Upgrade. JET Seminar, Abingdon 1993.

549. Laux, M.; Büchl, K.; Carlson, A.; Herrmann, A.; Kastelewicz, H.; Radtke, R.; Wenzel, U.: Detachment of the Divertor Plasma in ASDEX Upgrade. 20th EPS Conf. on Contr. Fusion and Plasma Phys., Lisbon 1993.

550. Laux, M.; Weinlich, M.; Carlson, A.; Günther, K.; Hildebrandt, D.; Neuhauser, J.; Pech, P.; Reiner, H.-D.; Richter, T.; Wolff, H.: Sondencharakteristiken bei flachem Einfall eines starken Magnetfeldes. Verhandl. DPG (VI) **28**, 75, P4.5 (1993).

551. Leuterer, F.: ECRH: Ausblick. Technologie Seminar "Heizung", Schloß Ringberg, Tegernsee 1993.

552. Leuterer, F.: ECRH - Wellenausbreitung, Absorption, Stromtrieb. Technologie Seminar "Heizung", Schloß Ringberg, Tegernsee 1993.

553. Lieder, G.; Napiontek, B.; Radtke, R.; Dorn, C.; Field, A.; Fußmann, G.; Kallenbach, A.; Schumacher, U.: Das Divertorspektrometer an ASDEX-Upgrade. Seminar IPF, Univ. Stuttgart 1993.

554. Lieder, G.; Napiontek, B.; Radtke, R.; Field, A.; Fußmann, G.; Kiemer, K.; Laux, M.; Mayer, H.-M.; Naujoks, D.; Schumacher, U.; Zohm, H.: Spektroskopische Messungen mit hoher räumlicher und zeitlicher Auflösung im Divertor von ASDEX Upgrade. Verhandl. DPG (VI) **28**, 83, P9.4 (1993).

555. Lieder, G.; Radtke, R.; Field, A.; Fußmann, G.; Kallenbach, A.; Kiemer, K.; Mayer, H.-M.; Schumacher, U.; ASDEX-Upgrade-Team; ICRH-Team: Spektroskopische Messungen mit hoher räumlicher und zeitlicher Auflösung im Divertor von ASDEX-Upgrade. Verhandl. DPG (VI) **28**, 83, P9.4 (1993).

556. Linden, W. von der; Donath, M.; Dose, V.: Resolution Enhanced Photoemission-Spectroscopy Based on Maximum Entropy Deconvolution. 13th Int. MaxEnt Workshop, Santa Barbara 1993.

557. Linden, W. von der; Donath, M.; Dose, V.: Maximum Entropy and Hidden Information in Experimental Data: Example: Exchange Splitting in Ni. Verhandl. DPG (VI) **28**, 1199, MA15.2 (1993).

558. Linsmeier, Ch.: Metall-Träger-Wechselwirkungen and Rh/TiO_2-Modellkatalysatoren. Seminar für Oberflächenchemie und Katalyse. Univ. München 1993.

559. Linsmeier, Ch.: Untersuchungen zu 'Strong Metal-Support Interactions' an Modellkatalysatoren. SFB-Seminar, Filzmoos 1993.

560. Linsmeier, Ch.; Knözinger, H.; Taglauer, E.:* Ion Scattering Characterization of SMSI Effects in Rh/TiO_2-Model Catalysts. Europacat-I, Montpellier 1993.

561. Lohnert, H.: Die Hochspannungsanlage des IPP. Technologie Seminar "Heizung", Schloß Ringberg, Tegernsee 1993.

562. Lortz, D.: Teil IV: Thermodynamik. Univ. München, SS 1993.

563. Lortz, D.; Zeiler, A.: Tokamak Stability without Wall Stabilization. 5th Europ. Fusion Theory Conf., Madrid 1993.

564. Martinelli, A.P.; Behrisch, R.; Peacock, A.T.:* Modification of the Carbon and Beryllium Walls in JET by Erosion, Redeposition and Deuterium Trapping after the 1991 Discharge Period. 6th Int. Conf. on Fusion Reactor Materials, Stresa 1993.

565. Mayer, H.-M.; Scherzer, B.; Eckstein, W.: Reflexion and Trapping von Deuterium an Graphit bei niedriger Energie. Verhandl. DPG (VI) **28**, 92, P13.5 (1993).

566. Mayer, H.-M.; Scherzer, B.; Eckstein, W.: Trapping and Reflection Coefficients for Deuterium in Graphite at Low Energy and Oblique Incidence. IBA 11, Balatonfüred 1993.

567. McCormick, K.: Erste Meßergebnisse mit dem Lithiumstrahl. Garching 1993.

568. McCormick, K.: Observed Scaling of SOL Parameters in Tokamaks. 5th Workshop on Magnetic Confinement Fusion: Plasma Boundary Physics Phenomena in Tokamaks and Stellarators, Santander 1993.

569. Melkus, W.: Die Hochspannungsmodulatoren der Heizsysteme. Technologie Seminar "Heizung", Schloß Ringberg, Tegernsee 1993.

570. Memmel, N.: Das Wachstum ultradünner Eisenschichten auf Cu(001). Workshop Oberflächenphysik, Erlangen 1993.

571. Memmel, N.: Growth, Structure and Stability of Ultrathin Iron Films on Cu(001). Seminar über Ordnung und Unordnung an Oberflächen, Garching 1993.

572. Memmel, N.: Growth, Structure and Stability of Ultrathin Iron Films on Cu(001). 13th Europ. Conf. Surface Science, Warwick 1993.

573. Memmel, N.: Wachstum, Struktur und Stabilität ultradünner Eisen Filme auf Cu(001). Poster. SFB-Seminar, Filzmoos 1993.

574. Merkel, P.: The Neumann Problem in Toroidal Domains Solved by an Integral Equation Technique for the Surface Current. Int. Sherwood Fusion Theory Conf., Newport 1993.

575. Meyer-Spasche, R.: Gleichgewichte und Stabilität II. Techn. Univ. München, WS 1992/93.

576. Meyer-Spasche, R.: Real Life Problems. Postgraduate Course on Reaction-Diffusion Equations. Univ. Basel 1993.

577. Meyer-Spasche, R.: Vom Gleichgewicht zum Chaos: Bifurkationsprobleme. Techn. Univ. München, SS 1993.

578. Meyer-Spasche, R.: Vom Gleichgewicht zum Chaos: nichtlineare Dynamik. Techn. Univ. München, WS 1993/94.

579. Monaco, F.: Steuerung und Überwachung der ECRH-Anlage. Technologie Seminar "Heizung", Schloß Ringberg, Tegernsee 1993.

580. Münich, M.: Gyrotrons und Gyrotronbetrieb. Technologie Seminar "Heizung", Schloß Ringberg, Tegernsee 1993.

581. Naujoks, D.; Roth, J.; Field, A.; Krieger, K.; Laux, M.; Lieder, G.: Erosions- und Redepositionsmessungen im ASDEX-Upgrade Divertor. Verhandl. DPG (VI) **28**, 123, P15.23 (1993).

582. Neu, R.; ASDEX-Upgrade-Team: X-Ray Diagnostics at ASDEX Upgrade. First Carolus Magnus Summer School on Plasma Physics, Vaals 1993.

583. Neu, R.; Fußmann, G.; Schumacher, U.: Bestimmung der Sauerstoffkonzentration in ASDEX-Upgrade aus der Intensität der OVIII (2p-1s) Strahlung. Verhandl. DPG (VI) **28**, 97, P14.19 (1993).

584. Niedermeyer, H.: Der Macintosh als Werkzeug des Physikers. Garching 1993.

585. Niedermeyer, H.; Balbin, R.; Carlson, A.; Endler, M.; Estrada*, T.; Geist, T.; Giannone, L.; Hartfuß, H.-J.; Hidalgo*, C.; Holzhauer, E.; Konrad, C.; Rudyj, A.; Sanchez*, J.; Sattler, S.; Siller, G.; Theimer, G.; Weinlich, M.; WVII-AS-Team:* Random Fluctuations of Density Temperature and Potential in Wendelstein 7-AS. Nieuwegein 1993.

586. Niedermeyer, H.; Balbin, R.; Carlson, A.; Endler, M.; Giannone, L.; Hidalgo*, C.; Holzhauer, E.; Rudyj, A.; Theimer, G.; Weinlich, M.; WVII-AS-Team:* Edge Turbulence in ASDEX and W7-AS. Newport 1993.

587. Niedermeyer, H.; Balbin, R.; Carlson, A.; Endler, M.; Giannone, L.; Hidalgo*, C.; Rudyj, A.; Theimer, G.; Weinlich, M.; WVII-AS-Team:* Turbulence in the Boundary Layer of ASDEX and W7-AS. Cadarache 1993.

588. *Niedermeyer, H.; Baldzuhn, J.; Bomba, B.; Brakel, R.; Burhenn, R.; Cattanei, G.; Dodhy, A.; Dorst, D.; Elsner, A.; Endler, M.; Erckmann, V.; Gasparino, U.; Geist, T.; Giannone, L.; Grigull, P.; Hacker, H.; Hartfuß, H.-J.; Heinrich, O.; Herre, G.; Hildebrandt, D.; Hofmann, J.V.; Jänicke, R.; Karger, F.; Kick, M.; Lazaros, A.; McCormick, K.; Ohlendorf, W.; Pech, P.; Ringler, H.; Rudyj, A.; Sardei, F.; Sattler, S.; Schneider, F.; Schneider, U.; Siller, G.; Stroth, U.; Tutter, M.; Unger, E.; Wagner, F.; Weller, A.; Wolff, H.; Würsching, E.; Zöpfel, S.; et al.:* The LH-Transition on W7-AS. Newport 1993.

589. *Noterdaeme, J.-M.:* ICRH: AUG, Tokamaks weltweit. Technologie Seminar "Heizung", Schloß Ringberg, Tegernsee 1993.

590. *Noterdaeme, J.-M.; Europ.-ICRF-Teams:* ITER Technical Meeting on RF Heating and Current Drive. Garching 1993.

591. *Noterdaeme, J.-M.; Ballico, M.; Brambilla, M.; Hoffmann, C.:* ITER ICRF System Design: Coupling and Heat Deposition Profiles. 7th Meeting of the Coordinating Comm. on Fast Wave Current Drive and Heating, Culham 1993.

592. *Noterdaeme, J.-M.; ICRH-Team; ASDEX-Upgrade-Team:* Plans for Screenless Antenna Operation at IPP. 6th Meeting of the Coordinating Comm. on Fast Wave Current Drive and Heating, Stockholm 1993.

593. *Noterdaeme, J.-M.; Brambilla, M.; Hoffmann, C.; ICRH-Team:* Recent Results from ASDEX-Upgrade and Contribution to ITER. 5th Meeting of the Coordinating Comm. on Fast Wave Current Drive and Heating, Culham 1993.

594. *Nührenberg, J.:* Divertor for W7-X. W7-X Stellarator Meeting, Schloß Ringberg, Tegernsee 1993.

595. *Nührenberg, J.:* Stellarator Optimization. Presentation of the Wendelstein 7-X Stellarator Project. NET, Garching; PPPL, Princeton; GA, San Diego 1993.

596. *Nührenberg, J.:* Theory of Neoclassical and Anomalous Transport in Stellarators. Workshop on Physics Issues to be Investigated in Parallel with ITER and Required Devices, Cadarache 1993.

597. *Ott, W.:* Aufbau und Wirkungsweise von Injektoren. Technologie Seminar "Heizung", Schloß Ringberg, Tegernsee 1993.

598. *Ott, W.:* Computation of Space Charge Compensation in Ion Beams - Preliminary Results. Joint Design Comm., Garching 1993.

599. *Passek, F.; Donath, M.; Dose, V.:* Magnetic Surface State on Ni(111) Becomes Non-Magnetic by Oxygen Adsorption. Verhandl. DPG (VI) **28**, 1518, SF10.6 (1993).

600. *Pautasso, G.; Gruber, O.; Lackner, K.; Schneider, W.; ASDEX-Upgrade-Team:* Simulation of Plasma Halo Currents During VDE in ASDEX Upgrade. Verhandl. DPG (VI) **28,** 98, P14.22 (1993).

601. *Penningsfeld, F.-P.:* NBI-Heizung an Stellaratoren. Technologie Seminar "Heizung", Schloß Ringberg, Tegernsee 1993.

602. *Pereverzev, G.V.; Leuterer, F.; Wilhelm, R.:* Estimates on Heat Wave Propagation in ASDEX-Upgrade. 5th Joint Russian-German Meeting on ECRH and Gyrotrons, Garching, Stuttgart, Karlsruhe 1993.

603. *Pfirsch, D.:* Einführung in die Theoretische Plasmaphysik 1 (Mikroskopische Theorie). Techn. Univ. München, SS 1993.

604. *Pfirsch, D.:* Einführung in die Theoretische Plasmaphysik 2 (Makroskopische Theorie). Techn. Univ. München, SS 1993.

605. *Pfirsch, D.:* Nonlinear Instabilities Relating to Negative Energy Perturbations. Univ. New York; Univ. Darmouth 1993.

606. *Pinkau, K.:* Forschungsmotivation und Entscheidungsprozesse in der Großforschung. Garching 1993.

607. *Pinkau, K.:* Forschungsverantwortung und Risikoabschätzung. Garching 1993.

608. *Pinkau, K.:* Fusionsenergie, Möglichkeit zukünftiger Energieversorung. Aachen 1993.

609. *Pinkau, K.:* Fusionsforschung mit toroidalem magnetischem Einschluß. Darmstadt 1993.

610. *Pinkau, K.:* Kernfusion - Forschungsstand und Aussichten. München 1993.

611. *Pinkau, K.:* The European Fusion Research Programme. Tokio 1993.

612. *Pinkau, K.:* Worin gründen die heutigen Vorbehalte gegenüber der Technik? München 1993.

613. *Poschenrieder, W.:* Vakuumphysik und -technologie in der Fusionsforschung. Schule für Vakuumphysik, Bad Honnef 1993.

614. *Puri, S.:* Sources for Bootstrap Current. Technologie Seminar "Heizung", Schloß Ringberg, Tegernsee 1993.

615. *Ramos, G.; Scherzer, B.:* Radiation Damage and Trapping of Helium in HOPG-Graphite. IBA 11, Balatonfüred 1993.

616. *Rau, F.:* Comparison of High-b Discharges in W7-AS at Varied "Mirror Ratio". W7-AS Seminar, Heisenberg-Zentrum, Garching 1993.

617. *Reiter, S.:* Untersuchung gestufter Oberflächen mit Tunnelmikroskopie im UHV. Mitarbeiterseminar Prof. J. Peisl, Univ. München 1993.

618. *Renner, H.:* Divertor Concept for the Modular Stellarator HELIAS Reactor. UCLA, Los Angeles 1993.

619. *Renner, H.:* Divertor Concept for W7-X. Presentation of the Wendelstein 7-X Stellarator Project. NET, Garching; PPPL, Princeton; GA, San Diego 1993.

620. *Renner, H.:* Divertor for W7-X. W7-X Stellarator Meeting, Schloß Ringberg, Tegernsee 1993.

621. *Renner, H.:* Influence of the Magnetic Configuration on the Plasma-Wall Interaction in the Stellarators W7-A and W7-AS. Cadarache 1993.

622. *Renner, H.:* "Island": Ergodised Boundary Target Plates - Integrated Pumps. W7-X Stellarator Meeting, Schloß Ringberg, Tegernsee 1993.

623. *Renner, H.*: Stellarators - Achievements and Perspectives. Cadarache 1993.

624. *Ringler, H.:* Interessante Thomsonprofilmessungen. Garching 1993.

625. *Roth, J.*. Material Problems in Fusion Research. Techn. Univ. Budapest 1993.

626. *Ryter, F..; et al.:* H-Mode Operation und ELMs in ASDEX Upgrade. ASDEX Upgrade Seminar, Schloß Ringberg, Tegernsee 1993.

627. *Ryter, F.; et al.:* H-Mode Results in ASDEX Upgrade. 4th H-Mode Workshop, Naka 1993.

628. *Ryter, F.; et al.:* Perturbative Experiments in Tokamaks: Untersuchungen des lokalen Transports und anderer physikalischer Vorgänge. Technologie Seminar "Heizung", Schloß Ringberg, Tegernsee 1993.

629. *Sandl, P.; Bertel, E.:* Surface States, Local Bonding, and Surface Reconstruction. Verhandl. DPG (VI) **28**, 1523, SF12.2 (1993).

630. *Sandl, P.; Roos, E.; Bertel, E.:* Surface States, Local Bonding, and Surface Reconstruction: Na on Cu(110). 13th Europ. Conf. Surface Science, Warwick 1993.

631. *Sapper, J.:* Stellarator Technology and Heating. Presentation of the Wendelstein 7-X Stellarator Project. NET, Garching; PPPL, Princeton; GA, San Diego; UCLA, Los Angeles 1993.

632. *Sapper, J.:* The Next Generation of Superconducting Stellarator and Helical Devices. Europ. Conf. on Applied Superconductivity, Göttingen 1993.

633. *Sapper, J.; Schauer, F.:* W7-X: Structural Components, Magnet, Cryogenics, Supporting Structure, Vessel, R&D Programme. W7-X Stellarator Meeting, Schloß Ringberg, Tegernsee 1993.

634. *Sardei, F.:* Open Magnetic Surfaces and Resonant Topology for Modelling Plasma Edge Transport in W7-AS. Garching 1993.

635. *Sardei, F.; Grigull, P.; Herre, G.; Kißlinger, J.; Richter-Gloetzl, M.:* Parametrization of Open Magnetic Structures for Modelling Plasma Transport in the Boundary of W7-AS. Varenna 1993.

636. *Sardei, F.; Grigull, P.; Herre, G.; Kißlinger, J.; Richter-Gloetzl, M.; WVII-AS-Team; ECRH-Group:* Open Magnetic Surfaces for Modelling Plasma Transport in the Boundary of Stellarators. El Escorial 1993.

637. *Sattler, S.:* Fluktuationen der Elektronentemperatur gemessen durch Intensitätsinterferometrie an W7-AS. Garching 1993.

638. *Sattler, S.:* Temperature Fluctuation Measurements with a Novel Type Correlation Radiometer on W7-AS. 5th Joint Russian-German Meeting on ECRH and Gyrotrons, Garching 1993.

639. *Sattler, S.; Hartfuß, H.-J.:* Intensitätsinterferometrie, Messung von Temperaturfluktuationen am Stellarator Wendelstein 7-AS. Verhandl. DPG (VI) **28**, 133, P15.59 (1993).

640. *Schimmel*, Th.; Winzer*, B.; Küppers, J.; Schwörer*, M.:* Layer by Layer Growth and Decomposition of an Organic Crystal Observed in Real Time with Scanning Force Microscopy. Verhandl. DPG (VI) **28**, 1527, SF13.4 (1993).

641. *Schimmel*, Th.; Winzer*, B.; Küppers, J.; Schwörer*, M.:* Polymerization and Layer by Layer Growth of Diacetylene Single Crystals Investigated with Scanning Force Microscopy. Polymer and Materials Research Symp., Bayreuth 1993.

642. *Schneider, R.; Reiter*, D.; Neuhauser, J.; Baelmans, T.; Braams*, B.; Kastelewicz, H.:* 2-D Modellierung der Plasmarandschicht im Tokamak: von ASDEX bis zu ITER. Verhandl. DPG (VI) **28**, 82, P14.85 (1993).

643. *Schömann, S.:* Atomoptik und -interferometrie. Seminar MPQ, München 1993.

644. *Schömann, S.:* Exakte Numerik des zweidimensionalen Maxwellschen Rades. Seminar, Univ. München 1993.

645. *Schwab, C.:* 3D Gobal Ideal MHD Stability with the CAS3D Code. NIFS, Nagoya 1993.

646. *Scott, B.:* Asymptotic Expansion Methods in Analytical Models of Turbulence. Univ. of Texas, Austin 1993.

647. *Scott, B.:* Simulation of the Tokamak. Univ. of Texas, Austin 1993.

648. *Söldner, F.X.:* Lower Hybrid Current Drive Scenarios on JET. JET Science Meeting, Culham 1993.

649. *Söldner, F.X.:* Lower Hybrid Launchers on JET. IAEA Meeting on Radio-Frequency Launchers for Plasma Heating and Current Drive, JAERI, Naka 1993.

650. *Söldner, F.X.:* Prospects of Advanced Scenarios on JET in the Light of Recent Experiments. JET Profile Control Seminar, Culham 1993.

651. *Söldner, F.X.:* Status and Programme on ASDEX Upgrade. Techn. Univ. St. Petersburg 1993.

652. *Speth, E.:* NBI-Reaktoranforderungen. Technologie Seminar "Heizung", Schloß Ringberg, Tegernsee 1993.

653. *Speth, E.:* NBI: Ausblick. Technologie Seminar "Heizung", Schloß Ringberg, Tegernsee 1993.

654. *Speth, E.:* Off-Axis-Heizexperimente mit Neutralinjektion. Technologie Seminar "Heizung", Schloß Ringberg, Tegernsee 1993.

655. *Speth, E.:* Physik der Neutralteilchenheizung: Prozesse im Plasma. Technologie Seminar "Heizung", Schloß Ringberg, Tegernsee 1993.

656. *Stäbler, A.:* Experimente mit Neutralinjektion an Tokamaks. Technologie Seminar "Heizung", Schloß Ringberg, Tegernsee 1993.

657. *Stäbler, A.:* Experimente mit NI an Tokamaks - JET, JT 60-U, TFTR, D III-D, AUG. Technologie Seminar "Heizung", Schloß Ringberg, Tegernsee 1993.

658. *Stäbler, A.:* NBI into ASDEX-Upgrade; Commissioning of the System. Joint Development Comm. Meeting, Garching 1993.

659. *Stäbler, A.:* Start of NBI into ASDEX-Upgrade. Joint Development Comm. Meeting, Culham 1993.

660. *Stäbler, A.:* Steuerung der Neutralinjektion an ASDEX-Upgrade. Technologie Seminar "Heizung", Schloß Ringberg, Tegernsee 1993.

661. *Stroth, U.:* Transienter Transport bei Leistungsstufen von ECRH und Transport in Entladungen mit Dichtestufen. Garching 1993.

662. *Taglauer, E.:* Studies of Surface Structure, Segregation and Preferential Sputtering of Binary Alloys: the Example of Fe_3Al. Europ. Science Foundation Workshop on Alloy Surfaces and Thin Metallic Films, Le Sappey 1993.

663. *Taglauer, E.:* Thermal Roughening of Cu Surfaces. Seminar Ordnung und Unordnung an Oberflächen, Garching 1993.

664. *Taglauer, E.; Liegl, A.:* Ion Scattering Study of the Cu(115) Surface and its Roughening Transition. 13th Europ. Conf. Surface Science , Warwick 1993.

665. Taglauer, E.; Liegl, A.: Untersuchungen zur Aufrauhung von Cu(115)-Oberflächen mit Ionenstreuung. Seminar. Inst. Kristallographie und Mineralogie, Univ. München 1993.

666. Tasso, H.: Hamiltonian, Phase Space and Statistics of Continua. Spring Coll. on Plasma Physics, Int. Centre Theoret. Physics, Trieste 1993.

667. Tasso, H.: Linear and Nonlinear Stability in Resistive Magnetohydrodynamics. Spring Coll. on Plasma Physics, Int. Centre Theoret. Physics, Trieste 1993.

668. Tasso, H.: Lyapunov Stability of Large Systems of van der Pol-Like Oscillators and Connection with Turbulence and Fluctuations Spectra. Spring Coll. on Plasma Physics, Int. Centre Theoret. Physics, Trieste 1993.

669. Tasso, H.: Nonlinear Resistive MHD Stability. 5th Europ. Fusion Theory Conf., Madrid 1993.

670. Tasso, H.: Renormalization Group in Magnetohydrodynamic Turbulence. Spring Coll. on Plasma Physics, Int. Centre Theoret. Physics, Trieste 1993.

671. Teubel, A.: Numerische Codes für NBI-Heizung. Technologie Seminar "Heizung", Schloß Ringberg, Tegernsee 1993.

672. Theimer, G.; Endler, M.; Giannone, L.; Niedermeyer, H.; Rudyj, A.: Modellierung von Fluktuationen des Raumladungspotentials an der Dichte im Randschichtplasma von ASDEX durch eine statistische Superposition von Einzelereignissen. Greifswald 1993.

673. Unger, E.: Ergebnisse der Gasoszillationsexperimente. Garching 1993.

674. Unger, E.; Hacker, H.: Messungen im Extremen Ultraviolett am Wendelstein 7-AS. Verhandl. DPG (VI) **28**, 134, P15.65 (1993).

675. Verplancke, P.: Langmuirsonden im Plasmarand bei ICRF: Simulation und Messung. Technologie Seminar "Heizung", Schloß Ringberg, Tegernsee 1993.

676. Vollmer, O.: Diagnostik und Datenerfassung der NI an ASDEX-Upgrade. Technologie Seminar "Heizung", Schloß Ringberg, Tegernsee 1993.

677. Vollmer, O.: NBI: Diagnostik und Datenerfassung. Technologie Seminar "Heizung", Schloß Ringberg, Tegernsee 1993.

678. Vollmer, O.: NBI into ASDEX-Upgrade; Commissioning of the System (cont.). Joint Development Comm. Meeting, Garching 1993.

679. Vollmer, O.; Stäbler, A.; Feist, J.-H.; Freudenberger, K.; Heinemann, B.; Lohnert, H.; Obermayer, S.; Riedl, R.; Schärich, W.; Speth, E.; Wittenbecher, K.: Commissioning and First Operation of the ASDEX Upgrade Neutral Beam System. 15th IEEE/NPS Fusion Symp. on Engineering, Hyannis 1993.

680. Vonbank, M.: Magnetismus von Oberflächen und dünnen Filmen. Techn. Univ. Wien 1993.

681. *Wagner, F.:* 4th H-Mode Workshop in Japan. Zusammenfassung, Garching 1993.

682. Wagner, F.: Anforderungen des Stellarator-Programms. Schloß Ringberg, Tegernsee 1993.

683. Wagner, F.: Answers to the Questions of R.Weynants Regarding Divertors. Cadarache 1993.

684. Wagner, F.: Confinement in Tokamaks and Stellarators. Hefei 1993.

685. Wagner, F.: Contributions from W7-AS and Related Program-Summary. Lisbon 1993

686. Wagner, F.: The H-Mode of W7-AS. Garching 1993.

687. Wagner, F.: H-Mode of W7-AS Stellarator. Naka 1993.

688. Wagner, F.: New Subjects of H-Mode. Naka 1993.

689. Wagner, F.: Operating Diagnostics on W7-AS. Lisbon 1993

690. Wagner, F.: Operational Limits in Stellarators. Cadarache 1993.

691. Wagner, F.: The Physics of the H-Mode. Hefei 1993.

692. Wagner, F.: W7-AS Results in Relation to W7-X. Los Angeles, Princeton, San Diego 1993.

693. Wagner, F.: Wo steht die Fusionsforschung? Erreichtes - Offene Fragen. Garching 1993.

694. Weinlich, M.; Carlson, A.; Günther, K.; Laux, M.; Neuhauser, J.: Einfluß von Strömen quer zum Magnetfeld auf Messungen mit Langmuirsonden. Verhandl. DPG (VI) **28**, 116, P14.85 (1993).

695. Weller, A.: Globale Instabilitäten im Stellarator Wendelstein 7-AS und ihre Relation zu Tokamak Ergebnissen. Stuttgart 1993.

696. Weller, A.: NI-getriebene globale Alfvén-Wellen (GAE) in W7-AS, Vergleich der experimentellen Daten mit ersten Ergebnissen von MHD-Rechnungen. Garching 1993.

697. Wesner, F.: Aufbau, Komponenten und Wirkungsweise des ICRH-Systems. Technologie Seminar "Heizung", Schloß Ringberg, Tegernsee 1993.

698. Wesner, F.; et al.: ICRH-Ausblick. Technologie Seminar "Heizung", Schloß Ringberg, Tegernsee 1993.

699. Wilhelm, R.: Mikrowellenplasmen für großflächige Oberflächenbeschichtungen. Elektrotechn. Kolloquium, Univ. Braunschweig 1993.

700. Wilhelm, R.: Möglichkeiten für Stromtrieb und ihre Bewertung. Technologie Seminar "Heizung", Schloß Ringberg, Tegernsee 1993.

701. Wilhelm, R.: Plasmaheizung und Stromtrieb durch Hochfrequenzwellen. Physik Kolloquium, Univ. Bochum 1993.

702. Wobig, H.: Experiments and Prospects for Confinement in Stellarators. Workshop on Physics Issues to be Investigated in Parallel with ITER and Required Devices, Cadarache 1993.

703. Wobig, H.: Parameter Range and Heating in W7-X. W7-X Stellarator Meeting, Schloß Ringberg, Tegernsee 1993.

704. Wobig, H.: Plasma Parameters for Reactors and for W7-X. Presentation of the Wendelstein 7-X Stellarator Project. NET, Garching; PPPL, Princeton; GA, San Diego; UCLA, Los Angeles 1993.

705. Wobig, H.: The Theoretical Basis of Drift-Optimized Stellarator Reactor. Int. Sherwood Fusion Theory Conf., Newport 1993.

706. Würsching, E.; Burhenn, R.; Grigull, P.; Hofmann, J.V.; Niedermeyer, H.; Stäbler, A.; Weller, A.; WVII-AS-Team: Untersuchungen zum Dichtelimit am W7-AS Stellarator. Greifswald 1993.

707. Yao, Q.; Boozer, A.H.: A Study of the Guiding Center Approximation. Int. Sherwood Fusion Theory Conf., Newport 1993.

708. Zohm, H.: Atomphysik und Quantenmechanik. Vorlesung Physik III, Univ. Augsburg, WS 1992/93 und WS 1993/94.

709. Zohm, H.: Dynamical Behaviour of the H-Mode in ASDEX-Upgrade. 4th H-Mode Workshop, JAERI, Naka 1993.

710. Zohm, H.: Dynamics of the H-Mode in ASDEX-Upgrade. Fusion Science Meeting, Culham 1993.

711. Zohm, H.: Dynamik der H-Mode in ASDEX-Upgrade. Plasmakolloquium IPF, Univ. Stuttgart 1993.

712. Zohm, H.: H-Mode in ASDEX-Upgrade and Dynamics of the L-H Transition. JET Theory Seminar, Culham 1993.

713. Zohm, H.: Kern- und Elementarteilchenphysik. Vorlesung Physik IV, Univ. Augsburg, SS 1993.

714. Zohm, H.: m=2 Mode Stabilization with ECRH/ECCD. Joint German-Russian Workshop on ECRH, Garching 1993.

715. Zohm, H.; Büchl, K.; Gernhardt, J.; Herrmann, A.; Lackner, K.; Lieder, G.; Salmon, N.; Schittenhelm, M.; Seidel, U.; ASDEX-Upgrade-Team; ICRH-Group: Untersuchung von ELMs in ASDEX Upgrade. Verhandl. DPG (VI) **28**, 72, P3.1 (1993).

716. Zohm, H.; Eckern, U.:* Seminar zur Magnetohydrodynamik heißer Plasmen. Univ. Augsburg, WS 1993/94.

717. Zohm, H.; Ryter, F.: Review of H-Mode Results from ASDEX-Upgrade. Fusion Science Meeting, Culham 1993.

Internal Laboratory Reports

IPP 1-274 *Lang, P.; Andelfinger, C.; Beck, W.; Buchelt, E.; Büchl, K.; Cierpka, P.; Kollotzek, H.; Lang, R.; Prausner, G.; Söldner, F.X.;Ulrich, M.; Weber, G.:* The New Centrifuge High-Speed Pellet Injector for ASDEX Upgrade. 1993.

IPP 1-275 *Kiemer, K.:* Untersuchung von Wasserstofflinienstrahlung in der Plasmarandschicht. 1993.

IPP 1-276 *Zohm, H.;ASDEX-Upgrade-Team; ICRH-Group; NI-Group:* Dynamic Behaviour of the L-H Transistion in ASDEX-Upgrade. 1993.

IPP 1-277 ASDEX Upgrade Results Publications and Conference Contributions Period 6/92 to 9/93. 1993.

IPP 2-307 *Beidler, C.; Hitchon, W.N.G.:* Ripple Transport in Helical-Axis Advanced Stellarators - A Comparison With Classical Stellarator/Torsatrons. 1993.

IPP 2-316 *Harmeyer, E.; Kißlinger, J.; Rau, F.; Wobig, H.:* Studies on a Stellarator Reactor of the Helias Type: The Modular Coil System. 1993.

IPP 2-318 *Beidler, C.; Harmeyer, E.; Kißlinger, J.; Ott, I.; Rau, F.; Wobig, H.:* Studies on a Stellarator Reactor of the Helias Type: The Power Balance. 1993.

IPP 2-319 *Nührenberg, J.; Zheng, L.-J.:* Invariant Expression for the Divergence of Braginskii's Gyroviscous Tensor for Localized Modes. 1993.

IPP 2-320 *Schauer, F.:* Transiente mechanische Störungen in intern gekühlten Supraleiterkabeln: Stabilitätskriterium und Stabilität des W7-X-Prototypleiters von LMI. 1993.

IPP 2-321 *Spada, M.:* A Sufficient Condition for the Lack of Cellular Convection in a Dissipative Plasma Column. 1993.

IPP III-186 Proceedings of 8th Joint Workshop on Electron Cyclotron Emission and Electron Cyclotron Resonance Heating, Gut Ising 1992. Vol. 1.2. 1993.

IPP III-189 *Bessenrodt-Weberpals, M.; Wagner, F.; ASDEX-TEAM:* The Isotope Effect in ASDEX. 1993.

IPP III-190 *Feng, Y.:* Formulation and Application of the Neutral Particle Beam Deposition Code SINBAD. 1993.

IPP III-191 W7-AS/W7-X Contributions to the 20th Europ. Conf. on Controlled Fusion and Plasma Heating, Lisboa 1993. 1993.

IPP III-192 *Kroiss, H.:* MEN - Menu and Dialog Software. 1993.

IPP III-193 *Sattler, S.:* Fluktuationen der Elektronentemperatur gemessen durch Intensitätsinterferometrie am Stellarator W7-AS. 1993.

IPP 4-258 *Ott, W.; Penningsfeld, F.-P.:* Spectroscopic Determination of Species and Divergence of Hydrogen Beams in the W7-AS Neutral Beam Injectors. 1993.

IPP 4-259 *Ott, W.:* Offset Steering in Multiamp Ion Sources - Revisited. 1993.

IPP 4-260 *Pereverzev, G.V.:* Paraxial WKB Solution of a Scalar Wave Equation. 1993.

IPP 4-262 *Engelhard, M.:* Messung und Modellierung absoluter Radikaldichten in einem ECR-Methanplasma = Measurements and Modelling of Absolut Radical Densities in an ECR-Methane Plasma. 1993.

IPP 4-263 *Ballico, M.; Puri, S.:* Calculation of the Self-Consistent Current Distribution and Coupling of an RF Antenna Array. 1993.

IPP 4-264 *Ballico, M.* The W7-AS Data Acquisition and Automatic Antenna Matching System. 1993.

IPP 4-265 *Penningsfeld, F.-P.:* Fast Access to Neutral Injection Heating Profiles in W7AS. 1993.

IPP 5-51 *Becker, G.:* Profile Constraining Mechanism for T_e Profile Invariance in Tokamaks. 1993.

IPP 5-52 *Brambilla, M.:* Linear Propagation and Absorption of the Fast Wave Near the First Ion Cyclotron Harmonic. 1993.

IPP 5-53 *Rozhansky*, V.A.; Lengyel, L.:* Calculation of Electrostatic Fields in Vapour Shields Evolving at Ablating Surfaces. 1993.

IPP 5-54 ASDEX Upgrade Results Publications and Conference Contributions Period 6/92 to 9/93. 1993.

IPP 5-56 *Brambilla, M.:* Quasilinear Ion Distribution Function During First Harmonic Ion Cyclotron Heating. 1993.

IPP 6-311 *Throumoulopoulos, G.N.; Pfirsch, D.:* Negative Energy Waves in a Magnetically Confined Guiding Center Plasma. 1993.

IPP 6-312 *Pfirsch, D.; Pohl, F.:* Test of a Multiple Time Scale Formalism Applied to the Nonlinear Evolution of Negative-Energy Modes. 1993.

IPP 6-313 *Pfirsch, D.:* Nonlinear Instabilities Relating to Negative-Energy Modes. 1993.

IPP 6-314 *Tasso, H.:* Linear and Nonlinear Stability in Resistive Magnetohydrodynamics. 1993.

IPP 6-315 *Kaiser, R.; Salat, A.:* Surface Current Equilibria from a Geometric Point of View. 1993.

IPP 6-316 *Tasso, H.:* Lyapunov Stability of Large Systems of van der Pol-Like Oscillators and Connection with Turbulence and Fluctuations Spectra. 1993.

IPP 6-317 *Correa-Restrepo, D.; Pfirsch, D.:* Negative-Energy Perturbations in General and in Arbitrary One-Dimensional Vlasov-Maxwell Equilibria Spectra. 1993.

IPP 6-318 *Throumoulopoulos, G.; Pfirsch, D.:* Negative-Energy Modes in a Magnetically Confined Plasma in the Framework of Maxwell-Drift Kinetic Theory. 1993.

IPP 8-2 *Bachmann, P.; Belitz*, H.J.:* Elastic Processes in Hydrogen-Helium Plasmas: Collison Data. 1993.

IPP 9-82 *Eckstein, W.; Garcia-Rosales, C.; Roth, J.; Ottenberger, W.:* Sputtering Data. 1993.

IPP 9-92 *Franzen, P.:* Hochtemperaturreemission von Wasserstoff aus Graphit = Reemission of Hydrogen from Graphite at High Temperatures. 1993.

IPP 9-95 *Jandl, C.:* Untersuchung des dynamischen Inventars von Wasserstoff in Graphit unter Beschuss aus einem RF-Plasma = Investigation of the Dynamic Inventory of Hydrogen in Graphite Exposed to a RF Discharge. 1993.

IPP 9-96 *Geipel, G.:* Manifestation magnetischer Phasenübergänge in Auger Elektronen und Auftrittspotential-Spektroskopie = Manifestation of Magnetic Phase Transitions in Auger Electron and Appearance Potential Spectroscopy. 1993.

IPP 9-97 *Hytry, R.:* Innenbeschichtung eines Hohlleiters mit Hilfe einer ECR-Laufentladung = Inner Coating of a Waveguide by Means of an ECR Running Discharge. 1993.

IPP R-44 *Strunz, R.:* Implementierung eines parallelisierten Buneman-Verfahrens für ein Multitransputersystem. 1993.

IPP R-45 *Ballico, M.; Lederer, H.:* PVM on Alpha AXP Workstations in a Customer Applications Environment. 1993.

External Laboratory Reports

AEA-Fus-230 *Hender,*, T.C.: Fitzpatrick*, F.; Morris*, A.W.; Zohm, H.; et al.:* Errot Fields and their Correction in ITER. Culham, Abingdon 1993.

JET-P(93)59 *Costley*, A.E.; Gasparino, U.; Kasparek*, W.:* Report on the 8th Joint Workshop on Electron Cyclotron Emission and Electron Cyclotron Resonance Heating (EC8), Gut Ising 1992. JET, Abingdon 1993.

JET-P(93)65 *Gormezano *, C.; Baranov*, Y.; Dobbing*, J.; Söldner, F.X.; et al.:* High Power Lower Hybrid Current Drive on JET: Results and Prospects. JET, Abingdon 1993.

JET-P(93)92 *Martinelli, A.P.; Behrisch, R.; Peacock*, A.T.:* Modification of the Carbon and Beryllium Walls in JET by Erosion, Redeposition and Deuterium Trapping after the 1991 Discharge Period. JET, Abingdon 1993.

NIFS-242 *Kardaun, O.; Itoh*, S.-I.; Itoh*, K.; Kardaun*, J.W.P.F.:* Discriminant Analysis to Predict the Occurence of ELMs in H-Mode Discharges. Nat. Inst. for Fusion Science, Nagoya 1993.

Author Index

* No Member of the IPP

Teams

ASDEX-Team: R.Aratari, G.Becker, M.Bessenrodt-Weberpals, B.Bomba, H.-S.Bosch, K.Büchl, R.Büchse, A.Carlson, G.Dodel, A.Eberhagen, M.Endler, W.Engelhardt, H.-U.Fahrbach, G.Fussmann, O.Gehre, J.Gernhardt, L.Giannone, O.Gruber, G.Haas, T.Hartinger, W.Herrmann, J.V.Hofmann, H.Hohenöcker, E.Holzhauer, K.Hübner, G.Janeschitz, A.Kallenbach, O.Kardaun, F.Karger, M.Kaufmann, O.Klüber, M.Kornherr, K.Krieger, J.Kucinski, K.Lackner, R.Lang, F.Leuterer, R.Loch, G.Lisitano, H.-M.Mayer, K.McCormick, D.Meisel, V.Mertens, E.R.Müller, H.Murmann, J.Neuhauser, H.Niedermeyer, J.-M.Noterdaeme, W.Poschenrieder, H.Röhr, J.Roth, A.Rudyj, N.Ruhs, F.Ryter, W.Sandmann, F.Schneider, U.Schneider, R.Schubert, G.Siller, E.Simmet, F.X.Söldner, E.Speth, A.Stäbler, K.-H.Steuer, U.Stroth, E.Taglauer, N.Tsois*, H.Verbeek, O.Vollmer, F.Wagner, K.Wira, F.Wesner, D.Zimmermann, H.Zohm.

ASDEX-Upgrade-Team: W.Köppendörfer, M.Albrecht, M.Alexander, C.Andelfinger, K.Asmussen, M.Ballico, G.Becker, K.Behler, A.Bergmann, M.Bessenrodt-Weberpals, H.-S.Bosch, M.Brambilla, F.Braun, K.Büchl, A.Carlson, R.Chodura, O.De Barbieri, H.J.De Blank, S. De Pena Hempel, C.Dorn, R.Drube, R.Dux, A.Eberhagen, W.Engelhardt, J.Engstler, H.-U.Fahrbach, H.-U.Feist, W.Feneberg, D.Fieg, A.Field, J.C.Fuchs, G.Fußmann, C.Garcia-Rosales, O.Gehre, J.Gernhardt, S.Götsch, J.Gruber, O.Gruber, K.Günther, G.Haas, B.Heinemann, G.Herppich, A.Herrmann, W.Herrmann, F.Hofmeister, H.Hohenöcker, H.Hupfloher, D.Jacobi, F.Jenichen, B.Jüttner, W.Junker, A.Kallenbach, O.Kardaun, T.Kass, M.Kaufmann, K.Kiemer, H.Kollotzek, M.Kornherr, H.Krause, K.Krieger, B.Kurzan, K.Lackner, P.Lang, R.Lang, M.Laux, L.Lengyel, F.Leuterer, G.Lieder, K.-F.Mast, H.-M.Mayer, P.McCarthy, D.Meisel, R.Merkel, V.Mertens, M.Münich, H.Murmann, B.Napiontek, D.Naujoks, G.Neu, R.Neu, J.Neuhauser, J.-M.Noterdaeme, J.Oswald, G.Pautasso, W.Poschenrieder, S.Puri, G.Raupp, H.Richter, T.Richter, H.Röhr, J.Roth, F.Ryter, N.Salmon, H.Salzmann, W.Sandmann, H.-B.Schilling, M.Schittenhelm, H.Schneider, R.Schneider, W.Schneider, K.Schönmann, G.Schramm, J.Schweinzer, S.Schweizer, B.Scott, U.Seidel, F.X.Söldner, E.Späth, A.Stäbler, K.-H.Steuer, J.Stober, B.Streibl, W.Suttrop, W.Teutterer, M.Troppmann, M.Ulrich, G.Venus, H.Vernickel, O.Vollmer, H.Wedler, M.Weinlich, U.Wenzel, F.Wesner, A.Wieczorek, R.Wilhelm, R.Wunderlich, D.Zasche, H.P.Zehrfeld, H.Zohm.

ECRH-Group: W.Kasparek, G.Müller, P.G.Schüller, M.Thumm.

Gyrotron-Group: H.U.Nickel, M.Thumm.

H-Mode-Database-Working-Group: O.Kardaun, F.Ryter, U.Stroth, A.Kus, J.C.DeBoo*, D.P.Schissel*, G.Bramson*, T.N.Carlstrom*, K.Thomsen*, D.J.Campbell*, J.G.Cordey*, J.P.Christiansen, Y.Miura*, N.Suzuki*, M.Mori*, T.Matsuda*, H.Tamai*, T.Takizuka*, S.-I.Itoh*, K.Itoh*, S.M.Kaye*.

ICRH-Team: M.Ballico, W.Becker, F.Braun, R.Fritsch, F.Hofmeister, C.Hoffmann, J.-M.Noterdaeme, S.Puri, P.Verplancke, H.Wedler, F.Wesner.

NI-Group: M.Ciric, J.-H.Feist, K.Freudenberger, B.Heinemann, W.Kraus, W.Melkus, S.Obermayer; W.Ott, F.-P.Penningsfeld, F.Probst, R.Riedl, W.Schärich, B.Sombach, E.Speth, A.Stäbler, R.Süß, A.Teubel, O.Vollmer, K.Wittenbecher.

NI-Team(ASDEX): E.Speth, A.Stäbler, O.Vollmer.

NI-Team(WVII-AS): K.Freudenberger, W.Melkus, W.Ott, F.-P.Penningsfeld, F.Probst, E.Speth, R.Süß, A.Teubel.

PSI-Group: R.Behrisch, A.P.Martinelli, V.Prozesky, J.Roth, E.Taglauer.

WVII-AS-Team: R.Balbin, J.Baldzuhn, K.Behringer, B.Bomba, R.Brakel, R.Büchse, R.Burhenn, G.Cattanei, A.Dodhy, D.Dorst, K.Dyabilin, A.Eslner, M.Endler, K.Engelhardt, V.Erckmann, U.Gasparino, J.Geiger, T.Geist, S.Geissler, L.Giannone, P.Grigull, G.Grünwald, H.Hacker, H.-J.Hartfuß, O.Heinrich, G.Herre, C.Hidalgo, M.Hirsch, J.V.Hofmann, J.Hofner, E.Holzhauer, R.Isler, R.Jänicke, J.Junker, F.Karger, M.Kick, A.Kislyakov, J.Kisslinger, C.Konrad, H.Kroiss, G.Kühner, N.F.Larinova, A.Lazaros, T.Luce, P.Luttner, H.Maaßberg, C.Mahn, W.Mandl, K.McCormick, H.Niedermeyer, W.Ohlendorf, F.Rau, H.Renner, H.Ringler, A.Rudyj, N.Ruhs, J.Saffert, J.Sapper, F.Sardei, S.Sattler, F.Schneider, U.Schneider, G.Siller, U.Stroth, G.Theimer, M.Tutter, E.Unger, F.Wagner, R.Waltz, U.Weber, A.Weller, H.Wobig, E.Würsching, S.Wurdack, D.Zimmermann, M.Zippe, S.Zöpfel.

WVII-X-Team: C.Beidler, W.Dommaschk, H.Greuner, G.Grieger, E.Harmeyer, F.Herrnegger, J.Junker, N.Karulin, J.Kisslinger, W.Lotz, P.Merkel, H.Münch, J.Nührenberg, M.Pillsticker, F.Rau, H.Renner, J.Sapper, F.Schauer, A.Schlüter, I.Schönewolf, C.Schwab, U.Schwenn, M.Spada, E.Strumberger, D.Sünder, A.Wieczorek, H.Wobig, L.-J.Zheng

WVII-X-Technical-Group: W.Bitter, H.Greuner, E.Harmeyer, R.Holzthüm, S.Huber, N.Jaksic, S.Kamm, F.Kerl, H.Münch, M.Pillsticker, J.Sapper, F.Schauer, I.Schoenewolf, J.Simon-Weidner, B.Somach, J.Tretter, F.Werner, A.Wieczorek.

University Contributions to IPP Programme

LEHRSTUHL FÜR EXPERIMENTALPHYSIK VI DER UNIVERSITÄT BAYREUTH

(Prof. Dr. Jürgen Küppers)

Elementary steps of chemical erosion of graphite based materials by hydrogen. Influence of boron on the chemical erosion mechanism.

(J. Biener, C. Lutterloh, A. Schenk, U. A. Schubert, B. Winter)

The cooperation activities of IPP and the University of Bayreuth are concentrated on investigating fusion relevant plasma-wall interaction processes. Accordingly, the surface chemistry of hydrogen on possible reactor wall materials (Be, C, C/B) is the primary research topic.

It has been shown that model systems consisting of several monolayers thick, ion beam deposited C:H films at a graphite monolayer on a Pt single crystal surface can be used to study the elementary steps of graphite erosion by hydrogen atoms. With these models the thermally activated step which leads to erosion via methane was identified as the breaking of a C-C bond in a hydrogen-containing carbon network. Furthermore, vibrational spectroscopy allowed sp^3-hybridized CH_x groups to be identified as the origin of erosion towards methane.

The walls of a vessel housing a magnetically confined hydrogen plasma are subjected to substantial fluxes of neutrals and ions. It is therefore necessary to know what reactions may occur at a graphite surface under the impact of the above particles.

For identification of these reactions C:H films which contain either a mixture of sp^2 and sp^3 or only sp^3 CH_x groups were subjected to a flux of hydrogen atoms effusing from a heated source. Vibrational spectroscopy revealed that the CH groups at the surface are hydrogenated to sp^3 upon hydrogen impact. From the fluence dependence of this reaction it can be concluded that approx. every tenth H atom hydrogenates a carbon centre. As a consequence, it can be safely assumed that under real conditions at the surface of a graphite tile in a fusion device all reactive carbon centres will be fully hydrogenated to sp^3 CH_3 groups.

The reaction caused by the flux of thermal H atoms impinging at the C:H film surface as revealed by spectroscopy can be formulated as follows:

$$H \rightarrow (network)\text{-}(sp,sp^2)CH \rightarrow (network)\text{-}(sp^3)CH_3 \qquad (1)$$

A reaction which occurs at a rate which is roughly 10 times slower than the above hydrogenation reaction is a hydrogen molecule recombination reaction of an incoming H atom with a H atom in a surface CH_3 group:

$$H \rightarrow (network)\text{-}CH_3 \rightarrow H_2\,(gas) + (network)\text{-}{}^*CH_2 \qquad (2)$$

The Eley-Rideal reaction (2) leaves a radical carbon centre at the surface which can be hydrogenated by a subsequently incoming H atom. The overall effect of reaction (2) and subsequent hydrogenation is therefore the transfer of (not too) energetic H atoms into thermal hydrogen molecules, which we call "chemical cooling" of a plasma, by reactions which occur at graphite surfaces.

The unsaturated centre produced in reaction (2) can initiate a chemical erosion step via

$$(network^*)\text{-}CH_3 \rightarrow (network) + CH_3\,(gas) \qquad (3)$$

Reaction (3) occurs for about every second excited centre produced in reaction (2), ie this erosion reaction is two times slower than the Eley-Rideal reaction. Its gaseous product, a CH_3 radical, is the same as that of the thermally excited excited erosion reaction towards methane. However, as reaction (3) is mediated by the impact of atoms at the surface of the C:H film, its activation barrier is so small that it already occurs at much lower temperature than the thermal erosion reaction, which has its rate maximum at approx. 850 K. Accordingly, even around 350 K erosion of C:H films via mechanism (3) is observed.

As the flux of hydrogen particles impinging on the wall in a fusion experiment is considerable, reaction (3) might be effective at wall segments which do not get hot enough to allow considerable thermally excited erosion products.

Spectroscopic investigations were also performed at boron

doped C:B:H films which were deposited from ethane/ trimethyl-borane mixtures. Vibrational spectroscopy revealed that boron doped films contained less sp and sp^2 hybridized CH groups than C:H films, several 10 per cent boron eventually suppressing the formation of these groups completely. Surprisingly, this effect is visible even at boron doping concentrations of a few per cent. This proves that boron is chemically incorporated into a C:H network, rather than embedded on interstitial sites of the network.

A second phenomenon introduced by boron doping is the shift of the maximum of the chemical erosion rate towards lower temperature, approx. 100 K at 30% B concentration. This effect is also seen from the lowest B concentrations. Thirdly, B doping of C:H films causes a decrease of the erosion yield, defined as the ratio of hydrocarbon products and total amount of hydrogenic species released from the film upon thermally activated decomposition. The shift of the erosion rate maximum on the temperature scale and the erosion yields of the present C:B:H films perfectly match the data measured at boron doped graphites used as wall materials, eg USB 10 and related B doped graphites.

This coincidence further supports the conclusion that the present thin film systems are very good models for the study of the chemical erosion mechanisms of graphite based materials by H.

The origin of boron induced effects on the erosion behaviour of graphite can be understood on the basis of vibrational spectra. Boron suppresses the formation of sp and sp^2 CH groups, ie it forces the carbon network to exclusively build sp^3 hybridized C-C and C-H bonds. Accordingly, the aromaticity of the films should decrease and their capacity for hydrogen increase, as was observed. As the B-C bond is stronger than the C-C bond, the bonding strengths of groups to the network is modified by boron. The decrease of the bond strength with which methyl groups are attached to the network then causes a reduction of the temperature at which the chemical erosion rate assumes its maximum.

Publications and conference reports

V. Lossev and J. Küppers
Adsorption of hydrogen on Be(0001) surfaces.
Surf. Sci. 284 (1993) 175

J. Biener, A. Schenk, B. Winter, C. Lutterloh, U. A. Schubert, and J. Küppers
Spectroscopic identification of C-H species in C:H films using HREELS.
Surf. Sci. Lett. 291 (1993) L725

J. Biener, A. Schenk, B. Winter, C. Lutterloh, U. A. Schubert, and J. Küppers
The Mechanism of Chemical Erosion of C:H Films: a HREELS and TDS study.
Proc. 3S'93, Editors: G. Betz and P. Varga, Vienna 1993

J. Biener, U. A. Schubert, A. Schenk, B. Winter, C. Lutterloh, and J. Küppers
A surface reaction with atoms: Hydrogenation of sp- and sp^2-hybridized carbon by thermal H(D) atoms.
J. Chem. Phys. 99 (1993) 3125

J. Biener, U. A. Schubert, A. Schenk, B. Winter, C. Lutterloh, and J. Küppers
Modeling the Elementary Steps of Low-Pressure Diamond Deposition.
Adv. Mater 5 (1993) 639

J. Biener, A. Schenk, B. Winter, and J. Küppers
HREEL Spectroscopy of Thin Ion Beam Deposited C:H(D) Films.
J. Electron Spectr. and Related Phen. 64/65 (1993) 331

Oral presentations

J. Biener, A. Schenk, B. Winter, C. Lutterloh, U. A. Schubert, and J. Küppers
Structure and thermal decomposition of thin ion-beam deposited C:H films
13th General Conference of the EPS, Regensburg, Germany, March 1993

J. Biener, A. Schenk, B. Winter, C. Lutterloh, U. A. Schubert, and J. Küppers
The Mechanism of Chemical Erosion of C:H Films: a HREELS and TDS study.
Symposium on Surface Science 9, Kaprun, Austria, May 1993

J. Küppers
Die chemische Erosion von Graphit durch H
Univ. Bochum 8.6.1993

J. Biener, A. Schenk, B. Winter, and J. Küppers
HREEL Spectroscopy of Thin Ion Beam Deposited C:H(D) Films.
Vibrations at Surfaces VII, Santa Margherita, Italy, June 1993

J. Biener, A. Schenk, B. Winter, U. A. Schubert, C. Lutterloh, and J. Küppers
Hydrogenation of Amorphous C:H surfaces by Thermal H(D) Atoms.
13th European Conference on Surface Science, Warwick, UK, August 1993

LEHRSTUHL FÜR MESSTECHNIK (LMT) DER UNIVERSITÄT DES SAARLANDES

(Prof. Dr. A. W. Koch)

In cooperation with IPP a two-wavelength electronic speckle pattern interferometer (ESPI) was constructed. It is specially designed to measure the surface topography - roughness and contour maps - of tokamak wall materials. Graphite tiles of ASDEX and JET were investigated ex situ.

1. MEASUREMENT OF TARGET EROSION AND REDEPOSITON BY MEANS OF SPECKLE INTERFEROMETRY

H. Stotz, M. Ruprecht, D. Tutsch

1.1 Principle of Measurement

The intensity of laser light reflected and diffracted by rough surfaces exhibits a specific structure, the speckle pattern. The phase information of this pattern is retrieved by superposing a reference beam on the speckled object beam in a Mach-Zehnder-type interferometer[1]. The resulting image is detected by a computer-controlled CCD-camera. The superposition of two speckle images recorded at two different laser wavelengths (λ_1, λ_2) yields contour maps of the surface to be investigated. The fringe separation is given by the synthetic wavelength:

$$\Lambda = \lambda_1 \cdot \lambda_2 / [2 \cdot (\lambda_1 - \lambda_2) \cos \Theta] ,$$

where Θ is the angle of reflection.

1.2 Results

Data acquisition and processing were automated. Contrast enhancement, filtering and superposition of the speckle images are performed by the computer program[2]. Fig. 1 shows a two-wavelength speckle superposition before and after digital image processing. The fringe separation in this case was 5 µm.

1.3 Long-range Speckle Interferometry

A long-range speckle interferometer is under construction that will permit measuring distances above 8 to 10 m and, by means of image linking, probing areas of approx. 50×50 cm^2.

Currently a pulsed laser system is being installed which allows exposure times down to 7 ns and high pulse energies of approx. 550 mJ in the visible spectral region. The experimental setup aims at the use of speckle interferometry as an in situ non-intrusive monitor for wall erosion and redeposition in experimental fusion devices /54/.

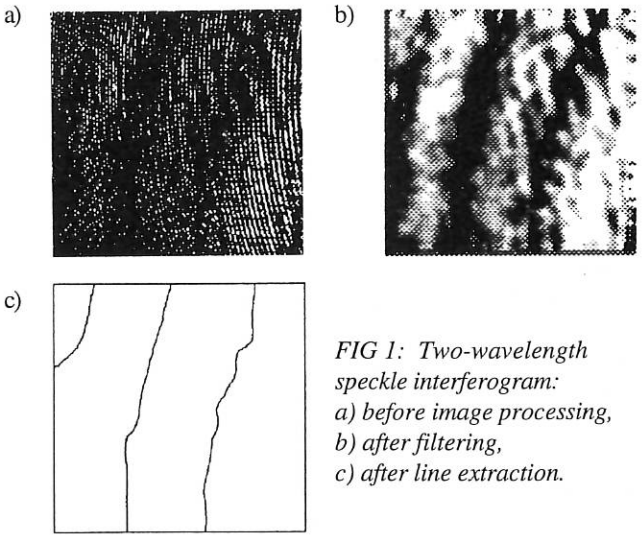

FIG 1: Two-wavelength speckle interferogram:
a) before image processing,
b) after filtering,
c) after line extraction.

---

[1] *Tutsch, D.:* Aufbau eines Zweiwellenlängen-Interferometers mit computergestützter Bildaufnahme und Bildverarbeitung für die Speckle-Oberflächenuntersuchung, Diploma Thesis, Universität des Saarlandes, May 1993.

[2] *Stotz, H.:* Rechnergestützte Auswertung von Speckle-Interferenzbildern zur Bestimmung drei-dimensionaler Oberflächenstrukturen, LMT Laboratory Report, Universität des Saarlandes, September 1993.

ISOTOPE SEPARATOR LABORATORY, PHYSICS DEPARTMENT, TECHNICAL UNIVERSITY OF MUNICH

(Dr. E. Hechtl)

The sputtering yields of nickel bombarded with argon ions were measured as a function of the impinging ion energy and the angle of ion incidence.

SPUTTERING OF SOLID SURFACES WITH HEAVY IONS

(E. Hechtl, A. Wagner)

Measurements of the sputtering yield of nickel were made in the energy range below 1 keV down to the lowest energies feasible under the conditions given in each case. Of particular interest in this investigation was the yield close to the threshold energy of sputtering. Data in this energy range are needed especially to test the TRIM.SP model calculations. The choice of a noble gas projectile affords the possibility of finding the sputtering yield without knowing the particle reflection coefficient.

The sputtering data were determined by the weight loss method, i.e. the loss of target material due to the ion irradiation is determined with an ultramicrobalance. The irradiations were performed with our isotope separator in conjunction with an ion optical deceleration system. The ion energy can therefore be said to result from the acceleration and deceleration voltages for energies above about 100 eV. With smaller energies, it is necessary to determine the energy of the ions more precisely. This was done by measuring the ion current at the target position by applying an additional deceleration voltage. It turned out that the ions have an additional energy of about 20 eV originating from the plasma in the ion source.

Measurement of the sputtering yield of nickel bombarded with argon ions at normal ion incidence delivered data in good agreement with the TRIM.SP calculation. Owing to the decreasing yields at these low energies it was too time—consuming to measure below 100 eV for normal ion incidence. The yield measurements as a function of the angle of ion incidence showed the yield to be maximum at an angle of about 45°. The measurements were therefore continued with an angle of ion incidence of 45° in order to measure yields at lower energies. These measurements were made down to energies as low as 50 eV.

Comparison with the TRIM.SP calculation shows good agreement only in the higher energy range above about 500 eV, whereas in the lower energy range the calculated data differ by up to 30% from the measured data. The effect of the choice of the interaction potential is not sufficient to account for this difference. The surface roughness on the other hand may well be the cause of this discrepancy. So far a completely smooth surface has been assumed in the calculation.

Conference contribution
Hechtl, E., Eckstein, W., and Roth, J.: Reflection and self—sputtering of nickel at oblique angles of ion incidence, ICACS—15, London, Ontario, Canada, July 26—30, 1993.

Institut für Plasmaforschung (IPF)
der Universität Stuttgart
(Prof. Dr. U. Schumacher)

1. ELECTRON CYCLOTRON RESONANCE HEATING (ECRH)

U. Schumacher, V.Erckmann*), W. Förster, G. Gantenbein**), W. Kasparek, H. Kumrić, G.A. Müller, J. Pretterebner, P.G. Schüller, J. Schwarz**), D. Wagner

1.1 ECRH at 70 and 140 GHz

In the W7-AS stellarator the plasma is produced and heated by electron cyclotron resonance absorption. This heating method (ECRH) needs microwave irradiation of the plasma at 70 GHz or 140 GHz to meet the resonance condition at the value of the confining magnetic field.
The 70 GHz system is used for 2nd harmonic heating at 1.25 T, while the 140 GHz system is applied at 2.5 T. Specific experiments concerning the physics of noninductive plasma current drive by ECR absorption were performed, where the influence of trapped electrons could be studied due to the possibility of changing the structure of the stellarator magnetic field.
Another series of experiments with additional NBI heating demonstrated ECRH to be a tool for density control in NBI heated plasmas.
Experiments with ECRH at 2.5 T and 140 GHz with power levels of up to 700 kW achieved ion heating at densities of 10^{20} m^{-3}, which is comparable to ion heating by NBI.

1.2 Microwave Technology for ECRH at 140 GHz

1.2.1 Quasi-optical 140 GHz transmission system

After one year of successful operation, the Russian $TE_{22,6}$ gyrotron was replaced by an upgraded tube early in 1993. For this purpose, the quasi-optical transmission line was modified to match the new gyrotron beam and especially to produce a flattened power distribution on the torus window. This technique allowed extension of the pulse length of the gyrotron to 1.1 s at a power level of 450 kW. Also, a power of 900 kW could be transmitted with a maximum pulse length of 350 ms.
Between March and August 1993 a series of experiments were performed with this system, e.g. studies of the iota limits and power and density thresholds of the occurrence of the H-mode; combined heating with NBI, where again density clamping was observed if EC power and NBI power were applied at a similar level; by modulating the gyrotron, transport studies by heat wave propagation were performed. Details can be found in the stellarator part of this report.
Additionally, this system was used for first experiments on collective Thomson scattering (see Sec. 1.3).

1.2.2 2 MW ECRH system for W7-AS

In 1993, the design of the 2 MW, 140 GHz ECRH system for W7-AS was finished. Preparations to replace two of the existing 70 GHz systems by 140 GHz had been completed; the construction of the new systems was started.
The new 140 GHz installations will consist of a gyrotron with a built-in quasi-optical mode converter emitting a collimated microwave beam. The specified power is 500 kW at a pulse length of 3 s (these parameters could already be demonstrated for this gyrotron during tests at Kurchatov Institute).
The transmission systems will consist of a compact matching optics which focuses the beam into a corrugated waveguide, where the power is transported in the form of an HE_{11} mode. Optimum matching between the beam and waveguide is provided by special horns (Sec. 1.2.4.4). After a 25 m long waveguide run, the power is launched into a polarizer box, where the polarization of the microwaves is adjusted for optimum coupling into the plasma. The remaining distance of 15 m to the stellarator is overcome with the help of a quasi-optical line consisting of 4 mirrors. The last mirror produces a flattened power distribution on the vacuum barrier window to allow operation of up to 3 s. Inside the vacuum vessel, the same antenna as before (with the 70 GHz system) is used; only the steering mirrors and the pick-up waveguides for beam diagnostics had to be adapted to the higher frequency.

*) *IPP Garching*
**) *since 1.11.93*

1.2.3 *2 MW ECRH system for ASDEX Upgrade*

For the planned ECRH system on ASDEX Upgrade, preferential support was granted by EURATOM. The design of the system is almost complete; the most critical issue was the influence of the stray magnetic field of ASDEX Upgrade on the gyrotrons. Similarly to that of W7-AS, the ECRH system of ASDEX Upgrade will use both beam waveguides and corrugated HE_{11} waveguides to transmit the power to the tokamak. The construction of many components of the first transmission line is already completed. First high-power tests using a gyrotron loaned from IAP Nizhni Novgorod are planned for April 94 (see also Technology Division).

1.2.4 *Development of special components*

1.2.4.1 *Quasi-optical mode converters for gyrotron output modes*

In 1993, the development of quasi-optical mode converters which transform the gyrotron cavity mode direct to modes appropriate for transmission was almost completed. Several prototypes designed for different input modes were successfully tested. As an example, the far-field radiation pattern of a $TE_{10,4}$-to-TEM_{00} converter envisaged to be built into a 140 GHz gyrotron at KfK is shown in Fig. 1.1. For optimization of the antenna, several modes were superposed to synthesize a gaussian beam. The pattern exhibits a low sidelobe level and cross-polarization, which is below -20 dB.
Another example is the $TE_{15,2}$-to-TEM_{00} converter to be used externally to the gyrotron for a 140 GHz collective Thomson scattering experiment at JET. This converter, designed by ray-tracing calculations, also yielded good results (see far-field pattern in Fig. 1.2).
The measurements showed that both ray descriptions and coupled waveguide equations can be used to optimize the aperture field of the converter, which is regarded as the key-point of a high-efficiency device.

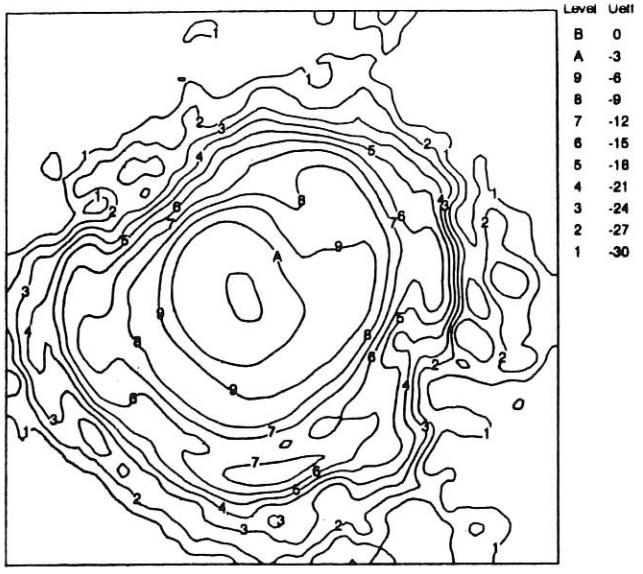

FIG. 1.1: Far-field pattern of a $TE_{10,4}$-to-TEM_{00} quasi-optical converter designed by coupled mode equations.

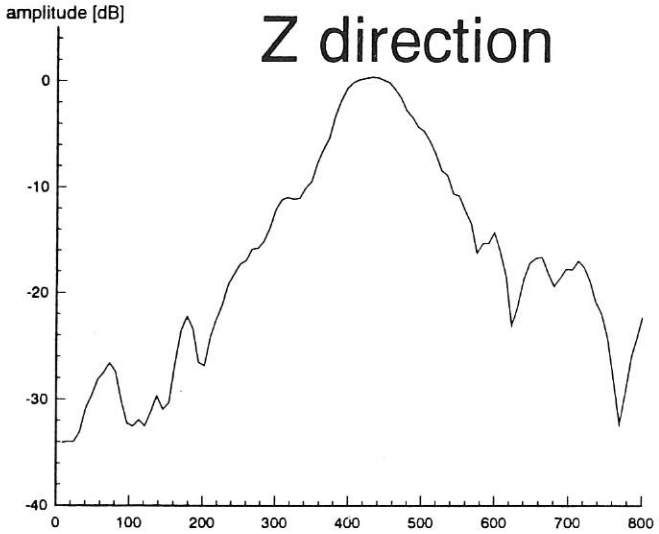

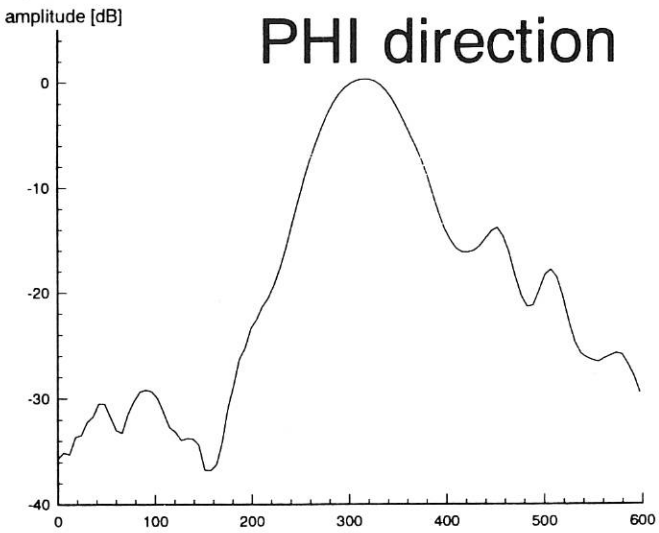

FIG. 1.2: Far-field pattern in the Z and PHI directions of a $TE_{15,2}$-to-TEM_{00} converter designed by using a ray description.

1.2.4.2 *Development of the MAGICTRAC converter*

The development of the MAGICTRAC converter in collaboration with LLNL as an alternative solution to quasi-optical mode converters was completed. The measurements showed that this principle can be used with good efficiency (typically 90%). In contrast to a Vlasov-type converter, the system can be built more compact, but the construction is more complex and the alignment is quite sensitive.

1.2.4.3 *Bragg mode converter*

Bragg reflectors consisting of periodic, cylindrically symmetric corrugations in the waveguide wall can produce adjustable

reflection up to nearly unity in definite modes by the principle of constructive interference. Window tapering of the corrugations leads to high mode purity and a ripple-free frequency dependence. The corrugation amplitudes are optimized with a scattering matrix code. Two Bragg reflectors with different corrugation periods can be combined in order to achieve mode conversion of one forward travelling mode into another. In this case a third backward travelling "working mode" which provides the energy exchange between the input and output forward travelling mode is trapped inside the converter.
To demonstrate the principle, a $TE_{11} \rightarrow TM_{11}$-mode converter at 28 GHz, where the TM_{12} mode acts as a working mode in the backward direction, was built and its properties were measured. In order to measure all three participating modes a k-spectrometer was placed in between the two Bragg reflectors. The measurement (Fig. 1.3) shows excellent agreement with the theoretical predictions.

1.2.4.4 Converters for matching of gaussian beams to HE_{11} transmission lines

The optimum coupling of a free-space gaussian beam into a corrugated waveguide can be achieved by particular mode mixtures of HE_{11} and HE_{12} hybrid modes. The wanted amount of the HE_{12} mode can be generated from the HE_{11} in a corrugated mode converter with periodic diameter variation (A) or in a corrugated taper (B). The encouraging results of detailed measurement with (A) at 70 GHz stimulated the development of very compact converters - radiating horns (B). The designed horns for installation in the 140 GHz transmission lines for W7-AS are in production.

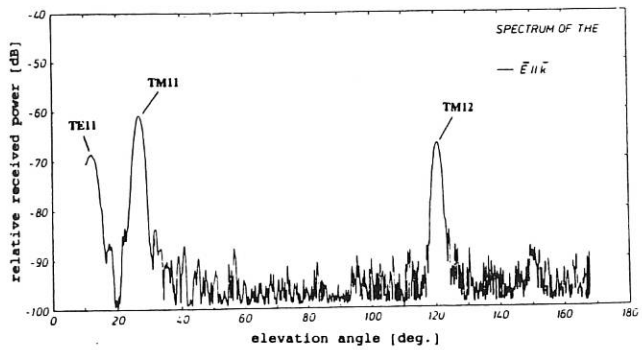

FIG. 1.3: k-spectrum of the $TE_{11} \rightarrow TM_{11}$-Bragg mode converter.

A) Periodic HE_{11}-HE_{12} mode converters

The mode content of the particular HE_{11} - HE_{12} mixtures [a) 97.5%+2.5% , b) 91%+9% and c) 80%+20%] produced by different optimized converters could be confirmed by k-spectrometer measurements and far-field measurements. In Fig. 1.4 the far-field patterns of a pure HE_{11} (dotted line) and of a mode mixture of 91% HE_{11} and 9% HE_{12} mode are shown.
Both far-field and k-spectrometer measurements yield pronounced reduction of side-lobes and cross-polarization as well as reduction of the beam waist.

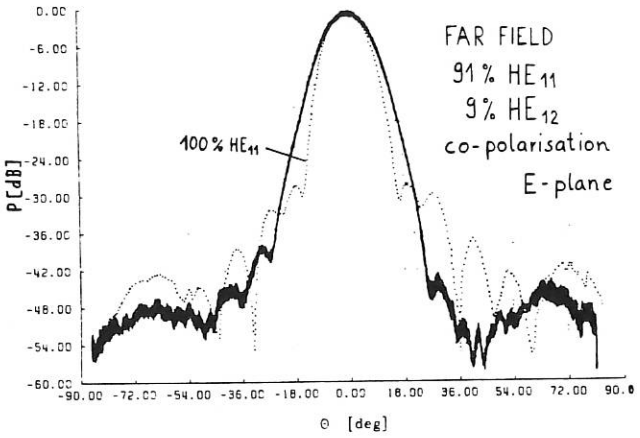

FIG. 1.4: Far-field patterns of a mode mixture of 91% HE_{11} and 9% HE_{12} mode (slot line) and a 100% HE_{11} mode (dotted line).

At 70 GHz, improvement compared with the coupling of a pure HE_{11} mode is achieved and further developments at 140 GHz were performed with optimized corrugated horns.

B) Horn design

For high-power applications, where a large waveguide diameter is needed, periodic mode-converters become very long. Therefore compact mode converting tapers were designed with a taper profile of the type proposed by Vlasov and Shapiro and described by $a(z) = a_0 [1 + (z/\alpha\ k\ a^2)^2]$. The optimization of the taper was done at 140 GHz with different diameters and by varying α in the formula. The mode mixture at the output is 85% HE_{11} and 15% HE_{12}. Even for large waveguide diameters of 87.0 mm the length of a taper giving similar results is about 540 mm. Additionally to the k-spectrometer and far-field measurements, the coupling between the waveguide and gaussian beam was confirmed by a resonator technique: the plane mirror of a Fabry-Perot resonator was replaced by the mode converter with a back-short. The design of the cavity is such that the beam waist is matched to the waveguide input and that no free-space modes are degenerated with the fundamental TEM_{00}. From the measured free spectral range ($\Delta\nu_F$) and half-width of the resonance line for the TEM_{00} mode ($\Delta\nu_L$) the finesse of the resonator ($F=\Delta\nu_F/\Delta\nu_L$) can be determined. The coupling efficiency is given by

$$\eta \approx 3 + \frac{\pi^2}{2F^2} - \sqrt{(1 + \frac{\pi^2}{2F^2})^2 - 1} - 2R ,$$

where R is the reflectivity of the mirrors.
The resonator measurement results are presented in Fig. 1.5. The efficiency of radiated mode mixtures from different horns is given in Table 1.

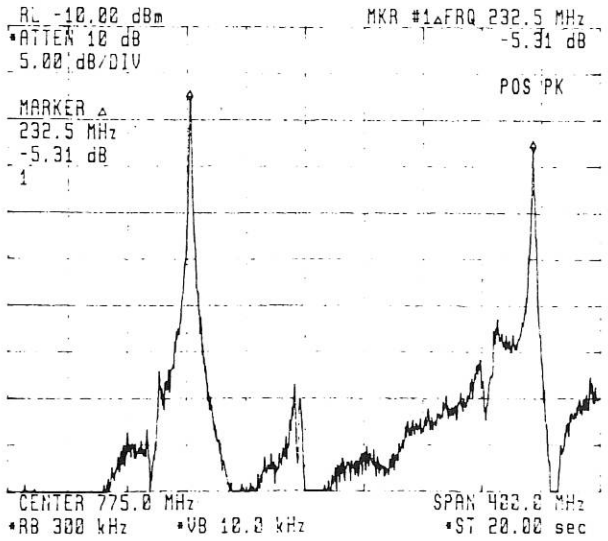

FIG. 1.5: Measurement of free spectral range and half-width of the resonant line.

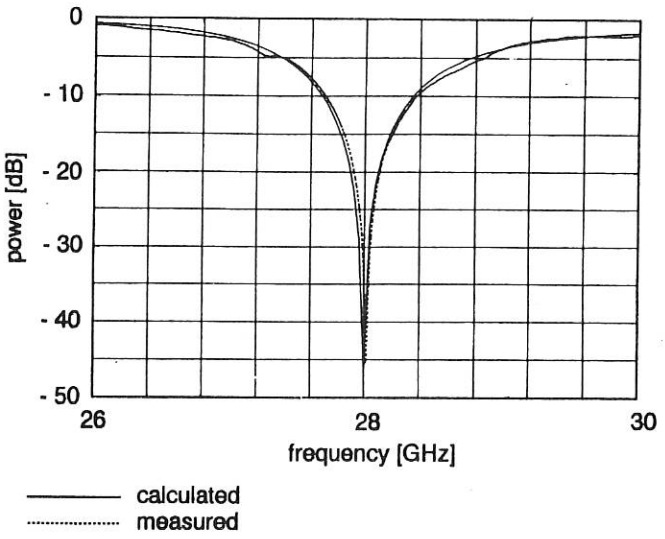

FIG. 1.6: Measured and calculated transmission curves of the 28 GHz notch filter.

Short Position	Horn 1	Horn 2	Corr. waveguide
0 mm	η=0.993	η=0.998	-----
71.3 mm	η=0.995	η=0.994	η=0.963
142.5 mm	η=0.993	η=0.993	η=0.978
213.8 mm	η=0.989	η=0.993	η=0.966
285.0 mm	η=0.989	η=0.991	η=0.977

TABLE 1: Efficiency of radiated mode mixtures from different horns

Very good agreement with calculated data (η=99.8%) is achieved. Improvement of the coupling efficiency between corrugated waveguides and free-space beams will therefore be realized with optimized horns.

1.2.4.5 Waveguide notch filters

Short inner waveguide reflectors and notch filters can be realized by using the effect of transverse resonances. A trapped mode is resonantly excited with the help of waveguide discontinuities. The effect is shown using a rectangular waveguide at 28 GHz with a symmetrical step in the width. The width and length of the larger cross-section were optimized using a scattering matrix code. In this case a TE_{30}-mode is resonantly excited in the larger section, whereas in the smaller cross-section only the TE_{10}-mode can propagate. Calculations and measurements performed at 28 GHz show good agreement between theory and experiment (Fig. 1.6).

1.2.4.6 Sawtooth oscillators for gyrotron collector coil supply

Since the 140 GHz Thorij gyrotrons are made for long pulses of up to 3 s, there is a need to vary the hit section of the electron beam at the gyrotron's collector to prevent thermal damage of the tube. The deflection is caused by a magnetic field which itself is produced by a toroidal solenoid. So there is need of a modulable power supply for this element. Because the magnetic field is directly proportional to the coil current (with a fixed geometry), the best possibility of driving it is with a sawtooth current. For this purpose a power supply with the following specifications was developed:

Peak current:	70 A (0 to 70 A adjustable)
Pulse period:	20 ms to 500 ms (adjustable)
Rise time:	5 ms
Fall time:	15 ms to 495 ms (adjustable)
Load:	R=1.0 Ω; L=150 mH

This supply is able to run loads with time constants of up to 150 ms, with simultaneous minimum pulse duration of 20
The effectivity of this supply was made very high, so that additional provisions for cooling are not necessary.

1.2.5 Loads for high-power microwaves

Two types of loads are applied to the operation of the Russian 140 GHz gyrotrons. A compact calorimetric load in which silicon oil serves as microwave absorbing liquid is used for exact high-power measurements. These are taken with short-

pulse operation (1-5 ms) at an average power of up to 5 kW. For adjustment of the gyrotron parameters to the full pulse length of 3 s a mobile absorber load was designed which consists of an absorbing cavity made of absorbing sand-lime bricks. Both loads allow measurement near the output window of the gyrotrons and at various positions along the transmission lines.

1.2.6 Conceptual design of a 50 MW ECRH/ECCD system for ITER

For the ITER international fusion reactor project, studies of different launching antennas for a variety of EC wave applications were performed. A major goal was to minimize the impact on the shield while fulfilling the physics requirements. On this basis, a quasi-optical antenna for ITER was designed. It can be switched between perpendicular and oblique toroidal injection and can thus be used for start-up, heating and current drive. The main features of this design are: (I) a power of 50 MW is delivered to the plasma; (II) only one horizontal port is needed; (III) minimum size of the shield penetration can be obtained; (IV) 40% of the port width is used for structure and shielding; (V) minimal extension of the primary vacuum boundary; (VI) the average power in the shield aperture is 420 MW/m^2.
This work was a contribution to a presentation at the 4th meeting of the Technical Advisory Committee (TAC-4) of ITER in San Diego.

1.3 Collective Thomson Scattering Diagnostic

(in collaboration with G.G. Denisov*), A.A. Fraiman*), T.Geist**), E. Holzhauer, V.N. Isaev*), L.V. Lubyako*), H.U. Nickel***), O.B. Smolyakova*), E.V. Suvorov*), M. Thumm***))

In 1993, first scattering experiments from thermal, collective electron density fluctuations in the W7-AS plasma were performed. The aim of these experiments is to measure the ion temperature or, more generally, the energy distribution of the different ion species in the plasma. This diagnostic could ultimately be used to get information on the energy spectrum of alpha particles generated in fusion reactions. For the measurements two installations originally envisaged for ECRH at 70 GHz and 140 GHz were used.
In the 70 GHz scattering system, two adjacent transmission lines were available, one for the launcher and one for the receiver. The gyrotron at the receiving line was disconnected and replaced by a heterodyne receiver. This was followed by a 9-channel filter bank to resolve the expected thermal spectra. By proper steering of the antennas in the vessel, different scattering geometries (scattering vector perpendicular and oblique to the magnetic field, shift of the scattering volume) could be realized.

*) Institute of Applied Physics, Nizhni Novgorod,
**) IPP Garching,
***) Kernforschungszentrum Karlsruhe

As the stellarator depends on ECRH for ionization and heating, a major problem for the 70 GHz experiments was the presence of an EC resonance layer in the scattering volume, which is optically thick. To discriminate the scattered signal from the EC emission, which dominates the scattered power by more than one order of magnitude, 10 kHz modulation of the gyrotron and synchronous detection of the scattered signal were successfully used.
Measured data are shown in Fig. 1.7. For comparison, a calculated spectrum is given, where effects by the finite refractive index of the plasma are neglected. The width of the measured spectrum (extending from 160 MHz to 400 MHz), which is at the thermal level, agrees with the theoretical value. At lower frequencies, the scattered power strongly overcomes the thermal level, which might indicate the presence of suprathermal fluctuations. However, at present exact theoretical models are missing for experiments where the EC resonance is located in the plasma. Further experiments are planned where this situation can be avoided.

At 140 GHz, the quasi-optical ECRH system was used for the launcher, and a separate receiver antenna was built. The complex and very sensitive receiving system (quasi-optical notch filter, heterodyne receiver, 32-channel filter bank, A/D converters) was fabricated at IAP Nizhni Novgorod.

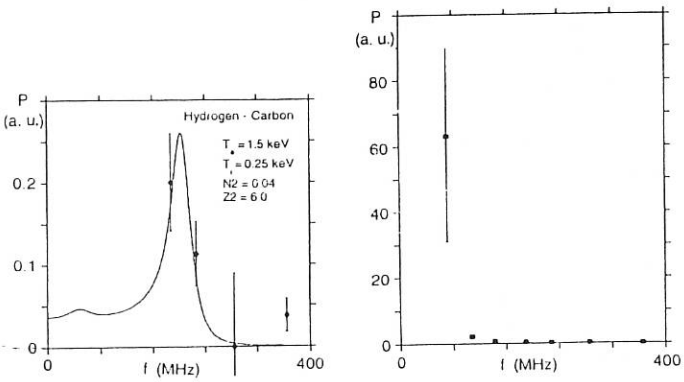

FIG. 1.7: Left: calculated and measured spectrum with 4% carbon impurities.
Right: the same spectrum with extended scale with the suprathermal part below 150 MHz.

Measurements were performed at a magnetic field of 1.25 T, where the fourth harmonic ECE radiation is weak (<2eV) and direct detection of the scattered signal could be used. The main problem for this experiment up to now has been the high level of stray radiation due to both the scattering geometry and the very strong frequency chirp during the switch-on phase (<1ms) of the gyrotron. The stray radiation coming from this part of the pulse could not be suppressed by the narrow notch filter. It was therefore not possible to identify unequivocally the scattered signal. Further experiments with an optimized scattering geometry and an upgraded receiver system with the capability of suppressing chirped frequency components due to pulsed operation of the gyrotrons are in preparation.

2. PLASMA EDGE DIAGNOSTICS

K. B e h r i n g e r, U. Fantz, H. Jentschke, K. Hirsch, E. Holzhauer, M. Niethammer, T. Schütte, K. Schwörer, G. Volk

2.1 Carbon Erosion Measurements

The interaction of materials with plasmas is being investigated within the framework of "Sonderforschungsbereich 259", dealing with the heat load problems of thermal protection systems during re-entry of spacecraft into the atmosphere. For this purpose, arc jets are operated in air-like mixtures at Institut für Raumfahrtsysteme, IRS. The IPF contribution to this project consists of plasma diagnostics and erosion measurements by means of emission spectroscopy and laser scattering. Due to the requirement of low weight, but high mechanical strength, carbon fibres (C/C) have been the basis for most materials considered so far. When exposed to the plasma, the material probes are heated to surface temperatures of about 1500-2000 °C. At these temperatures, the sublimation rate of carbon is still small and the erosion is mainly due to chemical processes with the oxygen and nitrogen molecules, atoms and ions. These processes can be largely reduced by silicon treatments, resulting in the formation of SiC (C/SiC), or by similar methods.

The integral erosion rates of these materials are obtained in the usual way from weight loss. Spectroscopic measurements of particle fluxes from the surface of the probes must be based on measurements of the respective particle number densities and their velocities. It is probably a reasonable assumption in this case that the particles leave the surface with the thermal velocity corresponding to the surface temperature. Since these atoms or molecules are not completely ionized in the low-temperature plasma, the simple method of flux measurements on the basis of so-called S/XB ratios, which is usually applied in fusion research, cannot be used (it is not even absolutely sure that all molecules break up in these plasmas, so that the fluxes can be measured from the atom densities alone). However, both methods of flux measurements require excitation rate coefficients of the elements in question, or, more precisely, collisional-radiative models. The experience gained in the plasma jet experiments can therefore be transferred, at least to some extent, to similar investigations in fusion research.

In 1992, the erosion of boron graphite (BC) was investigated in the plasma jet, in addition to the usual C/C and C/SiC probes. This material was similar to those used as limiters in some fusion experiments and consisted of 85% graphite and 15% boron. When the BC sample was exposed to the same heat flow as pure carbon, its surface temperature was about 150 °C higher (≈1850 °C instead of ≈1700 °C), obviously due to its much lower heat conductivity. The following erosion rates were measured by means of weight loss under these conditions (erosion Φ in mm/h):

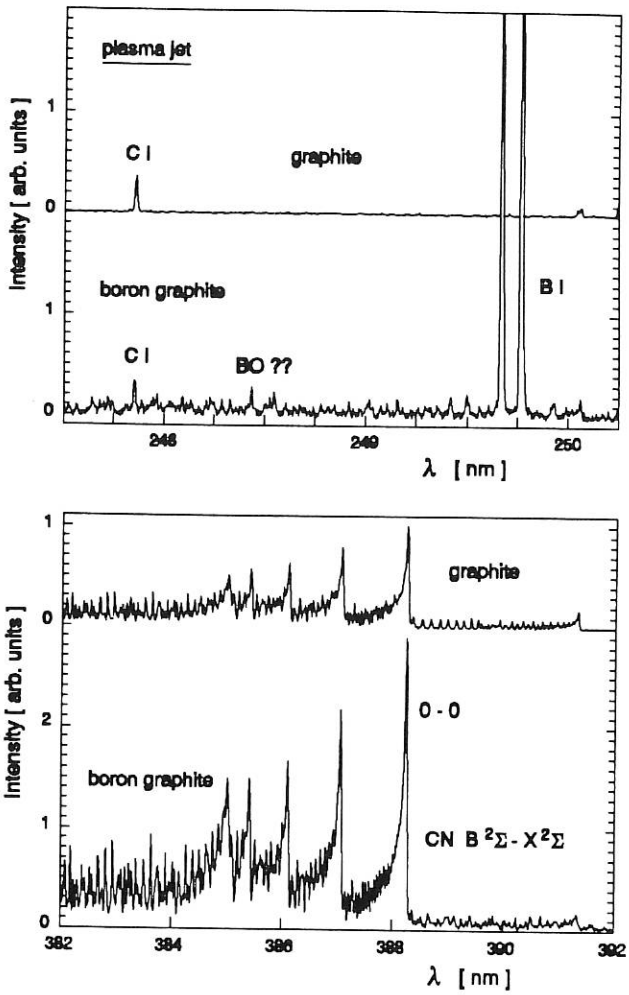

FIG. 2.1: C and B spectral lines and CN molecular bands emitted by the plasma in front of graphite and boron graphite probes.

Φ (C)	:	13.6
Φ (BC)	:	11.2
Φ (C/SiC)	:	0.4
Φ (SiC)	:	0.02

The silicon-containing materials showed the above reduced erosion after some initial formation of the surface.

The spectra emitted by the plasmas in front of the probes contain spectral lines of carbon (very weak for low erosion), silicon or boron lines, as well as strong molecular bands, especially of CN. Examples of the cases of pure graphite and boron graphite are given in Fig. 2.1. The lower part shows the CN bands, which, for an unknown reason (possibly the higher surface temperature) are stronger in the case of BC. The upper traces show the carbon spectral line and lines of boron in the 250 nm wavelength region. Similar spectra have been seen e.g. on W7-AS. The excitation rate coefficients for these lines had already been calculated for fusion plasma diagnostics (see Annual Report 1992), that for carbon from a collisional-radiative model; for the strong boron resonance line a corona calculation is probably sufficient. Under the conditions of the arc jet

plasma ($T_e \approx$ 1 eV), the boron excitation rate coefficient is a factor of about 200 higher than that of carbon. The results in Fig. 2.1 therefore show roughly the correct flux ratio of 6:1.

It should be pointed out that the observed boron erosion is again not explainable by evaporation, which should be three orders of magnitude lower. As in the case of carbon, chemical processes must be responsible, e.g. the formation of boron-nitride. In contrast, the measured silicon fluxes are lower than the calculated evaporation rate, indicating the formation of a protective surface layer.

2.2 First Results of High-resolution Spectroscopy in H_2 and D_2 RF Discharges

2.2.1 Echelle spectrometer

Since the end of 1993 a Sopra echelle spectrometer has been available for high-resolution spectroscopy, e.g. required for measuring line profiles (Stark and Doppler widths) and line shifts (flow velocities), as well as for detailed studies of molecular spectra. This instrument with 1.5 m focal length and double path offers a resolution of about 0.6 pm at 300 nm and 1.5 pm at 700 nm wavelength (resolution = 500,000). At present, only scanning mode with photoelectric recording is possible. The echelle spectrometer and a coupled predisperser are controlled by a PC and the data are digitally recorded. After some initial tests with spectral lamps, the first objects to be studied were the line profiles of H_α and D_α lines emitted by RF discharges in hydrogen and deuterium.

2.2.1 RF discharges used for first investigations

RF discharges were used for the first application of the echelle spectrometer in a plasma experiment. The RF power (industrial frequency 27 MHz) is capacitively coupled to a Pyrex cylinder (length = 150 mm, inner diameter 60 mm) with quartz windows at both ends. Filling pressures of atomic and molecular gases range from 5 Pa to several 100 Pa. A microwave interferometer operating at 70 GHz is used to measure the line-integrated electron number density. At present, continuous operation without additional cooling is possible for input powers ≤ 200 W resulting in electron densities $n_e \approx 10^{11}$ cm^{-3}, depending on the type and pressure of the filling gas. The plasma discharge can be pulsed to reduce cooling problems, as well as for the study of relaxation phenomena. In the longer term it is planned to extend the electron density range of the plasma to $>10^{12}$ cm^{-3}, corresponding to values relevant to fusion edge plasmas. Furthermore, a Maxwellian electron energy distribution can be expected at these densities, which makes interpretation of spectroscopic data much easier, but is often not realized in low-density plasmas.

The H_α and D_α line profiles discussed below were obtained in steady-state operation of this RF discharge with a filling pressure of 15 Pa and an RF power of 100 W.

2.2.3 H_α and D_α line profiles

In low-power and low-density discharges, the heavy particle temperatures T_g hardly increase over room temperature, while the electrons have energies of some eV. In molecular hydrogen, hydrogen atoms are usually produced by dissociation via the repulsive triplet ground state of the H_2 molecules, and the atoms will initially have a so-called Franck-Condon energy of about 3 eV. However, they will soon be cooled down to T_g by the very effective heavy-particle collisions. The corresponding Doppler profiles should then be relatively narrow, so that the hydrogen line fine structure could be clearly seen. However, since the majority of particles is in the molecular state, an appreciable fraction of H_α or D_α photons could be due to dissociative excitation. In the latter case, the radiating particles have kinetic energies of several eV, again gained from the repulsive upper molecular potential curves.

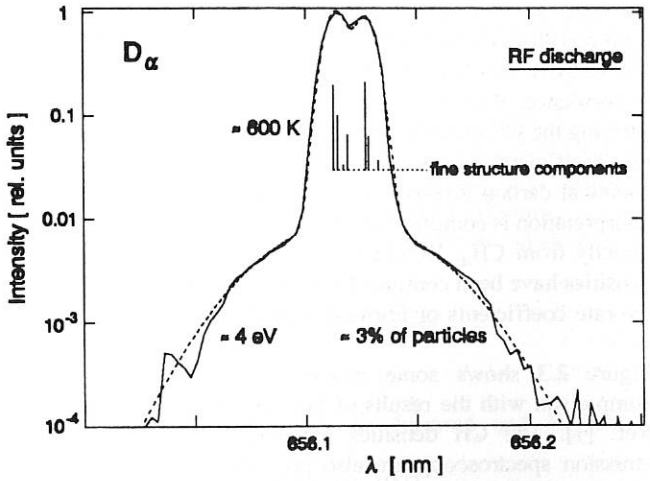

FIG. 2.2: Measurement of the D_α line profile in a low-pressure RF discharge and corresponding profile calculations.

The H_α fine structure consists of seven individual transitions between n=3 and n=2. Their relative intensities can be calculated by assuming a Boltzmann distribution over the very closely spaced sublevels. Taking into account the corresponding Doppler broadening, the result should correspond to the experimental profiles.

A comparison of measured and calculated D_α profiles is shown in Fig. 2.2 in a semi-logarithmic presentation. This particular recording was done with moderate spectral resolution (≈5 pm) aiming at study of the far line wings. The double peak in the line centre is due to the fine structure and can be analyzed better by means of other profile measurements with higher resolution. However, in any case, the higher wavelength peak should be the more intense one, according to the fine structure calculations, which is not found experimentally in Fig. 2.2. The discrepancy can be reconciled by assuming some 30% underpopulation of the $3d_{5/2}$ sublevel, as demonstrated by the calculated curve in Fig. 2.2. The narrow profile in the line centre corresponds to a temperature of about 600 K, i.e. the gas temperature of the discharge. Below the 1% intensity level,

the D_α line in Fig. 2.2 exhibits a second, much broader profile corresponding to a "temperature" of about 4 eV. This part of the spectrum must be due to the dissociative excitation process, which is responsible for roughly 3% of the emitted photons.The profile is almost Gaussian, but actually reflects the shape of the molecular potential curves. From such spectroscopic measurements, as well as other plasma diagnostics methods, ratios of the respective rate coefficients can be derived and possibly conclusions drawn on the electron energy distribution.

2.3 CH/CD Density Measurements in ECR Plasmas

Microwave discharges in methane (CH_4 and CD_4) and in methane-noble gas mixtures are being investigated by optical emission spectroscopy and active laser techniques. The usual 2.45 GHz frequency is used to generate these plasmas and the filling pressure can be varied between about 2 and 20 Pa. Emission spectra of the $A^2\Delta$-$X^2\Pi$ electronic transition have been recorded and analyzed (see e.g. Annual Report 1991) and the CH/CD densities have been measured by laser-induced fluorescence (LiF, Annual Report 1992) with the aim of deriving the CH electron impact excitation rate coefficient. This rate coefficient is a necessary prerequisite for investigating the chemical carbon erosion in fusion experiments. The intended interpretation is complicated by alternative excitation paths, e.g. directly from CH_4. Results for the CH and hydrogen number densities have been compared with model calculations [1] using the rate coefficients of Ehrhardt and Langer [2].

Figure 2.3 shows some recent experimental LiF data in comparison with the results of plasma modelling according to Ref. [1]. The CH densities obtained by means of optical emission spectroscopy are also presented. Unfortunately, the radiation due to electron excitation from the CH ground state is only responsible for a small fraction of the total intensity of the CH A-X transition, while the major part is due to the CH_4 dissociative excitation. A dilution with noble gases like argon reduces this competitive process, thus allowing a more precise measurement of the excitation rate coefficient. However, the good agreement of LiF and emission spectroscopy in Fig. 2.3 at higher pressures demonstrates that the values used at present are not far from reality. They are possibly somewhat on the low side.

The LiF measurements shown in Fig. 2.3 allow another important conclusion. For the same external parameters, the CD densities in CD_4 plasmas are virtually identical to the CH densities in CH_4 plasmas. Even though this result had always been expected, there is now proof that the difference in mass plays no major role in the dissociation processes.

[1] K. Behringer, Plasma Phys. and Contr. Fusion 33 (1991) 997

[2] A.B. Ehrhardt, W.D. Langer, Collisional Processes of Hydrocarbons in Hydrogen Plasmas, PPPL-2477, Sept. 1987

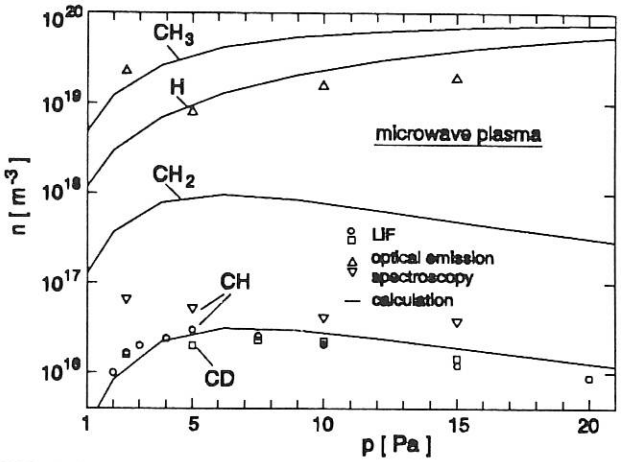

FIG. 2.3: Number densities in methane microwave discharges measured by emission spectroscopy and laser-induced fluorescence.

PUBLICATIONS AND CONFERENCE REPORTS RELATED TO THE COOPERATION BETWEEN IPF AND IPP

Allmendinger, A., R. Platz, and G. Dodel:
"Megahertz far-infrared frequency shifting via multiple diffraction by a rotating grating".
Rev. Sci. Instrum. 64 (1993) 1705-1713

Costley, A.E., U. Gasparino and W. Kasparek:
"Report on the 8th joint workshop on electron cyclotron emission and electron cyclotron resonance heating".
Nuclear Fusion 33 (1993), p. 1239-1245.

Schunke, B., C.W. Gowers, K. Hirsch and P. Nielsen:
A laser diode as a light source for calibrating the time base of a streak camera".
Rev. Sci. Instr. 64 (1993) 3338-3339

Tran, M.Q., H. Cao, J.Ph. Hogge, W. Kasparek, T.M. Tran and P.J. Paris:
"Properties of diffraction gratings used as output couplers in a quasi-optical gyrotron".
J. Appl. Phys. 73 (1993), 2089-2102.

8th Joint Workshop on Electron Cyclotron Emission and Electron Cyclotron Resonance Heating, Gut Ising, Oct. 19-21, 1992

Kasparek, W.:
"Millimetre wave systems for high-power ECRH, status and future trends".
Proc. EC-8 (March 1993), p. 423-444.

Wagner, D., J. Pretterebner, M. Thumm:
"Eigenmode mixtures in circum ferentially corrugated waveguides".
Proc. EC-8 (March 1993), p. 575-585.

Frühjahrstagung der Deutschen Physikalischen Gesellschaft, Fachausschuß Plasmaphysik, Greifswald (Germany), March 9-11, 1993

Kasparek, W., G.A. Müller, P.G. Schüller, V. Erckmann, W7-AS Team:
"Experimente am Stellarator W7-AS zur Heizung und Stromtrieb in Plasmen mit Millimeterwellen".
Verhandl. DPG (IV) 28 (1993) P VI.

Platz, R. und G. Dodel:
"Frequenzverschiebung von Ferninfrarotstrahlung im Megahertzbereich zur Anwendung bei der Heterodyninterferometrie und der Laserlichtstreuung mit Heterodynnachweis".
Verhandl. DPG (VI) 28 (1993) P 14.79

9th IAEA Workshop on Stellarators and other Helical Confinement Systems, Garching (Germany) May 10-14, 1993.

Erckmann, V., W. Kasparek, G.A. Müller, P.G. Schüller, V.I. Il'in, V.I. Kurbatov, S. Malygin and V.I. Malygin:
"Status and prospects of 140 GHz ECRH".
Proc., p. 602-610.

ITG (VDE)-Workshop on THz/Submillimeter Wave Technology, Sindelfingen (Germany), May 28, 1993

Alius, H. and G. Dodel:
"Modulation of submillimeter radiation by optically induced free carrier density modulation in semiconductors".

5th Joint Russian-German Meeting on ECRH and Gyrotrons, Garching-Stuttgart-Karlsruhe (Germany), June 28-July 2, 1993.

Erckmann, V., E. Holzhauer, W. Kasparek and E.V. Suvorov:
"Status of collective Thomson scattering experiments at 70 GHz and 140 GHz on W7-AS".
Proc., p. 207-230.

Graubner, T., H. Kumrić and W. Kasparek:
"Some applications of coupled mode equations on corrugated waveguide components".
Proc., p. 273-288.

Kasparek, W., G.A. Müller, P.G. Schüller, V. Erckmann, T. Geist, H.-U. Nickel, M. Thumm et al:
"Experimental experience with the quasi-optical ECRH transmission system on W7-AS and recent development".
Proc., p. 389-306.

Kasparek, W., H. Brinkschulte, F. Leuterer, M. Münich and M. Zouhar:
"The ASDEX-upgrade ECRH transmission system".
Proc., p. 307-326.

Möbius, A., J. Pretterebner and M. Thumm:
"Compact quasi-optical $TE_{22,6}$ to TEM_{00} converter with feed waveguide deformations".
Proc., p. 545-554.

Müller, G.A., H. Alius and W. Bartusch:
"28 GHz microwave processing of ceramics, status of the project at IPF".
Proc., p. 333-342.

Wagner, D., J. Pretterebner and M. Thumm:
"Design of coaxial gyrotron cavities using a scattering matrix code".
Proc., p. 555-565.

2nd International Workshop on Strong Microwaves in Plasmas, Nizhni Novgorod (Russia), August 15-22, 1993.

Denisov, G.G., V. Erckmann, A.A. Fraiman, T. Geist, E. Holzhauer, V.N. Isaev, W. Kasparek, A.G. Litvak, L.V. Lubyako, G.A. Müller, H.-U. Nickel, P.G. Schüller, O.B. Smolyakova, E.V. Suvorov and M. Thumm:
"Collective scattering of powerful gyrotron radiation at W7- AS".

18th International Conference on Infrared and Millimeter Waves,
Colchester (UK), September 6-10, 1993.

Graubner, T., W. Kasparek and H. Kumrić:
"Optimization of coupling between HE_{11} waveguide mode and gaussian beam".
Proc., p. 477-478.

Pretterebner, J., A. Möbius, M. Thumm and A. Wien:
"Compact quasi-optical $TE_{22,6}$ to TEM_{00} converter with feed waveguide deformations".
Proc., p. 322-323.

Verhoeven, A.G.A., W.A. Bouger, V.L. Bratman, M. Caplan, G.G. Denisov, B.S.Q. Elzendorn, A.M. van Ingen, W. Kasparek, P. Manintveld, H.U. Nickel, J. Pretterebner, A.V. Savilov, M.Yu Schmelyov, C. Shang, M. Thumm, A. Tulopov, W.H. Urbanus, D. Wagner and M.J. van der Wiel:
"Status of the design of the 200 GHz FOM-Fusion FEM".
Proc., p. 19-20.

Wagner, D., J. Pretterebner and M. Thumm:
"Mode coupling in overmoded, varying radius coaxial gyrotron cavities".
Proc., p. 326-327.

Wagner, D., J. Pretterebner and M. Thumm:
"Transverse resonances in oversized waveguides".
Proc., p. 422-423.

The 4th H-mode Workshop,
JAERI-NAKA (Japan), Nov. 15-17, 1993

Holzhauer, E., G. Dodel, M. Endler, J. Gernhardt, L. Giannone, M. Manso, K. McCormick, V. Mertens, H. Niedermeyer, A. Rudyj, F. Serra, A. Silva, G. Theimer, P. Varela, F. Wagner, H. Zohm and ASDEX Team:
"The H-mode in the ASDEX tokamak".
Paper IO 1.

DOCTORAL THESIS

Volk, G.:
"Zeitaufgelöste Bestimmung von Plasmaparametern der stillen Entladung in Stickstoff".

DIPLOMA THESES

Graubner, T.:
"Optimierung der Anpassung zwischen einem gaußschen Strahl und der HE_{11}-Hohlleitermode".

Wagner, K.P.:
"Modifikation des Intensitätsprofils eines gaußschen Strahles".

How to reach
Max-Planck-Institut für Plasmaphysik (IPP)

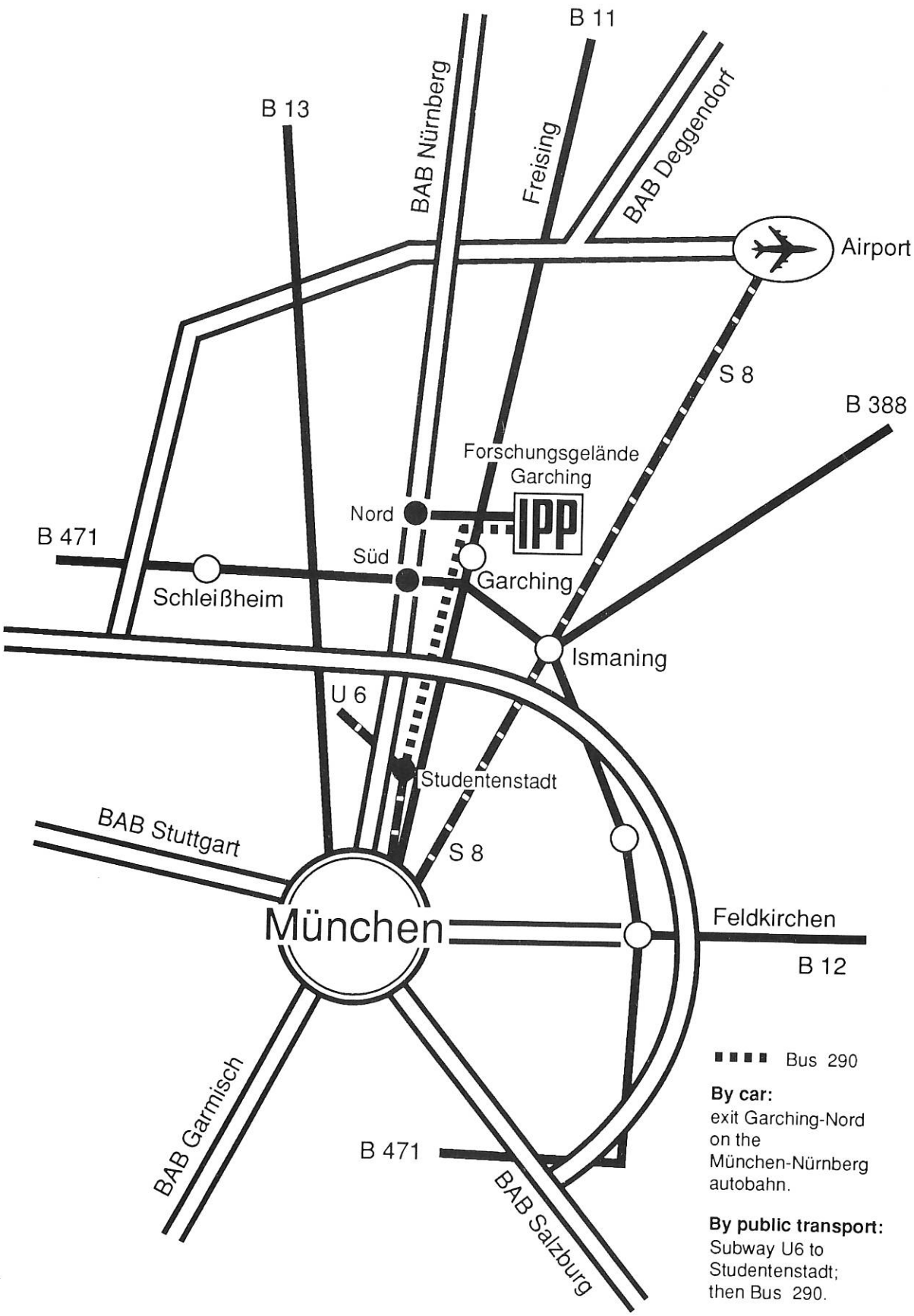

By car:
exit Garching-Nord on the München-Nürnberg autobahn.

By public transport:
Subway U6 to Studentenstadt; then Bus 290.

ANNUAL REPORT 1993

Max-Planck-Institut für Plasmaphysik (IPP) · 85748 Garching bei München
Telephone (0 89) 32 99-01 · Telefax (0 89) 32 99-22 00

Printing: SV-Kommunalschriften-Druckerei, München

Printed in Germany
ISSN 0179-9347

This work was performed under the terms of the agreement between Max-Planck-Institut für Plasmaphysik and the European Atomic Energy Community to conduct joint research in the field of plasma physics.


IPP